

# **Molecular mechanisms of TIMP-3 turnover in Sorsby Fundus Dystrophy**

**Jacob Henry John Betts**

Doctor of Philosophy (PhD)



**University of East Anglia**

Norwich Medical School

2024

This copy of the thesis has been supplied on condition that anyone who consults it is understood to recognise that its copyright rests with the author and that use of any information derived therefrom must be in accordance with current UK Copyright Law. In addition, any quotation or extract must include full attribution.

# Abstract

Sorsby fundus dystrophy (SFD) is an autosomal dominant macular dystrophy, caused by mutations in tissue inhibitor of metalloproteinases 3 (TIMP-3), leading to central vision loss. SFD is characterised by extracellular accumulation of mutant TIMP-3 proteins in the Bruch's membrane (BrM), although molecular mechanism(s) facilitating this accumulation are unknown. In other cell types, extracellular levels of TIMP-3 are regulated post-translationally by the balance between its endocytosis via low-density lipoprotein receptor-related protein 1 (LRP1) and extracellular binding to heparan sulfate (HS).

To establish how SFD TIMP-3 proteins accumulate extracellularly, I investigated whether retinal pigment epithelial (RPE) cells endocytose wild-type (WT) and SFD variants (H181R, Y191C, S204C) of TIMP-3, and whether this occurs via LRP1. WT and SFD TIMP-3 were recombinantly expressed in HEK-293 cells and isolated by affinity chromatography. Endocytosis of these proteins from conditioned media of ARPE-19 and hTERT RPE-1 cells was assessed by immunoblotting and confocal microscopy. Endocytosis of Y191C and S204C was significantly slower than WT TIMP-3, whereas H181R had unimpaired endocytosis. Receptor-associated protein (RAP) blocked uptake of WT and SFD TIMP-3, however siRNA knockdown of *LRP1* had no effect on WT TIMP-3 uptake. Endocytosis assays performed in LRP1-null mouse fibroblasts demonstrated that endocytosis of SFD TIMP-3 proteins is largely independent of LRP1. This suggests that RPE cells are distinct from other cells analysed to date, in that they endocytose WT and SFD TIMP-3 via an LRP other than LRP1.

Delayed endocytosis of Y191C and S204C TIMP-3 is likely a key molecular mechanism by which they accumulate in the BrM. However, the unimpaired endocytosis of H181R indicates heterogeneity in SFD molecular mechanisms. Further studies are needed to clarify binding of SFD TIMP-3 to HS, as this may be an alternative mechanism of accumulation. Targeting SFD TIMP-3 endocytosis or clearance may be a potential therapeutic approach to treat SFD.

## **Access Condition and Agreement**

Each deposit in UEA Digital Repository is protected by copyright and other intellectual property rights, and duplication or sale of all or part of any of the Data Collections is not permitted, except that material may be duplicated by you for your research use or for educational purposes in electronic or print form. You must obtain permission from the copyright holder, usually the author, for any other use. Exceptions only apply where a deposit may be explicitly provided under a stated licence, such as a Creative Commons licence or Open Government licence.

Electronic or print copies may not be offered, whether for sale or otherwise to anyone, unless explicitly stated under a Creative Commons or Open Government license. Unauthorised reproduction, editing or reformatting for resale purposes is explicitly prohibited (except where approved by the copyright holder themselves) and UEA reserves the right to take immediate 'take down' action on behalf of the copyright and/or rights holder if this Access condition of the UEA Digital Repository is breached. Any material in this database has been supplied on the understanding that it is copyright material and that no quotation from the material may be published without proper acknowledgement.

# Table of Contents

<b>Abstract .....</b>	<b>2</b>
<b>Abbreviations .....</b>	<b>7</b>
<b>List of figures .....</b>	<b>9</b>
<b>List of tables.....</b>	<b>12</b>
<b>Acknowledgments .....</b>	<b>13</b>
<b>Chapter 1: Introduction .....</b>	<b>14</b>
1.1 <b>Sorsby Fundus Dystrophy.....</b>	<b>15</b>
1.2 <b>Similarities between SFD and other retinal dystrophies .....</b>	<b>19</b>
1.2.1    Age-related macular degeneration.....	19
1.2.2    Other retinal diseases .....	20
1.3 <b>Structure of the retina.....</b>	<b>20</b>
1.3.1    RPE cells .....	22
1.3.2    The Bruch's membrane.....	23
1.4 <b>The TIMP family .....</b>	<b>31</b>
1.4.1    Inhibition of metalloproteinases .....	32
1.4.2    TIMP structure .....	34
1.4.3    TIMP-3 .....	35
1.5 <b>SFD TIMP-3 mutant proteins .....</b>	<b>38</b>
1.6 <b>Why does TIMP-3 accumulate in SFD? .....</b>	<b>52</b>
1.6.1    Mechanisms regulating TIMP-3 abundance .....	53
1.7 <b>The scavenger receptor LRP1.....</b>	<b>55</b>
1.7.1    LRP1 structure and biological function .....	55
1.7.2    Mechanisms and regulation of LRP1-mediated endocytosis .....	58
1.7.3    Other LRPCs .....	61
1.8 <b>Hypotheses and aims of the project.....</b>	<b>62</b>
<b>Chapter 2: Materials and methods .....</b>	<b>64</b>
2.1 <b>Materials .....</b>	<b>65</b>
2.1.1    General chemicals .....	65
2.1.2    Disposable plastics .....	66
2.1.3    Cultured cells and cell culture reagents .....	67

2.1.4 SDS-PAGE and immunoblotting reagents .....	68
2.1.5 Antibodies and fluorescent stains .....	69
2.1.6 Molecular biology reagents .....	69
2.1.7 Laboratory instrumentation .....	74
2.1.8 Software.....	74
<b>2.2 Methods.....</b>	<b>75</b>
2.2.1 Mammalian cell culture .....	75
2.2.2 SDS-PAGE and immunoblotting .....	75
2.2.3 Molecular biology methods .....	78
2.2.4 HEK-293 transfections of wild-type and SFD TIMP-3, and stable expression of TIMP-3 and pro-MMP-1.....	80
2.2.5 Wild-type and SFD TIMP-3 and pro-MMP-1 isolation.....	81
2.2.6 Pro-MMP-1 activation .....	83
2.2.7 Transfection of ARPE-19 cells .....	84
2.2.8 Apoptosis of ARPE-19 cells induced by TIMP-3 and SFD TIMP-3 mutants .....	85
2.2.9 Endocytosis assays .....	86
2.2.10 Cell viability assays .....	86
2.2.11 Immunofluorescent microscopy to visualise endocytosis of TIMP-3 and SFD TIMP-3 .....	87
2.2.12 RNAscope analysis of TIMP3 and LRP1 expression.....	88
2.2.13 siRNA knockdown of LRP1 .....	89
2.2.14 Statistical analysis .....	90
<b>Chapter 3: Generation and characterisation of SFD TIMP-3 mutants.....</b>	<b>91</b>
<b>3.1 Introduction.....</b>	<b>92</b>
<b>3.2 Results.....</b>	<b>94</b>
3.2.1 Generation of pCEP4 expression vectors encoding E162K, H181R, Y191C and S204C SFD TIMP-3.....	94
3.2.2 Expression of WT and SFD TIMP-3 mutants in HEK-293 cells .....	95
3.2.3 Isolation of WT and SFD TIMP-3 from conditioned medium of HEK-293 cells .....	98
3.2.4 Reduction and alkylation of isolated WT, H181R, Y191C and S204C TIMP-3 .....	105
3.2.5 Expression and isolation of FLAG-tagged pro-MMP-1 .....	107
<b>3.3 Discussion .....</b>	<b>110</b>

<b>Chapter 4: What are the effects of SFD TIMP-3 mutants on RPE gene expression and health?.....</b>	<b>117</b>
<b>4.1    Introduction.....</b>	<b>118</b>
<b>4.2    Results.....</b>	<b>119</b>
4.2.1    Optimisation of ARPE-19 cell transfection with pCEP4 plasmids encoding WT and SFD TIMP-3 mutants .....	119
4.2.2    Optimised ARPE-19 cell transfection with pCEP4 plasmids encoding WT and SFD TIMP-3 mutants .....	126
4.2.3    Expression of LRP, metalloproteinase, proteoglycan, cytokines and oxidative stress genes induced by ARPE-19 transfection with WT and SFD TIMP-3 .....	129
4.2.4    Effect of WT, H181R and S204C TIMP-3 on ARPE-19 apoptosis .....	135
<b>4.3    Discussion .....</b>	<b>138</b>
<b>Chapter 5: Turnover of TIMP-3 and SFD TIMP-3 variants by RPE cells.....</b>	<b>146</b>
<b>5.1    Introduction.....</b>	<b>147</b>
<b>5.2    Results.....</b>	<b>148</b>
5.2.1    Evaluating the effect of TNC-B on ARPE-19 and hTERT RPE-1 cell viability .....	148
5.2.2    Endocytosis of WT, H181R, Y191C and S204C TIMP-3 by ARPE-19 cells .....	151
5.2.3    Endocytosis of WT, H181R, Y191C and S204C by hTERT RPE-1 cells .....	158
5.2.4    WT, H181R, Y191C and S204C TIMP-3 were not degraded in conditioned media.....	163
5.2.5    Visualisation of WT, H181R, Y191C and S204C TIMP-3 endocytosis by immunofluorescent microscopy .....	165
5.2.6    WT and H181R TIMP-3 bound to heparin-Sepharose beads .....	167
<b>5.3    Discussion .....</b>	<b>169</b>
<b>Chapter 6: Establishing the role of LRP1 in the endocytosis of TIMP-3 in RPE cells.....</b>	<b>177</b>
<b>6.1    Introduction.....</b>	<b>178</b>
<b>6.2    Results.....</b>	<b>179</b>

6.2.1 Endocytosis of WT, H181R, Y191C and S204C TIMP-3 by mouse embryonic fibroblast and PEA-13 cells .....	179
6.2.2 LRP1 is expressed by retinal pigment epithelial cell lines and in primary retinal tissue.....	184
6.2.3 Endocytosis of WT, H181R, Y191C and S204C TIMP-3 was blocked by RAP 187	
6.2.4 Effect of siRNA knockdown of LRP1 on endocytosis of WT TIMP-3 in RPE cells .....	193
6.2.5 mRNA expression of LRP-related receptors in ARPE-19 and hTERT RPE-1 cells .....	205
<b>6.3 Discussion .....</b>	<b>206</b>
<b>Chapter 7: Discussion .....</b>	<b>218</b>
<b>7.1 Key findings .....</b>	<b>219</b>
<b>7.2 Molecular mechanisms of SFD TIMP-3 accumulation .....</b>	<b>219</b>
7.2.1 WT TIMP-3 is taken up by RPE cells .....	219
7.2.2 Endocytosis of Y191C and S204C TIMP-3 by RPE cells is significantly delayed .....	220
7.2.3 Endocytosis of H181R TIMP-3 by RPE cells is unimpaired.....	220
7.2.4 Uptake of WT, H181R, Y191C and S204C TIMP-3 is LRP-dependent but distinct from LRP1 .....	222
7.2.5 Limitations and further experiments examining endocytosis .....	224
<b>7.3 Other considerations of SFD TIMP-3 proteins .....</b>	<b>226</b>
7.3.1 Dimerisation status of SFD TIMP-3 proteins.....	226
7.3.2 Broader effects of SFD TIMP-3 proteins on RPE cells .....	227
7.3.3 Regulation of SFD TIMP-3 protein expression .....	228
<b>7.4 Additional areas for future investigation .....</b>	<b>229</b>
<b>7.5 Therapeutic implications .....</b>	<b>230</b>
<b>Bibliography .....</b>	<b>233</b>

# Abbreviations

ADAM	A disintegrin and metalloprotease
ADAMTS	A disintegrin-like and metalloprotease domain with thrombospondin motifs
AMD	Age-related macular degeneration
APMA	4-aminophenylmercuric acetate
APS	Ammonium persulfate
BrM	Bruch's membrane
CFH	Complement factor H
CNV	Choroidal neovascularisation
CS	Chondroitin sulfate
DMSO	Dimethyl sulfoxide
DS	Dermatan sulfate
DTT	Dithiothreitol
ECM	Extracellular matrix
ERK	Extracellular signal-regulated kinase
FBS	Foetal bovine serum
FMO	Fluorescence minus one
GAGs	Glycosaminoglycans
GWAS	Genome wide association study
HA	Hyaluronan
hiPSC	Human-induced pluripotent stem cell
HS	Heparan sulfate
HSPG	Heparan sulfate proteoglycan
IFT88	Intraflagellar transport 88
KS	Keratan sulfate
LB	Luria broth
LDLRAD	Low density lipoprotein receptor class A domain containing
LRP1	Low-density lipoprotein receptor-related protein 1
MCP1/CCL2	Macrophage chemoattract protein 1
MEFs	Mouse embryonic fibroblasts
MMPs	Matrix metalloproteinases
PBS	Phosphate buffered saline
PEA	<i>Pseudomonas aeruginosa</i> antigen-selected

POS	Photoreceptor outer segment
RAP	Receptor associated protein
RPE	Retinal pigment epithelial
RT-qPCR	Real time quantitative polymerase chain reaction
SDS	Sodium dodecyl sulfate
SF	Serum-free
SFD	Sorsby fundus dystrophy
sLRP1	Shed low-density lipoprotein receptor-related protein 1
TBS	Tris buffered saline
TCA	Trichloroacetic acid
TEMED	2-amino-2-methyl-1,3-propanediol N,N,N',N'-tetramethylethylenediamine
TGF	Transforming growth factor
TIMP-3	Tissue inhibitor of metalloproteinases 3
TNC	Tris/sodium/calcium assay buffer
TNC-B	TNC-Brij
TNF	Tumour necrosis factor
tPA	Tissue plasminogen activator
Trypsin-EDTA	Trypsin-ethylenediaminetetraacetic acid
VEGF	Vascular endothelial growth factor
VEGFR2	Vascular endothelial growth factor receptor 2
WT	Wild-type

# List of figures

Figure 1.1: SFD causes loss of central vision.....	15
Figure 1.2: Predicted tertiary structure of TIMP-3 showing residues mutated in SFD.....	17
Figure 1.3: Structure of the eye, showing key layers of the retina.....	21
Figure 1.4: Retinal section of a human eye, highlighting the key layers.....	22
Figure 1.5: Summary of the regulatory mechanisms determining TIMP-3 expression.....	52
Figure 1.6: Main domain and motif structures of LRP1. ....	55
Figure 3.1: Agilent QuikChange II XL site-directed mutagenesis protocol (adapted from Agilent product literature).....	94
Figure 3.2: Optimisation of HEK-293 transfection with pCEP4 plasmids encoding Y191C and S204C TIMP-3. ....	96
Figure 3.3: Optimisation of HEK-239 transfection with H181R TIMP-3 pCEP4 plasmid.....	98
Figure 3.4: Isolation and titration of WT TIMP-3 in TNC-B by anti-FLAG affinity chromatography. ....	99
Figure 3.5: Isolation and titration of H181R, Y191C and S204C SFD TIMP-3 in TNC-B by anti-FLAG affinity chromatography.....	101
Figure 3.6: Isolation of E162K TIMP-3 in TNC-B by anti-FLAG affinity chromatography and comparison with WT TIMP-3.....	103
Figure 3.7: Purity of WT, H181R, Y191C and S204C TNC-B elution fractions as detected by silver staining.....	104
Figure 3.8: Isolation of WT, H181R, Y191C and S204C TIMP-3 in SF DMEM by anti-FLAG affinity chromatography. ....	105
Figure 3.9: Reduction and alkylation of isolated WT, H181R, Y191C and S204C TIMP-3 in TNC-B or SF DMEM.....	107
Figure 3.10: Expression, isolation and activation of FLAG-tagged pro-MMP-1...	109
Figure 4.1: Optimisation of ARPE-19 transfection with pCEP4 plasmids encoding WT, Y191C and S204C TIMP-3 with jetPRIME, Lipofectamine 3000, or Lipofectamine LTX transfection reagents.....	121
Figure 4.2: Initial optimisation of ARPE-19 transfection with pCEP4 plasmids encoding WT T3, H181R, Y191C and S204C. ....	123
Figure 4.3: Further optimisation of ARPE-19 transfection with pCEP4 plasmids encoding WT T3, H181R, Y191C and S204C. ....	125

Figure 4.4: Optimised transfection of ARPE-19 cells with pCEP4 plasmids encoding WT, H181R, Y191C and S204C TIMP-3.....	127
Figure 4.5: Transfection of ARPE-19 cells with pCEP4 plasmids encoding WT, H181R, Y191C and S204C TIMP-3 did not change LRP-receptor mRNA expression.....	130
Figure 4.6: Transfection of ARPE-19 cells with pCEP4 plasmids encoding WT, H181R, Y191C and S204C TIMP-3 did not change <i>MMP</i> or <i>ADAM</i> mRNA expression.....	132
Figure 4.7: Transfection of ARPE-19 cells with pCEP4 plasmids encoding WT, H181R, Y191C and S204C TIMP-3 did not change proteoglycan mRNA expression.....	133
Figure 4.8: Transfection of ARPE-19 cells with pCEP4 plasmids encoding WT, H181R, Y191C and S204C TIMP-3 did not change cytokine or oxidative stress gene mRNA expression.....	134
Figure 4.9: Gating strategy and FMO controls for Annexin V and propidium iodide.....	136
Figure 4.10: Treatment of ARPE-19 cells with WT, H181R and S204C TIMP-3 did not induce apoptosis.....	137
Figure 5.1: TNC-B at high volumes caused ARPE-19 cell death, whereas TNC alone did not.....	148
Figure 5.2: TNC-B at high volumes caused hTERT RPE-1 cell death, whereas TNC alone did not.....	150
Figure 5.3: WT TIMP-3 was endocytosed by ARPE-19 cells.....	152
Figure 5.4: H181R TIMP-3 was endocytosed at a similar rate to WT TIMP-3, but endocytosis of Y191C and S204C TIMP-3 by ARPE-19 cells was slower.....	154
Figure 5.5: WT TIMP-3 and H181R TIMP-3 were readily endocytosed by ARPE-19 cells, but endocytosis of Y191C and S204C TIMP-3 was significantly delayed. .	156
Figure 5.6: Higher molecular weight species were not endocytosed by ARPE-19 cells.....	157
Figure 5.7: WT TIMP-3 was endocytosed by hTERT RPE-1 cells.....	158
Figure 5.8: H181R TIMP-3 was endocytosed at a similar rate to WT TIMP-3, but endocytosis of Y191C and S204C TIMP-3 by hTERT RPE-1 cells was slower...	160
Figure 5.9: WT TIMP-3 and H181R TIMP-3 were readily endocytosed by hTERT RPE-1 cells, but endocytosis of Y191C and S204C TIMP-3 was significantly delayed. .	162

Figure 5.10: Conditioned media alone did not cause significant loss of WT, H181R, Y191C and S204C TIMP-3 .....	164
Figure 5.11: WT and H181R TIMP-3 were endocytosed by ARPE-19 cells. ....	166
Figure 5.12: Y191C and S204C TIMP-3 were endocytosed by ARPE-19 cells... ..	167
Figure 5.13: There was no discernible difference in WT and H181R TIMP-3 binding to heparin-Sepharose beads. ....	168
Figure 6.1: LRP1-null PEA-13 cells had reduced uptake of WT TIMP-3 compared to WT MEF cells.....	180
Figure 6.2: Endocytosis of H181R TIMP-3 was not reduced in LRP1-null PEA-13 cells.....	181
Figure 6.3: Y191C and S204C TIMP-3 were endocytosed by LRP1-null PEA-13 and WT MEF cells.....	183
Figure 6.4: LRP1 is expressed by ARPE-19 and hTERT RPE-1 cell lines. ....	184
Figure 6.5: RNAscope analysis of human retinal tissue sections revealed widespread mRNA expression of <i>LRP1</i> and <i>TIMP3</i> . ....	186
Figure 6.6: Addition of RAP to the conditioned medium of ARPE-19 cells resulted in TIMP-3 accumulation in the conditioned medium. ....	187
Figure 6.7: Addition of RAP to the conditioned medium of ARPE-19 and hTERT RPE-1 cells inhibited WT TIMP-3 endocytosis. ....	189
Figure 6.8: RAP inhibited endocytosis of WT TIMP-3, H181R TIMP-3, Y191C TIMP-3 and S204C TIMP-3 by ARPE-19 cells.....	191
Figure 6.9: Expression of <i>LRP1</i> was reduced by ThermoFisher siRNA knockdown, but this had no effect on TIMP-3 uptake by ARPE-19 cells. ....	194
Figure 6.10: Optimisation of Dhamacon siRNA knockdown of <i>LRP1</i> in ARPE-19 cells.....	197
Figure 6.11: Expression of <i>LRP1</i> was reduced by Dhamacon siRNA knockdown and this reduced TIMP-3 uptake by ARPE-19 cells. ....	199
Figure 6.12: Optimisation of Dhamacon siRNA knockdown of <i>LRP1</i> in hTERT RPE-1 cells. ....	202
Figure 6.13: Expression of <i>LRP1</i> in hTERT RPE-1 cells was reduced by Dhamacon siRNA knockdown, but this had no effect on TIMP-3 endocytosis. ..	204
Figure 6.14: ARPE-19 and hTERT RPE-1 cells expressed a range of LRP-related receptors at the mRNA level. ....	206
Figure 7.1: Proposed mechanisms of SFD TIMP-3 accumulation. ....	224

# List of tables

Table 1.1: Mutations in TIMP-3 associated with SFD and their age of onset.....	16
Table 1.2: Proteins components of the humans BrM. ....	25
Table 1.3: Summary of TIMP characteristics. Adapted from (Brew & Nagase, 2010; Murphy, 2011). .....	31
Table 1.4: SFD TIMP-3 variants and their ability to dimerise and inhibit MMPs. ....	41
Table 1.5: SFD TIMP-3 variants and their ability to inhibit angiogenesis and bind to the ECM.....	44
Table 1.6: Glycosylation state of SFD TIMP-3 mutants, their apoptotic activity and other properties.....	50
Table 1.7: Summary of endocytic pathways. Based on (G. J. Doherty & Mcmahon, 2009; Thottacherry et al., 2019).....	59
Table 2.1: General chemicals and their manufacturers. ....	65
Table 2.2: Disposable labware and their manufacturers.....	66
Table 2.3: Cell culture reagents. ....	67
Table 2.4: SDS-PAGE and immunoblotting reagents.....	68
Table 2.5: Antibodies and their applications.....	69
Table 2.6: Molecular biology reagents and their manufacturers. ....	70
Table 2.7: Human KiCqStart primers (purchased from Merck). ....	71
Table 2.8: Forward and reverse primers designed for site-directed mutagenesis of TIMP-3 (purchased from Merck).....	73
Table 2.9: Sequencing primers designed for sequencing the pCEP4 plasmid. ....	73
Table 2.10: Laboratory instruments and their manufacturers. ....	74
Table 2.11: Software. ....	74
Table 2.12: SDS-PAGE and immunoblotting buffer recipes.....	77
Table 2.13: Modified PCR reagent conditions for Agilent QuikChange Site-Directed mutagenesis kit.....	79
Table 2.14: Modified PCR conditions for Agilent QuikChange Site-Directed mutagenesis kit.....	79
Table 2.15: RNAScope buffers.....	89
Table 5.1: Sample number required to detect various differences in the means of endocytosis disappearance assays at a power of 95 %.....	171
Table 6.1: Summary of LRP-dependence of WT, H181R, Y191C and S204C TIMP-3 endocytosis in MEF and RPE cells.....	216

# Acknowledgments

My deepest thanks go to my primary supervisor, Dr Linda Troeberg, for her thorough support and guidance throughout the last 3 years. From capturing my interest in TIMP-3, to drawings of experimental concepts and for laughing and troubleshooting with me when my experiments went wrong, I could not have asked for a better supervisor. This PhD has been a very fulfilling experience and I'm excited to see where you continue to take this work. I would like to express my gratitude to Professor Anthony Day for providing great insight and support, as well as for being so welcoming and kind when I visited Manchester last year. Thanks to Professor Ian Clark, for encouragement and helpful suggestions. I'd also like to thank Dr Sheona Drummond, for performing and capturing the lovely RNAscope images in this thesis.

I gratefully acknowledge the kind support of the Macular Society for this scholarship; this work would not have been possible without their funding.

My wonderful fiancé, Annabel Laver, has been a core of support throughout these past 3 years and has spent many hours producing some of the figures in this thesis. As this PhD chapter closes, I eagerly look forward to our next chapter together as a married couple.

Lastly, I would like to thank my dear parents, Jeremy and Caroline Betts. Thank you for being my biggest champions, I would never have reached this stage without such great parents.

# **Chapter 1: Introduction**

## 1.1 Sorsby Fundus Dystrophy

SFD is an autosomal dominant macular dystrophy that progresses to bilateral central vision loss, making it difficult to recognise faces, read, and perform tasks that rely on central vision (**Figure 1.1**). It was originally identified by Sorsby and Mason who described several families with central vision loss in their early 40s and similar fundal presentation to that observed in patients with age-related macular degeneration (AMD) (Sorsby & Mason, 1949). The prevalence of SFD is not well established, but is estimated to be in the region of 1 in 220 000 (Christensen et al., 2017), with typical onset between the 4<sup>th</sup> and 6<sup>th</sup> decades of life, although this depends on the particular mutation (**Table 1.1**).



**Figure 1.1: SFD causes loss of central vision.**

SFD causes loss of central vision due to invasion of blood vessels into the outer retina and/or atrophy of RPE cells and death of photoreceptors. Figure adapted from National Institutes of Health.

SFD is caused by mutations in the gene encoding for TIMP-3 (Weber et al., 1994a; Weber et al., 1994b). 21 mutations have been reported to cause SFD to date (**Table 1.1 & Figure 1.2**). Mutations were originally named excluding the 23 amino acid signal peptide of TIMP-3, however as proposed by Bakall et al. (2014), SFD mutations are now named to comply with the Human Genome Variation Society, and numbering includes the signal peptide. The first identified SFD mutation was S204C (Weber et al., 1994a) and this has since garnered a considerable amount of research, most likely because it is the most commonly occurring mutation in the UK (Wijesuriya et al., 1996). Most SFD mutations occur in the C-terminal region of TIMP-3 and involve substitution to a cysteine amino acid, but some do not conform to this pattern. For example, L10H and G12R mutations occur in the signal peptide (Guan et al., 2022) and C24R and S38C occur in the N-terminal domain. Also, not all mutations result in the substitution to a cysteine amino acid, e.g., L10H, G12R, C24R, E162K, E162X, H181R, and a mutation within the splice acceptor site between intron 4 and exon 5. It is important to note that although the E162X mutation doesn't involve an amino acid substitution, this truncation does still give rise to an unpaired cysteine residue. Interestingly, some patients diagnosed with other macular dystrophies (e.g., retinitis pigmentosa in a father and son, and neovascular

AMD in an unrelated male and 2 unrelated females) have been found to carry mutations in TIMP-3 (DeBenedictis et al., 2020; Warwick et al., 2016). It is unclear whether these patients have undiagnosed SFD or whether TIMP-3 mutations contribute to other retinal pathologies.

**Table 1.1: Mutations in TIMP-3 associated with SFD and their age of onset.**

Mutation	Mutation (without signal peptide)	Age of Onset (years)	Original Publication
Leu10His & Gly12Arg	N/A	Early (2 <sup>nd</sup> Decade)	(Guan et al., 2022)
Cys24Arg	Cys1Arg	Early	(Bakall et al., 2014)
Ser38Cys	Ser15Cys	40-50	(Schoenberger & Agarwal, 2013)
Intron 4/Exon 5 Splice Site	Intron4/Exon 5 Splice Site	50-80	(Tabata et al., 1998)
Ser149Cys	Ser126Cys	30-50	(L. Huang et al., 2021)
Tyr151Cys	Tyr128Cys	Early	(Bakall et al., 2014)
Glu162Lys	Glu139Lys	30-50	(Saihan et al., 2009)
Glu162STOP	Glu139STOP	20-40	(Langton et al., 2000)
Tyr174Cys	Tyr151Cys	30-40	(Gliem et al., 2015)
Tyr177Cys	Tyr154Cys	50-60	(Gliem et al., 2015)
Ser179Cys	Ser156Cys	20-30	(Felbor et al., 1995)
His181Arg	His158Arg	50-70	(Lin et al., 2006)
Tyr182Cys	Tyr159Cys	50-60	(Fung et al., 2013)
Gly189Cys	Gly166Cys	20-40	(Felbor et al., 1997)
Gly190Cys	Gly167Cys	30-40	(Jacobson et al., 1995)
Tyr191Cys	Tyr168Cys	30-40	(Felbor et al., 1996)
Ser193Cys	Ser170Cys	30-40	(Barbazetto et al., 2005)
Tyr195Cys	Tyr172Cys	20-40	(Jacobson et al., 2002)
Trp198Cys	Trp175Cys	Early	(Bakall et al., 2014)
Ser204Cys	Ser181Cys	30-60	(Weber et al., 1994a)

SFD shares clinical and pathological characteristics with AMD (Gourier & Chong, 2015), with a key hallmark of both being a thickening of the BrM and the build-up of yellow drusen deposits in the retinal extracellular matrix (ECM), the BrM. Drusen are composed of large amounts of lipid and accumulated protein, and in the case of SFD, this protein is accumulated mutant TIMP-3 (Chong et al., 2000; Fariss et al., 1998). TIMP-3 accumulation is also associated with other retinal dystrophies, including AMD and Retinitis Pigmentosa (Fariss et al., 1998; Jones et al., 1994; Kamei & Hollyfield, 1999). Interestingly, fibulin-3, a binding partner of TIMP-3 (Klenotic et al., 2004), accumulates in Malattia Leventinese (Marmorstein et al., 2002), also implicating a role for TIMP-3 in this macular degenerative disease. Retinal cells that express TIMP-3 include the RPE cells (Della et al., 1996) and the choroidal endothelial cells (Vranka et al., 1997); both cell types enclose and are adjacent to the BrM (**Figure 1.3 & Figure 1.4**). The existing body of literature focuses predominantly on RPE cells, however choroidal endothelial cells are also an important source of TIMP-3 and novel human choroidal endothelial cell lines

have been developed (Loeven et al., 2018) that could be used to study their role in SFD.

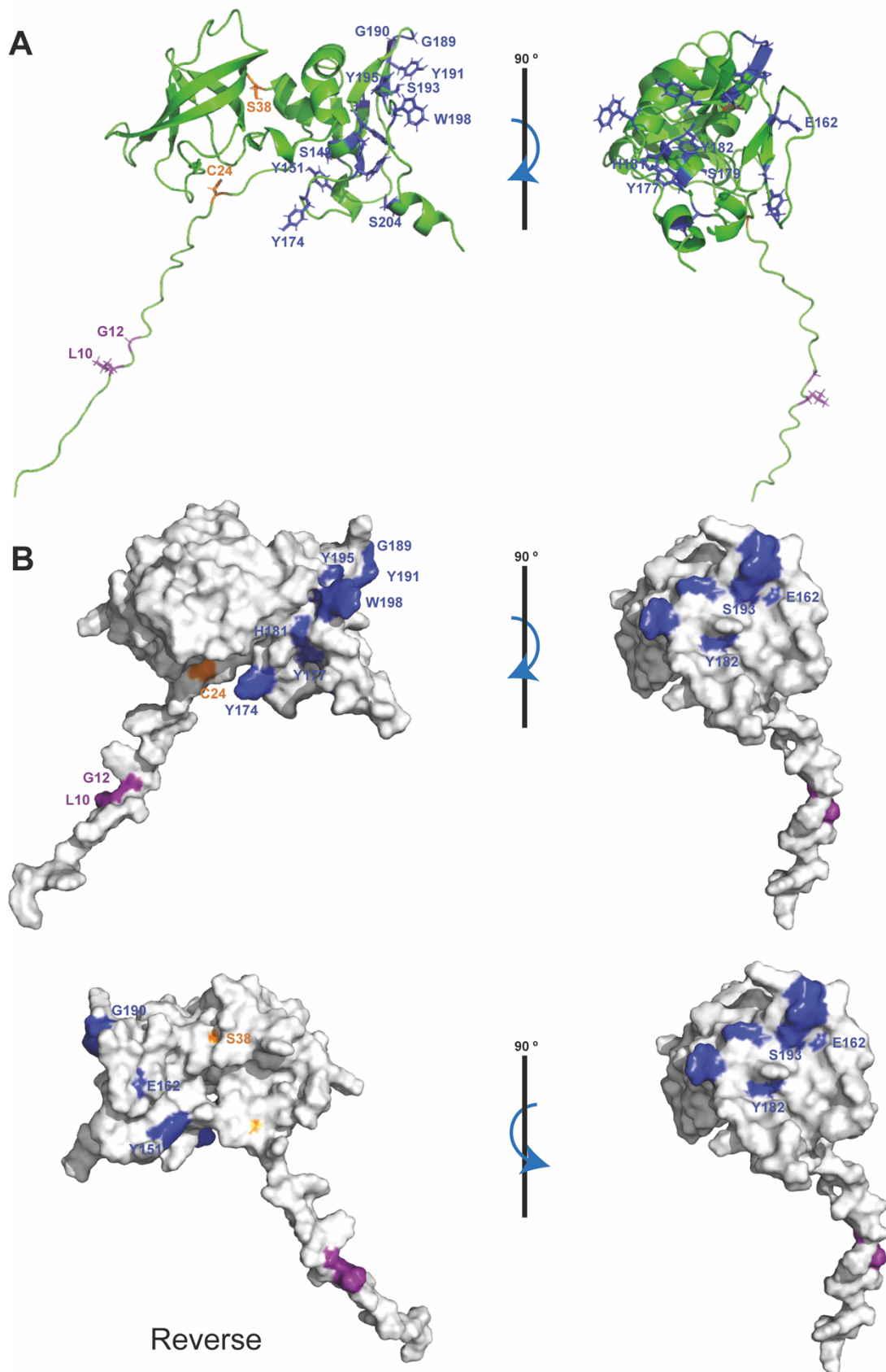


**Figure 1.2: Predicted tertiary structure of TIMP-3 showing residues mutated in SFD.**  
 A model of human TIMP-3 was generated in AlphaFold and analysed in PyMOL. SFD mutations in the signal peptide are coloured in purple, those in the N-terminal domain are in orange, and those in the C-terminal region are blue. **(A)** The ribbon structure of TIMP-3. **(B)** Surface residues mutated in SFD. Obtained from Betts and Troeberg (2024).

Progressive SFD manifests as two forms: either choroidal neovascularisation (CNV), where leakage from new vessels developing from the choroid and invading the outer retina causes acute visual loss, or progressive loss of central vision that occurs as a result of RPE atrophy and death of the photoreceptors they support (Betts & Troeberg, 2024). This mirrors AMD, which also presents in 'wet' CNV and 'dry' RPE atrophy forms. Vitamin A was initially used as a treatment for SFD, but only targeted a common presenting symptom of SFD, night blindness (Jacobson et al., 1995), not experienced by all patients. In previous decades there was a poor outlook for SFD patients with CNV, with photodynamic therapy or argon and krypton laser photocoagulation being available options but having limited effectiveness and CNV often recurring (Peiretti et al., 2005; Sivaprasad et al., 2008; S. C. Wong et al., 2003). The introduction of anti-vascular endothelial growth factor (VEGF) therapy in the 2000s for CNV treatment considerably improved the visual prognosis for SFD patients (Balaskas et al., 2012; Gemenetzi et al., 2011; Gray et al., 2012; Kapoor & Bakri, 2013). For SFD patients with RPE atrophy, there are currently no treatments or cure available in the UK, but there are many ongoing clinical trials (Cabral De Guimaraes et al., 2022). In February 2023, pegcetacoplan, a complement C3 inhibitor was approved by the Food and Drug Administration in the US, for treatment of dry AMD. Given that dry AMD is similar in presentation to RPE atrophy in SFD (Gourier & Chong, 2015), it seems possible that this treatment could be adopted for SFD. However, a clear link has been established between complement system dysregulation in AMD (Gehrs et al., 2010; Whitmore et al., 2015), and this is not known for SFD, although inflammation is suggested to occur. More recent studies have suggested that base editing could modify the mutated TIMP-3 allele to restore expression of WT TIMP-3 (Elsayed et al., 2022). For those mutations where base editors cannot correct the sequence to code for the correct amino acid, it has been suggested that an alternative base could be introduced that would generate a mutation in TIMP-3 that would be 'more well tolerated' compared to the SFD mutation (Elsayed et al., 2022).

## 1.2 Similarities between SFD and other retinal dystrophies

### 1.2.1 Age-related macular degeneration

AMD is the leading cause of irreversible sight loss in the Western world (Wong et al., 2014), affecting more than 600 000 people in the UK alone (“Age-related macular degeneration - Macular Society,”). Due to the increasing ageing population, the prevalence of AMD is expected to rise, with projections that ~288 million people globally will suffer from AMD by 2040 (Wong et al., 2014).

AMD shares many similarities with SFD in terms of clinical and pathological presentation (Gourier & Chong, 2015), although AMD occurs considerably later than SFD, often affecting those over 60 years of age (Fleckenstein et al., 2024). Both result in progressive loss of central vision and late-stage disease is characterised by atrophy of RPEs and photoreceptors and/or invasion and subsequent leakage of immature blood vessels in the outer retina. Key pathological features include a vast thickening of the BrM, and also deposition of lipid- and protein-filled deposits called drusen. Drusen formation typically occurs with age and generally drusen are small and found in the periphery of the retina where they don't affect visual function, however in AMD and SFD drusen form in the macula and have detrimental effects on visual function (Booij et al., 2010). Drusen are composed mainly of lipids such as esterified and unesterified cholesterol, but also contain accumulated proteins, which in the case of AMD includes a plethora of proteins, including vitronectin, TIMP-3, complement factor H (CFH), complement components C3 and C8 and crystallins (Crabb et al., 2002). Interestingly, many of these accumulated proteins, including TIMP-3 and CFH are known to bind HS (Keenan et al., 2014; Troeberg et al., 2014).

AMD has a much more complex aetiology than SFD, involving interactions between ageing, environmental and genetic risk factors (Fleckenstein et al., 2024). Ageing is the biggest risk factor, with onset typically occurring over the age of 55 (Ferris et al., 2013). A range of environmental risk factors are associated with AMD, including smoking, diet and low physical activity, and there is also a strong genetic component to AMD, with a large-scale genome wide association study (GWAS) identifying 52 single nucleotide polymorphisms at 34 loci associated with advanced AMD (Fritsche et al., 2015). This GWAS implicated genes with roles in inflammation and immunity, lipid metabolism and ECM homeostasis as conferring increased risk for AMD. One

such variation was in the *TIMP3* gene (Fritsche et al., 2015), as suggested by other investigators (Chen et al., 2010; Kaur et al., 2010), despite *TIMP3* historically being excluded from AMD risk genes (De La Paz et al., 1997). Polymorphisms in the *CFH* gene have been strongly implicated as important risk factors for AMD, with the Y402H polymorphism best characterised (Edwards et al., 2005; Hageman et al., 2005; Klein et al., 2005).

### 1.2.2 Other retinal diseases

SFD also has similarities with other retinal diseases such as Malattia Leventinese, Best Disease and Stargardt disease. These are all caused by mutations in a single gene and affect the macula, a specialised retinal area described in **1.3**. Malattia Leventinese is caused by mutations in *EFEMP1* that encodes fibulin-3, a binding partner of TIMP-3 (Klenotic et al., 2004) that also accumulates extracellularly in the BrM (Marmorstein et al., 2002). Best disease is caused by mutations in *BEST1* which encodes for bestrophin (Petrukhin et al., 1998), a transmembrane chloride channel that can regulate other ion channels and ion gradients (Johnson et al., 2017). Finally, Stargardt disease arises from mutations in *ABCA4*, encoding a membrane-bound transporter protein that processes accumulated retinoids during visual pigment metabolism (Tanna et al., 2017).

## 1.3 Structure of the retina

The retina is composed of a series of cell layers that enable vision (**Figure 1.3 & Figure 1.4**), including a layer of light-sensing photoreceptors and underlying pigmented RPE cells. Light is detected and processed by the photoreceptors (part of the outer retina), these are the rods and cones. Rods are important for dark-adapted, lower acuity vision, whereas cones provide higher visual acuity and colour vision (Lamb, 2015). In humans, the macula is a specialised central region in the retina with a dense concentration of cones (Lamb, 2015), providing high visual acuity upon which humans heavily rely. Other cells in the retina include bipolar, ganglion, horizontal and amacrine cells, which aid in processing visual signals from the photoreceptors to the optic nerve. These cells are supported by glial cells such as astrocytes, microglia and Müller glia cells (Mahabadi & Khalili, 2023).

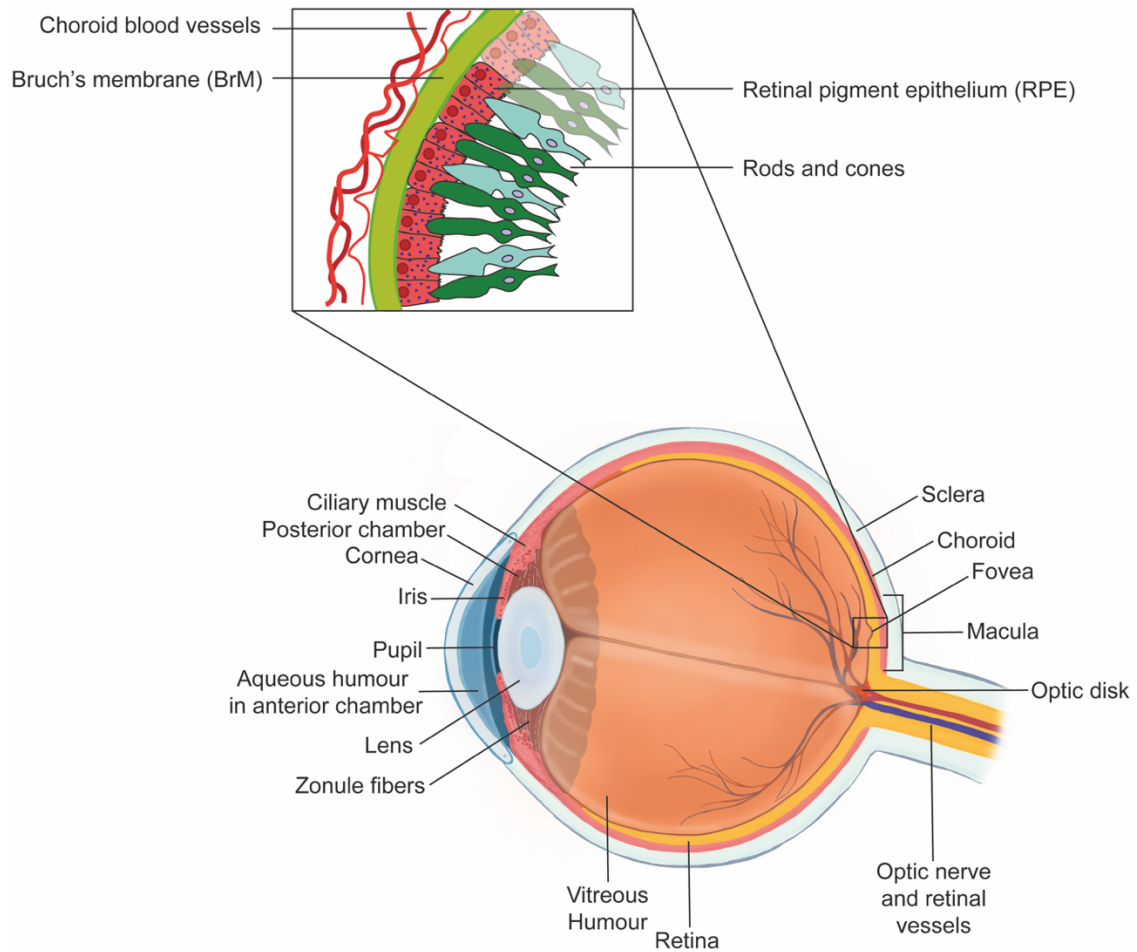


**Figure 1.3: Structure of the eye, showing key layers of the retina.**

Photoreceptors (rods and cones) in the retina are responsible for detecting light. They are nourished by a single underlying layer of RPE cells, which provide nutrients and removes waste to and from the photoreceptors. Below the RPE is a specialised ECM, the BrM and an underlying blood supply, the choroid. The BrM greatly thickens with age and in SFD and AMD, increasing diffusion distance between the choroid and the RPE. The ageing and disease state BrM contains drusen deposits composed of accumulated protein and lipid. Figure adapted from Betts and Troeberg (2024).

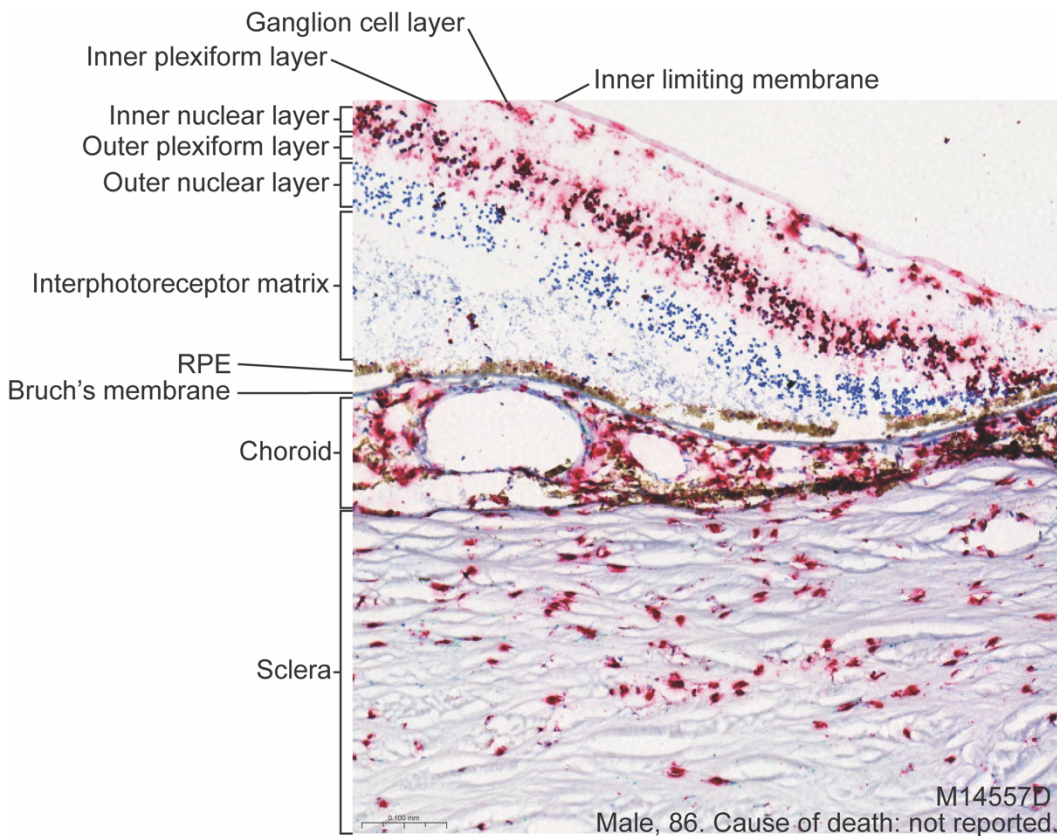


**Figure 1.4: Retinal section of a human eye, highlighting the key layers.**

The human retina is organised into distinct layers with cell bodies and nuclei. The RPE sits upon a basement membrane, the BrM, under which lies the choroidal vasculature supply. The apical microvilli of the RPE interdigitate with the photoreceptor outer segments. Retinal section taken from an 86-year-old male, with no reported retinal pathology and no cause of death reported. Scale bar represents 0.1 mm.

### 1.3.1 RPE cells

Photoreceptors are nourished by the RPE, a single polarised epithelial layer that sits under them. The RPE mediate bi-directional transport of nutrients to and waste from the photoreceptors. RPE cells are generally considered post-mitotic, thus their loss or damage in various retinal diseases described above is severely detrimental, however under certain pathological conditions, such as choroidal tumour growth or following retinal detachment, they have been reported to proliferate (Stern & Temple, 2015).

The RPE also fulfils many other functions including absorption of light, phagocytosis of photoreceptor outer segments (POS), protection against oxidative stress, distribution of electrical potential, and polar secretion of growth factors and proteins as reviewed elsewhere (Sparrow et al., 2010; Yang et al., 2021). RPE cells contain the pigment melanin (Tian et al., 2021), which allows them to absorb excess light entering the eye to prevent damage. The high amount of light entering the eye, places the retina under a high state of photo-oxidation, resulting in the generation

of free oxygen radicals. To combat this, RPE cells contain antioxidants such as superoxide dismutase and glutathione, as well as melanosomes that collect free oxygen radicals (Maurya et al., 2023).

RPE cells participate in the phagocytosis of photoreceptor outer segments, with each RPE cell being responsible for ~ 30 photoreceptors (Yang et al., 2021). Several RPE proteins are critical for this phagocytic function, including the receptor tyrosine kinase, MerTK, as well as  $\alpha\beta 5$  integrin. POS present phosphatidylserine on their membranes, acting as a phagocytic signal, which RPEs bind to via an  $\alpha\beta 5$  integrin (Yu et al., 2019) expressed on their apical membrane.

### **1.3.2 The Bruch's membrane**

The BrM is a specialised ECM located between the RPE and choroidal blood supply that was originally identified by Carl Ludwig Wilhelm Bruch in the middle of the 19<sup>th</sup> century and has since been defined as a 5 pentalaminar ECM (Booij et al., 2010). The BrM is present throughout the whole retina but there is evidence that there are structural and molecular differences between the BrM in the macula and the peripheral retina, with a thinner elastin layer (Chong et al., 2005) and a reduced expression of structural proteins such as collagens in the macula BrM (van Soest et al., 2007). BrM structure is known to change with age, genetics, environment and disease (Curcio and Johnson, 2012) as discussed below.

#### **1.3.2.1 Bruch's membrane function**

Arguably the most important role of the BrM is to act as a semi-permeable barrier to facilitate the exchange of biomolecules, fluid, oxygen and waste products between the RPE and the choroidal blood supply. Transport of biomolecules is primarily mediated by diffusion via passive processes, which are dependent on the hydrostatic pressure either side of the BrM in conjunction with the concentration of certain biomolecules and ions (Booij et al., 2010). Biologically important molecules passing from the choroid to the RPE through the BrM include nutrients, lipids, pigment precursors, vitamin A, oxygen, minerals, antioxidants, trace elements and serum components (Booij et al., 2010). These are taken up by the RPE or can bind and accumulate in the BrM. Biologically important molecules passing from the RPE to the choroid include carbon dioxide, water, ions, oxidised lipids and other waste products from the RPE. Lipoprotein particles function to transport vitamins, signalling molecules and other molecules required by photoreceptors, to and from the RPE by passing through the BrM (Curcio & Johnson, 2012). Due to the high

phagocytic capacity of the RPE (Kwon & Freeman, 2020; Mazzoni et al., 2014), they generate large amounts of metabolic waste, including partly digested/oxidised fragments of photoreceptor outer segments, as well as waste from the visual cycle which are transported across the BrM to the circulation.

The BrM is also critical for adhesion of RPE cells and facilitation of RPE differentiation. RPE cells attach to the BrM via integrin cell surface receptors, including integrin alpha subunits 1-6 and beta subunits 1 and 4 (Fang et al., 2009; Li et al., 2009; Zarbin, 2003) and overexpression of integrins in RPE cells has been shown to increase RPE adhesion to the BrM (Fang et al., 2009).

Together with tight junctions between RPE cells, the BrM is important for forming the outer blood-retina barrier (Booij et al., 2010), which prevents the transport of molecules larger than 300 kDa into the retina. The BrM also aids in the formation of the inner blood-retina barrier alongside retinal vascular endothelial cells. This inner barrier is generally thought to block the crossing of leukocytes (Booij et al., 2010), however leukocytes have been detected in the retina, when they become activated or under inflammatory conditions (Crane & Liversidge, 2008; Prendergast et al., 1998).

### 1.3.2.2 Bruch's membrane structure

Hogan and colleagues in the 1960s classified the BrM into 5 distinguishable layers based on their histological features (Hogan, 1961; Hogan & Alvarado, 1967). These layers are:

- 1) the basement membrane of the RPE,
- 2) the inner collagenous layer,
- 3) the elastin layer,
- 4) the outer collagenous layer, and
- 5) the basement membrane of the choroid.

Each of these layers contains specialised components, including types of collagens, laminins, glycosaminoglycans (GAGs) and proteoglycans, as well as other structural ECM proteins and regulatory proteins such as TIMP-3 (**Table 1.2**), as discussed in more detail below.

**Table 1.2: Proteins components of the humans BrM.**

Based on Booij et al. (2010) and Curcio and Johnson (2012).

Bruch's membrane layer	Composition
<b>RPE basement membrane</b>	Collagen IV & V, laminins 1, 5, 10 & 11, fibulins, HSPGs (including perlecan, agrin, collagen XVIII), CSPGs, nidogen-1
<b>Inner collagenous layer</b>	Collagen I, III & V, fibronectin, fibulins, HSPGs, CSPGs, dermatan sulfate, clusterin, vitronectin
<b>Elastin layer</b>	Elastin, collagen IV, VI, XVIII, fibronectin, fibulins, HSPGs, TIMP-3
<b>Outer collagenous layer</b>	Collagen I, III, IV, V & VI, fibronectin, fibulin-5, HSPGs, CSPGs, dermatan sulfate, clusterin
<b>Choroidal basement membrane</b>	Collagen IV & V, laminins, fibulins, HSPGs (including perlecan, agrin, collagen XVIII), CSPGs, endostatin

### 1.3.2.2.1 Collagens

There are 28 different types of collagens and they are the major insoluble fibrous protein of the ECM. The rope-like structure of collagens gives them tensile strength and enables collagens to function primarily to provide support and stability, as well as being binding partners for other proteins in the ECM. Furthermore, some collagens (e.g., type I, II, III collagen) can assemble into polymers called fibrils, which provide greater structural integrity for tissues and allow them to withstand mechanical stress such as shear and compression. Other collagens of interest are collagens IV, VII, XV, XVII and XIX, which are components of basement membranes (Karamanos et al., 2021) and are found in the RPE and choroidal basement membranes of the BrM.

### 1.3.2.2.2 Laminins

Laminin is an important component of basement membranes, with more than 16 members of the laminin family identified (Karamanos et al., 2021). Laminins are made of 3 polypeptide chains ( $\alpha$ ,  $\beta$ ,  $\gamma$ ) that are disulfide-bonded. Laminins are distributed based on cell and tissue type, for example, laminin-332 is found in the basement membrane of epithelial cells such as RPE cells (Rousselle & Beck, 2013), whereas laminin-411 is found in the basement membrane of vasculature such as the choroidal endothelium (Hall et al., 2022; Thyboll et al., 2002).

### 1.3.2.2.3 Glycosaminoglycans and proteoglycans

GAGs are unbranched polymers of repeated disaccharides. The disaccharide repeat is composed of an amino sugar that is usually sulfated (*N*-acetylglucosamine or *N*-acetylgalactosamine) and a second sugar that is a uronic (i.e., glucuronic or iduronic) acid. GAGs are highly negatively charged due to the presence of sulfate and carboxyl groups and as a consequence of this GAGs attract cations and retain

large amounts of water, which provides mechanical support to the ECM and enables it to withstand compression. There are 4 main groups of ECM GAGs: hyaluronan (HA), chondroitin and dermatan sulfate (CS and DS, respectively), HS and keratan sulfate (KS). Interestingly, hyaluronan is the only GAG that is entirely non-sulfated and is not covalently linked to a core protein. The distribution of GAGs throughout the retina has been profiled, with CS, DS, HA and HS being present in the BrM (Clark et al., 2011).

A GAG of particular interest is HS, which can be O-sulfated at the second carbon of the glucuronic acid by heparan sulfate 2-O-transferases, the sixth carbon of the N-acetylglucosamine by heparan sulfate 6-O-transferases 1-3, the third carbon of the N-acetylglucosamine by heparan sulfate 3-O-transferases 1-5, and lastly N-deacetylated and N-sulfated on N-acetylglucosamine by N-deacetylase/N-sulfotransferase 1-4 (Annaval et al., 2020). This provides HS with a very high binding capacity, with reports that HS can bind over 400 ligands (Ori et al., 2011; Vallet et al., 2022), including TIMP-3 (Lee et al., 2007; Yu et al., 2000). Exogenous heparin, a highly sulfated form of HS synthesised by mast cells, has been observed to block LRP1-mediated endocytosis of TIMP-3 (Scilabre et al., 2013), as has exogenously added HS (Troeberg et al., 2014). Interestingly, binding of TIMP-3 to HS was observed to increase TIMP-3 affinity for a disintegrin-like and metalloprotease domain with thrombospondin motifs (ADAMTS)-5 by 1000-fold (Troeberg et al., 2014), demonstrating that HS can bind ligands and modulate their endocytosis and biological activity. Additionally, HS can protect ligands from proteolysis, promote ligand interactions with their receptors or even prevent ligand-receptor interactions (Sarrazin et al., 2011).

In nature, GAG chains (except hyaluronan) exist covalently attached to a core protein to form proteoglycans. Due to the highly variable numbers, types and sulfation of attached GAG chains, proteoglycans can have an almost limitless potential of heterogeneity and potential information content. Proteoglycans are involved in mechanical resistance, hydration of tissues, sequestering growth factors, organisation of the ECM, and acting as co-receptors to initiate signalling cascades that govern cell growth and behaviour. Proteoglycans are involved in physiological processes such as tissue repair, wound healing and development, as well as pathological states such as osteoarthritis and cancer (Frantz et al., 2010; Karamanos et al., 2021).

The distribution of proteoglycan core proteins throughout the retina has been profiled with perlecan, agrin, collagen XVIII, versican, aggrecan and small leucine-rich repeat family members being present in the BrM (Keenan et al., 2012). Of particular abundance in the BrM is HS and heparan sulfate proteoglycans (HSPGs), including perlecan, agrin and collagen XVII, which are capable of binding to TIMP-3 (Troeberg et al., 2014), however their relative contributions as ECM reservoirs of TIMP-3 in the retina are unknown.

HSPGs are also known to be expressed on the RPE cell surface (Clark et al., 2011; Keenan et al., 2012). Interestingly, HSPGs have been identified as a key cell surface receptor for adeno-associated virus type 2 virions (Summerford & Samulski, 1998), with this virus manipulated as a vector to deliver *RPE65* (Bainbridge et al., 2008) and *REP1* (MacLaren et al., 2014) genes to treat patients with Leber congenital amaurosis and choroideremia, respectively.

#### 1.3.2.2.4 *Elastin*

Elastic fibres are comprised of two morphologically distinguishable components, including cross-linked elastin cores and fibrillin-based microfibrils. In mature form, elastin is highly hydrophobic, insoluble and also extremely resistant to proteolysis, thus providing tissues with the ability to stretch and recoil (Karamanos et al., 2021). As mentioned above, the elastin layer of the BrM in the macula is significantly thinner than that found in the periphery of the retina.

#### 1.3.2.3 Ageing changes to the Bruch's membrane

As in other tissues, there is a fine line between changes associated with 'normal' ageing and those associated with pathology of the BrM, with the distinction not clearly established. This section examines what are considered typical ageing changes in the BrM, including lipid accumulation, BrM thickening and changes in ECM composition.

The predominant change in the BrM associated with ageing is a substantial accumulation of lipids. Oil red O-binding and other studies revealed the accumulation of phospholipids, triglycerides, fatty acids and cholesterol, mainly in an esterified form (Pauleikhoff et al., 1990). These esterified cholesterol-rich deposits are ~7 fold more abundant in the macula than the peripheral retina (Curcio and Johnson, 2012; Holz et al., 1994). Round lipoprotein particles, between 60 –

100 nm in size, are first observed in the fibrils of the elastic layer of the BrM and progressively accumulate in the inner and outer collagenous layers of the BrM in late adulthood (Huang et al., 2008). Eventually, lipid deposits build-up in the space between the inner collagenous layer and the RPE basement membrane, disrupting anchoring of the RPE basement membrane to collagen fibrils (Curcio & Johnson, 2012).

Another prominent change is an overall thickening of the BrM by 2- to 3-fold (Booij et al., 2010) due to changes in ECM composition. For example, HSPGs have been reported to increase in size, with a tendency towards higher molecular weights (Hewitt et al., 1989). Keenan et al. (2014) reported a decrease in HS sulfation with age and a decrease in overall HS with a concurrent rise in heparanase-1 levels. A decrease in overall HS and HS sulfation is likely to have significant ramifications on the presence of HS-binding proteins, including growth factors, cytokines, complement factors, matrix metalloproteinases (MMPs) and TIMP-3, given that HS is known to bind over 400 ligands (Ori et al., 2011; Vallet et al., 2022). Furthermore, abundance of ECM modulators in the BrM changes with age. Abundance of TIMP-3 in the BrM increases with age (Kamei & Hollyfield, 1999), impairing ECM turnover. Given that TIMP-3 is also known to inhibit angiogenesis (Anand-Apte et al., 1997; Qi et al., 2003), this increase may reduce blood vessel proliferation in the BrM from the underlying choroid. Both increased (García-Onrubia et al., 2020) and decreased (Hussain et al., 2011) abundance of MMPs in the BrM with age has been reported, but there is general agreement that normal maintenance and turnover of the BrM is severely disrupted with age. Other ECM changes with age include an increase in collagen cross-linking, which results in decreased elasticity and turnover of the BrM (Booij et al., 2010). There is the deposition of various metal ions in BrM over time, including calcium, iron, and zinc, which are likely to decrease elasticity of the BrM, cause damage via oxidative stress and contribute to oligomerisation of CFH thereby impacting regulation of the complement cascade (Booij et al., 2010). Lastly, advanced glycation end products and age-related lipoperoxidation end products accumulate in the BrM over time and contribute to improper functioning and damage to the BrM.

Overall, age reduces the functional efficiency of the BrM, in terms of its elasticity and most importantly its bidirectional transport of water and biomolecules between the RPE and choroid, ultimately impairing vision.

#### 1.3.2.4 Bruch's membrane in disease

AMD is the classical disease discussed when considered the BrM in pathology. In AMD, extracellular lesions occur in the BrM, including formation of drusen and basal deposits between the RPE basement membrane and the inner collagenous layer. Basal deposits and drusen contain accumulated lipids and proteins that affect the RPE and photoreceptors by impairing transport mechanisms, causing inflammation and contributing towards CNV (Curcio and Johnson, 2012).

Drusen are yellow-white deposits 30-300  $\mu\text{m}$  in diameter that initially appear in the macular area, but are also present in the peripheral retina, where ultimately they are more abundant (Lengyel et al., 2004; Rudolf et al., 2008). Due to their wide variety, drusen are classified based on their size, location and shape to distinguish natural ageing processes from disease. Formation of drusen is considered a normal part of the ageing process (Ardeljan & Chan, 2013), but formation of soft drusen, which have more confluent borders is a clinical indicator of pathology, and highly associated with AMD progression (de Jong, 2006). Drusen are composed primarily of lipids, containing esterified and unesterified cholesterol and also phosphatidylcholine, other phospholipids and ceramide. They are also rich in apolipoproteins, including apolipoprotein B, likely to be sourced from RPE cells. Other components of drusen include proteins such as vitronectin, TIMP-3, complement factor H, complement components C3 and C8, crystallins and zinc (Booij et al., 2010), along with RPE-derived lipofuscin, melanin and amyloid assemblies. A novel proteomic approach performed by Crabb et al. (2002) identified over 120 additional proteins in drusen, including TIMP-3, as well as oxidatively modified proteins (Crabb et al., 2002). Drusen and basal deposits are also found in other macular dystrophies, including SFD and Malattia Leventinese (Galloway et al., 2017), demonstrating that lipid and protein accumulation in the BrM is a shared feature of multiple visual disorders. Drusen have been likened to atherosclerotic lesions and Alzheimer's plaques, although they share relatively few proteins in common (Booij et al., 2010).

Altered regulation of complement and inflammatory and immune responses in the BrM also contribute to retinal pathology. Mutations in CFH have been well documented, leading to increased activation of the complement system (Edwards et al., 2005; Hageman et al., 2005; Klein et al., 2005). Furthermore, changes in proteoglycan and GAG content (Booij et al., 2010; Hewitt et al., 1989), as well as

changes in GAG sulfation in the BrM (Keenan et al., 2014) have been shown to reduce the number of binding sites for CFH and reduce binding of genetic variants of CFH to the BrM, impairing complement regulation (Keenan et al., 2014). Immune cells such as macrophages and lymphocytes have been observed in the retina (Booij et al., 2010) and are thought to play a role in breakdown of the BrM and neovascularisation in AMD (Penfold et al., 1985). It has been suggested that modified lipofuscin in RPE cells acts as a non-self-antigen to trigger immune responses, and amyloid beta in drusen (Crabb et al., 2002) has been shown to activate complement components and invoke inflammation (Johnson et al., 2002; Wang et al., 2008).

Lastly, CNV is an important feature of many retinal diseases, in which blood vessels sprout and proliferate from the underlying choroid and break through and invade the BrM where they leak fluid. RPE cells release several pro-angiogenic factors, including VEGF and pigment epithelium derived factor, which facilitate blood vessel growth (Booij et al., 2010). Furthermore, macrophages have been implicated in the proliferation of new blood vessels in neovascular diseases (Zhou et al., 2017).

## 1.4 The TIMP family

SFD is caused by mutations in the *TIMP3* gene that encodes for the TIMP-3 protein, a key inhibitor of the metalloproteinase family of proteolytic enzymes. There are 21 mutations currently associated with SFD that are described in more detail in 1.5, although this list continues to grow (Vergaro et al., 2024).

There are four members of the mammalian TIMP family which were initially classified based on their ability to inhibit MMPs, but they can also inhibit other metalloproteinases including ADAMs (a disintegrin and metalloprotease) and ADAMTSs, although to varying degrees (Brew & Nagase, 2010) (**Table 1.3**).

**Table 1.3: Summary of TIMP characteristics. Adapted from (Brew & Nagase, 2010; Murphy, 2011).**

Property	TIMP-1	TIMP-2	TIMP-3	TIMP-4
Amino acid residues (mature protein sequence)	184	194	188	194
Protein localisation	Soluble/cell surface	Soluble/cell surface	Extracellular matrix/cell surface	Soluble/cell surface
Glycosylation	Yes (2 N-glycosylation sites)	No	Partial (1 N-glycosylation site)	No
MMP inhibition	Weak for MMP-14, -16, -19 and -24.	All	All	Most
Other metalloproteinase inhibition	For example, ADAM10	For example, ADAM12	Most ADAMs and ADAMTSs, e.g., ADAM10, 12, 17, 28 and 33 ADAMTS-1, -4, and -5 ADAMTS-2 (weak)	For example, ADAM17 and 28 ADAM33 (weak)
Pro-MMP interactions	Pro-MMP-9	Pro-MMP-2	Pro-MMP-2 and pro-MMP-9	Pro-MMP-2
Other binding partners	CD36 and LRP1/MMP-9	$\alpha 3\beta 1$ integrin and LRP1	EFEMP1, AngIIIR, VEGFR and LRP1	Not known
Apoptotic effects	Negative	Positive Negative	Positive Negative	Not known
Cell proliferation	Promotes	Promotes Inhibits	Promotes	Promotes Inhibits
Angiogenesis	Inhibits	Inhibits	Inhibits	Inhibits
Genetic defects	Implicated in retinal atrophy	Idiopathic scoliosis	SFD	Kawasaki disease

### **1.4.1 Inhibition of metalloproteinases**

TIMPs are known to inhibit metalloproteinases including MMPs, ADAMs and ADAMTs. These metalloproteinases and those particularly relevant in the retina are described below.

#### **1.4.1.1 MMPs**

Matrix metalloproteinases are calcium- and zinc-dependent endopeptidases that belong to the superfamily of metzincin proteases and are involved primarily in ECM turnover and matrix remodelling (Cabral-Pacheco et al., 2020; de Almeida et al., 2022; Nagase et al., 2006). There are 23 different MMPs found in humans, the structure of which is reviewed elsewhere (Nagase et al., 2006). MMPs have a diverse array of substrates including collagen and non-collagen ECM substrates, as well as non-ECM substrates. MMPs are regulated at multiple levels (Löffek et al., 2011), including transcriptional, activation and localisation, and by endogenous inhibitors comprising  $\alpha_2$ -macroglobulin and TIMP-1-4. Most MMPs are inhibited by all TIMPs, with the exception of TIMP-1 not inhibiting some of the membrane type-MMPs.

MMPs have important roles in ECM degradation and turnover, and are also involved in releasing cytokines and growth factors, regulating cell adhesion, migration and proliferation and so contributing to physiological processes like wound healing, bone development, angiogenesis and immunity (Löffek et al., 2011; Nagase et al., 2006). MMPs known to be expressed in the retina include MMP-1, MMP-2, MMP-3, MMP-9 and MMP-14 (Alexander et al., 1990; Caban et al., 2022; De Groef et al., 2015; Guo et al., 1999; Hunt et al., 1993; Singh & Tyagi, 2017). Changes in the abundance of MMPs in the BrM with age have been reported (García-Onrubia et al., 2020; Guo et al., 1999).

#### **1.4.1.2 ADAMs and ADAMTs**

ADAMs are involved in cleaving transmembrane ectodomains which results in the release of adhesion molecules, endocytic receptors, growth factor receptors and cytokines, leading to the term ‘shedases’ being coined to describe the proteolytically active ADAMs (Reiss & Saftig, 2009). The roles of proteolytically inactive ADAMs (e.g., ADAM1, ADAM2, ADAM3, ADAM5, ADAM6, ADAM7, ADAM11, ADAM18, ADAM22, ADAM23, ADAM29, ADAM32) are less well understood, apart from some (e.g., ADAM1, ADAM2, ADAM7, ADAM11, ADAM23,

ADAM29) which are involved in cell-cell fusion, cell adhesion and cell signalling through their intracellular domains. Physiologically, ADAMs are implicated in spermatogenesis, sperm-egg fusion, heart development, neurogenesis and morphogenesis in tissues such as the pancreas, lungs and kidneys. ADAMs have also been implicated in pathology, including diseases such as cancer, asthma, chronic inflammatory diseases and Alzheimer's disease (Duffy et al., 2009; Mullooly et al., 2016).

ADAMs are mainly inhibited by TIMP-3 (Calligaris et al., 2021), and of particular interest is the inhibition of ADAM17 by TIMP-3 (Amour et al., 1998). ADAM17 was the first sheddase to be characterised and is classically known to cleave the membrane-bound precursor form of tumour necrosis factor (TNF) to its soluble form (Black et al., 1997). ADAM17 also cleaves over 90 different substrates, with roles in development, cell adhesion and immune function.

There are 19 members of the ADAMTS family, with these enzymes being structurally similar to ADAMs, but lacking a transmembrane domain and having varying numbers of thrombospondin-like repeats. They are secreted enzymes that either bind to the ECM or are soluble molecules.

Functionally, ADAMTS-1 and -8 have anti-angiogenic properties, whilst ADAMTS-1, -4, -5, -8, -9 and -15 cleave aggrecan. ADAMTS-2, -3 and -14 are pro-collagen N-proteinases that catalyse the removal of the N-terminal peptide of pro-collagens to form mature collagen molecules. ADAMTS-1 and -4 can also cleave versican and brevican (Kelwick et al., 2015; Porter et al., 2005). Physiologically, ADAMTSs are involved in ECM turnover, ovulation and blood coagulation, and pathologically ADAMTSs have been implicated in osteoarthritis, thrombotic thrombocytopenic purpura, deficient lymphangiogenesis, pulmonary artery hypertension and cancer (Blobel & Apte, 2022; Kelwick et al., 2015; Malfait et al., 2002).

ADAM10, ADAM17, ADAMTS-1, ADAMTS-2, ADAMTS-3, ADAMTS-5, ADAMTS-6, ADAMTS-7 and ADAMTS-9 are known to be expressed in the retina (Bevitt et al., 2003; Campbell et al., 2019). The roles of ADAMs and ADAMTSs in the retina are not well defined, however ADAMs are involved in retinal development (Yan et al., 2011) and also pathogenesis, such as AMD (Or et al., 2014). The role of ADAM10 and ADAM17 as sheddases (Saftig & Reiss, 2011), poses great interest for shedding

of cell surface receptors and membrane-bound TNF in retinal health and disease. ADAMTSs have been implicated in angiogenesis regulation (Kumar et al., 2012), and hence may participate in blood vessel proliferation from the choroid in the retina.

### 1.4.2 TIMP structure

Structurally, the four TIMPs share similarities, being composed of an N-terminal domain of approximately 125 amino acids and a C-terminal region made-up of approximately 65 amino acids. The tertiary structures of TIMPs are stabilised by 6 intramolecular disulfide bonds that form between 12 cysteine residues in the TIMP amino acid sequence. Human TIMPs share about 40 % sequence homology, with TIMP-2 and TIMP-4 sharing 50 % sequence identity, whilst TIMP-3 has 38 % sequence identity with TIMP-2 and 30 % identity with TIMP-1 (Brew & Nagase, 2010). Full length TIMP-1 and TIMP-2 and N-TIMP-1 and N-TIMP-3 structures have been resolved by X-ray crystallography (Fernandez-Catalan et al., 1998; Iyer et al., 2007; Maskos et al., 2007; Morgunova et al., 2002; Tuuttila et al., 1998; Wisniewska et al., 2008), whilst full length TIMP-2 structure has also been determined in solution (Williamson et al., 1994). Most of these structures have been determined with TIMPs in complex with their target metalloproteinases, for example the structure of TIMP-2 was determined in complex with MMP-14 and N-TIMP-3 was determined in complex with ADAM17 (Wisniewska et al., 2008). These studies showed that TIMPs have a ‘wedge-shaped’ inhibitory ridge that is complementary in shape to the active site of target metalloproteinases, enabling them to form high-affinity, non-covalent complexes with target enzymes (Brew & Nagase, 2010). Generally, the interactions between TIMPs and metalloproteinases are mediated by 5 amino acid residues in the N-terminal domain of TIMPs, in the case of TIMP-3 this sequence is Cys-Thr-Cys-Ser-Pro (Spanò & Scilabre, 2022). TIMPs achieve inhibition of metalloproteinases via the  $\alpha$ -amino and carbonyl groups of the N-terminal Cys-1 residue chelating the  $Zn^{2+}$  ion of the active site of metalloproteinases. Furthermore, the OH group of Ser/Thr-2 on TIMPs interacts with the Glu in the MMP catalytic site to displace a water molecule that is critical for the peptide hydrolytic function of metalloproteinases (Murphy, 2011). The TIMP N-terminal domain alone is mostly sufficient to inhibit metalloproteinases, however there are a few exceptions, including the inability of N-TIMPs to inhibit ADAM10 (Rapti et al., 2008). Residues in the C-terminal region of TIMPs also participate in interactions with target metalloproteinases, however these interactions mainly play a stabilisation role and are not required for metalloproteinase inhibition (Brew & Nagase, 2010).

Despite structural similarities between the 4 TIMPs, TIMP-3 is unique in a number of respects including its localisation to the ECM, as well as its inhibitory range, which is greater than all of the other TIMPs (**Table 1.3**). Given that mutations in the *TIMP3* gene cause SFD, the following section will discuss TIMP-3 properties in more detail.

### 1.4.3 TIMP-3

#### 1.4.3.1 Physiological and pathological roles of TIMP-3

TIMP-3 has the broadest inhibitory function of all of the TIMPs (**Table 1.3**), inhibiting most ADAMs and ADAMTSs and consequently TIMP-3 null mice have the most severe phenotypes. *TIMP3* null mice exhibit lung defects including air space enlargement (Leco et al., 2001) and impaired bronchiolar branching (Gill et al., 2003), dilated cardiomyopathy (Fedak et al., 2004), spontaneous development of osteoarthritis (Sahebjam et al., 2007) and inflammatory arthritis (Mahmoodi et al., 2005). In terms of retinal pathology, *TIMP3* null mice display abnormal vascularisation in the choroid (Janssen et al., 2008) with vessels exhibiting strong dilation or fusing of multiple vessels. Interestingly, *TIMP3* null mice exhibited unchanged retinal histology, even though increased MMP activity was observed in the choroid, which one might expect would cause a thinning of BrM, but perhaps other TIMPs compensate to inhibit MMPs. Furthermore, aortic explants isolated from *TIMP3* null mice had enhanced capillary sprouting and it was observed that aortic endothelial cells from these mice had enhanced autophosphorylation of VEGF receptor 2 (VEGFR2) and phosphorylation of downstream signalling molecules such as extracellular signal-related kinase (ERK) 1/2 compared to cells from control mice. These phenotypes of *TIMP3* null mice are mostly thought to arise from unregulated remodelling of the ECM by MMPs, highlighting the important role of TIMP-3 in regulating MMP activity and in the case of retinal pathology, angiogenic activity. Additionally, *TIMP3* null mice display increased release of TNF and TNF-dependent signalling, due to increased ADAM17 activity, driving inflammation related pathologies of the liver, as well as sepsis, diabetes, nephritis and atherosclerosis (Kassiri et al., 2009; Martin et al., 2005; Mohammed et al., 2004; Stöhr et al., 2014).

TIMP-3 is also linked to various human diseases, including cardiovascular disease, cancer, and emphysema (Brew & Nagase, 2010; Fan & Kassiri, 2020; Su et al., 2019). Furthermore, a decrease in TIMP-3 is observed in osteoarthritic cartilage compared to healthy controls (Morris et al., 2010), which is thought to enable increased degradation of cartilage by enzymes such as ADAMTS-5 and MMP-13.

Mutations in the *TIMP3* gene are linked to disease, namely SFD (Weber et al., 1994a, Weber et al., 1994b), as detailed in section 1.1. Interestingly, variants in the *TIMP3* gene are also linked to AMD (Fritzsche et al., 2015; Kaur et al., 2010), however the roles of these variants has not been defined.

#### 1.4.3.2 Structure

Human TIMP-3 is synthesised as a precursor protein that is 211 amino acids in length. The precursor contains a 23 amino acid signal peptide that facilitates secretion of TIMP-3 from cells and is cleaved off during the secretory process (Wilde et al., 1994). When separated by electrophoresis, mature TIMP-3 typically migrates as 2 bands. Unglycosylated TIMP-3 is present at ~24 kDa whereas glycosylated TIMP-3, formed as a result of N-linked glycosylation at a site near the carboxyl terminus at position Asn-184 (Apte et al., 1994b; Langton et al., 1998; Leco et al., 1994), has a mass of ~27 kDa. TIMP-3 is composed of a ~120 amino acid N-terminal domain, with the remaining ~80 amino acids forming the C-terminal region of TIMP-3. TIMP-3's tertiary structure relies on the formation of 6 intramolecular disulfide bonds between 12 cysteine residues, which results in a wedge-like structure with an inhibitory ridge that is complementary to target metalloproteinases (Brew & Nagase, 2010). The crystal structure of N-TIMP-3 in complex with ADAM17 has been resolved (Wisniewska et al., 2008), but the structure of full-length TIMP-3 has not. A model of full-length TIMP-3 has been generated based on its homology with TIMP-2 (Doherty et al., 2016), which agrees with the predicted structure from AlphaFold (Figure 1.2) (Betts & Troeberg, 2024).

#### 1.4.3.3 Extracellular matrix binding

TIMP-3 is unique among TIMPs in its ability to bind to the ECM, with other TIMPs being soluble. TIMP-3 binds to sulfated GAGs in the ECM including HS and CS (Yu et al., 2000). These same investigators also demonstrated co-localisation of TIMP-3 with HS, which could be abolished by digestion of tissues with heparinase III or chondroitinase ABC. Mutagenesis studies revealed that basic residues from both the N- (Lys26, Lys27, Lys30 and Lys76) and C-terminal (Arg163 and Lys165) domains are required for TIMP-3 binding to the ECM (Lee et al., 2007). Binding of TIMP-3 to HS has been shown to enhance TIMP-3 affinity and inhibitory function for ADAMTS5 (Troeberg et al., 2014) and MMP-13 (Yamamoto et al., 2016). Additionally, TIMP-3 binding to the ECM glycoprotein fibulin-3 has been demonstrated in vitro (Klenotic et al., 2004). It has been suggested that the

interaction of fibulin-3 with TIMP-3 inhibits TIMP-3 binding to ADAM10 and ADAM17, resulting in increased enzyme activity (Nandhu et al., 2014).

#### **1.4.3.4 Apoptotic activity of TIMP-3**

High levels of TIMP-3 are cytotoxic to cells including HeLa cells (Baker et al., 1999), vascular smooth muscle cells and even RPE cells (Majid et al., 2002). This is likely due to stabilisation of death receptors on the cell surface, induced by TIMP-3 inhibition of ADAM10 and ADAM17, which are known to cleave and shed cell surface death receptors (Ahonen et al., 2003; Weinlich et al., 2010). Death receptors include TNF receptor 1, FAS and TNF-related apoptosis-inducing ligand receptor-1 (Ahonen et al., 2003; Bond et al., 2002; Smith et al., 1997). TIMP-3 has also been shown to promote cell death in ischaemic cortical neurons by inhibiting shedding of FAS ligand and so promoting FAS activation (Wetzel et al., 2007). Interestingly, TIMP-3 has also been reported to cause cell death intracellularly in synovial fibroblasts, via a mechanism distinct from TIMP-3's ability to inhibit ADAM10/17 ectodomain shedding, but involving NF- $\kappa$ B regulation (Drynda et al., 2005).

#### **1.4.3.5 Inhibition of angiogenesis**

TIMP-3 is a potent inhibitor of angiogenesis. It inhibits chemotaxis of human umbilical vein endothelial cells in a dose-dependent fashion in vitro (Anand-Apte et al., 1997) and can inhibit basic-fibroblast-growth-factor-2-induced blood vessel growth in a chorioallantoic membrane assay (Anand-Apte et al., 1997). TIMP-3's anti-angiogenic function is reported to be mediated by its ability to competitively block VEGF binding to VEGF receptor 2 (Qi et al., 2003). Furthermore, TIMP-3 is thought to inhibit angiogenesis by binding to angiotensin II type-2 receptor, with over expression of TIMP-3 and angiotensin II type-2 receptor shown to additively inhibit angiogenesis (Kang et al., 2008). In vivo evidence demonstrates that TIMP-3 null mice have increased VEGF signalling (Ebrahem et al., 2011), culminating in abnormalities in vascularisation of the retinal choroidal layer (Ebrahem et al., 2011; Janssen et al., 2008), which corroborates in vitro results to show that TIMP-3 is an important inhibitor of angiogenesis.

## 1.5 SFD TIMP-3 mutant proteins

Various properties of SFD TIMP-3 mutant proteins have been studied to date, including dimerisation state, MMP inhibition and inhibition of angiogenesis (Betts & Troeberg, 2024). These studies have mainly focused on a few of the currently known 21 SFD mutations. There is also a wide body of evidence showing that SFD TIMP-3 mutants accumulate extracellularly in the BrM and it has been suggested that they are more resistant to turnover than WT TIMP-3 (Langton et al., 2005). These concepts are discussed below (**Table 1.4**, **Table 1.5** & **Table 1.6**).

### 1.5.1 Dimerisation of SFD TIMP-3 proteins

Most investigators have observed that SFD mutants have a propensity to form dimers, multimers and higher molecular weight complexes (Arris et al., 2003; Langton et al., 2000, 2005; Weber et al., 2002; Yeow et al., 2002) (**Table 1.4**), although this hasn't been seen by all groups (Qi et al., 2002). Those SFD TIMP-3 mutations that introduce a free cysteine are hypothesised to cause intermolecular disulfide bond formation with other TIMP-3 monomers to generate dimers (Christensen et al., 2017). However, this process would not result in the formation of multimers as there wouldn't be additional free cysteines to form further intermolecular disulfide bonds (Betts & Troeberg, 2024). A model proposed by Li et al. (2005) suggests that dimers could be formed between WT and SFD TIMP-3 monomers, with nucleophilic attack across a disulfide bond in the WT TIMP-3, generating an unpaired cysteine residue and allowing for the formation of higher molecular weight complexes.

One of the main points of evidence for intermolecular disulfide bond formation in SFD dimers is comparison of western blot migration under non-reducing and reducing conditions. Addition of reducing agents (e.g.,  $\beta$ -mercaptoethanol or dithiothreitol [DTT]) causes dimeric bands to disappear, with a concurrent increase in the intensity of monomeric bands (Alsaffar et al., 2022; Arris et al., 2003; Langton et al., 2000, 2005).

SFD mutants not involving the generation of a free cysteine residue have also been reported to form dimers, for example E162K and H181R (Alsaffar et al., 2022; Saihan et al., 2009). This indicates that there is a dimerisation mechanism independent of free cysteine-driven intermolecular disulfide bond formation and

raising the possibility that even SFD mutations involving a free cysteine residue may form dimers via this currently unknown mechanism (Betts & Troeberg, 2024).

### 1.5.2 Metalloproteinase inhibition by SFD TIMP-3 proteins

The majority of published literature concludes that SFD mutants retain their ability to inhibit MMP-2 and MMP-9 (**Table 1.4**). This has largely been investigated by reverse zymography in a range of cell types not relevant to the eye, such as patient-derived fibroblast cells or non-human cell lines such as BHK or COS-7 cells (Arris et al., 2003; Qi et al., 2022; Langton et al., 2000; Yeow et al., 2002), but has also been looked at in ARPE-19 cells (Langton et al., 2005) and human-induced pluripotent stem cells (hiPSC)-RPE cells (Hongisto et al., 2020) (Betts & Troeberg, 2024). Others have also found that SFD TIMP-3 mutants retain their ability to inhibit MT1-MMP-dependent activation of pro-MMP-2 (Langton et al., 2005; Soboleva et al., 2003). It is surprising that only MMP-2 and MMP-9 have been extensively studied, given that RPE cells also express other MMPs, including MMP-1 and MMP-3 (Alexander et al., 1990; Guo et al., 1999; Hunt et al., 1993). Furthermore, the MMP inhibitory capacity of most of the 21 SFD mutants has not been investigated, so this is an area which requires more research, especially as there has been some disagreement in the literature, with some reports of impaired inhibitory activity (Qi et al., 2002).

Multiple groups have concluded from reverse zymography that SFD mutants (e.g., S179C, Y191C and S204C) retain their ability to inhibit MMP-2 and MMP-9 in both monomeric and dimeric forms (Arris et al., 2003; Qi et al., 2022; Langton et al., 1998, 2005; Yeow et al., 2002), although there are some important points to consider in relation to these conclusions. Firstly, a lot of earlier studies transfected SFD mutants into cells that endogenously expressed WT TIMP-3, meaning WT TIMP-3 could be responsible for inhibition observed at monomer molecular masses. This possibility cannot be ruled out unless the appropriate controls (e.g., WT TIMP-3 alone or untransfected cells) are run on the same gel and compared. Additionally, the composition of dimers was not known. If we consider the model proposed by Li et al. (2005), it is plausible that WT TIMP-3 could be part of an observed dimer and this WT TIMP-3 could be responsible for the bands observed by reverse zymography. Whether the monomeric forms of SFD TIMP-3 mutants can inhibit MMPs hasn't been extensively investigated. Hongisto et al. (2020) demonstrated that monomeric S204C retained MMP inhibitory capacity in a collagenase activity

assay, but there is a lack of other evidence looking at monomeric forms. Lastly, reverse zymography gives no indication of the kinetics or affinity of inhibition by mutant TIMP-3 proteins.

One group has investigated the kinetic interactions of SFD TIMP-3 mutants with MMPs (Yeow et al., 2002) and they described the S179C mutant has lower  $k_{on}$  values for MMP-2, MMP-3, MMP-9 and MMP-13. This does not necessarily mean that S179C has decreased inhibition, because it could also have a slower  $k_{off}$  rate, meaning that its  $K_i$  for these MMPs could be similar to that of WT TIMP-3. More research is warranted to establish kinetic parameters of a broader spectrum of SFD mutants for target metalloproteases.

Given that SFD mutants appear to retain MMP inhibition, their extracellular accumulation in the BrM could cause increased inhibition of MMPs, leading to the huge thickening of the BrM that is observed in SFD (Capon et al., 1989). In turn this could greatly increase the diffusion distance and hence impair the exchange of fresh nutrients and waste between the choroid and metabolically-active RPE, leading to accumulation of sub-RPE deposits and geographic atrophy.

To my knowledge, only one study has investigated the ability of SFD TIMP-3 mutants to inhibit ADAMs and ADAMTSs. Fogarasi et al. (2008) showed that the S179C mutant inhibited ADAM17, ADAMTS-4 and -5, as effectively as WT TIMP-3. Additional studies are needed to determine whether other SFD TIMP-3 mutants retain inhibition of these and other ADAMs and ADAMTSs.

**Table 1.4: SFD TIMP-3 variants and their ability to dimerise and inhibit MMPs.**

Mutation	Age of Onset (years)	Dimerisation/ multimerisation	MMP Inhibition
<b>Leu10His &amp; Gly12Arg</b>	Early (2 <sup>nd</sup> Decade)	Not clear. Dimeric species shown in cytoplasmic, membrane, nuclear extracts and ECM (for Gly12Arg) but no difference compared to WT TIMP-3 in <b>HEK-293 cells</b> (Guan et al., 2022)	Not known.
<b>Cys24Arg</b> <b>Ser38Cys</b>	Early 40-50	Not known. Monomeric, <b>Patient Fibroblasts</b> (Naessens et al., 2019) Yes, <b>ARPE-19 cells</b> (F. A. Alsaffar et al., 2022)	Not known. Not known.
<b>Intron 4/Exon 5 Splice Site</b>	50-80	Yes, <b>ARPE-19 cells</b> (Alsaffar et al., 2022)	Not known.
<b>Ser149Cys</b> <b>Tyr151Cys</b>	30-50 Early	Not known. Yes, <b>ARPE-19 cells</b> (Alsaffar et al., 2022)	Not known. Not known.
<b>Glu162Lys</b>	30-50	Yes, <b>ARPE-19 cells</b> (Saihan et al., 2009)	MMP-2 and MMP-9 inhibition retained – <b>Reverse zymography</b> (Saihan et al., 2009)
<b>Glu162STOP</b>	20-40	Yes, <b>Transfected insect cells</b> (Arris et al., 2003) and <b>ARPE-19 cells</b> (Langton et al., 2005) Dimer molecular weight is ~26 kDa, which is similar to WT TIMP-3 so can be hard to distinguish.	Monomer retained MMP-2 inhibition in transfected cells, but not in patient-derived fibroblasts – <b>Reverse zymography</b> (Arris et al., 2003) MMP-2/9 inhibition in ECM extracts from ARPE-19 cells, but hard to distinguish from WT TIMP-3. No inhibition of MT1-MMP activation of pro-MMP-2. – <b>Reverse zymography &amp; zymography</b> (Langton et al., 2005)
<b>Tyr174Cys</b> <b>Tyr177Cys</b>	30-40 50-60	Not known. Yes, <b>ARPE-19 cells</b> (Alsaffar et al., 2022)	Not known. Not known.
<b>Ser179Cys</b>	20-30	No, <b>ARPE-19 cells</b> (Qi et al., 2002) Yes, <b>ARPE-19 cells</b> (Langton et al., 2005), <b>BHK cells</b> (Yeow et al., 2002), <b>mouse RPE &amp; human fibroblasts</b> (Weber et al., 2002), <b>COS-7 cells</b> (Langton et al., 2000), <b>porcine aortic endothelial cells</b> (Lin et al., 2006; Qi & Anand-Apte, 2022).	2-3-fold lower $k_{on}$ values for MMP-2/3/9/13 – <b>Association rate assay</b> (Yeow et al., 2002) Attenuated inhibition of MT1-MMP activation of pro-MMP-2. Increased secretion and activation of pro-MMP-2/9 in ARPE-19 cells – <b>Reverse zymography &amp; zymography</b> (Qi et al., 2002) Monomer but not higher molecular weight species (~35 kDa) retain inhibition of MMP-2 and MMP-9 – <b>Reverse zymography</b> (Soboleva et al., 2003) MMP-2/9 inhibition in ECM extracts. Did not inhibit MT1-MMP activation of pro-MMP-2 – <b>Reverse zymography &amp; zymography</b> (Langton et al., 2005) Spleen tissue isolated from S179C +/- mice did not inhibit MMP-2 or MMP-9 and there was an increase in MMP-9 activity – <b>Reverse zymography &amp; zymography</b> (Qi et al., 2009) Reduced MMP-2/9 inhibition in ECM and CM of porcine aortic endothelial cells. Glycosylation-dependent. Increased secretion of MMP-2/9. – <b>Reverse zymography &amp; zymography</b> (Qi & Anand-Apte, 2022)
<b>His181Arg</b>	50-70	Not explicitly concluded but 39-50 kDa species	Proposed model suggests that H181R could reduce pro-MMP-2 activation (Lin et al., 2006)

		observed – <b>Skin fibroblasts</b> (Lin et al., 2006) Yes, <b>ARPE-19 cells</b> (Alsaaffar et al., 2022).	
<b>Tyr182Cys</b>	50-60	Yes, <b>ARPE-19 cells</b> (Alsaaffar et al., 2022)	Not known.
<b>Gly189Cys</b>	20-40	Yes, <b>COS-7 cells</b> (Langton et al., 2000)	MMP inhibition retained in ECM from COS-7 cells – <b>Reverse zymography</b> (Langton et al., 2000)
<b>Gly190Cys</b>	30-40	Yes, <b>BHK cells</b> (Yeow et al., 2002)	MMP-2/9 inhibition retained – <b>Reverse zymography</b> (Yeow et al., 2002)
<b>Tyr191Cys</b>	30-40	Yes, <b>BHK cells</b> (Yeow et al., 2002), <b>Porcine aortic endothelial cells</b> (Qi & Anand-Apte, 2022).	MMP-2/9 inhibition retained – <b>Reverse zymography</b> (Yeow et al., 2002) Reduced MMP-2/9 inhibition in the ECM and CM of porcine aortic endothelial cells. Glycosylation-dependent. Increased secretion of MMP-2/9 – <b>Reverse zymography &amp; zymography</b> (Qi & Anand-Apte, 2022)
<b>Ser193Cys</b>	30-40	Not known.	Not known.
<b>Tyr195Cys</b>	20-40	Not known.	Not known.
<b>Trp198Cys</b>	Early	Not known.	Not known.
<b>Ser204Cys</b>	30-60	Yes, <b>COS-7 cells</b> (Langton et al., 1998), <b>BHK cells</b> (Yeow et al., 2002), <b>patient-derived fibroblasts</b> (Weber et al., 2002), <b>Patient-derived fibroblasts</b> (Arris et al., 2003), <b>ARPE-19 cells</b> (Langton et al., 2005), <b>hiPSC-RPE cells</b> (Hongisto et al., 2020), <b>porcine aortic endothelial cells</b> (Qi & Anand-Apte, 2022).	MMP-2/9 inhibition retained – <b>Reverse zymography</b> (Langton et al., 1998) MMP-2/9 inhibition retained – <b>Reverse zymography</b> (Yeow et al., 2002) MMP-2/9 inhibition retained and no effect on expression of MMP-2/9 in patient-derived fibroblasts – <b>Reverse zymography</b> (Arris et al., 2003) MMP-2/9 seen in ARPE-19 cells. Could inhibit MT1-MMP activation of pro-MMP-2 – <b>Reverse zymography &amp; zymography</b> (Langton et al., 2005) MMP inhibition retained – <b>EnzChek collagenase/gelatinase assay</b> (Hongisto et al., 2020) Reduced MMP-2/9 inhibition in ECM and CM of porcine aortic endothelial cells. Glycosylation-dependent – <b>Reverse zymography</b> (Qi & Anand-Apte, 2022) Less effective at inhibiting MMP-2/9 but due to the significant increase in S204C accumulation, overall inhibition of MMP-2/9 was the same – <b>Reverse zymography</b> (Engel et al., 2022)

### 1.5.3 Inhibition of angiogenesis by SFD TIMP-3 proteins

Late-stage SFD typically manifests with CNV, where dysregulated angiogenesis results in the inappropriate proliferation and invasion of blood vessels into the outer retina. TIMP-3 has anti-angiogenic activity (Anand-Apte et al., 1997) and it is thought to mediate this effect by competitively blocking the binding of VEGF to VEGFR2 (Qi et al., 2003).

There are contrasting reports in the literature on how SFD TIMP-3 mutants impact angiogenesis, with unchanged, reduced and no inhibition of angiogenesis reported in different studies.

The S179C TIMP-3 variant has received considerable investigation in this area and has been reported by one group in two studies (Qi et al., 2002, 2009) to induce

angiogenesis, despite WT TIMP-3 being reported to inhibit angiogenesis (Anand-Apte et al., 1997). This group reported that application of conditioned media containing S179C TIMP-3 induced neovascularisation on a chick chorioallantoic membrane (Qi et al., 2002). The mechanism behind this is likely to be increased binding of VEGF to VEGFR2, due to an observed increased expression of VEGFR2 in both a mouse S179C model and an S179C SFD patient (Qi et al., 2009). More recent evidence from the same group (Qi & Anand-Apte, 2022) demonstrated enhanced phosphorylation of VEGFR2 in response to VEGF in endothelial cells expressing S179C, relative to cells expressing WT TIMP-3. In a mini-Boyden assay chamber, they found that endothelial cells expressing S179C, Y191C and S204C TIMP-3 variants migrated more than cells expressing WT TIMP-3 when stimulated with VEGF. Interestingly, they report that deglycosylation of these SFD mutants further exacerbated their angiogenic potential.

A recent publication suggests that RPE cells expressing S179C TIMP-3 promote angiogenesis from the choroid by increasing RPE secretion of basic fibroblast growth factor (Qi et al., 2019). Thus, SFD TIMP-3 mutants may also promote angiogenesis and CNV by a mechanism distinct from VEGF signalling and dependent on an fibroblast growth factor receptor-1-dependent pathway.

A more agnostic mass spectrometry approach adopted by Hongisto et al. (2020) examined that the conditioned medium of hiPSC-RPE expressing S204C and found an upregulation of proteins involved in angiogenesis-related pathways compared to WT TIMP-3-expressing cells, including chemoattractant protein 1, platelet-derived growth factor and angiogenin. This supports the hypothesis that SFD mutants may induce or promote angiogenesis.

Additionally, a recent report by Alsaffar et al. (2022) agrees somewhat with the above studies (Qi et al., 2022; Qi et al., 2002, 2009) and suggests that a wide range of SFD mutants (S38C, E162K, E162X, S179C, H181R, S204C) have reduced inhibition of VEGFR2 signalling, although they didn't induce angiogenesis as suggested above.

In contrast, another investigation on the same S179C TIMP-3 mutant reported that it inhibits angiogenesis to the same extent as WT TIMP-3 (Fogarasi et al., 2008). A fibrin bead assay showed that tube formation from mice aortic endothelial cells was

not statistically different if they expressed WT or S179C TIMP-3, and that S179C TIMP-3 was able to inhibit binding of VEGF to VEGFR2 as effectively as WT TIMP-3 (Fogarasi et al., 2008).

The reasons for these discrepancies may be due to the different cell types and experimental setups used. For example, some groups use conditioned media from ARPE-19 cells expressing S179C (Qi et al., 2002), whilst others use ECM extract from transfected ARPE-19 cells (Alsaffar et al., 2022), and further still others use aortic endothelial cells isolated from mice expressing S179C TIMP-3 (Fogarasi et al., 2008).

**Table 1.5: SFD TIMP-3 variants and their ability to inhibit angiogenesis and bind to the ECM.**

Mutation	Inhibition of angiogenesis retained?	ECM localisation/binding
Leu10His & Gly12Arg	Not known.	<b>Yes</b> , but decreased amounts of L10H and G12R detected in ECM, possibly due to altered cellular secretion (Guan et al., 2022)
Cys24Arg	Not known.	Not known.
Ser38Cys	Reduced (~50 %) compared to WT TIMP-3 when expressed by ARPE-19 cells in HUVEC assay (Alsaffar et al., 2022)	<b>Yes</b> , patient fibroblasts (Naessens et al., 2019), ARPE-19 cells (Alsaffar et al., 2022). Decreased amounts detected in ECM, possibly due to altered cellular secretion (Guan et al., 2022)
Intron 4/Exon 5 Splice Site	Not known.	<b>Yes</b> , ARPE-19 cells (Alsaffar et al., 2022)
Ser149Cys	Not known.	Not known.
Tyr151Cys	Not known.	<b>Yes</b> , ARPE-19 cells (Alsaffar et al., 2022)
Glu162Lys	Reduced (~50 %) compared to WT TIMP-3 when expressed by ARPE-19 cells in HUVEC assay (Alsaffar et al., 2022)	<b>Yes</b> , ARPE-19 cells (Saihan et al., 2009)
Glu162STOP	Reduced (~50 %) compared to WT TIMP-3 when expressed by ARPE-19 cells in HUVEC assay (Alsaffar et al., 2022)	<b>Yes</b> , Patient fibroblasts (Arris et al., 2003) and reduced turnover in ARPE-19 cells (Langton et al., 2005)
Tyr174Cys	Not known.	Not known.
Tyr177Cys	Not known.	<b>Yes</b> , ARPE-19 cells (Alsaffar et al., 2022)
Ser179Cys	Induced angiogenesis in CAM assay (J. H. Qi et al., 2002), increased VEGF:VEGFR2 binding (Qi et al., 2009) and upregulation of VEGFR2 in porcine aortic endothelial cells expressing S179C. Increased VEGFR2 signalling (Qi and Anand-Apte, 2022). Inhibited angiogenesis as effectively as WT TIMP-3 (Fogarasi et al., 2008) Reduced (~50 %) angiogenesis compared to WT TIMP-3 when expressed by ARPE-19 cells in HUVEC assay (Alsaffar et al., 2022)	<b>Yes</b> , BHK cells expressing S179C had slower detachment from the ECM vs WT TIMP-3 after treatment with EDTA and EGTA (Yeow et al., 2002) <b>Yes</b> , mice retinal sections (Weber et al., 2002), ARPE-19 cells in monomeric form, so difficult to distinguish from WT TIMP-3 (Qi et al., 2002), more S179C present in the ECM of fibroblasts than WT TIMP-3, but same rate of turnover as WT TIMP-3 (Soboleva et al., 2003), reduced turnover in ARPE-19 cells (Langton et al., 2005) and porcine aortic endothelial cells (Qi & Anand-Apte, 2002).
His181Arg	Reduced (~50 %) angiogenesis compared to WT TIMP-3 when expressed by ARPE-19 cells in HUVEC assay (Alsaffar et al., 2022)	<b>Yes</b> , patient fibroblasts (Lin et al., 2006) and ARPE-19 cells (Alsaffar et al., 2022)
Tyr182Cys	Not known.	<b>Yes</b> , ARPE-19 cells (Alsaffar et al., 2022)
Gly189Cys	Not known.	<b>Yes</b> , COS-7 cells (Langton et al., 2000)
Gly190Cys	Not known.	<b>Yes</b> , BHK cells (Yeow et al., 2002)

<b>Tyr191Cys</b>	Upregulation of VEGFR2 in porcine aortic endothelial cells expressing S179C. Increased VEGFR2 signalling (Qi & Anand-Apte, 2022)	<b>Yes</b> , BHK cells (Yeow et al., 2002) and Porcine aortic endothelial cells (Qi & Anand-Apte, 2022)
<b>Ser193Cys</b>	Not known.	Not known.
<b>Tyr195Cys</b>	Not known.	Not known.
<b>Trp198Cys</b>	Not known.	Not known.
<b>Ser204Cys</b>	No difference in basal secretion of VEGF from hiPSC-RPE but an increase in angiogenesis-related proteins such as angiogenin and PDGF (Hongisto et al., 2020)  Reduced (~50 %) compared to WT TIMP-3. Expressed by ARPE-19 cells in HUVEC assay (Alsaaffar et al., 2022)  Upregulation of VEGFR2 in porcine aortic endothelial cells expressing S179C. Increased VEGFR2 signalling (Qi & Anand-Apte, 2022)	<b>Yes</b> , COS-7 cells (Langton et al., 1998) <b>Yes</b> , BHK cells expressing S179C had slower detachment from the ECM than WT TIMP-3 when treated with EDTA/EGTA (Yeow et al., 2002) <b>Yes</b> , patient fibroblasts (Arris et al 2003), reduced turnover in ARPE-19 cells (Langton et al., 2005), porcine aortic endothelial cells (Qi & Anand-Apte, 2022) and higher presence in the ECM of hiPSC-RPE but this may not indicate increased binding (Engel et al., 2022).

#### 1.5.4 Accumulation and turnover of TIMP-3 in SFD

Accumulation of TIMP-3 in the BrM is a classic hallmark of SFD and has received considerable attention in the literature (Betts & Troeberg, 2024; Christensen et al., 2017). Extracellular accumulation of TIMP-3 has been observed in SFD patients (Chong et al., 2000), mouse models of SFD (Weber et al., 2002), as well as *in vitro* in cell lines and hiPSC-RPE models (Engel et al., 2022; Galloway et al., 2017; Langton et al., 2005; Majid et al., 2007; Soboleva et al., 2003; Yeow et al., 2002).

Interestingly, intracellular accumulation of TIMP-3 has also been observed for S204C TIMP-3 in a hiPSC-RPE model (Hongisto et al., 2020) as well as for mutations in TIMP-3 that occur in the signal peptide, L10H and G12R, in HEK-293 cells (Guan et al., 2022). The mechanism by which intracellular TIMP-3 accumulation occurs is unknown and may be due to either impaired secretion of TIMP-3, which is likely to be the case for mutations occurring in the signal peptide, or due to impaired breakdown of TIMP-3 after cellular uptake.

The primary hypothesis for this extracellular accumulation of SFD TIMP-3 mutants relates to the formation of dimers and multimers (1.5.1), with some mutants have demonstrated to be more resistant to turnover by RPE cells. Langton et al. (2005) cultured ARPE-19 cells transfected with plasmids encoding E162X, S179C or S204C and cultured these cells to allow for ECM deposition containing the mutant TIMP-3. They subsequently replaced transfected cells with fresh untransfected ARPE-19 cells and measured the disappearance of SFD TIMP-3 from the ECM over 96 h. Over the first 48 h, SFD TIMP-3 mutants were cleared as efficiently as WT TIMP-3, corroborating previous observations (Soboleva et al., 2003). However after

96 h, significantly more of all SFD variants analysed remained in the ECM compared to WT TIMP-3, primarily as dimeric and multimeric species (Langton et al., 2005), indicating that SFD TIMP-3 mutants have significantly reduced turnover.

SFD TIMP-3 mutants may also have increased binding to the ECM. S179C, G190C, Y191C and S204C have all been shown to be more thermodynamically stable than WT TIMP-3 when bound to the ECM and were able to retain a degree of MMP inhibitory activity when heated to 100 °C (Majid et al., 2007), so perhaps these SFD mutants form covalent interactions with the ECM. Alternatively, changes to the BrM ECM itself could result in altered post-translational trafficking of TIMP-3. A key study performed by Keenan et al. (2014) found that the mean quantity of HS in the human BrM significantly decreased with age, along with a decrease in the degree of sulfation of HS. Given that HS is a major binding partner for CFH in the BrM, they demonstrated that the decrease in overall HS and a change in its sulfation could disrupt ECM binding of complement factor H, particularly the 402H form that is associated with AMD and causes overactivation of complement. The same could apply to TIMP-3, with a decrease in HS and its sulfation disrupting TIMP-3 trafficking and activity. The average age of donors in the 'old' group in this study was 82 years, so these changes in the BrM may be more relevant for the accumulation of SFD mutants that present later in life such as the intron 4/exon 5 splice site mutation, Y177C, H181R and Y182C (**Table 1.1**).

TIMP-3 can also bind to other ECM components including fibulin-3 (Klenotic et al., 2004), which is known to accumulate in another macular dystrophy called Malattia Leventinese (Marmorstein et al., 2002). Fibulin-3 is upregulated in a hiPSC-RPE model expressing S204C TIMP-3 (Hongisto et al., 2020), and accumulation of fibulin-3 would potentially promote extracellular TIMP-3 accumulation in SFD.

Accumulation of TIMP-3 could also be due to intermolecular crosslinking of ECM components as a result of the high photo-oxidative environment in the retina (Christensen et al., 2017; Crabb et al., 2002).

Despite well-characterised extracellular TIMP-3 accumulation in SFD, mRNA levels of TIMP-3 are not elevated in SFD patients (Chong et al., 2003), indicating that accumulation may be due to dysregulated post-translational regulation of TIMP-3 protein levels. Therefore, mutations in TIMP-3 may affect its binding to HS in the

ECM or its endocytosis and breakdown, ultimately leading to its extracellular accumulation.

### 1.5.5 Mechanisms of pathology

Sections **1.5.1, 1.5.2 & 1.5.3** summarise evidence for how SFD mutations may affect TIMP-3 protein functions, in terms of dimerisation, MMP inhibition and altered inhibition of angiogenesis. The following section will review how these altered protein functions may affect retinal cells and be responsible for the pathology observed in SFD.

#### 1.5.5.1 *Apoptosis*

It has been observed by others that cellular morphology is altered in cells expressing SFD variants, with Soboleva et al. (2003) reporting that mouse fibroblasts expressing the S179C variant have a pavement-like appearance with more random orientations and less uniform formation, as well as a higher cytoplasmic to nuclear ratio compared to WT TIMP-3-expressing fibroblasts. This indicates that the expression of SFD mutants is damaging to cells and that they could possibly induce cell death, as is observed in SFD geographic atrophy.

Indeed, as discussed in **1.4.3.4**, it has been shown that overexpression of WT TIMP-3 induces apoptosis in a variety of cell types, including HeLa (Baker et al., 1999), vascular smooth muscle cells and even RPE cells (Majid et al., 2002). Only one study has reported a modest increase in the ability of SFD TIMP-3 variants to induce apoptosis in RPE cells compared to WT TIMP-3 (Majid et al., 2002). They performed plasmid-mediated over-expression of S179C, G190C, Y191C and S204C TIMP-3 in RPE cells and measured increased cell death via trypan blue staining, propidium iodide staining and *in situ* DNA end labelling. The authors state that although they do detect increased apoptosis in SFD TIMP-3-expressing RPE cells, this difference was small and unlikely to fully account for the SFD phenotype. Another point of consideration is that the expression level of Y191C TIMP-3 was significantly lower than WT TIMP-3 but still induced a significantly higher degree of apoptosis than WT TIMP-3-expressing RPE cells, indicating that this particular mutant has a particularly pronounced apoptotic effect (Majid et al., 2002). Even if SFD TIMP-3 mutants are not inherently more pro-apoptotic than WT TIMP-3, their increased accumulation in

the BrM (Chong et al., 2000) could enable them to induce more RPE apoptosis than WT TIMP-3 and so to increase death of the photoreceptors they support.

#### 1.5.5.2 *Metabolism*

It is possible that the expression of SFD mutants could alter cellular metabolism, which may be especially important given that RPE cells are very metabolically active in their essential turnover of POS (Kwon & Freeman, 2020). It has been shown that expression of the S179C TIMP-3 variant decreases overall mitochondrial activity and lactate concentration, indicating a decrease in overall metabolic activity (Soboleva et al., 2003). Conversely, more recent proteomic and RNAseq analysis together with stable isotope tracing experiments indicate that ARPE-19 cells expressing S179C or hiPSC-RPE cells expressing S204C have enhanced glucose utilisation and glycolytic activity compared to RPE cells expressing WT TIMP-3 (Grenell et al., 2024). Furthermore, broader metabolomic approaches have shown alterations in metabolic activity of hiPSC-RPE expressing the S204C variant (Engel et al., 2022). This includes changes in metabolites such as tyrosine, aspartate, GTP and FAD, as well as a reduction in the flux from malate to pyruvate. Additionally, a significant increase in 4-hydroxyproline was detected, indicating increased ECM breakdown. Glutathione was significantly decreased, rendering hiPSC-RPE more susceptible to oxidative damage; this has also been observed in an SFD mouse model (Wolk et al., 2020), and could majorly contribute to the loss of RPE and geographic atrophy observed in late-stage SFD. Overall, the evidence for changes in metabolism is limited, however it is compelling and should receive a greater degree of investigation, as understanding how SFD TIMP-3 mutants globally affect cells in the retina is likely to be important for development of treatments.

#### 1.5.5.3 *Inflammation*

There is some evidence to suggests that inflammation plays a role in SFD, despite SFD originally being thought of as a pseudo-inflammatory condition (Capon et al., 1988; Hoskin et al., 1981). Spaide (2021) reported the successful use of a monoclonal anti-TNF antibody, adalimumab, in the treatment of a woman with the S204C mutation who presented with CNV in 2003. Initially, the adopted treatment was intravitreal injections of the corticosteroid triamcinolone, followed by anti-VEGF therapy in the form of bevacizumab. Both of these treatments had limitations with bevacizumab resulting in signs of exudation and haemorrhage and triamcinolone having long-term complications such as bacterial infection due to immune system

suppression. Adalimumab was subsequently used for 18-months, during which time the patient showed cessation of CNV disease activity and had 20/20 visual acuity in the right eye. Given that TIMP-3 is the primary physiological inhibitor of ADAM17, it can regulate local ADAM17-dependent cleavage of the membrane-bound precursor of TNF to its soluble form (Black et al., 1997). Thus it is possible that SFD mutations affect TIMP-3's ability to regulate ADAM17-dependent cleavage of TNF. Impaired ADAM17 inhibition could promote inflammation, which would be reduced by anti-TNF treatments such as adalimumab. The efficacy of adalimumab therapy suggests that SFD may have an inflammatory components, at least in this patient.

To my knowledge, only one study has investigated the ability of TIMP-3 variants to inhibit ADAM17 (Fogarasi et al., 2008). WT mouse liver extracts were treated with increasing concentrations of recombinant WT and S179C TIMP-3, expressed from *E. coli* and refolded on a metal affinity chromatography column. ADAM17 activity, as measured by hydrolysis of a fluorogenic substrate, was blocked to a similar extent by WT and S179C TIMP-3, indicating no change in inhibition was induced by this SFD mutation. The authors do point out that their TIMP-3 preparations may contain some incorrectly folded material and this may undermine their conclusions; this is indeed possible as TIMP-3's tertiary structure contains 6 intramolecular disulfide bonds. Overall, the ability of SFD TIMP-3 mutants to inhibit ADAM17 has not been extensively profiled.

More recent evidence from hiPSC-RPE models further indicates a role for inflammation in SFD pathogenesis. An increase in expression of complement genes such as *C1R*, *C1S* and *C3*, as well as increased levels of *MCP1/CCL2* have been identified in hiPSC-RPE cells expressing S204C TIMP-3 (Galloway et al., 2017; Hongisto et al., 2020), all of which indicate inflammation. Changes in the expression of complement genes have previously linked inflammation with AMD – *CFH* is heavily associated with AMD pathogenesis (Edwards et al., 2005; Hageman et al., 2005; Klein et al., 2005) and treatment of RPE cells with TNF has been shown to downregulate *CFH* expression (Chen et al., 2007). Thus, it is possible that dysregulation of the complement pathway may also drive SFD pathogenesis. Furthermore, monocyte chemoattractant protein-1 (*MCP1/CCL2*) has been shown to have increased expression by retinal Müller cells under stressful high light exposure conditions (Rutar et al., 2011), attracting macrophages expressing chemokine receptor type 2 to sites of retinal damage. It may be these macrophages

that produce higher levels of TNF due to reduced inhibition of ADAM17-dependent shedding by SFD TIMP-3 variants, although as stated above, reduced ADAM17 inhibition is not supported by the currently available literature (Fogarasi et al., 2008). Further examination of local and systemic inflammatory responses in SFD patients and murine models is thus warranted, ideally over the course of SFD pathogenesis to capture changes as SFD TIMP-3 accumulates in the retina.

### 1.5.6 Extraocular effects of SFD mutations

Given that TIMP-3 is expressed widely, having particularly high expression in the lung, adipose tissue and the synovium (Apte et al., 1994a; Leco et al., 1994), it seems likely that SFD patients would also present with effects in other tissues. It has been reported that members from 2 families expressing the Y191C variant also have pulmonary pathology despite no previous history of emphysema (Meunier et al., 2016). Other SFD patients being referred for lung function tests have been found to be normal (Tsokolas et al., 2018). In the latter study, patients referred for lung function were also referred for bone densitometry tests, with these yielding normal results (Tsokolas et al., 2018). The second group of 2 patients examined had a different mutation in TIMP-3, namely the S204C variant, thus it could be that SFD can have extraocular effects but that these vary depending on the specific SFD TIMP-3 mutation. Overall, there is currently limited evidence to support extraocular effects of SFD TIMP-3 variants, suggesting the retina is the most affected site.

**Table 1.6: Glycosylation state of SFD TIMP-3 mutants, their apoptotic activity and other properties.**

Mutation	Glycosylation	Apoptotic activity	Other
Leu10His & Gly12Arg	More highly glycosylated than WT TIMP-3 in cytoplasmic, membrane and nuclear extracts of HEK-293 cells (Guan et al., 2022)		Impaired secretion of both in HEK-293 cells (Guan et al., 2022)
Cys24Arg Ser38Cys	Increased glycosylation detected in one patient fibroblast sample (Naessens et al., 2019)		Possible aberrant intramolecular disulfide bonds between S38C and Cys36 (Naessens et al., 2019) Impaired secretion in HEK-293 cells (Guan et al., 2022)
Intron 4/Exon 5 Splice Site			
Ser149Cys			
Tyr151Cys			
Glu162STOP			

<b>Glu162Lys</b>			No effect on MMP-2/9 expression – (Arris et al., 2003)
<b>Tyr174Cys</b>			
<b>Tyr177Cys</b>			
<b>Ser179Cys</b>	Bound to ECM of porcine aortic endothelial cells mainly in a glycosylated form vs WT TIMP-3 which was present in an unglycosylated form. Deglycosylation promoted aggregation at higher MW in the ECM, reduced MMP inhibition and increased MMP secretion (Qi & Anand-Apte, 2022)	Overexpression caused more cell death than WT TIMP-3 in primary RPE cells (Majid et al., 2002)	ARPE-19 cells expressing S179C had decreased adhesion to laminin, increased migration and invasive potential (Qi et al., 2002) Change in cellular morphology and metabolism in patient fibroblasts. No effect on MMP-2/9 expression (Soboleva et al., 2003) Unimpaired inhibition of ADAM17 & ADAMTS4/5. MMP-2 protein expression unchanged in chondrocyte cultures as measured by zymography (Fogarasi et al., 2008)
<b>His181Arg</b>	No difference vs WT TIMP-3 (Lin et al., 2006)		No unpaired cysteine residue.
<b>Tyr182Cys</b>			
<b>Gly189Cys</b>			
<b>Gly190Cys</b>		Overexpression caused more cell death than WT TIMP-3 in primary RPE cells (Majid et al., 2002)	
<b>Tyr191Cys</b>	Bound to ECM of porcine aortic endothelial cells mainly in a glycosylated form vs WT TIMP-3 which was present in an unglycosylated form. Deglycosylation promoted aggregation at higher MW in the ECM, reduced MMP inhibition and increased MMP secretion (Qi & Anand-Apte, 2022)	Overexpression caused more cell death than WT TIMP-3 in primary RPE cells (Majid et al., 2002)	Two patients with Y191C variant presented with lung pathology (Meunier et al., 2016)
<b>Ser193Cys</b>			
<b>Tyr195Cys</b>			
<b>Trp198Cys</b>			
<b>Ser204Cys</b>	45-55kDa bands showed a similar pattern of glycosylation to WT TIMP-3 in BHK cells (Yeow et al., 2002)	Overexpression caused more cell death than WT TIMP-3 in primary RPE cells (Majid et al., 2002)	Basolateral accumulation of S204C within hiPSC-RPE cells rather than accumulation in the ECM (Hongisto et al., 2020) Increased levels observed in hiPSC-RPE and their ECM. S204C hiPSC-RPE were more susceptible to oxidative stress and had altered metabolism (Engel et al., 2022) Clinical improvement in patient treated with anti-TNF biologic, adalimumab (Spaide, 2021) Patients reported to have normal lung function and bone density (Tsokolas et al., 2018)

## 1.6 Why does TIMP-3 accumulate in SFD?

Accumulation of TIMP-3 in the BrM is a classic hallmark of SFD (Betts & Troeberg, 2024; Christensen et al., 2017) with extracellular accumulation of TIMP-3 observed in SFD patients (Chong et al., 2000), mouse models of SFD (Weber et al., 2002), as well as *in vitro* in cell lines and hiPSC-RPE models (Engel et al., 2022; Galloway et al., 2017; Langton et al., 2005; Majid et al., 2007; Soboleva et al., 2003; Yeow et al., 2002).

Despite this well-characterised extracellular accumulation of TIMP-3 protein in SFD, TIMP-3 mRNA levels are not elevated in SFD patients (Chong et al., 2003), indicating that accumulation may be due to dysregulated post-translational regulation of TIMP-3.

As detailed below, TIMP-3 abundance is tightly regulated at several levels, including epigenetic regulation by promoter methylation, transcriptional regulation by cytokines and growth factors, post-transcriptional regulation by miRNAs, as well as post-translational regulation by ECM binding and receptor-mediated endocytosis and lysosomal degradation (Spanò & Scilabria, 2022) (**Figure 1.5**).

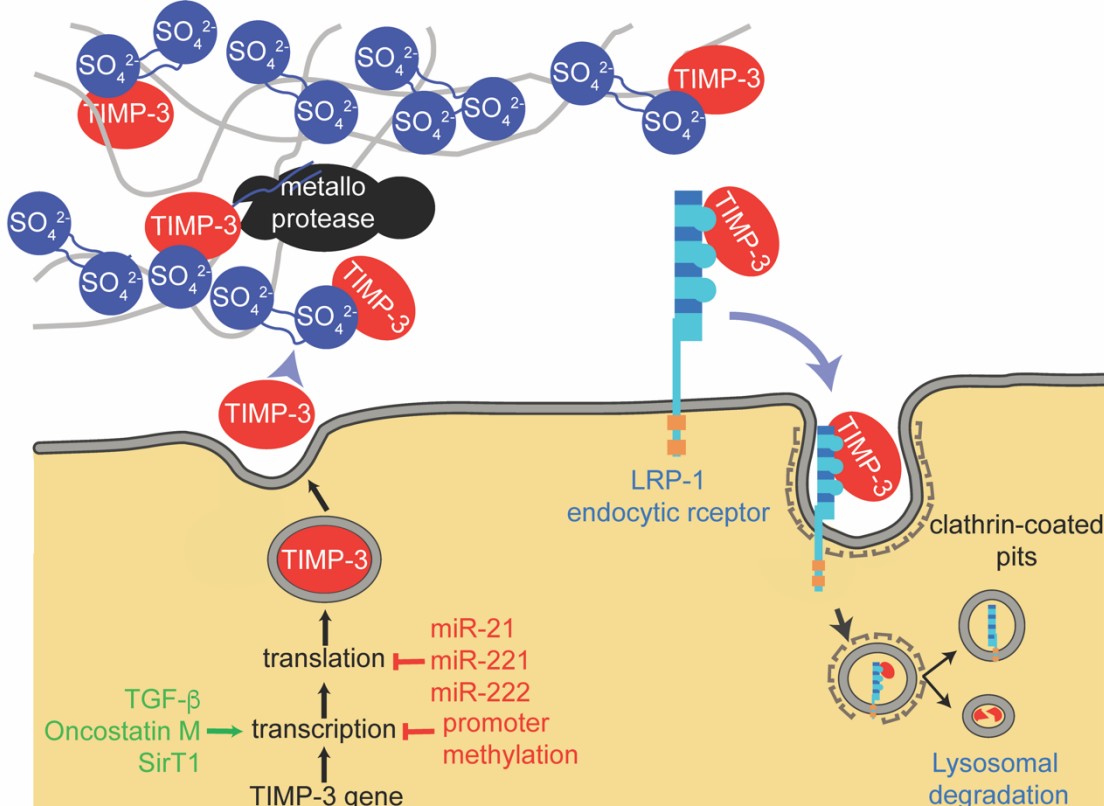


**Figure 1.5: Summary of the regulatory mechanisms determining TIMP-3 expression.** Expression of *TIMP3* can be stimulated or repressed at the transcriptional level, as well as post-transcriptionally by several miRNAs. A large portion of TIMP-3 expression levels is determined post-translationally by the balance between binding to HS in the ECM or endocytosis and lysosomal degradation.

## 1.6.1 Mechanisms regulating TIMP-3 abundance

### 1.6.1.1 Transcriptional regulation

*TIMP3* expression in chondrocytes has been observed to be stimulated by TGF- $\beta$ , which signals through the ERK/MAPK signalling pathway, resulting in the phosphorylation of the Sp-1 transcription factor, allowing it to bind to the *TIMP3* promoter (Qureshi et al., 2005). A distinct signalling pathway involving Smad-2, -3 and -4 and the phosphatidylinositol 3-kinase/Akt signalling pathway has also been shown to result in TGF- $\beta$ -induced upregulation of *TIMP3* in human chondrocytes (Qureshi et al., 2007). *TIMP3* expression is also induced by oncostatin M via the JAK/STAT signalling pathway (Li et al., 2001). Conversely, *TIMP3* expression is suppressed by viral proteins and mutant tumour suppressor genes, including viral proteins from Epstein-Barr virus and mutant p53 (Spanò & Scilabria, 2022).

### 1.6.1.2 Post-transcriptional regulation

Several miRNAs, including miR-21, miR-181b, miR-206 miR-221 and miR-222 can bind to the 3'-untranslated region of TIMP-3 mRNA and result in transcript degradation (Spanò & Scilabria, 2022). miR-21 is upregulated in many tumours, and it facilitates tumour invasion by inhibiting TIMP-3 expression (Gabriely et al., 2008; Song et al., 2010; Wang et al., 2010). miR-21 is also implicated in downregulating TIMP-3 expression in physiological conditions such as wound healing (Yang et al., 2011). Further post-transcriptional regulation of *TIMP3* mRNA is not well documented, however the overall mRNA expression of *TIMP3* is reduced in SFD (Chong et al., 2003). Whether this is due to less transcription or reduced stability of *TIMP3* mRNA is not known but raises the possibility of further post-transcriptional regulation.

### 1.6.1.3 Post-translational regulation

*TIMP-3* protein levels can be regulated by secretion, which controls the levels of *TIMP-3* in the ECM and cellular compartments. For example, RPE cells display polarised secretion of *TIMP-3*, with more secretion occurring at the basolateral face (Hongisto et al., 2020), indicating that there are mechanisms regulating *TIMP-3* secretion to different membrane compartments. Additionally, impaired secretion has been reported for the SFD S204C *TIMP-3* protein (Hongisto et al., 2020), with significantly more detectable in the cell layer, which may be targeted for proteasomal degradation as suggested by Alsaffar. (2017).

Furthermore, TIMP-3 can be regulated post-translationally by endocytosis and lysosomal degradation via the scavenger receptor LRP1 (Scilabria et al., 2013). This has been demonstrated in several cell types, including chondrosarcoma cell lines and primary human macrophages (Doherty et al., 2016; Schubert et al., 2019; Scilabria et al., 2013). Furthermore, Scilabria et al. (2013) showed that there are LRP-independent pathways of TIMP-3 endocytosis, although analysis of LRP1 null PEA-13 cells demonstrated that these contribute less to TIMP-3 endocytosis than LRP1, at least in mouse embryonic fibroblasts (MEFs). TIMP-3 can be endocytosed alone or in complex with other ligands such as the metalloproteinases that TIMP-3 targets (Carreca et al., 2020). For example, TIMP-3-MMP-1 complexes have a 7-fold higher affinity for LRP1 than MMP-1 alone (Carreca et al., 2020). TIMP-3 preferentially binds to the N-terminal domain of ligand binding cluster II of LRP1 (Scilabria et al., 2017), with lysine residues ~21 Angstroms apart (e.g., K26A/K45A or K42A/K110A) on a basic patch of TIMP-3 mediating this interaction (Doherty et al., 2016). LRP-resistant TIMP-3 mutants were shown to have longer half-lives in cartilage and to inhibit ADAMTS-mediated cartilage degradation more effectively. The ectodomain of LRP1 can be shed by proteases including ADAM10 and ADAM17 (Liu et al., 2009), with shed LRP1 able to bind to TIMP-3 and prevent its endocytosis (Scilabria et al., 2013). In macrophages, this shedding is induced by LPS, and is thought to cause a time-dependent increase in TIMP-3 levels that inhibits ADAM17-mediated TNF release (Schubert et al., 2019). Additionally, as discussed in **1.4.3.3**, TIMP-3 can bind to cell surface and ECM HS, which blocks its binding to LRP1 and so inhibits its endocytosis (Scilabria et al., 2013; Troeberg et al., 2014). Thus, TIMP-3 protein abundance is regulated by the balance between its endocytosis via LRP1 and binding to extracellular or pericellular HS. This balance is thought to be dysregulated in diseases such as osteoarthritis, where there is a decrease in extracellular TIMP-3 (Morris et al., 2010), leading to increased cartilage degradation mediated by enzymes such as ADAMTS-5 and MMP-13. Altered endocytosis or extracellular/pericellular HS-binding of TIMP-3 could also be involved in SFD pathogenesis, with a decrease in endocytic uptake of TIMP-3 and/or an increase in HS binding leading to extracellular accumulation of TIMP-3.

## 1.7 The scavenger receptor LRP1

### 1.7.1 LRP1 structure and biological function

LRP1 is a large endocytic and signalling receptor that is a member of the low-density lipoprotein receptor superfamily. LRP1 exhibits almost ubiquitous expression with particularly high expression in the brain, lung and liver (May et al., 2007), as well as RPE cells (Hollborn et al., 2004a). The active protein of LRP1 arises from a 600 kDa precursor protein that is processed by furin in the Golgi apparatus into a C-terminal 85 kDa membrane-bound portion containing the transmembrane and cytoplasmic domains, and an N-terminal 515 kDa portion that forms the extracellular domain of LRP1 and is responsible for interacting with extracellular ligands (May et al., 2007). Structurally, LRP1 is similar to other members of the low-density lipoprotein receptor superfamily and consists of several domains including cysteine-rich ligand-binding repeats, epidermal growth factor repeats,  $\beta$ -propeller domains, along with transmembrane and cytoplasmic domains, including 2 NP<sub>x</sub>Y motifs, 1 Y<sub>xx</sub>L motif and 2 di-leucine motifs (Figure 1.6).

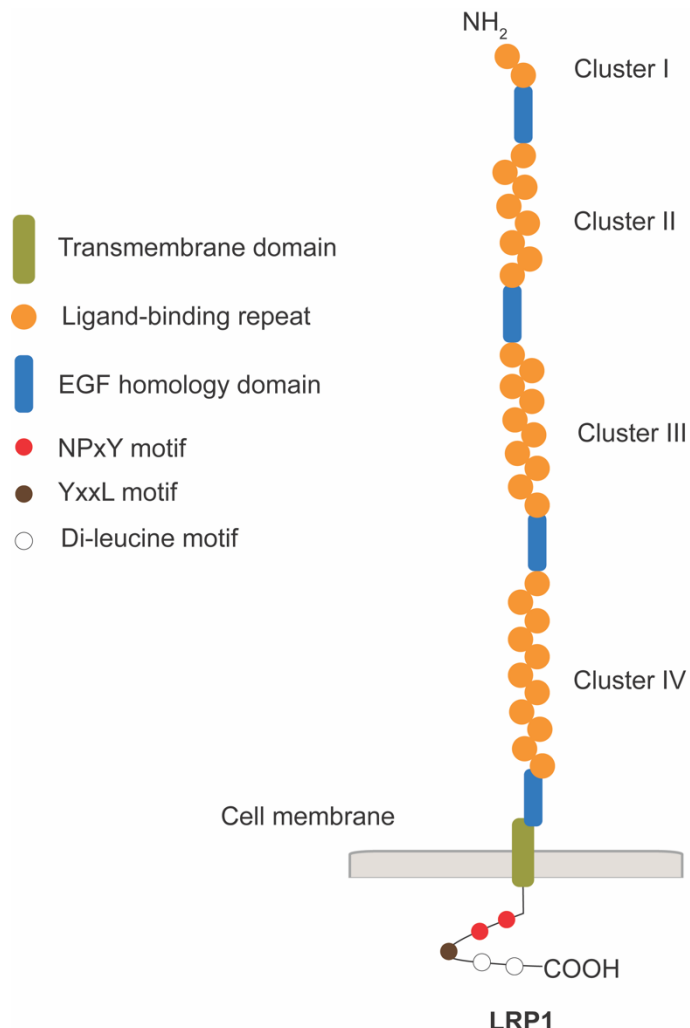


Figure 1.6: Main domain and motif structures of LRP1.

The domain structures of LRP1 includes cysteine-rich ligand-binding repeats, EGF homology domains comprised of epidermal growth factor repeats and  $\beta$ -propeller domains, as well as a transmembrane domain. Intracellularly LRP1 has 2 NPxY motifs, one YxxL motif and 2 di-leucine repeats.

LRP1 was discovered as having an endocytic role in the late 1980s and early 1990s. The prototypic LRP1 ligand is activated  $\alpha_2$ -macroglobulin, which is endocytosed by LRP1 following proteolysis of its bait region (Holtet et al., 1994; Jensen et al., 1989; Kristensen et al., 1990).

Several studies including with more recent proteomic approaches have demonstrated that LRP1 interacts with over 100 ligands via its extracellular domain (Bres & Faissner, 2019; Mogensen et al., 2022; Yamamoto et al., 2022). These ligands are very diverse and include lipoproteins, ECM proteins, growth factors, proteases and their inhibitors and cytokines, e.g., apolipoprotein E, lipoprotein lipase, heat-shock protein-96, MMP-2, MMP-9, MMP-13, ADAMTS-5, TIMP-1, TIMP-2 and TIMP-3 (Knauer et al., 1996; Scilabria et al., 2013; Thevenard et al., 2014; Willnow, 1999; Yamamoto et al., 2013). Specifically in the human cornea, LRP1 has been shown to interact with a variety of ligands including annexin A4, apolipoprotein E, serotransferrin and serum amyloid P-component, implicating LRP1 in exocytic and transport pathways in the eye (Mogensen et al., 2022). Additional LRP1 was demonstrated to interact with complement C3, C4-A and C4-B, as well as immunoglobulins, and high mobility group protein B1, demonstrating that LRP1 is involved in regulating immune responses in the cornea (Mogensen et al., 2022).

LRP1 is known to bind to a diverse array of ligands, raising the question of how it achieves specific binding to these. The sheer number of complement type repeats (31) in LRP1, along with different modes of ligand binding (i.e., direct and indirect) are thought to enable LRP1 to selectively bind to its many ligands. Activated  $\alpha_2$ -macroglobulin and tissue type plasminogen activator are known to bind directly to LRP1, but other ligands such as amyloid- $\beta$ -peptides and factor VIII are thought to initially bind with low affinity to GAG chains of cell surface HSPGs, which then 'pass on' these ligands to LRP1 (Kanekiyo et al., 2011; Sarafanov et al., 2001). Furthermore, there is also evidence that some ligands bind to GAG chains of HSPGs with high affinity and the ligand/GAG complex then binds to LRP1 – this is the case for sonic hedgehog protein in complex with the GAG chains of glycan-3 (Capurro et al., 2012).

The N-terminal extracellular region of LRP1 contains distinct ligand-binding clusters, named I, II, III and IV that are separated by EGF repeats (**Figure 1.6**). These ligand-binding clusters contain, 2, 8, 10 or 11 ligand-binding repeats. In each ligand-binding repeat, three aspartic acid residues create an acidic pocket that enables electrostatic interactions with lysine residues on the ligand (Fisher et al., 2006). For example, structural studies with the chaperone protein, receptor associated protein (RAP), in complex with LRP1 have revealed that lysine residues ~ 21 Angstroms apart are critical for binding to ligand-binding repeats of LRP1 and mutation of these residues abolished binding of RAP to LRP1 (Dolmer et al., 2013; Jensen et al., 2006; Van Den Biggelaar et al., 2011). Lysine residues 21 Angstroms apart on TIMP-3 have also been shown to be critical for its binding to LRP1 (Doherty et al., 2016). Furthermore, TIMP-3 has been shown to bind to cluster II of LRP1 (Scilabria et al., 2017) and indeed clusters II and IV are thought to bind most LRP1 ligands.

To prevent LRP1 from associating with ligands during the secretory pathway, LRP1 associates with the chaperone protein RAP, which is able to bind strongly to all ligand-binding domains and can be used experimentally to block endocytosis of ligands such as TIMP-3 (Doherty et al., 2016; Scilabria et al., 2013), as well as to identify new ligands that bind to LRP1 (Mogensen et al., 2022; Yamamoto et al., 2022).

It is noteworthy that LRP1 mediates the endocytosis of many ECM proteins, including MMPs, ADAMTSs and TIMPs as discussed above, demonstrating that LRP1 regulates ECM turnover. This is highlighted in disease processes such as osteoarthritis where a reduced LRP1 expression leads to a greater extracellular presence of proteases such as ADAMTS-5 and MMP-13 and increased ECM degradation (Yamamoto et al., 2017).

In addition to its well-documented endocytic role, LRP1 is also known to participate in signalling. The cytoplasmic domain of LRP1 is composed of ~ 100 amino acids and includes 2 NPxY and 2 dileucine repeats which participate in intracellular signalling. Binding of extracellular ligands to LRP1 can induce phosphorylation of the tyrosine residue in the NPxY motifs, resulting in modulation of signalling pathways such as the mitogen-activated protein kinase pathway (Barnes et al., 2001; Hu et al., 2006; Muratoglu et al., 2010). Furthermore,  $\gamma$ -secretase is an

intramembrane protease that is involved in cleaving the intramembrane domain of LRP1 in a process called regulated intramembrane proteolysis (Kinoshita et al., 2003). The released intracellular domain of LRP1 can translocate to the nucleus where it can bind transcription factors, including the IRF3 transcription factor, and modulate transcription (Zurhove et al., 2008).

LRP1 knockout mice have been generated with embryonic homozygous knockout of LRP1 being lethal (Herz et al., 1992), demonstrating the critical role of LRP1 in development. Thus, various inducible or heterozygous LRP1 knockout mice have also been generated. These studies reveal altered metabolism in different cell types including endothelial cells (Mao et al., 2017) and neurons, as well as altered lipid handling (Liu et al., 2010), highlighting the key roles of LRP1 in both signalling and endocytosis. Aberrant lipid handling has also been observed in adipocyte-specific LRP1 knockout mice, leading to the development of inflammation and atherosclerosis (Konaniah et al., 2017). Additionally, conditional LRP1 knockout mice have revealed the importance of LRP1 in the regulation of bone mass and cartilage development (Lu et al., 2018; Yan et al., 2022).

### **1.7.2 Mechanisms and regulation of LRP1-mediated endocytosis**

Endocytosis is a process by which cells take up extracellular materials, including nutrients, receptor-ligand complexes, fluids, cell debris and microorganisms. Endocytic pathways are broadly divided into two major categories, clathrin-dependent and clathrin-independent pathways. The classically defined mechanism of endocytosis is mediated via a clathrin-dependent pathway, which includes LDL receptors (Doherty and McMahon, 2009) and LRP1 is now known to mediate the internalisation of ligands via clathrin-coated pits (Lillis et al., 2005). However, there are a wide variety of clathrin-independent pathways, with endocytic pathways being further subdivided based on their requirement for dynamin. These pathways have been extensively reviewed elsewhere (Doherty and McMahon, 2009; Thottacherry et al., 2019) and are briefly summarised in **Table 1.7**.

**Table 1.7: Summary of endocytic pathways. Based on (G. J. Doherty & McMahon, 2009; Thottacherry et al., 2019).**

Endocytic mechanism	Clathrin-dependent	Dynamin-dependent
Clathrin-mediated	Yes	Yes
Caveolae/caveolin-1-dependent	No	Yes
Clathrin-independent carrier/GPI-AP enriched early endosomal compartment	No	No
Fast endophilin-mediated	No	Yes
Arf6 dependent	No	No
Flotillin dependent	No	No
Phagocytosis	No	Yes
Micropinocytosis	No	No

Clathrin-mediated endocytosis controls the endocytosis of receptor-ligand complexes. Endocytic receptors contain specific sequences in their cytoplasmic domains (NPxY motifs in the case of LRPCs) that are recognised by adaptor proteins, including assembly polypeptide 2 (Smith et al., 2017). Upon ligand binding to the receptor, this initiates the recruitment of clathrin via adaptor proteins and polymerisation to form clathrin-coated pits. To aid in the invagination of the membrane and the formation of membranous vesicles, there is bending of local portions of the membrane that is stabilised by curvature sensing/curvature stabilising Bin-amphiphysin-RVS domain-containing proteins (Thottacherry et al., 2019). A large GTPase, dynamin, is recruited at the neck of a clathrin-coated pit and via GTP hydrolysis causes vesicle scission, allowing intracellular release of clathrin-coated vesicles (Thottacherry et al., 2019). Clathrin is subsequently removed from the vesicle by HSC70 (Cho et al., 2015), which allows the uncoated vesicle to fuse with the target-sorting endosome, discussed below.

Uncoated vesicles carrying cargo fuse with early endosomes via proteins that promote vesicle fusion such as Rab-5, SNARE proteins and early endosome antigen 1 (Cho et al., 2005; Dumas et al., 2001). Early endosomes act as a major sorting hub and receive cargo from the clathrin-mediated pathway, as well as other endocytic pathways. Early endosomes localise to the periphery of the cytoplasm and recruit a ‘Retromer’ component to the cytosolic surface which is comprised of sorting nexins and associated proteins to facilitate retrieval of cargoes or receptors from endosomes to the plasma membrane or the trans-Golgi network for re-use (Keeling et al., 2018). As early endosomes mature, there is a progressive acidification of their lumen, which is achieved by vacuolar ATPases in the membrane

bilayer, which pumps hydrogen ions into the vacuole lumen (Elkin et al., 2016; Maxson & Grinstein, 2014). Intraluminal vesicles also form which alongside early endosomes can mature to late endosomes (Keeling et al., 2018). Progressive acidification of the lumen causes dissociation of ligands from their receptors, allowing receptors to be recycled back to the plasma membrane or the Golgi apparatus and for ligands to be sorted towards late endosomes for degradation (Hsu & Prekeris, 2010). Other key hallmarks of endosomal maturation involve a 'Rab' conversion from Rab-5 to Rab-7, which are commonly used markers to distinguish between early and late endosomes, as well as progressive movement of endosomes from the cell periphery along microtubules towards the outer nuclear region where lysosomes reside (Keeling et al., 2018). Late endosomes express a variety of Rab proteins, including Rab-4, -8, -10, -11, -13 and -22a, which refines sorting of cargoes to specific lysosomal compartments and also sort receptors to specific recycling endosomes returning to the plasma membrane (Hsu & Prekeris, 2010). Delivery of late endosomes to lysosomes achieves degradation of ligands, for which lysosomes are well equipped as they contain over 50 lysosomal membrane proteins including a variety of transporters, as well as 60 different hydrolytic enzymes. The highly acidic environment of lysosomes results in degradation and yields products such as monosaccharides, amino acids and free fatty acids (Perera & Zoncu, 2016).

LRP1-mediated endocytosis has complex regulation beginning with initial internalisation that occurs at clathrin-coated pits. The intracellular domain of LRP1 is vital for internalisation of ligands and NPxY, YxxL and di-leucine motifs have been shown to participate in the rapid endocytosis of LRP1 (Deane et al., 2008). Mutation of NPxY motifs reduces ligand internalisation (Roebroek et al., 2006) but alternatively, the YxxL motif has been suggested to be the dominant endocytosis signal for LRP1 (Li et al., 2000). It is not entirely clear how these intracellular motifs of LRP1 facilitate internalisation, however they are capable of interacting with a variety of adaptor and scaffold proteins which are likely to mediate this. Internalised ligands are ultimately delivered to lysosomes where they are degraded with LRP1 recycled back to the cell membrane. Conversely, LRP1 can also be degraded, thus providing a mechanism by which the cell surface levels of LRP1 can be controlled (Bres & Faissner, 2019).

LRP1-mediated internalisation can also be regulated by the distribution of LRP1 in the membrane. In certain cell types (e.g., vascular smooth muscle cells (Weaver et al., 1996)), LRP1 locates exclusively to clathrin-coated pits, however in other cell types (e.g., human fibroblasts and neurons (Laudati et al., 2016)), LRP1 localises to clathrin-coated pits but also areas that are high in cholesterol and sphingolipids, so-called lipid rafts. LRP1 internalisation via a caveolin-dependent pathway has been reported to occur in lipid rafts in hepatic cells and MEFs (Kanai et al., 2014). Additionally, LRP1 has been seen to concentrate at the site of cilia assembly in chondrocytes and disruption of the cilia protein intraflagellar transport 88 (IFT88) impairs the localisation of LRP1 and LRP1-mediated endocytosis of proteases such as ADAMTS-5 and MMP-13 (Coveney et al., 2018). Here we see that the distribution of LRP1 in the cell membrane varies depending on cell type.

LRP1-mediated endocytosis is also regulated by proteolytic shedding of the ectodomain portion of LRP1, releasing a soluble form of the receptor. Typically, LRP1 is cleaved at the membrane-proximal site to release the 515 kDa  $\alpha$  chain (termed shed LRP1, sLRP1), with a 55 kDa extracellular portion of the  $\beta$  chain remaining on the cell surface. sLRP1 is able to bind ligands and so can competitively inhibit endocytosis of ligands, including TIMP-3 (Scilabre et al., 2013). The shedding of LRP1 thus reduces endocytosis by reducing the number of endocytic receptors available on the cell surface and also by generating a decoy receptor that binds to and prevents endocytosis of ligands. Several proteases have been proposed to shed LRP1, and this is dependent on cell type. For example, ADAM10 and ADAM17 have been shown to mediate shedding of LRP1 in MEFs, as well as in the brain (Q. Liu et al., 2009), while ADAM17 and MMP-14 are involved in LRP1 shedding in chondrocytes (Yamamoto et al., 2017). Interestingly, LRP1 shedding is reportedly stimulated by binding of ligands, including tissue plasminogen activator (tPA), RAP and calreticulin (Brifault et al., 2017; Polavarapu et al., 2007). However, the mechanism by which these ligands stimulate or mediate shedding is not known.

### 1.7.3 Other LRP<sub>s</sub>

LRP1b is a close homologue of LRP1, and they share a very similar domain structure, including a 59 % identical amino acid sequence (Knisely et al., 2007). LRP1b also has well-reported endocytic functions, sharing many of the same ligands as LRP1, including urokinase plasminogen activator and tPA (Haas et al.,

2011; C. X. Liu et al., 2001). Despite sharing many of the same ligands as LRP1, LRP1b is reported to mediate a slower rate of endocytosis (Knisely et al., 2007).

LRP2, also called megalin, is a 600 kDa protein and is the largest of the LRP family of receptors. LRP2 has a well-characterised endocytic role and is involved in internalisation of vitamins/vitamin binding complexes, hormones, lipoproteins (May et al., 2007) and also protease/inhibitor complexes, including TIMP-2: proMMP-2 (Johanns et al., 2017). LRP2 has also been shown to internalise the signalling factor BMP4. LRP2 is important for reabsorption of vitamins in the kidney, highlighted by loss of LRP2 resulting in increased excretion of 25-hydroxy-vitamin D in the urine (Nykjaer et al., 1999). Interestingly, RPE cells also express LRP2 (Storm et al., 2014), however its role in these cells is not defined, although it is likely to be involved in endocytosis.

Briefly, other LRP receptors include LRP4, LRP5 and LRP6, which have signalling roles. LRP4 has been proposed to modulate signalling pathways that regulate development of limbs. This is highlighted by the fact that homozygous *LRP4*-null mice exhibit reduced overall growth, and fusion and duplication of digits on the fore and hind limbs (Johnson et al., 2005). LRP5 and LRP6 are well documented to be involved in Wnt signalling (Ren et al., 2021), which is reflected in *LRP5/6*-null mice having severely impaired development of the gut (Zhong et al., 2012) and also impaired gastrulation (Kelly et al., 2004).

There are also many other members of the LRP superfamily, including LRP8, 10, 11, 12, as well as related receptors including low density lipoprotein receptor class a domain containing (LDLRAD) 1, 2 and 3. Endocytic properties of these is less well explored.

## 1.8 Hypotheses and aims of the project

TIMP-3 is known to accumulate extracellularly in the BrM in SFD (Chong et al., 2000; Engel et al., 2022; Galloway et al., 2017; Langton et al., 2005; Soboleva et al., 2003; Yeow et al., 2002) and SFD TIMP-3 mutants have been shown to be more stable in the ECM (Majid et al., 2007) and to have impaired turnover by RPE cells (Langton et al., 2005). TIMP-3 has been shown to be endocytosed by various cell types, including chondrocytes, primary human macrophages and also mouse embryonic fibroblasts (Doherty et al., 2016; Schubert et al., 2019; Scilabria et al., 2013) with

this process mediated primarily by LRP1 (Scilabra et al., 2013). TIMP-3 is also able to bind to sulfated GAG chains, such as HS that are present on proteoglycans (Troeberg et al., 2014; Yu et al., 2000) with perlecan, and agrin being abundantly expressed in the BrM (Keenan et al., 2012).

I hypothesise that SFD TIMP-3 mutations impair the trafficking of mutant TIMP-3 between HSPGs in the BrM and endocytosis via LRP1 on the cell surface of RPE cells, resulting in accumulation of SFD mutant TIMP-3. More specifically, I predict that SFD TIMP-3 mutants have impaired LRP1-mediated endocytic clearance by RPE cells.

Therefore, I aimed to:

- 1) Express and isolate WT and SFD TIMP-3 proteins from a mammalian expression system (Chapter 3) and investigate some of the broader effects of SFD TIMP-3 mutants on RPE cells, including effects on gene expression (Chapter 4).
- 2) Investigate whether RPE cells endocytose WT and the 3 SFD TIMP-3 mutants H181R, Y191C and S204C (Chapter 5).
- 3) Investigate whether internalisation of SFD TIMP-3 mutants H181R, Y191C and S204C by RPE cells was impaired compared to WT TIMP-3 (Chapter 5).
- 4) Determine whether LRP1 is responsible for WT TIMP-3 uptake by RPE cells (Chapter 6).

## **Chapter 2: Materials and methods**

## 2.1 Materials

### 2.1.1 General chemicals

General laboratory chemicals used are listed in **Table 2.1**.

**Table 2.1: General chemicals and their manufacturers.**

Reagent	Manufacturer
Protease inhibitor cocktail tablets	Merck
Acetic acid (glacial, $\geq 99\%$ )	ThermoFisher
Bromophenol blue	Merck
Coomassie brilliant blue	Merck
Ethanol	VWR
Glycerol	ThermoFisher
Hydrochloric acid	ThermoFisher
Isopropanol (propan-2-ol)	ThermoFisher
Methanol	ThermoFisher
Phosphate buffer saline (PBS)	In-house
Triton X-100	Merck
Gelatin	Acros Organics
Ammonium chloride	Merck
Sodium hydroxide (NaOH) 1 M	ThermoFisher
Formaldehyde solution 4 %, pH 6.9	Merck
Sodium chloride (NaCl) $\geq 99.5\%$	ThermoFisher
Bradford reagent	Merck

## 2.1.2 Disposable plastics

Disposable labware used is listed in **Table 2.2**.

**Table 2.2: Disposable labware and their manufacturers.**

Labware	Manufacturer
Cell strainer (40 µm)	Greiner Bio
Vacuum filter (0.22 µm)	Corning
Cell scraper (1.8 cm blade)	Corning
Cryovials	Corning
Tissue culture plates (96-well, 12-well, 6-well)	Corning
10 cm tissue culture plate	Greiner Bio
15 cm tissue culture plate	ThermoFisher
10 cm petri dishes	Sarstedt
96-well plate (clear bottom, opaque walls)	ThermoFisher
384-well RT-qPCR plates	Armadilo, ThermoFisher
Pipetting tips (10 µl, 200 µl, 1000 µl)	Sarstedt
Sterile stripettes (5 ml, 10 ml, 25 ml)	Sarstedt
Microcentrifuge tubes (0.5 ml, 1.5 ml, 2 ml)	Eppendorf
Protein LoBind Tubes (1.5 ml)	Eppendorf
Sterile syringes (10 ml)	ThermoFisher
Sterile tubes (15 ml, 50 ml)	Sarstedt
Sterile filter (0.22 µm)	ThermoFisher
PD-10 column	GE Healthcare

### 2.1.3 Cultured cells and cell culture reagents

HEK-293, ARPE-19, PEA-13 (*Pseudomonas aeruginosa* antigen-selected) and mouse embryonic fibroblast (MEF) cells were acquired from laboratory stocks, after original purchase from American Type Culture Collection. hTERT RPE-1 cells were a gift from Professor Simon Clark (University of Tübingen, Germany). ARPE-19 and hTERT RPE-1 cells are classified as normal, having no disease phenotype, by the American Type Culture Collection. **Table 2.3** summarises cell culture reagents used.

**Table 2.3: Cell culture reagents.**

Reagent	Manufacturer (Distributor)
DMEM (4.5 g/L D-Glucose, L-Glutamine, no pyruvate)	Gibco, catalogue #41965-039
Heat-inactivated foetal bovine serum (FBS)	Merck
Penicillin (10 000 U/ml) - streptomycin (10 000 µg/ml)	Merck
Sodium pyruvate (100 mM)	Gibco
Opti-MEM	Gibco
Hygromycin B solution (50 mg/ml)	Gibco
Sodium chlorate	Acros Organics
Primocin solution (50 mg/ml)	InvivoGen
Phosphate-buffered saline (PBS) tablets	ThermoFisher
Dimethyl sulfoxide (DMSO)	ThermoFisher
0.25 % Trypsin-ethylenediaminetetraacetic acid (1 x) (Trypsin-EDTA)	Gibco
Cell dissociation solution	Gibco
Lipofectamine LTX transfection reagent	Invitrogen (ThermoFisher)
Lipofectamine 3000 transfection reagent	Invitrogen (ThermoFisher)
jetPRIME transfection reagent	Polyplus (Sartorius)

## 2.1.4 SDS-PAGE and immunoblotting reagents

Reagents used for SDS-PAGE and immunoblotting are detailed in **Table 2.4**.

**Table 2.4: SDS-PAGE and immunoblotting reagents.**

Reagent	Manufacturer
30% (w/v) acrylamide/bis-acrylamide	Severn Biotech
2-amino-2-methyl-1,3-propanediol N,N,N',N'-tetramethylethylenediamine (TEMED)	ThermoFisher
Ammonium persulfate (APS)	ThermoFisher
Sodium dodecyl sulfate (SDS)	ThermoFisher
PageRuler/PageRuler Plus prestained protein ladder for SDS-PAGE	ThermoFisher
Tris(hydroxymethyl)aminomethane (Tris) base	ThermoFisher
Glycine	ThermoFisher
Trans-Blot Turbo Transfer Buffer	Bio-Rad
Intercept blocking buffer in Tris-buffered saline (TBS)	LiCOR
TBS	In-house
Tween 20	ThermoFisher
Mini-PROTEAN TGX Gels 4-15%	Bio-Rad
Trichloroacetic acid (TCA, 6.1 N solution)	MP Biomedicals
Revert Total Protein Stain	LiCOR
Pierce silver stain kit	ThermoFisher
Immobilon membrane (low fluorescence)	Merck

## 2.1.5 Antibodies and fluorescent stains

The antibodies used and their applications are listed in **Table 2.5**.

**Table 2.5: Antibodies and their applications.**

Antibody	Host species	Manufacturer	Detected by	Application
Anti-FLAG M2 (1°)	Mouse	Merck	RDye 800 CW anti- mouse IgG	Immunoblotting and fluorescence microscopy
Anti-LRP1 8G1 (1°)	Mouse	Abcam	RDye 800 CW anti- mouse IgG	Immunoblotting
Anti-TIMP-3 AB6000 (1°)	Rabbit	Merck	IRDye 680RD anti-rabbit IgG	Immunoblotting
RDye 800 CW anti- mouse IgG (2°)	Goat	LiCOR	N/A	Immunoblotting
IRDye 680RD anti-rabbit IgG (2°)	Goat	LiCOR	N/A	Immunoblotting
Alexa Fluor-488-conjugated anti- mouse IgG (2°)	Goat	Invitrogen ThermoFisher	N/A	Fluorescence microscopy

## 2.1.6 Molecular biology reagents

All reagents used in molecular biology procedures such as site-directed mutagenesis, RNA extraction, DNA extraction, cDNA synthesis and real time quantitative polymerase chain reaction (RT-qPCR) can be found in **Table 2.6**. Primers used for RT-qPCR are summarised in **Table 2.7**. Primers designed for site-directed mutagenesis and sequencing of the pCEP4 plasmid are found in **Table 2.8** and **Table 2.9**, respectively.

**Table 2.6: Molecular biology reagents and their manufacturers.**

Consumable	Manufacturer (Distributor)
RNEasy Kit (RNA extraction kit)	QIAGEN
RNase-Free DNase set	QIAGEN
cDNA synthesis kit	Applied Biosystems
qPCR BIO SyGreen Mix (qPCR mix)	PCR Biosystems
RNase/DNase free water	QIAGEN and Invitrogen (ThermoFisher)
QuikChange site-directed mutagenesis kit	Agilent Technologies
Miller's Luria Broth (LB) base	Invitrogen (ThermoFisher)
LB Agar	Invitrogen (ThermoFisher)
Carbenicillin	ThermoFisher
Plasmid Maxi Kits (DNA extraction kit)	QIAGEN
One Shot TOP10 Chemically Competent <i>E. coli</i>	Invitrogen (ThermoFisher)
Wizard Plus SV Minipreps DNA purification system (DNA extraction kit)	Promega
β-Mercaptoethanol	Merck
Iodoacetamide	ThermoFisher
RNAscope 2.5 HD Duplex reagent kit	ACD Bio, Biotechne
C1 TIMP3 RNAscope probe	ACD Bio, Biotechne catalogue #433101
C2 LRP1 RNAscope probe	ACD Bio, catalogue #836621-C2
LRP1 Silencer Select siRNA	ThermoFisher, catalogue # 4392420
Silencer Select Negative Control siRNA	ThermoFisher, catalogue # 4390843
ON-TARGETplus SMARTpool LRP1 siRNA	Dharmacon, catalogue #L-004721-00-005
ON-TARGETplus Non-targeting pool	Dharmacon, catalogue #D-001810-10-05

**Table 2.7: Human KiCqStart primers (purchased from Merck).**

Gene name	Forward sequence 5'-3'	Reverse sequence 5'-3'
<i>GAPDH</i>	ACAGTTGCCATGTAGACC	TTGAGCACAGGGTACTTTA
<i>LDLR</i>	GAGGACAAAGTAGTTTGGACAG	GTAGGTTTCAGCCAACAAG
<i>vLDLR</i>	GGTTACAAGTGTGAATGTAGTC	CTTCCTCTCTAAGCCAAGTC
<i>LRP1</i>	ACATATAGCCTCCATCCTAATC	GCTTATACCAGAATACCACTC
<i>LRP1b</i>	CAGTCTGTGAGGATTTGTC	TAGTACTGACATCTGTCTCC
<i>LRP2</i>	GCCGATGCATTATCAAAC	TCACATCCATCTTCATCTCC
<i>LRP3</i>	CTGTCTGGTGAACATCTTC	AAGCTGATGGTAATCATGTC
<i>LRP4</i>	AAATCCAAGTTCACTGATCC	CCTCTTCTTATAGCACAGC
<i>LRP5</i>	CAAGATCGAGGTGATCAATG	TCAGTCCAGTAGATGAAGTC
<i>LRP6</i>	AATGTTCATCGAGTGATTG	CTTCATGTCACTGATGAGTTC
<i>LRP8</i>	ACAATATTGAATGGCCAAAC	AAACACAGCTATCCAAAAG
<i>LRP10</i>	AGAACCTTAATGATAACTCAGTG	CACCTCCTGGAGTCATATC
<i>LRP11</i>	GGTGGAAAAGTCTCAGAAAG	AGGAACACTATCTGGCATC
<i>LRP12</i>	CAAGAGTGGAAGCAGAATTG	GCCTGATTAGGTGAACAAAC
<i>LDLRAD3</i>	CTGTATTGACAAGAGCTTCATC	TTCTTGAGAACCTTCACAGC
<i>SORL1</i>	GCATTTAATGAAAGCAGGG	ACGGTGAACGTGTAATTATG
<i>TIMP3</i>	CATGTGCAGTACATCCATAC	AGGTGATACCGATAGTTCAG
<i>MMP1</i>	AAAGGGAATAAGTACTGGGC	CAGTGTTCCTCAGAAAGAG
<i>MMP2</i>	GTGATCTTGACCAGAACATACC	GCCAATGATCCTGTATGTG
<i>MMP3</i>	GCAGTTAGAGAACATGGAG	ACGAGAAATAATTGGTCCC
<i>MMP8</i>	AAGTTGATGCAGTTTCCAG	CTGAACCTCCCTAACATT
<i>MMP9</i>	AAGGATGGGAAGTACTGG	GCCCAGAGAAGAAGAAAAG
<i>MMP13</i>	AGGCTACAACCTGTTCTTG	AGGTGTAGATAGGAAACATGAG
<i>MMP14</i>	ATGGCAAATTCGTCTTCTTC	CGTTGAAACGGTAGTACTTG
<i>ADAM8</i>	CAATGCAGAGTCCAGATG	TTTCTGATATAGCTGTCCAC
<i>ADAM9</i>	AGGTATGACATGATGGGAAG	CATACTATCCAAGTAGTTGCC
<i>ADAM10</i>	CACATGATTCTGGAACAGAG	GTTGTTAACGTTGTCCCCAG
<i>ADAM12</i>	AGTTTACAGACCCTGAAC	TAGAAGCTTCATCTCCTCC
<i>ADAM15</i>	AGCTAATACTCGGGGAAATG	GTCCCATTACATCTATTGTC
<i>ADAM17</i>	CAGATTCGCATTCTCAAGTC	CTAGCAACATCTCACATCC
<i>ADAM19</i>	GTTTCAGAAGAACATCGACGAG	GACCAGAGGGTAGAATATGG
<i>ADAM20</i>	AATGGAACACTGAAAGACAC	TGTCTAGAGCAGAACAGAAC
<i>ADAM28</i>	ATCCAGTGTCTACACCTAAG	CTTGAGTCGAGAGCAAATAC
<i>ADAM30</i>	AACTGTAGCATTGGACTTTG	CCATCCTGCTTATAAACGTC
<i>ADAM33</i>	CCCAGGATACATAGAAACCC	GCAGATAATAGCTGGCATT
<i>IL6</i>	GCAGAAAAAGGCAAAGAAC	CTACATTGCCAAGAGC
<i>TNF</i>	AGGCAGTCAGATCATCTTC	TTATCTCTCAGCTCCACG

GSS	CACAAGCAAGTCCTAAAAGAG	ATGGTGTGATTCGATCTG
<i>GPX1</i>	CTACTTATCGAGAATGTGGC	CAGAATCTCTCGTTCTTGG
SOD1	GAGCAGAAGGAAAGTAATGG	GATTAAGTGAGGACCTGC
SOD2	ATCATAACCCTAATGATCCCAG	AGGACCTTATAGGGTTTCAG
ACAN	CACCCCCATGCAATTGAG	AGATCATCACCAACACAGTC
<i>AGRN</i>	GATCTTCTTGTGAACCCTG	TATCTTCCACACAGAACTCC
<i>HSPG2</i>	CCACTACTTCTATTGGTCCC	GTATTGGATTGGTGGAGATTAC
VCAN	CCAGTGTGAACTTGATTTG	CAACATAACTTGAAGGCAG
<i>COL11A1</i>	ACAAGGT CCTATTGGATACC	CCTTTCACCTTAGATCCC

**Table 2.8: Forward and reverse primers designed for site-directed mutagenesis of TIMP-3 (purchased from Merck).**

Mutant	Primer sequence 5'-3'	Tm (°C)	GC (%)	Base length
E162K	<b>Forward:</b> CCTTGCTTGACTTCCAAGAACAGTGTCTCTGG ACCGACATGCTC  <b>Reverse:</b> GAGCATGTCGGTCCAGAGACACTTGTCTTGGAAAG TCACAAAGCAAGGC	87.1	50.9	51
H181R	<b>Forward:</b> ACCCGGCTACCAGTCCAAACGCTACGCCCTGCATC CGGCAGAAGGG  <b>Reverse:</b> CCGCCCTCTGCCGGATGCAGGCGTAGCGTTGGA CTGGTAGCAGGG	91.2	63	46
Y191C	<b>Forward:</b> TGCATCCGGCAGAAGGGCGGCTGCTGCAGCTGGT ACCGAGGATGGG  <b>Reverse:</b> CGGACGTAGGCCGTCTCCCGCCGACGACGTCGA CCATGGCTCCTAC	95.5	67.3	46
S204C	<b>Forward:</b> AGGATGGGCCCGGATAATGCATCATCAATGC CACAGACCCCG  <b>Reverse:</b> CCTACCCGGGGGGGCCTATTACGTAGTAGTTACG GTGTCTGGG	92.8	59.5	47

**Table 2.9: Sequencing primers designed for sequencing the pCEP4 plasmid.**

Primer sequence 5'-3'	Tm (°C)	GC (%)	Base length
<b>Forward:</b> GGAGGTCTATATAAGCAGAGCTCG	63.2	50	24
<b>Reverse:</b> CTGCATTCTAGTTGTGGTTGTCC	65.5	45.8	24

## 2.1.7 Laboratory instrumentation

Table 2.10 summarises laboratory instruments used.

**Table 2.10: Laboratory instruments and their manufacturers.**

Instrument	Manufacturer (Distributor)
Trans-Blot Turbo Transfer System (immunoblotting)	Bio-Rad
LiCOR Odyssey CLx fluorescent imager	LiCOR
T1000 thermal cycler	Bio-Rad
QuantStudio 7 Flex RT-qPCR system	Applied Biosystems (ThermoFisher)
BD FACSsymphony A1 flow cytometer	BD Bioscience
Mini-PROTEAN Tetra Vertical Electrophoresis Cell and PowerPac Basic power supply	Bio-Rad
SPECTROstar Omega plate reader	BMG LABTECH
NanoDrop One microvolume spectrophotometer	ThermoFisher
5804 R centrifuge	Eppendorf
EVOS M5000 microscope	Invitrogen (ThermoFisher)
HERAcell 150i tissue-culture incubator	ThermoFisher
MICRO STAR 17R microcentrifuge	VWR
SPECTRAmax GEMINI XPS fluorometric plate reader	Molecular Devices
BioTek Cytation 7 plate reader	Agilent

## 2.1.8 Software

Table 2.11 details all the software used for data and statistical analysis.

**Table 2.11: Software.**

Omega BMG LABTECH 5.11	Image J 1.53 t
MARS data analysis software 3.20 R2	SnapGene Viewer 7.0
Image Studio version 4.0.21	SlideViewer 2.7.0.191696
SoftMax Pro version 7.1	QuantStudio Real-Time PCR Software v1.7.2
GraphPad Prism version 10.1.1	Gen5 3.14

## 2.2 Methods

### 2.2.1 Mammalian cell culture

#### 2.2.1.1 Culturing cells

HEK-293, ARPE-19, hTERT RPE-1, MEF and PEA-13 cells were cultured in growth DMEM, defined as DMEM supplemented with 1 % (v/v) penicillin-streptomycin, 1 % (v/v) sodium pyruvate and 10 % (v/v) FBS. Cells were incubated at 37 °C, 5 % (v/v) CO<sub>2</sub> and passaged every 2-3 days. For some experiments, cells were cultured in serum-free (SF) DMEM, defined as DMEM supplemented with 1 % (v/v) penicillin - streptomycin and 1 % (v/v) sodium pyruvate.

### 2.2.2 SDS-PAGE and immunoblotting

Prior to SDS-PAGE, proteins in some conditioned media samples were precipitated by addition of TCA. The resultant low pH from addition of TCA disrupts the electrostatic interactions between charged amino acids in the proteins, reducing solubility and causing the proteins to precipitate. TCA was added to 5 % (v/v) and samples incubated overnight at 4 °C. The solution was centrifuged (16 000 RCF, 10 min, 4 °C) and the pellet was resuspended in non-reducing 2x Tris-glycine SDS-PAGE sample buffer (**Table 2.12**).

In some cases, samples were mixed with reducing 4x Tris-glycine SDS-PAGE sample buffer, the composition for which is seen in **Table 2.12**. Briefly, samples under reducing conditions were first incubated with β-mercaptoethanol (20 mM final concentration) for 45 min at 56 °C, followed by cooling for 15 min at room temperature. Samples were then incubated with iodoacetamide (20 mM final concentration) for 30 min at room temperature and finally mixed with 4x non-reducing Tris-glycine SDS-PAGE sample buffer.

Unless otherwise stated, 15 µl of sample (7.5 µl sample and 7.5 µl of sample buffer) was electrophoresed on 12 or 15 % Tris-glycine polyacrylamide gels (**Table 2.12**) or on 4-15 % precast Mini-PROTEAN TGX Gels 4-15% (**Table 2.4**) and transferred to a low fluorescence PVDF membrane (Merck) using the Transblot Turbo System. In some cases (indicated in the specific figure legends) a total protein stain was performed (Revert Total Protein Stain, LiCOR) following the manufacturer's protocol and then imaged using LiCOR Odyssey CLx imager. Blots were de-stained using the supplied de-staining solution (LiCOR) and membranes were incubated in Intercept blocking buffer (LiCOR, 1 h, room temperature). Following this,

membranes were incubated with a primary antibody detailed in **Table 2.5** at a 1:1000 dilution contained in primary antibody solution (2.5 ml Intercept buffer, 2.5 ml TBS, 0.2 % Tween 20, overnight at 4 °C with gentle shaking). Membranes were washed 4 times for 5 min each in TBS-Tween 20 (0.1 % Tween 20) and incubated with an appropriate secondary antibody detailed in **Table 2.5**. Secondary antibodies were applied at a 1:4000 dilution in secondary antibody solution (2.5 ml Intercept buffer, 2.5 ml TBS, 0.2 % Tween 20 and 0.2 % SDS) for 1-2 h at room temperature with gentle shaking. PVDF membranes were washed again (4 x 5 min) in TBS-Tween 20 (0.1 % Tween 20) and imaged using an LiCOR Odyssey CLx imager. Quantification of bands of interest was performed in Image Studio Version 4.0.21 and then subsequently normalised to total protein signal in each lane.

**Table 2.12: SDS-PAGE and immunoblotting buffer recipes.**

Buffer	Recipe
Non-reducing SDS-PAGE sample buffer 2x	100 mM Tris-HCl, pH 6.8 2 % (w/v) SDS 15 % (v/v) glycerol 0.01 % (w/v) bromophenol blue
Non-reducing SDS-PAGE sample buffer 4x	200 mM Tris-HCl, pH 6.8 4 % (w/v) SDS 24 % (v/v) glycerol 0.01 % (w/v) bromophenol blue
10x SDS-PAGE running buffer	250 mM Tris-base 1.92 M Glycine 30 mM SDS pH 8.3
Lower (resolving) gel (For 15 % gel)	7.5 ml 30 % (w/v) acrylamide 3.8 ml 1.5 M Tris (pH 8.8) 3.4 ml Milli-Q-H <sub>2</sub> O 150 µl 10 % (w/v) SDS 150 µl 10 % (w/v) APS 6 µl TEMED
Upper (stacking) gel	1.0 ml 30 % (w/v) acrylamide 750 µl 1.0 M Tris (pH 6.8) 4.1 ml Milli-Q H <sub>2</sub> O 60 µl 10 % (w/v) SDS 60 µl 10 % (w/v) APS 6 µl TEMED
TBS	24 g Tris-Base 88g NaCl pH 7.6 1 l final volume

## 2.2.3 Molecular biology methods

### 2.2.3.1 RNA isolation and reverse transcription PCR

RNA extraction was performed using RNeasy RNA extraction kits (QIAGEN) following the manufacturer's protocol and the concentration of isolated RNA was measured using a Nanodrop (NanoDrop One). Using a high-capacity cDNA synthesis kit (Applied Biosystems), 400-500 ng of RNA was reverse transcribed to cDNA in a T1000 Thermal Cycler (Bio-Rad) according to the manufacturer's instructions. The PCR product was then diluted 1:4 with RNase-free water (QIAGEN or Invitrogen).

### 2.2.3.2 Real time quantitative PCR

RNA expression was quantified by RT-qPCR with samples loaded in 384-well plates (Armadillo, ThermoFisher Scientific) and run on a QuantStudio 7 Flex system (Applied Biosystems). For each reaction, an overall volume of 5  $\mu$ l was used, which was composed of 2.5  $\mu$ l SYBR-Green master mix (PCR Biosystems), 0.5  $\mu$ l of a mix of gene-specific forward and reverse primers (each 1  $\mu$ M final concentration), 1  $\mu$ l of RNase/DNase free water and 1  $\mu$ l of diluted cDNA sample. Changes in expression of the gene of interest was compared to a housekeeper gene, *GAPDH*, and changes in expression were calculated using the  $\Delta\Delta CT$  method, with  $\Delta CT$  values calculated between the gene of interest and the housekeeper gene *GAPDH*, and then the differences in  $\Delta CT$  values between experimental and control samples was calculated as  $\Delta\Delta CT$ . Melt curves were analysed on each run to ensure that only a single species of PCR product was generated.

### 2.2.3.3 Site-directed mutagenesis

TIMP-3 with a C-terminal FLAG tag contained in a pCEP4 expression vector was used as the template for site-directed mutagenesis to generate the SFD mutants H181R, Y191C and S204C TIMP-3. pCEP4 is a large plasmid at 10.4 kb, so the Agilent QuikChange II XL Site-Directed Mutagenesis Kit was used, as it has been optimised for use with large plasmids. Specific mutagenesis primers were designed following Agilent's guidelines for primer length, % GC content and melting temperature (**Table 2.8**) and were synthesised by Merck.

Previous experiments in our group found that the Agilent QuikChange guidelines resulted in low colony numbers, so the protocol was modified according to the previously-optimised method (Doherty et al., 2016). The 50  $\mu$ l PCR product was

digested using DpnI restriction enzyme (10 U/μl) for 1 h at 37 °C. 2 μl of this reaction was transformed into XL10-Gold ultracompetent cells by heat shock at 42 °C (30 s), followed by recovery in 500 μl of NZY<sup>+</sup> broth supplemented with 20 % (w/v) glucose (1 h, 37 °C). Transformed bacteria (250 μl) were plated on LB-agar plates (containing 100 μg/ml carbenicillin) and incubated overnight at 37 °C. Colonies were selected and grown in 3 ml Miller's LB containing 100 μg/ml carbenicillin (overnight, 37 °C, with shaking at ~200 RPM). Plasmids were isolated from overnight cultures using the Promega Wizard Plus SV Minipreps DNA Purification Systems kit, and sent for sequencing (Genewiz) using specifically-designed sequencing primers seen in **Table 2.9**.

**Table 2.13: Modified PCR reagent conditions for Agilent QuikChange Site-Directed mutagenesis kit.**

Reagent	Agilent Guidelines	Modified Protocol
10x reaction buffer (μl)	5	5
Ds DNA Template (ng)	10	10
Forward primer (μl of 10 μM stock)	125	100
Reverse primer (μl of 10 μM stock)	125	100
dNTP mix (μl)	1	1
QuikSolution reagent (μl)	3	3
ddH <sub>2</sub> O (μl)	To 50 μl	To 50 μl
Final volume (μl)	50	50
PfuUltra high fidelity polymerase (2.5U/μl)	1	1

**Table 2.14: Modified PCR conditions for Agilent QuikChange Site-Directed mutagenesis kit.**

Segment	Cycles	Temperature (°C)		Time (s)	
		Guidelines	Conditions Used	Guidelines	Conditions Used
1	1	95	95	60	60
2	18	95	95	50	60
		60	60	50	60
		68	68	624	1435
3	1	68	68	420	420

#### **2.2.3.4 Bacterial transformation and plasmid purification**

Following the manufacturer's guidelines, One Shot TOP10 Chemically Competent *E. coli* (Invitrogen, ThermoFisher) were transformed by heat-shock with pCEP4 plasmid constructs encoding either C-terminally-FLAG-tagged WT TIMP-3, SFD TIMP-3 (E162K, H181R, Y191C and S204C) or N-terminally-FLAG-tagged pro-MMP-1.

Transformed bacteria were spread onto agar plates containing 100 µg/ml carbenicillin (ThermoFisher), with plates inverted and cultured overnight at 37 °C. Single colonies were picked and cultured in 3 ml Miller's LB overnight at 37 °C with shaking at ~ 200 RPM, followed by further culture in 200 ml Miller's LB overnight at 37 °C with shaking at ~ 200 RPM. Bacteria were harvested by centrifugation at 13 000 RCF and plasmids isolated using the Qiagen Plasmid Maxi Kit.

#### **2.2.4 HEK-293 transfections of wild-type and SFD TIMP-3, and stable expression of TIMP-3 and pro-MMP-1**

HEK-293 cells were plated at a cell density of 500 000 cells per well in 6-well plates and cultured overnight in growth DMEM (2.2.1) and transfected using Lipofectamine 3000 reagent on the following day with pCEP4 vectors encoding C-terminally FLAG-tagged human WT, H181R, Y191C or S204C TIMP-3. To do this, wells were washed three times in 2.5 ml SF DMEM, and media replaced with 2 ml Opti-MEM. Plasmid DNA (0.5-5.0 µg) was added to transfection reagents according to the manufacturer's protocols and incubated at room temperature for 10-15 min before being added to cells for 24-36 h to allow for transfection.

Wild-type and SFD mutant TIMP-3 expression in the conditioned media of cells was measured by immunoblotting. To this end, Opti-MEM media containing transfection reagents was replaced with 2 ml SF DMEM supplemented with 30 mM sodium chlorate ( $\text{NaClO}_3$ ) for a further 24-36 h. Media were collected and protein precipitated by the addition of TCA as described in 2.2.2 followed by electrophoresis and immunoblotting for TIMP-3 protein using anti-TIMP-3 AB6000 and anti-FLAG M2 primary antibodies.

After determining a suitable plasmid amount for transfection, populations of HEK-293 cells expressing wild-type and the SFD TIMP-3 were selected based on inclusion of a hygromycin-resistance gene on the pCEP4 plasmid. HEK-293 cells

were transfected with expression plasmids using Lipofectamine 3000 as described above. Instead of changing the media to SF DMEM with 30 mM NaClO<sub>3</sub>, media were changed to 2 ml growth DMEM containing hygromycin B (100, 200, 400, 600 and 800 µg/ml) after 24 h. Media were changed every 2-3 days and wells observed for cell death, indicating absence of the plasmid. Expression of WT or SFD TIMP-3 was then quantified by immunoblotting. Electrophoresis and immunoblotting was performed as described in **2.2.2** using anti-TIMP-3 AB6000 and anti-FLAG M2 antibodies. From these data, the lowest hygromycin B concentration giving high TIMP-3 expression was selected.

HEK-293 cells transfected with a pCEP4 vector encoding N-terminally FLAG-tagged human pro-MMP-1 were obtained from laboratory stocks (originally made by Dr Linda Troeberg) and seeded on 6-well plates. To select for cells containing this plasmid construct, hygromycin B was added at 0, 100, 200, 400, 600 and 800 µg/ml, with cells regularly passaged at ratios of 1:5 and 1:10 and media changed every 2-3 days. As above, wells were observed for cell death which either indicated cells not containing the plasmid or a concentration of hygromycin B that was too high for cells to tolerate. To choose an appropriate amount of hygromycin B for preparing pro-MMP-1, expression of pro-MMP-1 was analysed by washing cells (3 x 2 ml SF DMEM) and incubating them in 2 ml SF DMEM for 48 h. Media were harvested, TCA precipitated, electrophoresed and immunoblotted using M2 anti-FLAG as described in **2.2.2**.

### **2.2.5 Wild-type and SFD TIMP-3 and pro-MMP-1 isolation**

Recombinant TIMP-3 with a C-terminal FLAG tag was isolated following a method previously described (Troeberg et al 2009). HEK-293 cells were transfected with a pCEP4 plasmid encoding wild-type or SFD (E162K, H181R, Y191C, S204C) TIMP-3 and selected by treatment with hygromycin B, or HEK-293 cells already transfected with a pCEP4 construct expressing pro-MMP-1 were selected for with hygromycin B as described in **2.2.4**.

HEK-293 cells expressing wild-type or SFD TIMP-3 or pro-MMP-1 were cultured on 150 mm diameter cell cultures plates in 30 ml growth DMEM supplemented with the appropriate concentration of hygromycin B until confluent, at which time media were changed to 50 ml SF DMEM supplemented with 30 mM NaClO<sub>3</sub>. Fresh SF DMEM

was applied approximately every 48 h, and the harvested conditioned media were centrifuged at 400 RCF to remove dead cells and cellular membrane debris.

Conditioned media were filtered through a cell strainer (40  $\mu$ m, Greiner Bio), followed by vacuum filtration (0.22  $\mu$ m filter, Corning) to further remove cell debris. Media were then passed over a column of anti-FLAG M2-agarose beads (2 ml, Merck) that had previously been equilibrated in TNC buffer (50 mM Tris-HCl, pH 7.5, 150 mM NaCl, 10 mM CaCl<sub>2</sub>, 0.02 % NaN<sub>3</sub>, 0.05 % Brij 35). After loading the conditioned media at an approximate rate of 1-2 ml per minute, the column was washed in ~20 ml TNC buffer. To remove non-specifically bound proteins, the column was washed in ~20 ml of a high salt TNC buffer (50 mM Tris-HCl, pH 7.5, 600 mM NaCl, 10 mM CaCl<sub>2</sub>, 0.02 % NaN<sub>3</sub>, 0.05 % Brij 35), followed by a further wash in 50 ml TNC buffer or 50 ml SF DMEM, depending on the buffer used for elution. Elution of bound WT or SFD TIMP-3 or pro-MMP-1 was performed using either TNC buffer (without 0.02% NaN<sub>3</sub>) or SF DMEM (without 0.02 % NaN<sub>3</sub> and 0.05 % Brij 35) containing 200  $\mu$ g/ml FLAG peptide (Cambridge Biosciences, 3 x 5 ml). FLAG peptide competes with C-terminally FLAG-tagged WT/SFD TIMP-3 or N-terminally FLAG-tagged pro-MMP-1 for binding to the anti-FLAG M2-agarose beads, thus releasing the proteins from the anti-FLAG M2 beads and allowing them to be collected in elution buffer. The column was then washed with TNC buffer for storage at 4 °C.

To monitor TIMP-3 or pro-MMP-1 purification, samples from each stage of the purification were mixed with an equal volume of non-reducing 2x Tris-glycine SDS PAGE sample buffer. Samples were electrophoresed and immunoblotted using AB6000 or M2 anti-FLAG as detailed in **2.2.2**.

#### **2.2.5.1 Titration of isolated TIMP-3 preparations with MMP-1**

Immunoblotting was used to determine which elution fractions to pool, upon which the active concentration of eluted WT or SFD TIMP-3 was determined by titration against a known concentration of MMP-1 using the Mca-Pro-Leu-Gly-Leu-Dap(Dnp)-Ala-Arg-NH<sub>2</sub> substrate (Knight et al., 1992). This substrate works on the principle of fluorescence resonance energy transfer, whereby donor and acceptor fluorophores are incorporated either side of an MMP-cleavable bond in the Mca-Pro-Leu-Gly-Leu-Dap(Dnp)-Ala-Arg-NH<sub>2</sub> substrate (Knight et al., 1992) and upon cleavage, diffusion of the donor fluorophore away from the acceptor fluorophore

results in the appearance of fluorescence at the emission wavelength of the donor fluorophore.

Briefly, doubling dilutions of eluted WT or SFD TIMP-3 was mixed with active MMP-1 (final concentration, 50 nM) for 1 h at 37 °C. The Mca-Pro-Leu-Gly-Leu-Dap(Dnp)-Ala-Arg-NH<sub>2</sub> substrate was added to a final concentration of 1.5 μM in a final reaction volume of 200 μl. Fluorescence of each well was measured in an opaque-walled, clear-bottomed 96-well plate using a SPECTRAmax GEMINI XPS fluorometric plate reader (Molecular Devices). Measurements were taken for a period of 30 min at intervals of 30 sec, with excitation and emission wavelengths of 325 nm and 393 nm, respectively. Data was subsequently analysed and processed in SoftMax Pro (version 7.1). Pooled elution fractions were also analysed for purity by silver staining (ThermoFisher), following the manufacturer's instructions. Pro-MMP-1 was activated (**2.2.6**) and titrated against a known concentration of TIMP-1 (originally made by Dr Linda Troeberg).

## 2.2.6 Pro-MMP-1 activation

4-aminophenylmercuric acetate (APMA) has been widely used to activate pro-MMPs (Galazka et al., 1996; Nagase et al., 1992). Pooled eluted fractions of pro-MMP-1 were incubated with 1 mM APMA dissolved in DMSO at 37 °C for 30 min, followed by removal of APMA by flowing the sample over a PD10 desalting column (Cytiva). Equal volumes of sample were mixed with non-reducing 2x SDS-PAGE sample buffer (10 μl, final volume 20 μl) and 15 μl was electrophoresed on an 8 % Tris-glycine polyacrylamide gel. A Coomassie stain was performed to visualise protein, with gels incubated in Coomassie Brilliant Blue Stain [0.1 % (w/v) Coomassie Brilliant Blue, 50 % (v/v) methanol, 20 % (v/v) acetic acid, 29.9 % (v/v) dH<sub>2</sub>O] for 30 min at room temperature. Gels were then de-stained for 3 x 30 min or in some cases overnight, in de-staining solution [20 % (v/v) methanol, 10 % (v/v) acetic acid, 70 % dH<sub>2</sub>O]. LiCOR Odyssey CLx was used to image gels in the 680RD channel.

## 2.2.7 Transfection of ARPE-19 cells

Optimisation experiments involved the use of three separate transfection reagents: jetPRIME (Polyplus, Sartorius), Lipofectamine 3000 (ThermoFisher) and Lipofectamine LTX (ThermoFisher). ARPE-19 cells were plated at a density of 500 000 cells per well in a 6-well plate and incubated overnight in 2 ml growth DMEM. For Lipofectamine 3000 and LTX, media were replaced with 2 ml Opti-MEM but for jetPRIME, the media were not changed. pCEP4 plasmid vectors (0.5 – 5.0 µg) encoding C-terminally FLAG-tagged WT or SFD (H181R, Y191C, S204C) TIMP-3 were added to transfection reagents according to the manufacturer's instructions and incubated at room temperature for 10-15 min, before addition to cells. Cells were left for 24 h with media then changed to SF DMEM for a further 24 h. Conditioned media were collected, TCA precipitated as detailed in **2.2.2** and resuspended in 50 µl of 2x SDS-PAGE sample buffer. 15 µl of resuspended sample was analysed by immunoblotting using an anti-FLAG M2 antibody or an anti-TIMP-3 AB6000 antibody, followed by detection with a fluorescent anti-mouse IgG secondary antibody or a fluorescent anti-rabbit IgG secondary antibody, respectively. Quantification was performed using Image Studio version 4.0.21, with bands normalised to total protein stain in the same lane.

After further optimisation the finalised protocol for transfection with Lipofectamine LTX was as follows. ARPE-19 cells were plated at a density of 250 000 cells per well in a 12-well plate. Cells were incubated overnight in 2 ml growth DMEM and were washed 3 times in 2.5 ml SF DMEM the following morning. Media was replaced to 2 ml Opti-MEM and cells were transfected, using Lipofectamine LTX following the manufacturer's instructions, with 1-9 µg (detailed in figure legends) of pCEP4 plasmid vectors encoding C-terminally FLAG-tagged WT or SFD (H181R, Y191C, S204C) TIMP-3. After 4 h, media were changed to SF DMEM for a further 18 - 20 h. 24 h post-transfection, media were collected, TCA precipitated as detailed in **2.2.2** and resuspended in 50 µl of 2x SDS-PAGE sample buffer. 15 µl of resuspended sample was analysed by immunoblotting using an anti-FLAG M2 antibody, followed by detection with a fluorescent anti-mouse IgG secondary antibody. Cells remaining in the well were collected by addition of cell dissociation solution, followed by centrifugation at 400 RCF for 5 min. Some of the cells were used for cell viability assays as described in **2.2.8** and others were resuspended in 50 µl of 2x SDS-PAGE sample buffer and boiled for 5 mins at 100 °C, before undergoing immunoblotting with an anti-FLAG M2 antibody. ECM samples were collected by scraping the well

content with 50  $\mu$ l of 2x SDS-PAGE sample buffer and boiling at 100 °C for 5 min before immunoblotting using an anti-FLAG M2 antibody, followed by detection with a fluorescent anti-mouse IgG secondary antibody.

## 2.2.8 Apoptosis of ARPE-19 cells induced by TIMP-3 and SFD TIMP-3 mutants

Apoptosis of ARPE-19 cells in response to treatment with WT, H181R or S204C TIMP-3 was investigated using annexin V and propidium iodide staining followed by flow cytometry. Annexin V and propidium iodide staining are commonly used to detect apoptotic cells and have been used previously to investigate apoptosis of chondrocytes induced by N-TIMP-3 (Gendron et al., 2003). Flow cytometry experiments were performed with assistance from Katherine Hampton (University of East Anglia).

ARPE-19 cells were plated at a density of 250 000 cells per well in a 12-well plate and incubated overnight (37 °C, 5 % CO<sub>2</sub>) in 2 ml growth DMEM. Cells were then washed 3 times in 2.5 ml SF DMEM before incubation in 2 ml SF DMEM containing 100 nM WT, H181R or S204C TIMP-3 (all in SF DMEM). After 16 h, cells were trypsinized (200  $\mu$ l trypsin-EDTA) and collected in 1 ml of PBS. Cells were centrifuged at 400 RCF for 5 min, followed by resuspension in Annexin V Binding Buffer (50  $\mu$ l) (BioLegend). 1  $\mu$ l of FITC-Annexin V stain and 0.33  $\mu$ l of propidium iodide were added to cells in the Annexin V Binding Buffer, followed by a gentle vortex and incubation for 15 min at 4 °C. A further 200  $\mu$ l of Annexin V Binding Buffer was added to each sample and gently vortexed. A positive control for cell death was generated by repeated freeze-thawing at – 80 °C and room temperature.

Flow cytometry was performed using a FACSsymphony flow cytometer. Flow cytometer calibration was performed and passed before sample analysis using CS&T Research Beads (BD Biosciences, catalogue #655051). Compensations and fluorescence minus one were performed to exclude auto- and background fluorescence of cells and to accurately determine cells staining positive with the Annexin V and propidium iodide staining. The stains used are as follows: FITC-Annexin V (BioLegend, catalogue #640914) and Propidium Iodide Solution (BioLegend, catalogue #640914). FITC has excitation of 488 nm and an emission max of 525 nm (BioLegend), and propidium iodide also has an excitation of 488 nm but has an emission max of 610 nm (BioLegend).

## 2.2.9 Endocytosis assays

Endocytosis assays were performed in ARPE-19, hTERT RPE-1, PEA-13 and MEF cells.

For ARPE-19 and hTERT RPE-1 cells, cells were plated at a density of 250 000 cells per well in a 12-well plate, whereas PEA-13 and MEF cells were plated at a density of 500 000 cells per well in a 12-well plate. All cells were cultured overnight (37 °C, 5 % CO<sub>2</sub>) in 2 ml growth DMEM. Cells were then washed 3 times in 2.5 ml SF DMEM before incubation in 2 ml DMEM containing 2.5 nM WT or SFD TIMP-3, 1 % (v/v) penicillin-streptomycin, 1 % (v/v) sodium pyruvate and 0.2 % FBS, which acted to seed protein precipitation in TCA. After 0 – 24 h conditioned media were collected and TCA precipitated overnight as detailed in **2.2.2**. Immunoblotting was performed using an anti-FLAG M2 antibody, followed by quantification using Image Studio version 4.0.21, with bands normalised to total protein staining for each lane and expressed as a % of WT or SFD TIMP-3 present at 0 h.

In some experiments, cells were preincubated with 1 µM of RAP for 1 h before the addition of DMEM containing WT or SFD TIMP-3. RAP functions endogenously as a molecular chaperone for newly synthesised LDL receptors, aiding their trafficking from the endoplasmic reticulum to the Golgi (Lee et al., 2007) but it can be used experimentally to block LDL and LRP receptors (Doherty et al., 2016; Johanns et al., 2017; Scilabre et al., 2013).

## 2.2.10 Cell viability assays

Cell viability was assessed using the CellTiter 96 Aqueous One Solution Cell Proliferation Assay (Promega) following the manufacturer's instructions. This assay contains a tetrazolium compound, [3-(4,5-dimethylthiazol-2-yl)-5-(3-carboxymethoxyphenyl)- 2-(4-sulfophenyl)-2H-tetrazolium, inner salt; (MTS), and an electron coupling agent, phenazine methosulfate. The tetrazolium compound is bioreduced by cells to produce a coloured formazan product and the amount of formazan can be quantified by measuring absorbance at 490 nm, to indicate metabolic activity and hence cell viability.

Generally, after removal of conditioned media, cells were collected in cell dissociation solution from each well of a 12-well plate. Cells were centrifuged at 400 RCF for 5 min, followed by resuspension in 2 ml SF DMEM. From each well, 80 µl

of resuspended cells were plated in a 96-well plate with 20 µl of SF DMEM and 20 µl of CellTiter 96 Aqueous One Solution Cell Proliferation Assay. Cells were incubated for 90 min (37 °C, 5 % (v/v) CO<sub>2</sub>) and absorbance at 490 nm measured. For controls for cell death, cells were repeatedly freeze-thawed at – 80 °C and room temperature.

## **2.2.11 Immunofluorescent microscopy to visualise endocytosis of TIMP-3 and SFD TIMP-3**

### **2.2.11.1 Coating glass coverslips**

Glass coverslips (16 mm in diameter) were coated in 10 mg/ml gelatin (dissolved in dH<sub>2</sub>O) for 15 min at room temperature. The gelatin solution was removed and coverslips were fixed in 1 % (w/v) glutaraldehyde in TBS for 20 min at room temperature, followed by incubation with 1 M ammonium chloride for 15 min at room temperature to block any free glutaraldehyde. Coverslips were placed into a 12-well plate and washed 3 times in 2 ml 70 % (v/v) ethanol, followed by washing 3 times in 2.5 ml growth DMEM.

### **2.2.11.2 Visualising TIMP-3 internalisation by confocal microscopy**

ARPE-19 cells were plated at a density of 100 000 cells per coverslip in a 12-well plate. Cells were incubated overnight (37 °C, 5 % CO<sub>2</sub>) in 2 ml growth DMEM. Cells were then washed 3 times in 2.5 ml SF DMEM before incubation in 1 ml SF DMEM containing 40 nM WT or SFD TIMP-3 (all in SF DMEM), 1 % (v/v) penicillin-streptomycin, 1 % (v/v) sodium pyruvate and 0.2 % FBS for 1 – 12 h. Cells were washed in 2 ml PBS and fixed in 3 % (v/v) paraformaldehyde (Merck) in PBS for 10 min at 25 °C, followed by a further wash in 2 ml PBS and blocking in PBS containing 5 % (v/v) goat serum (ThermoFisher) and 3 % (v/v) FBS for 1 h at room temperature. Cells were permeabilised with PBS containing 0.1 % (v/v) Triton X-100 for 15 min at room temperature and then incubated with anti-FLAG M2 (mouse, 1:50) primary antibody in blocking solution for 3 h at 25 °C. After washing in 2 ml PBS (3 times), cells were incubated with the secondary antibody Alexa Fluor-488-conjugated goat anti-mouse IgG to visualise FLAG staining. Actin was stained with Alexa Fluor-647-conjugated phalloidin (Invitrogen, ThermoFisher), and nuclei visualised with DAPI staining (Invitrogen, ThermoFisher). Cells were then visualised with a Zeiss LSM 800 confocal microscope on a 60x objective lens and images viewed in Zen Blue software.

## 2.2.12 RNAScope analysis of *TIMP3* and *LRP1* expression

RNAScope is a novel method of RNA in situ hybridisation, whereby unique probes can amplify and enable detection of specific RNA sequences whilst achieving background suppression and preservation of tissue morphology (Wang et al 2012). In this study, specific probes were used for the detection of *TIMP3* and *LRP1* mRNA. RNAScope analysis was performed on frozen macular tissue sections, obtained from four donors, who had no reported visual pathology, via the Manchester Eye Tissue Repository. Donors had no reported visual pathology at the time of death. One donor, an 86-year-old male (M14557D) had no cause of death reported with tissue collected 1-day postmortem, and a second donor, a 51-year-old female (M14578C) also had no cause of death reported, with tissue collected 6 days postmortem. A third donor was a 39-year-old female (M15092D) whose cause of death was liver disease, with tissue collected 2-days postmortem and the last donor was a 51-year-old female (M14558C) whose cause of death was intracranial haemorrhage, with tissue collected 5-days postmortem. This protocol was performed by Dr Sheona Drummond (University of Manchester). Only data from donors M14557D and M14578C is presented. Buffers used in this protocol can be seen in **Table 2.15**.

Macular sections were washed 3-4 times with PBS in order to remove OCT embedding matrix, followed by incubation for 30 min at 60 °C. Slides were post-fixed in 10 % neutral buffered formalin for 15 min at 4 °C, and then sequentially washed in 50 %, 70 % and 100 % ethanol for 5 min each to achieve dehydration of the sample. A hydrophobic barrier was drawn around tissue sections and sections were incubated for 10 min at room temperature with 1-2 drops of hydrogen peroxide. Sections were rinsed in distilled water and incubated with a ready-made solution of pepsin (Merck) for 10 min at 40 °C and again with fresh pepsin for a further 10 min at 40 °C. Samples were washed again in distilled water and incubated with C1 *TIMP3* probe (ACD Bio, catalogue #433101) and a dilution (1:50) of C2 *LRP1* probe (ACD Bio, catalogue #836621-C2) for 2 h at 40 °C. Slides were washed in RNAScope buffer twice for 3 min each and stored in 5x SCC buffer overnight at room temperature.

The RNAScope 2.5 HD Duplex reagent kit (ACD Bio, catalogue #322430) was used to amplify and detect C1 and C2 probes. Slides were washed in the supplied wash buffer 2x for 2 min. Sequential incubations with amplification probes was performed

according to the manufacturer's instructions with detection for the red signal (C2 probe, i.e. LRP1) and detection for the green signal (C1 probe, i.e. TIMP3) performed as part of this workflow. Slides were counterstained with 3 dips in 50 % haematoxylin, then washed twice in dH<sub>2</sub>O, followed by 2 dips in 0.02 % ammonium hydroxide and two further washes in dH<sub>2</sub>O.

Samples were dried at 60 °C for 15-30 min and then cooled for 5 min at room temperature. Slides were dipped into fresh pure xylene and mounted with a coverslip in DPX. Samples were imaged on a 3D Histech Pannoramic P250 digital slide scanner.

**Table 2.15: RNAScope buffers.**

Buffer	Composition
20x SSC buffer	Invitrogen, ThermoFisher
RNAScope buffer	0.1x SSC 0.03 % (w/v) lithium dodecyl sulfate 10 ml of 20x SSC buffer (in a final volume of 2 l)

### 2.2.13 siRNA knockdown of LRP1

Two siRNA constructs were used to knockdown LRP1: (i) LRP1 Silencer Select siRNA from ThermoFisher (catalogue # 4392420) with its respective negative control Silencer Select Negative Control siRNA (ThermoFisher, catalogue # 4390843), and (ii) another ON-TARGETplus SMARTpool LRP1 siRNA from Dharmacon (catalogue #L-004721-00-005) with its negative control, ON-TARGETplus Non-targeting pool (Dharmacon, catalogue #D-001810-10-05).

Below details the final experimental protocol used for LRP1 siRNA knockdown after optimisation. ARPE-19 or hTERT RPE-1 cells were plated at a density of 250 000 cells per well in a 12-well plate. Cells were incubated overnight in 2 ml growth DMEM and washed 3 times in 2.5 ml SF DMEM the following morning. Media were replaced with 1 ml Opti-MEM and cells were transfected using Lipofectamine LTX following manufacturer's instructions, with 100 nM LRP1 Silencer Select siRNA (ThermoFisher), or 100 nM of Silencer Select Negative Control siRNA (ThermoFisher), or 25 nM ON-TARGETplus SMARTpool LRP1 siRNA (Dharmacon) or its respective negative control. For ThermoFisher siRNA constructs, cells were

left for 24 h and then washed in 2.5 ml SF DMEM 3 times, whereas for Dharmacon siRNA constructs, cells were left for 6 h with media then changed to growth DMEM for a further 18 h. 2.5 nM of purified WT TIMP-3, (in TNC Brij 0.05 %) was added to cells in 2 ml DMEM containing 0.2 % FBS. Samples were collected at 0, 4 and 6 h, TCA precipitated as detailed in **2.2.2** and resuspended in 50  $\mu$ l of 2x SDS-PAGE sample buffer. 15  $\mu$ l of resuspended sample was analysed by immunoblotting using an anti-FLAG M2 antibody, followed by detection with a fluorescent anti-mouse IgG secondary antibody. Quantification was performed using Image Studio version 4.0.21, with bands normalised to total protein within each lane. Data are expressed as percentages of normalised band intensity at time = 0 for each siRNA construct used.

#### **2.2.14 Statistical analysis**

Statistical analysis was performed in GraphPad Prism version 10.1.1. Data were assessed for normality using the Shapiro-Wilk test for normality and subsequently analysed using an unpaired t-test for two independent groups. Alternatively, a one- or two-way ANOVA was used when there were more than two independent groups and when there were one or two independent variables. Significance was accepted at \*  $p \leq 0.05$  on two-tailed tests. Details of correction for multiple comparisons performed are denoted in figure legends.

## **Chapter 3: Generation and characterisation of SFD TIMP-3 mutants**

### 3.1 Introduction

SFD is caused by mutations in the gene encoding for TIMP-3 (Weber et al., 1994a), with 21 mutations associated with SFD having been identified to date (Betts & Troeberg, 2024). The majority of SFD mutations occur in exon 5, corresponding to the C-terminal region of TIMP-3, and involve substitution to a cysteine residue or generation of an unpaired cysteine residue due to truncation (e.g., E162STOP) or mutation of a previously paired cysteine residue (e.g., C24R) (Betts & Troeberg, 2024). A smaller number of SFD mutations occur in the TIMP-3 signal peptide (e.g., L12H and G12R) (Guan et al., 2022) or the N-terminal domain (e.g., C24R and S38C). Also, not all mutations result in the generation of an unpaired cysteine residue, e.g., L10H, G12R, E162K and H181R (Betts & Troeberg, 2024).

The generally accepted premise is that SFD mutants of TIMP-3 form dimers, multimers and higher molecular weight complexes (Arris et al., 2003; Langton et al., 2000, 2005; Weber et al., 2002; Yeow et al., 2002) and that this is a pre-requisite required for disease (Alsaffar et al., 2022), although not all groups have observed such dimerisation (Qi et al., 2002). The general view is that SFD mutants form dimers via their free cysteine residues, which enable intermolecular disulfide bond formation with other TIMP-3 molecules, although SFD mutants that do not involve a change in the number of cysteine residue have also been reported to form dimers (E162K and H181R) (Alsaffar et al., 2022; Saihan et al., 2009).

Properties, including dimerisation and MMP inhibition, of SFD TIMP-3 mutants have largely been studied using cellular models (BHK, COS-7, ARPE-19) transfected with plasmids encoding SFD TIMP-3 mutants (Arris et al., 2003; Langton et al., 2000, 2005; Yeow et al., 2002). While this approach has some advantages, effects of other proteins expressed by the cells can be hard to control for. I thus aimed to express and isolate SFD TIMP-3 mutants (H181R, Y191C and S204C), as well as WT TIMP-3, to compare their biochemical properties and effects on cells in a more defined system. The N-terminal domain of WT TIMP-3 has been expressed in *E. coli* (Kashiwagi et al., 2001), but our group has had more success expressing the protein in mammalian cells (Troeberg et al., 2009). To my knowledge only one group has purified a recombinant SFD mutant, S179C TIMP-3 (Fogarasi et al., 2008), using *E. coli* as an expression system and refolding the protein post-purification. I opted to express SFD TIMP-3 mutants using the mammalian express systems optimised in our group, and isolated the proteins by their engineered C-terminal FLAG tag. This

would provide useful tools for assays aimed at understanding how SFD mutations affect TIMP-3 protein structure and function. The concentration of isolated TIMP-3 proteins was determined by titration and dimerisation status was investigated by reduction and alkylation prior to immunoblot analysis.

## 3.2 Results

### 3.2.1 Generation of pCEP4 expression vectors encoding E162K, H181R, Y191C and S204C SFD TIMP-3

Using a pCEP4 expression vector encoding human TIMP-3 with a C-terminal FLAG tag (Troebert et al., 2009) as a template, site-directed mutagenesis was performed to introduce point mutations to generate the SFD mutations, E162K, H181R, Y191C and S204C. Given the large size of the pCEP4 plasmid (10.4 kb), the Agilent QuikChange II XL Site-Directed Mutagenesis Kit was used for site-directed mutagenesis (**Figure 3.1**).

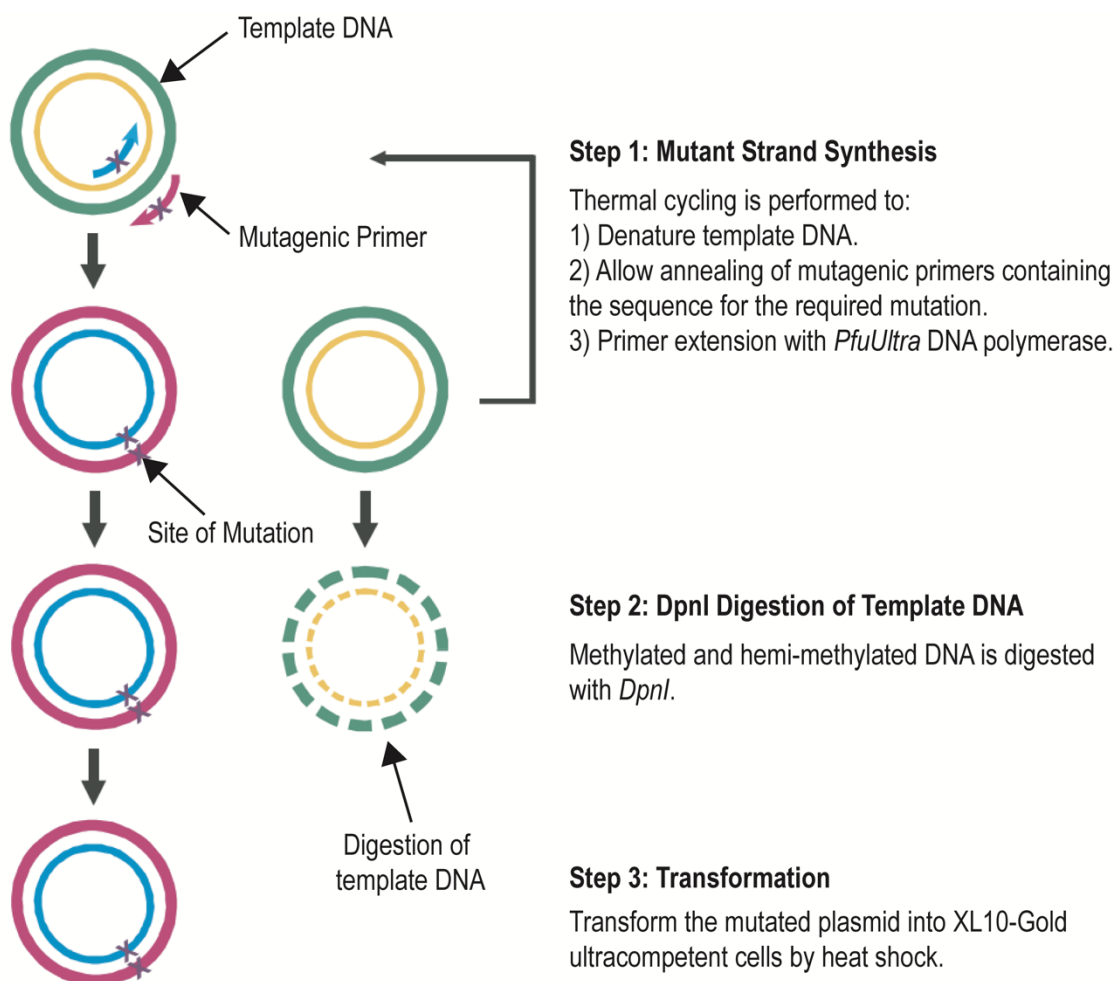


**Figure 3.1: Agilent QuikChange II XL site-directed mutagenesis protocol (adapted from Agilent product literature).**

SFD TIMP-3 mutants were made by PCR, using a pCEP4 expression vector encoding WT TIMP-3 as a template and mutagenic primers containing the specific base change(s) to introduce the desired mutation. A high fidelity *Pfu* DNA polymerase was used to reduce the chance of errors and random mutations. Methylated parental pCEP4 vector was digested with *DpnI* and the remaining non-methylated DNA (arising from PCR) was transformed by heat shock into *E. coli* XL-10-Gold ultracompetent cells, spread on LB-carbenicillin agar plates and left to grow overnight at 37 °C. Candidate colonies were grown in Miller's LB broth (100 µg/ml carbenicillin). DNA was isolated and sent for sequencing to confirm introduction of the desired mutation.

For E162K and H181R, low numbers of colonies were obtained, but sequencing of 4 of the 6 colonies and 3 of the 6 colonies respectively indicated that site-directed mutagenesis was successful at the first attempt using the mutagenic primers (**Table 2.8**). Similarly, sequencing of 2 of the 4 Y191C colonies indicated that site-directed mutagenesis was successful at the first attempt. However, initial attempts to obtain the S204C mutant were unsuccessful, with none of the colonies sequenced having the desired sequence. A new shorter reverse primer was designed (**Table 2.8**) to more closely match the  $T_m$  of the forward primer, and sequencing of the resultant colonies showed this approach successfully generated the desired mutant. Following generation of these mutants, plasmids were amplified using the QIAGEN plasmid Maxi Kit to increase plasmid concentration for use in subsequent transfections.

### 3.2.2 Expression of WT and SFD TIMP-3 mutants in HEK-293 cells

HEK-293 cells were transfected with several amounts of pCEP4 vector encoding FLAG-tagged Y191C or S204C TIMP-3 or an empty pCEP4 vector, which was used as a negative control. Cells were also transfected with a previously optimised (data not shown) amount (3  $\mu$ g) of pCEP4 vector encoding FLAG-tagged WT TIMP-3. After 40-68 h, conditioned media and RNA samples were collected, to quantify TIMP-3 expression at both the protein and mRNA levels using immunoblotting and RT-qPCR.

Using an anti-FLAG M2 antibody and an anti-TIMP-3 AB6000 antibody, expression of WT, Y191C and S204C TIMP-3 in the conditioned medium of transfected HEK-293 cells was observed (**Figure 3.2 A**). The AB6000 immunoblot showed that cells transfected with the empty pCEP4 vector expressed a protein of  $\sim$  25 kDa, the expected molecular mass of TIMP-3, in the conditioned medium at, but there were no detectable bands in the anti-FLAG blot, so this likely reflects endogenously expressed TIMP-3 (**Figure 3.2 A**). Quantification was thus performed only on anti-FLAG M2 blots, which solely reflected expression of TIMP-3 from the transfected expression plasmid. WT TIMP-3 was detected in the conditioned medium of HEK-293 cells as two bands just below and above  $\sim$  25 kDa, indicative of a glycosylated and non-glycosylated form of the protein. The upper of these bands appeared much stronger than the lower band, demonstrating greater expression of a glycosylated form (Troeberg et al., 2009). For Y191C TIMP-3, a band was observed at  $\sim$  25 kDa

for all amounts of plasmid on both the anti-FLAG M2 and anti-TIMP-3 AB6000 blots, with 3  $\mu$ g of plasmid giving the strongest expression upon quantification of anti-FLAG M2 bands (**Figure 3.2 A & B**). This correlated with the highest increase in *TIMP3* mRNA levels with an increase of over 600-fold (**Figure 3.2 C**). Similarly, transfection with S204C TIMP-3 resulted in bands at  $\sim$  25 kDa for all amounts of plasmid used (**Figure 3.2 A**). Upon quantification of anti-FLAG M2 bands, highest protein expression was seen with 5  $\mu$ g of S204C TIMP-3 plasmid (**Figure 3.2 B**), but this did not correlate with the highest mRNA expression of this mutant, which was achieved with 3  $\mu$ g of plasmid (**Figure 3.2 C**).

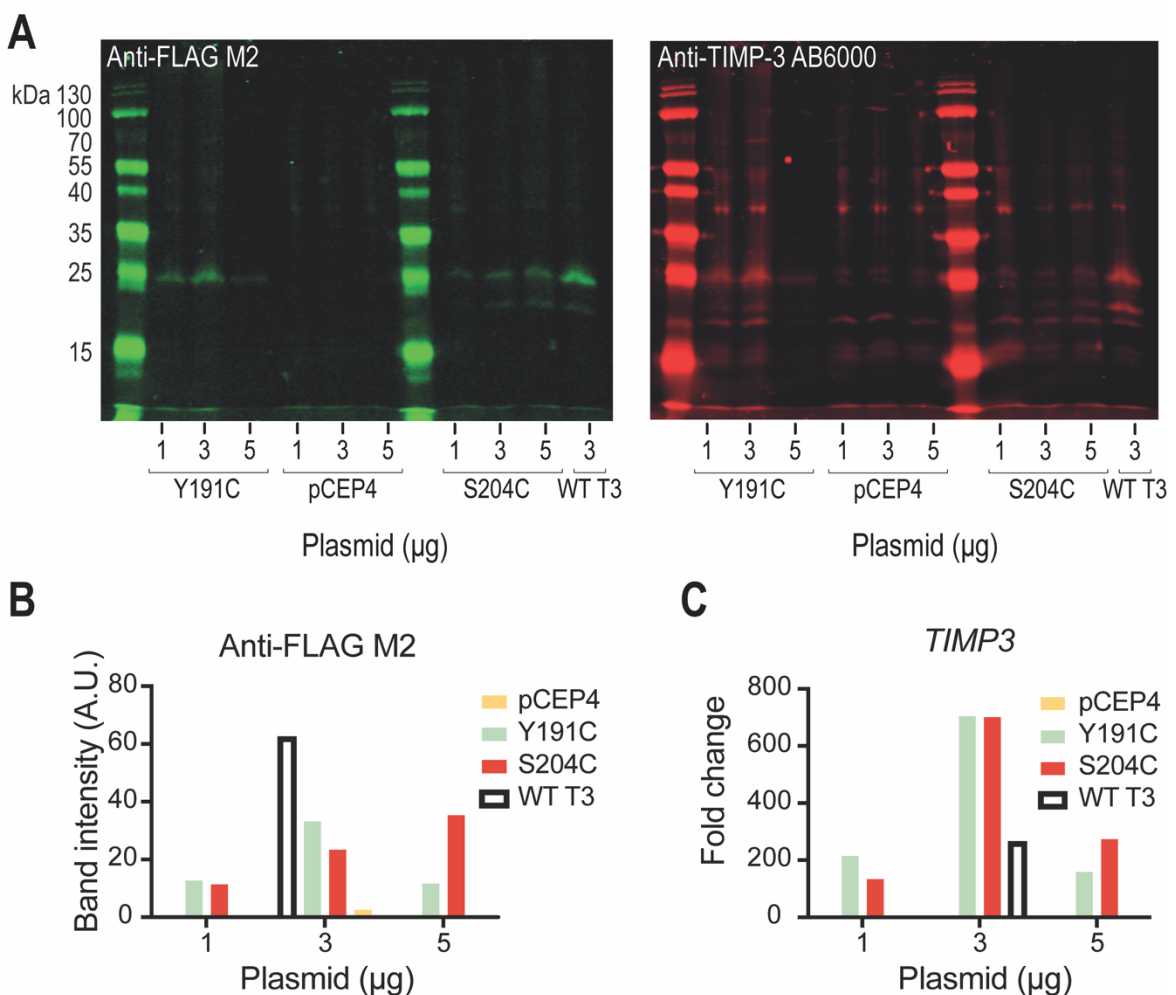


**Figure 3.2: Optimisation of HEK-293 transfection with pCEP4 plasmids encoding Y191C and S204C TIMP-3.**

HEK-293 cells (plated at  $5 \times 10^5$  per well in a 6-well plate) were cultured overnight in growth DMEM (2 ml). On the day of transfection, wells were washed in SF DMEM (3 x 2.5 ml) and media were replaced with Opti-MEM (2 ml). Cells were transfected with Lipofectamine 3000 and the indicated plasmid amounts following the manufacturer's instructions. After 24-36 h, media were changed to SF DMEM (2 ml) and cultured for a further 24 h. Conditioned media were then collected, TCA precipitated, and resuspended in 2x SDS-PAGE sample buffer (50  $\mu$ l). (**A**) Resuspended samples (15  $\mu$ l) were analysed by immunoblotting using an anti-FLAG M2 or anti-TIMP-3 AB6000 antibody, followed by detection with a fluorescent anti-mouse or anti-rabbit IgG secondary antibody, respectively. (**B**) Bands on the anti-FLAG M2 immunoblot were quantified. (**C**) RNA was extracted, cDNA synthesised and mRNA expression of *TIMP3* measured by RT-qPCR. Using the  $\Delta\Delta CT$  method, data were normalised against the housekeeper gene *GAPDH*, and expressed relative to HEK-293 cells transfected with an empty pCEP4 vector. n=1 replicate.

Protein expression of WT TIMP-3 (3 µg or plasmid) was stronger than that for Y191C or S204C TIMP-3 at 1, 3 or 5 µg of plasmid (**Figure 3.2 A & B**). However, at the mRNA level, highest expression was seen at 3 µg of Y191C and S204C TIMP-3, with expression of WT TIMP-3 about 50 % lower (**Figure 3.2 C**).

Given that HEK-293 cells expressed WT, Y191C and S204C TIMP-3 upon transfection, it was next determined whether H181R TIMP-3 could also be expressed in HEK-293 cells (**Figure 3.3**). HEK-293 cells were transfected with 1, 3 or 5 µg of pCEP4 vector encoding H181R TIMP-3 and previously optimised amounts of WT, Y191C and S204C TIMP-3 plasmids as seen in **Figure 3.2**. Conditioned media were collected from cells and probed using an anti-FLAG M2 antibody (**Figure 3.3 A**). Cells transfected with an empty pCEP4 vector, or cells treated with Lipofectamine 3000 alone, acted as a negative controls, with no detectable bands in the anti-FLAG M2 immunoblot (**Figure 3.3 A**). Strong bands corresponding to the expected molecular weight of TIMP-3 at ~ 25 kDa (Apte et al., 1994b; Langton et al., 1998; Leco et al., 1994) were observed at all amounts of H181R plasmid used, and upon quantification all amounts of the H181R plasmid resulted in similar protein expression (**Figure 3.3 B**). Faint bands were also detected above 70 kDa in the lanes for Y191C and S204C TIMP-3, especially in the Y191C TIMP-3 lane (**Figure 3.3 A**). Transfection with the H181R, Y191C and S204C plasmids resulted in similar TIMP-3 expression at the protein level, but transfection with 3 µg of WT TIMP-3 gave higher levels of expression in the conditioned medium.

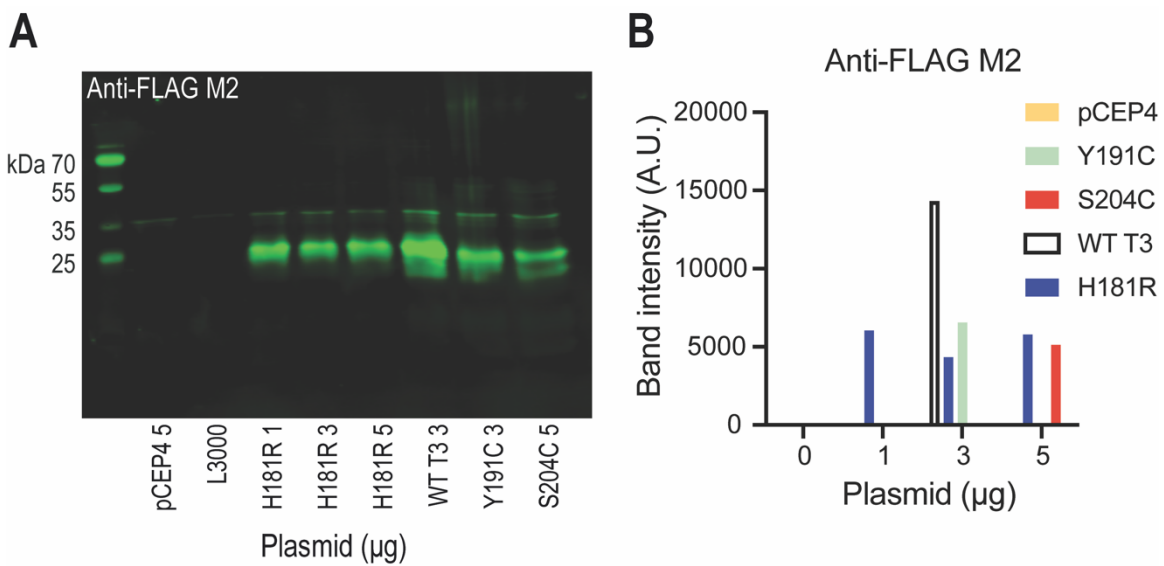


**Figure 3.3: Optimisation of HEK-239 transfection with H181R TIMP-3 pCEP4 plasmid.**  
 HEK-293 cells (plated at  $5 \times 10^5$  per well in a 6-well plate) were cultured overnight in growth DMEM (2 ml). On the day of transfection, wells were washed in SF DMEM (3 x 2.5 ml) and media were replaced with Opti-MEM (2 ml). Cells were transfected with Lipofectamine 3000 and the indicated plasmid amounts, including previously optimised amounts of pCEP4 vectors encoding Y191C and S204C, following the manufacturer's instructions. After 24-36 h, media were changed to SF DMEM (2 ml) and cultured for a further 24 h. Conditioned media were then collected, TCA precipitated, and resuspended in 2x SDS-PAGE sample buffer (50  $\mu$ l). (A) Resuspended samples (15  $\mu$ l) were analysed by immunoblotting using an anti-FLAG M2 followed by detection with a fluorescent anti-mouse secondary antibody. (B) Bands on the anti-FLAG M2 immunoblot were quantified.  $n = 1$  replicate.

### 3.2.3 Isolation of WT and SFD TIMP-3 from conditioned medium of HEK-293 cells

HEK-293 cells transfected with optimised amounts of pCEP4 vectors encoding WT, H181R, Y191C and S204C TIMP-3 (Figure 3.2 & Figure 3.3) were selected by the addition of hygromycin B (200  $\mu$ g/ml) to growth DMEM. Selected HEK-293 cells were then expanded, switched to SF DMEM containing 30 mM NaClO<sub>3</sub> to inhibit TIMP-3 endocytosis (Troebert et al., 2009), and conditioned media were collected every 48-72 h. WT TIMP-3 was isolated from conditioned media first, in TNC-Brij (TNC-B) buffer by anti-FLAG affinity chromatography (Figure 3.4).

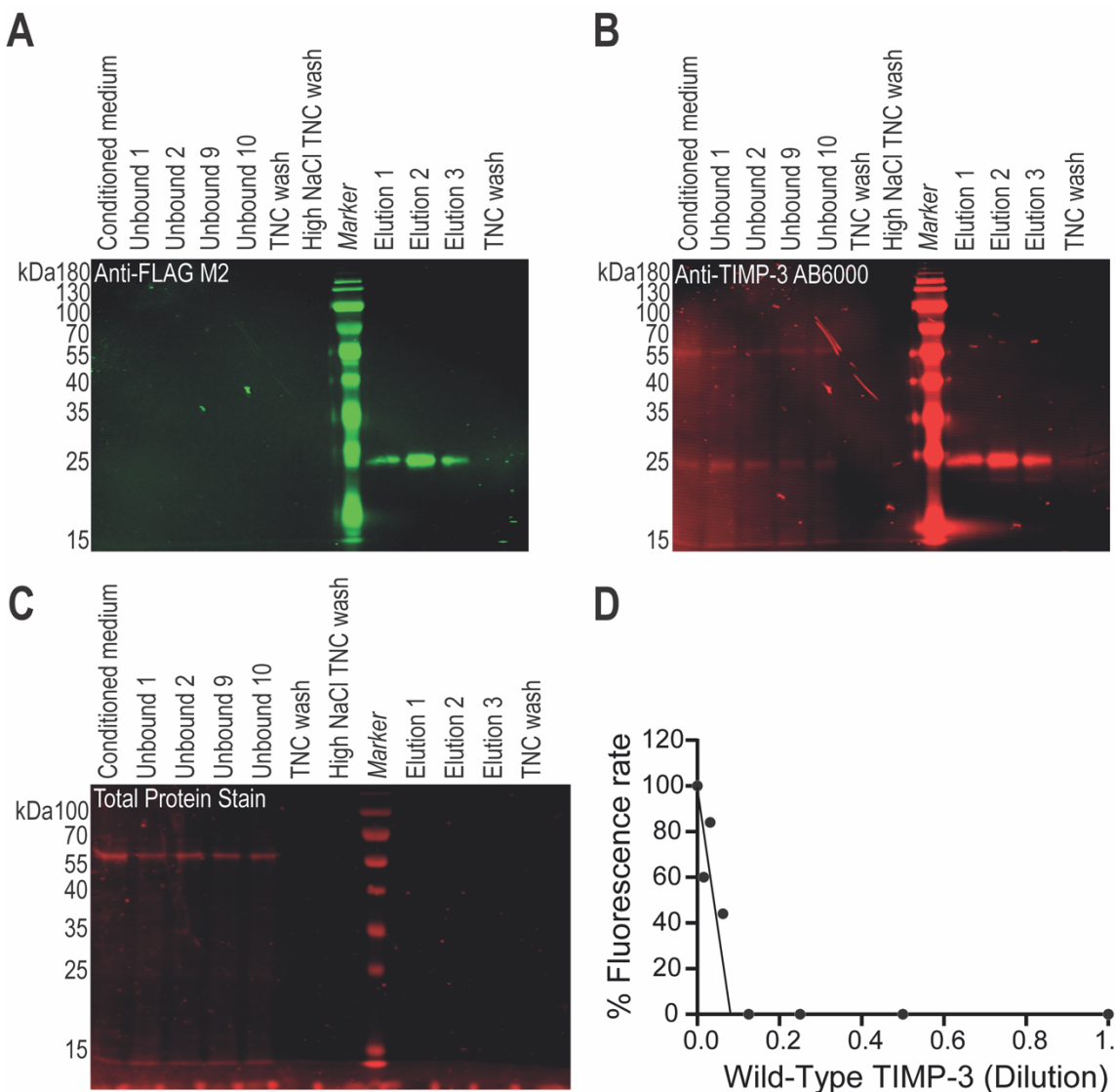


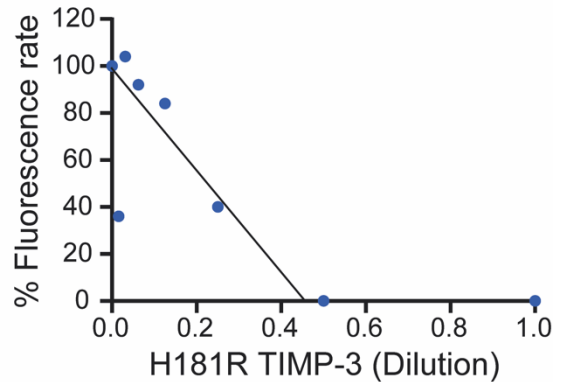
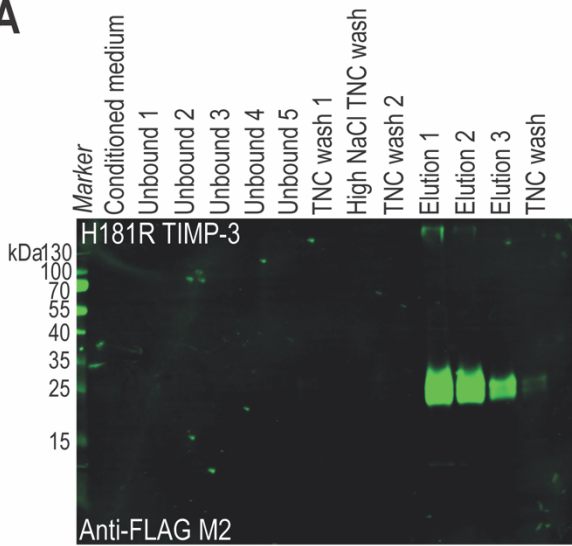
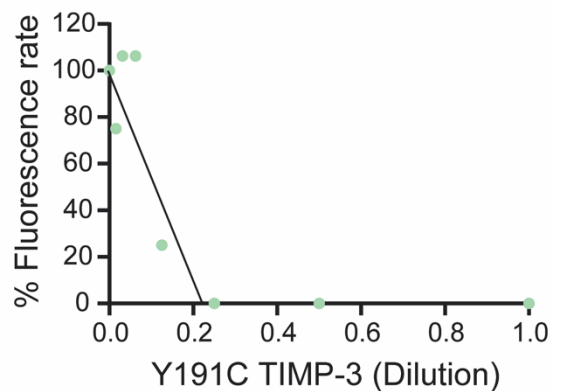
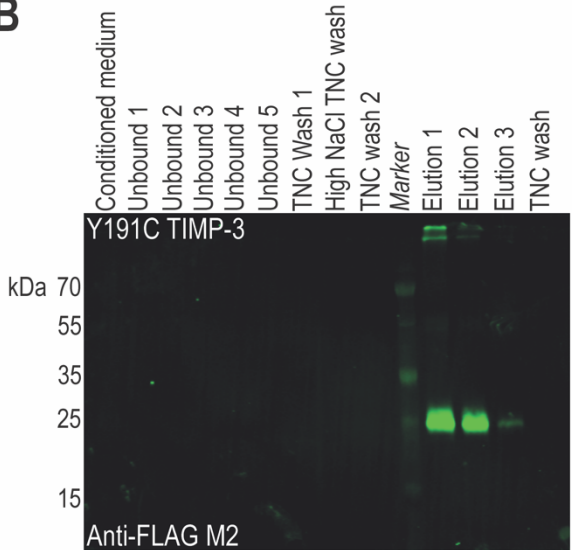
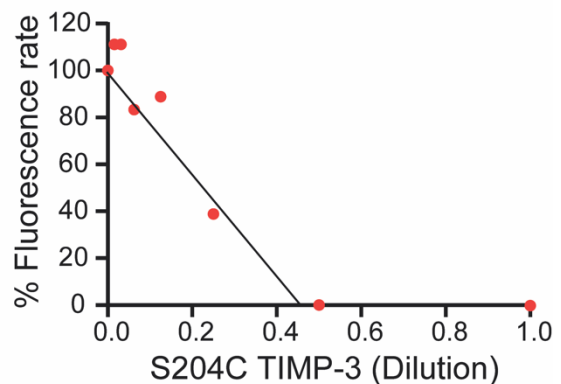
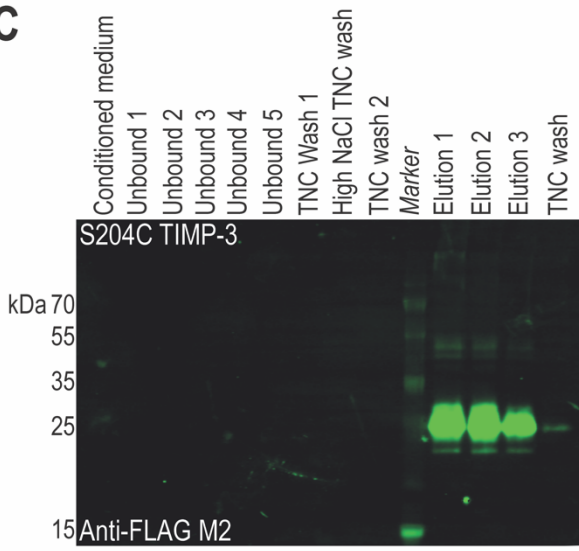
**Figure 3.4: Isolation and titration of WT TIMP-3 in TNC-B by anti-FLAG affinity chromatography.**

HEK-293 cells expressing WT TIMP-3 were grown to confluence in growth DMEM supplemented with 200 µg/ml hygromycin B. Once confluent, cells were cultured with SF DMEM supplemented with 30 mM NaClO<sub>3</sub>. Conditioned media were harvested every 48-72 h, centrifuged to remove cell debris, and stored at -20/80 °C until use. Thawed media were passed over an anti-FLAG M2-agarose column (1-2 ml) equilibrated in TNC-B, followed by a high salt (600 mM NaCl) TNC wash. WT TIMP-3 was eluted in 200 µg/ml FLAG peptide in TNC-B (3 x 5 ml). Fractions were analysed by immunoblotting using an anti-FLAG M2 or anti-TIMP-3 AB6000 antibody, followed by detection with a fluorescent anti-mouse or fluorescent anti-rabbit IgG secondary antibody, respectively. (C) A total protein stain of the blot was also performed before blocking using Revert Total Protein Stain (LiCOR). (D) The active concentration of isolated WT TIMP-3 was determined by titration against a known concentration of MMP-1. MMP-1 (50 nM final concentration) was incubated with doubling dilutions of WT TIMP-3 (37 °C, 1 h), before addition of Mca-Pro-Leu- Gly-Leu-Dap(Dnp)-Ala-Arg-NH<sub>2</sub> (1.5 µM final concentration, 30 min). The increase in fluorescence ( $\lambda_{ex}$  325 nm,  $\lambda_{em}$  393 nm) was measured and WT TIMP-3 concentration determined from a linear regression of a plot of % activity against TIMP-3 dilution.

Immunoblotting with anti-FLAG M2 revealed strong bands at ~ 25 kDa in the elution fractions, with no staining for FLAG in the initial or unbound fractions due to their dilute nature (Figure 3.4 A). Immunoblotting with the AB6000 polyclonal TIMP-3 antibody also showed strong clear bands at ~ 25 kDa in the eluted fractions, indicating successful isolation of TIMP-3 (Figure 3.4 B). On the AB6000 blot, there

were also clear bands at ~ 25 kDa and ~ 55 kDa in the unbound fractions, indicating that TIMP-3 lacking the FLAG tag was not isolated. Considerably fainter bands were visible beneath 25 kDa in elution fractions 2 and 3, possibly indicating some degradation of TIMP-3 in the conditioned medium during culture. Elution fractions 1-3 were pooled and doubling dilutions (50  $\mu$ l) were titrated with an equal volume of a known concentration of active MMP-1 (50  $\mu$ l of 200 nM, giving 50 nM final), using Mca-Pro-Leu-Gly-Leu-Dap(Dnp)-Ala-Arg-NH<sub>2</sub> substrate, more commonly known as Knight substrate (100  $\mu$ l of 3  $\mu$ M, giving 1.5  $\mu$ M final) (Knight et al., 1992) as an indicator of MMP-1 activity. The % of MMP-1 activity (relative to MMP-1 incubated without TIMP-3, defined as 100 %) was plotted against TIMP-3 dilution and a line of best fit was drawn to determine the dilution of WT TIMP-3 that completely inhibited MMP-1 activity (**Figure 3.4 D**). TIMP-3 inhibits MMP-1 with a 1:1 stoichiometry (Brew & Nagase, 2010), thus the active concentration of WT TIMP-3 was determined by multiplying the dilution factor by the starting concentration of MMP-1 (200 nM). In **Figure 3.4 D**, the dilution factor was ~ 10-fold, so the active WT TIMP-3 concentration was calculated as 2000 nM.

**Figure 3.5** shows that H181R, Y191C and S204C TIMP-3 were also successfully isolated in TNC-B buffer by FLAG affinity chromatography. Immunoblotting with an anti-FLAG M2 antibody revealed strong bands at ~ 25 kDa, the mass expected for TIMP-3, in elution fractions 1-3 for H181R and S204C TIMP-3 (**Figure 3.5 A & C**), whereas only elution fractions 1 and 2 showed strong staining at ~ 25 kDa for Y191C TIMP-3 (**Figure 3.5 B**). Additional higher molecular weight bands were also visible just below 55 kDa [for Y191C (**Figure 3.5 B**) and S204C TIMP-3 (**Figure 3.5 C**), but not H181R TIMP-3 (**Figure 3.5 A**)] and above the highest molecular weight marker [for H181R TIMP-3 (**Figure 3.5 A**), Y191C TIMP-3 (**Figure 3.5 B**) and S204C TIMP-3 (**Figure 3.5 C**)].

**A****B****C**

**Figure 3.5: Isolation and titration of H181R, Y191C and S204C SFD TIMP-3 in TNC-B by anti-FLAG affinity chromatography.**

HEK-293 cells expressing H181R, Y191C or S204C TIMP-3 were grown to confluence in growth DMEM supplemented with 200 µg/ml hygromycin B. Once confluent, cells were cultured with SF DMEM supplemented with 30 mM NaClO<sub>3</sub>. Conditioned media were harvested every 48-72 h, centrifuged to remove cell debris, and stored at -20/80 °C until use. Thawed media were passed over an anti-FLAG M2-agarose column (1-2 ml) equilibrated in TNC-B. (A, B & C left-hand side) Unbound

fractions were collected, and the column washed in TNC-B, followed by a high salt (600 mM NaCl) TNC wash. TIMP-3 mutants were eluted in 200 µg/ml FLAG peptide in TNC-B (3 x 5 ml). Fractions were analysed by immunoblotting using an anti-FLAG M2 antibody, followed by detection with a fluorescent anti-mouse IgG secondary antibody. **(A, B & C right-hand side)** The active concentrations of isolated H181R, Y191C, S204C TIMP-3 were determined by titration against a known concentration of MMP-1. MMP-1 (50 nM final concentration) was incubated with doubling dilutions of TIMP-3 (37 °C, 1 h), before addition of Mca-Pro-Leu- Gly-Leu-Dap(Dnp)-Ala-Arg-NH<sub>2</sub> (1.5 µM final concentration, 30 min). The increase in fluorescence ( $\lambda_{\text{ex}} 325 \text{ nm}$ ,  $\lambda_{\text{em}} 393 \text{ nm}$ ) was measured and TIMP-3 concentration determined from a linear regression of a plot of % activity against TIMP-3 dilution. Isolation and titration of H181R TIMP-3, Y191C TIMP-3 and S204C TIMP-3 is indicated in **(A)**, **(B)** and **(C)**, respectively.

Elution fractions 1-3 of each TIMP-3 were pooled and doubling dilutions were titrated with an equal volume of a known concentration of active MMP-1 as described above for WT TIMP-3. The % of MMP-1 activity was plotted against dilutions of H181R, Y191C or S204C TIMP-3 and a line of best fit was drawn to determine the dilution of H181R, Y191C or S204C TIMP-3 that completely inhibited MMP-1 activity (**Figure 3.5 A, B & C, right-hand side**). In the case of H181R, Y191C and S204C TIMP-3, calculated concentrations were 444 nM, 909 nM and 465 nM, respectively. These concentrations were all lower than that calculated for WT TIMP-3 (**Figure 3.4 D**).

E162K was also successfully isolated from HEK-293 conditioned media, as bands at ~ 25 kDa were detected in elution fractions on an anti-FLAG M2 immunoblot (**Figure 3.6 A**). Bands were also present between 40 and 55 kDa, similar to those observed for S204C TIMP-3 above, as well as at molecular weights higher than the molecular weight markers in elution fractions 2 and 3. When pooled and titrated, E162K TIMP-3 was unable to inhibit MMP-1 activity, even if undiluted material was used (data not shown), thus the pooled elution fractions of E162K TIMP-3 were compared with known concentrations of isolated WT TIMP-3 by anti-FLAG M2 immunoblotting (**Figure 3.6 B**). This revealed very weak bands at ~ 25 kDa for E162K, while WT TIMP-3 was clearly visible even at 25 nM, indicating that the yield of isolated E162K TIMP-3 was extremely low.

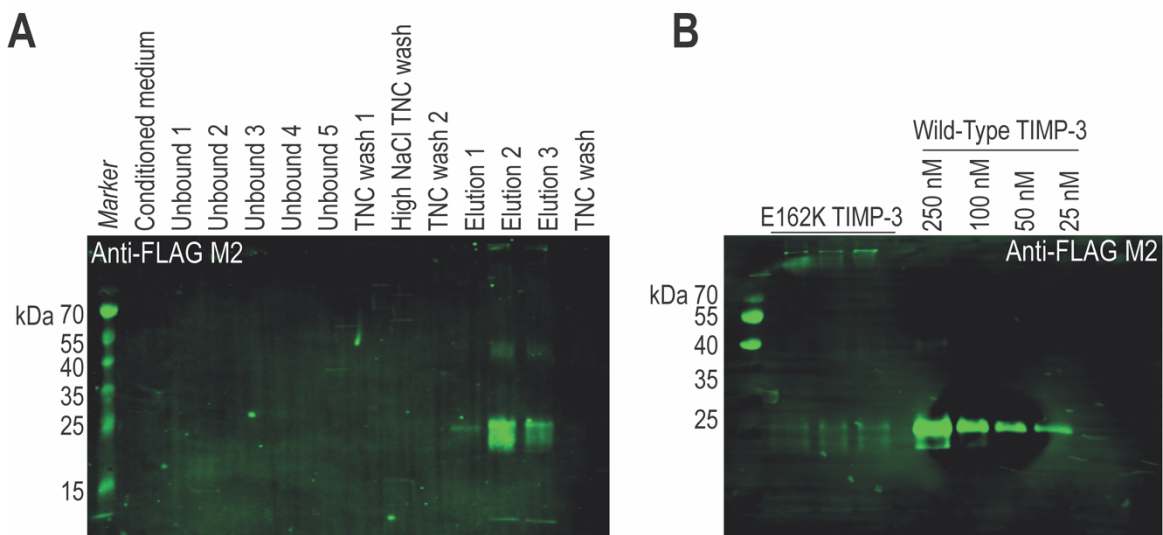


**Figure 3.6: Isolation of E162K TIMP-3 in TNC-B by anti-FLAG affinity chromatography and comparison with WT TIMP-3.**

HEK-293 cells expressing E162K TIMP-3 were grown to confluence in growth DMEM supplemented with 200 µg/ml hygromycin B. Once confluent, cells were cultured with SF DMEM supplemented with 30 mM NaClO<sub>3</sub>. Conditioned media were harvested every 48-72 h, centrifuged to remove cell debris, and stored at -20/80 °C until use. Thawed media were passed over an anti-FLAG M2-agarose column (1-2 ml) equilibrated in TNC-B. (A) Unbound fractions were collected, and the column washed in TNC-B, followed by a high salt (600 mM NaCl) TNC wash. E162K TIMP-3 was eluted in 200 µg/ml FLAG peptide in TNC-B (3 x 5 ml). Fractions were analysed by immunoblotting using an anti-FLAG M2 antibody, followed by detection with a fluorescent anti-mouse secondary antibody. (B) Pooled E162K elution fractions (15 µl) were analysed by immunoblotting alongside indicated concentrations of isolated WT TIMP-3, using an anti-FLAG M2, followed by detection with a fluorescent anti-mouse IgG secondary antibody.

Silver staining was performed to analyse the purity of WT, H181R, Y191C and S204C TIMP-3 that had been isolated in TNC-B (Figure 3.7). For all preparations, a band was present at ~ 25 kDa, which corresponds to the expected molecular weight of TIMP-3 (Figure 3.7). For WT TIMP-3, a band was also present above the molecular weight markers, indicating that the eluted sample was not entirely pure (Figure 3.7 A). Similar bands above the molecular weight markers were also seen in H181R, Y191C and S204C TIMP-3 elution fractions at a greater intensity than for WT TIMP-3 (Figure 3.7 B & C), with these bands particularly strong in Y191C and TCA-precipitated S204C preparations. There were also additional higher molecular weights bands in H181R, Y191C and S204C preparations that were not present in WT TIMP-3 preparations.

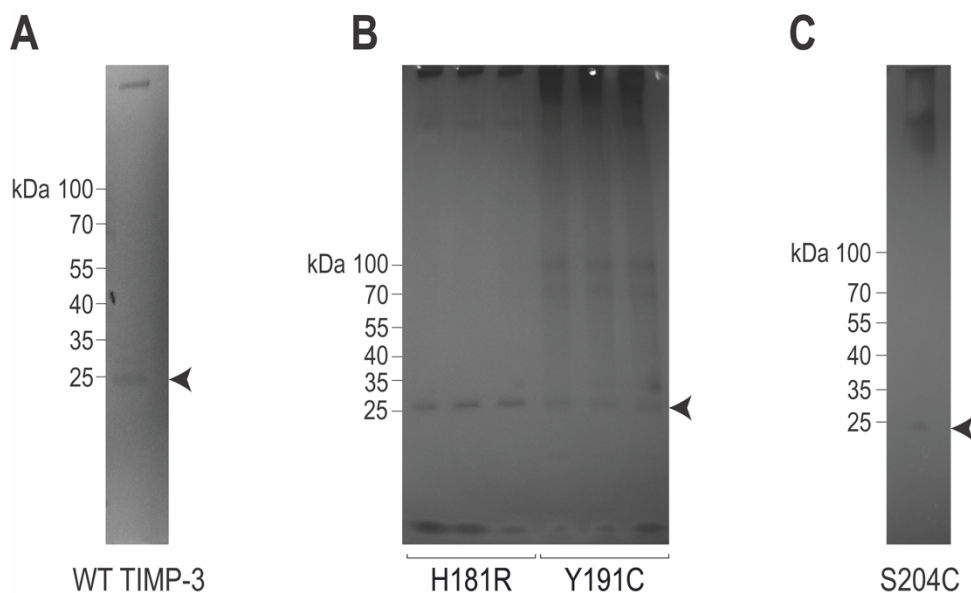


**Figure 3.7: Purity of WT, H181R, Y191C and S204C TNC-B elution fractions as detected by silver staining.**

Elution fractions of WT, H181R, Y191C and S204C TIMP-3 all in TNC-B were electrophoresed on a Mini-PROTEAN TGX Gel 4-15%, and silver stained (A) 2  $\mu$ l of WT TIMP-3 (100 ng) was mixed with 13  $\mu$ l of 2x SDS sample buffer and 15  $\mu$ l loaded for electrophoresis. (B) 5  $\mu$ l of H181R TIMP-3 and 7.6  $\mu$ l of Y191C TIMP-3 (100 ng) was mixed with 10  $\mu$ l and 7.4  $\mu$ l of 2x SDS sample buffer, respectively (final amount of 100 ng), with 15  $\mu$ l of each loaded for electrophoresis. (C) 500  $\mu$ l of 250 nM S204C TIMP-3 was TCA precipitated and resuspended in 30  $\mu$ l 2x SDS sample buffer, with 15  $\mu$ l (90 ng) loaded for electrophoresis.

In addition to isolation in TNC-B, anti-FLAG affinity chromatography was also used to isolate WT, H181R, Y191C or S204C TIMP-3 in SF DMEM, for use in planned cell culture experiments (Figure 3.8). For WT, H181R, Y191C and S204C TIMP-3, strong bands were visible in the elution fractions at  $\sim$  25 kDa, the expected molecular mass of TIMP-3. Additional weaker bands were also present above the molecular weight markers for all 4 of these TIMP-3 preparations (Figure 3.8 A, B, C and D). For isolated S204C TIMP-3, strong bands were present between 40 and 55 kDa (Figure 3.8 D), which were similar to those observed when S204C TIMP-3 was isolated in TNC-B (Figure 3.5 C), although these bands appeared to be more abundant in the SF DMEM elutions. Bands between 35 and 55 kDa were also seen in the elution fractions of SF Y191C TIMP-3 (Figure 3.8 C), but these appeared to be weaker than those in elution fractions of S204C TIMP-3. Titration of each TIMP-3 with active MMP-1 and Knight substrate revealed that WT TIMP-3 had the highest active concentration. Overall, isolated concentrations were lower in SF DMEM than in TNC-B (data not shown).

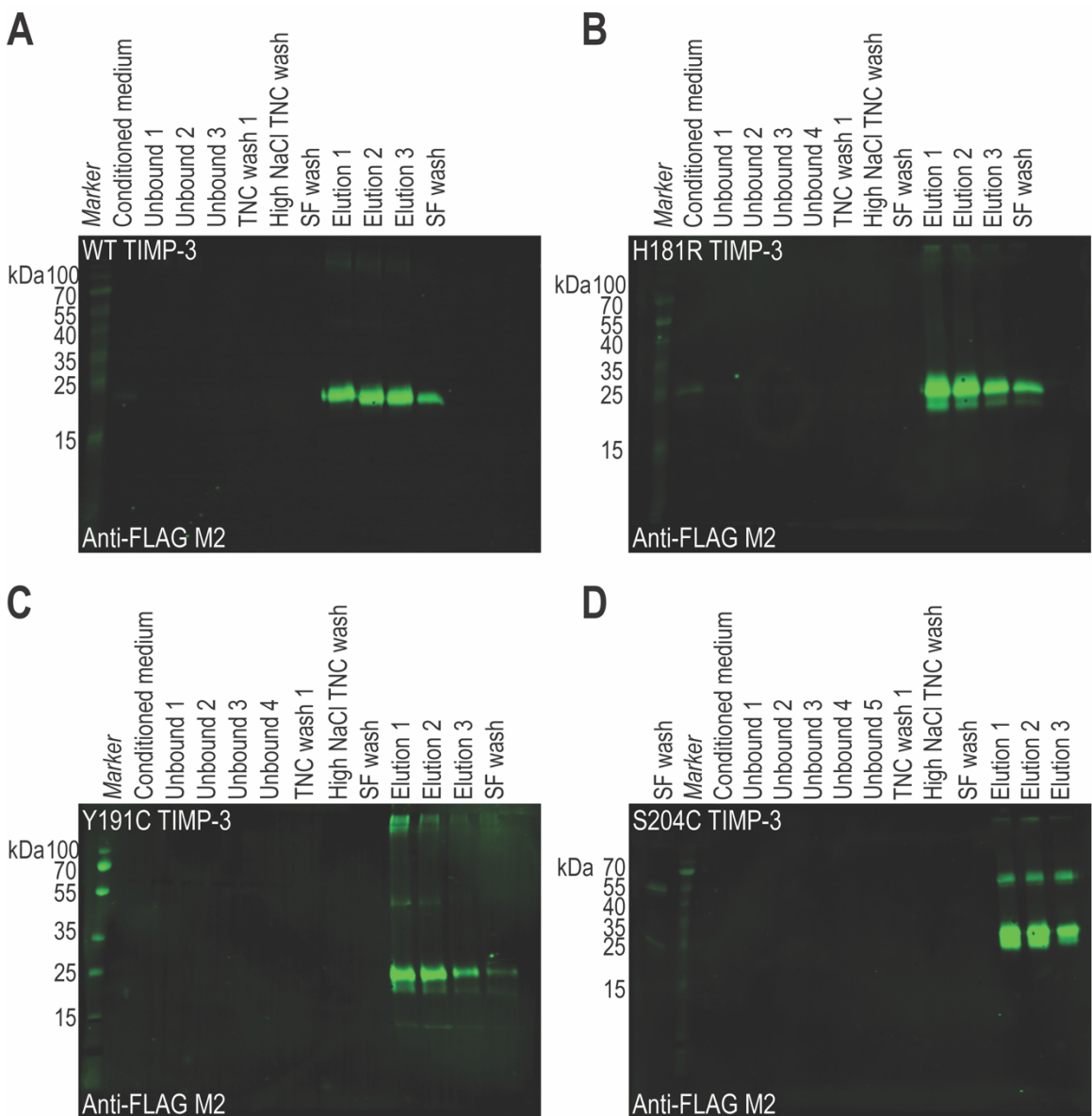


**Figure 3.8: Isolation of WT, H181R, Y191C and S204C TIMP-3 in SF DMEM by anti-FLAG affinity chromatography.**

HEK-293 cells expressing WT, H181R, Y191C or S204C TIMP-3 were grown to confluence in growth DMEM supplemented with 200 µg/ml hygromycin B. Once confluent, cells were cultured with SF DMEM supplemented with 30 mM NaClO<sub>3</sub>. Conditioned media were harvested every 48-72 h, centrifuged to remove cell debris, and stored at -20/80 °C until use. Thawed media were passed over an anti-FLAG M2-agarose column (1-2 ml) equilibrated in TNC-B. (A, B, C & D) Unbound fractions were collected, and the column washed in TNC-B, followed by a high salt (600 mM NaCl) TNC wash. TIMP-3 was eluted in 200 µg/ml FLAG peptide in SF DMEM (3 x 5 ml). Fractions were analysed by immunoblotting using an anti-FLAG M2 antibody, followed by detection with a fluorescent anti-mouse IgG secondary antibody. Isolation of WT, H181R TIMP-3, Y191C TIMP-3 and S204C TIMP-3 is indicated in (A), (B), (C) and (D), respectively.

### 3.2.4 Reduction and alkylation of isolated WT, H181R, Y191C and S204C TIMP-3

The presence of bands between 35 and 55 kDa in elution fractions of isolated WT and mutant TIMP-3 (Figure 3.5 & Figure 3.8) was reminiscent of TIMP-3 dimers and multimers that have previously been reported for SFD TIMP-3 mutants (Arris et al., 2003; Langton et al., 2000, 2005; Weber et al., 2002; Yeow et al., 2002).

Previous work has shown that these dimers were ablated under reducing conditions (Langton et al., 2005), so isolated WT and mutant TIMP-3 in both TNC-B and SF DMEM were subjected to reduction and alkylation before electrophoresis on SDS-PAGE gels, followed by immunoblotting with an anti-FLAG M2 antibody. **Figure 3.9 A** shows that WT, H181R, Y191C and S204C TIMP-3 (all in TNC-B) all migrated  $\sim$  25 kDa under non-reducing conditions and that this band shifted slightly upwards under reducing conditions, indicating the presence of disulfide bonds in the recombinant proteins. A  $\sim$  55 kDa band was visible under non-reducing conditions for Y191C and S204C TIMP-3, which also shifted upwards in reducing conditions. For WT and H181R TIMP-3, the 55 kDa band was visible only in reducing conditions, and not detected under non-reducing conditions; even when the blot was overexposed (**Figure 3.9 B**). Additionally, for Y191C TIMP-3, a band was visible above the molecular weight markers in non-reducing conditions, and this band disappeared with reduction. Bands above the molecular weight markers were also detectable in H181R and S204C TIMP-3 under non-reducing conditions when the blot was overexposed, and these appeared to shift upwards when reduced. Bands higher than the molecular weight markers for WT TIMP-3 were only visible under reducing conditions when the blot was overexposed.

Similarly, when isolated in SF DMEM (**Figure 3.9 C**), WT, H181R, Y191C and S204C TIMP-3 all migrated at  $\sim$  25 kDa under non-reducing conditions, with a slight shift upwards under reducing conditions. The  $\sim$  55 kDa band was visible under non-reducing conditions for Y191C and S204C TIMP-3, with an upwards shift in reducing conditions. The  $\sim$  55 kDa band was also present for WT TIMP-3 under non-reducing conditions, although only when the blot was overexposed (**Figure 3.9 D**), and this band also shifted slightly upwards in reducing conditions. For H181R, the  $\sim$  55 kDa band was visible only in reducing conditions. Non-reducing samples of Y191C in SF DMEM did not appear to contain the clear band seen above the molecular weight markers in TNC-B, although both Y191C and S204C TIMP-3 in SF DMEM did have the strong staining above the molecular weights in non-reducing and reducing conditions that were also seen in TNC-B (**Figure 3.9 C & D**).

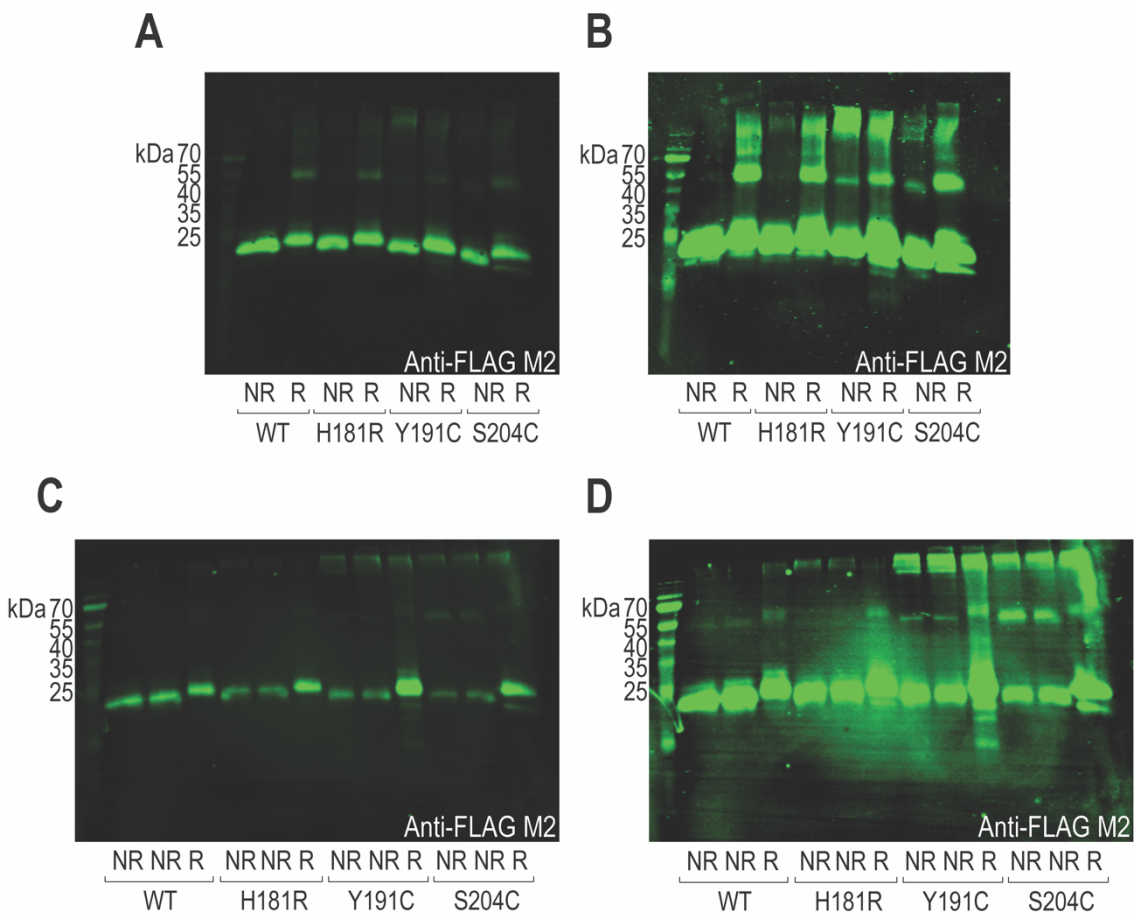


**Figure 3.9: Reduction and alkylation of isolated WT, H181R, Y191C and S204C TIMP-3 in TNC-B or SF DMEM.**

Isolated WT, H181R, Y191C and S204C TIMP-3 in TNC-B (**A** & **B**) or SF DMEM (**C** & **D**) were reduced and alkylated by incubation with  $\beta$ -mercaptoethanol (20 mM, 45 min, 56 °C) followed by cooling (15 min, room temperature) and incubation with iodoacetamide (20 mM, 30 min room temperature) before 4 x SDS sample buffer was added (giving a final TIMP-3 concentration of 50 nM). Preparations of WT, H181R, Y191C and S204C TIMP-3 under non-reducing conditions were also prepared in 4 x SDS sample buffer. Samples (15  $\mu$ l) were electrophoresed on 15 % Tris-glycine polyacrylamide gels and analysed by immunoblotting using an anti-FLAG M2 antibody, followed by detection with a fluorescent anti-mouse secondary. **B** and **D** represent overexposed blots of **A** and **C**, respectively. R denotes reducing conditions and NR indicates non-reducing conditions.

### 3.2.5 Expression and isolation of FLAG-tagged pro-MMP-1

HEK-293 cells that had previously been transfected with a pCEP4 vector encoding N-terminally FLAG-tagged pro-MMP-1 were cultured with several concentrations of the selection antibody hygromycin B. Media were collected and pro-MMP-1 expression was analysed by an anti-FLAG M2 immunoblot (**Figure 3.10 A**). Across all concentrations of hygromycin B tested, bands were visible at  $\sim$  55 kDa, corresponding to the expected molecular weight for pro-MMP-1 (Goldberg et al., 1986). The strongest band was observed at 400  $\mu$ g/ml of hygromycin B, so cells were cultured with this concentration of hygromycin B to generate conditioned media for isolation of the enzyme.

Conditioned medium from pro-MMP-1-transfected HEK-293 cells was collected and pro-MMP-1 was successfully isolated by anti-FLAG affinity chromatography into TNC-B buffer (**Figure 3.10 B**). Immunoblotting using an M2 anti-FLAG antibody revealed 2 strong bands in elution fractions between 55 and 70 kDa, indicative of pro-MMP-1 expression (Goldberg et al., 1986), and also several bands below 35 kDa, which are likely breakdown products of pro-MMP-1. Elution fractions were then tested for purity by performing a Coomassie stain, which revealed strong bands just above 55 kDa and some weaker bands below 55 kDa, likely to be pro and some active MMP-1, respectively (**Figure 3.10 C**). Importantly, Coomassie staining revealed no major contaminants in elution fractions.

Following successful isolation, pro-MMP-1 elution fractions were pooled and activated by incubation with 1 mM APMA dissolved in either DMSO or NaOH over a time-course of 180 min (**Figure 3.10 D**). APMA has been used in the literature for activation of pro-MMPs (Galazka et al., 1996; Nagase et al., 1992). For activation with APMA dissolved in either DMSO or NaOH, at 0 min there were strong bands present just above 55 kDa (likely to be pro-MMP-1) with weaker bands just below 55 kDa (likely to be active MMP-1). After 30 min this pattern reversed, with bands below 55 kDa appearing stronger, indicating successful activation of pro-MMP-1 to active MMP-1. With longer incubations (30 to 180 min), bands appeared below 35 kDa. These most likely correspond to the pro-domain of pro-MMP-1 that was removed during APMA-induced activation. APMA dissolved in DMSO generated stronger bands below 55 kDa after 30 min than APMA dissolved in NaOH, so APMA in DMSO was selected for subsequent activation of pro-MMP-1.

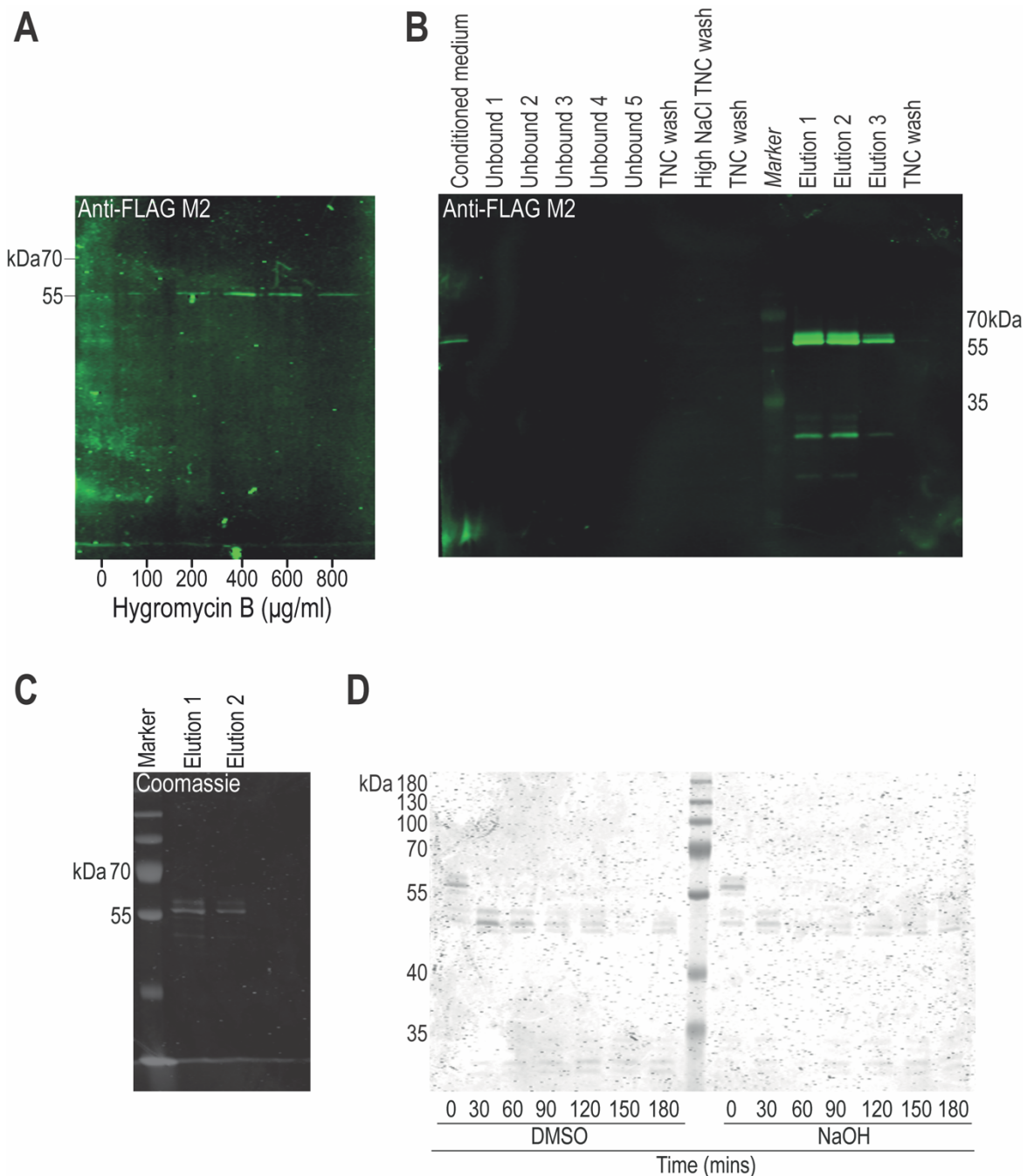


**Figure 3.10: Expression, isolation and activation of FLAG-tagged pro-MMP-1.**

(A) HEK-293 cells (plated at  $2.5 \times 10^5$  per well in a 6-well plate) expressing a pCEP4 vector encoding N-terminally FLAG-tagged pro-MMP-1 were cultured overnight in growth DMEM (2 ml) with the indicated amounts of hygromycin B. Conditioned media were collected, TCA precipitated, and resuspended in 2x SDS-PAGE sample buffer (50 µl). Resuspended samples (15 µl) were analysed by immunoblotting using an anti-FLAG M2, followed by detection with a fluorescent anti-mouse IgG secondary antibody. (B) HEK-293 cells expressing FLAG-tagged pro-MMP-1 were grown to confluence in growth DMEM supplemented with 400 µg/ml hygromycin B. Once confluent, cells were cultured in SF DMEM. Conditioned media were harvested every 48-72 h, centrifuged to remove cell debris, and stored at -20/80 °C until use. Thawed media were passed over an anti-FLAG M2-agarose column (1-2 ml) equilibrated in TNC-B. Unbound fractions were collected, and the column washed in TNC-B, followed by a high salt (600 mM NaCl) TNC wash. Pro-MMP-1 was eluted in 200 µg/ml FLAG peptide in TNC-B (3 x 5 ml). Fractions were analysed by immunoblotting using an anti-FLAG M2 antibody, followed by detection with a fluorescent anti-mouse IgG secondary antibody. (C) Eluted fractions were electrophoresed on an 8 % SDS-PAGE gel, followed by a Coomassie stain to check for impurities in the eluted sample. (D) Pro-MMP-1 was incubated with 1 mM APMA dissolved in DMSO or NaOH (37 °C, 3 h) and collected samples were electrophoresed on an 8 % SDS-PAGE gel, followed by a Coomassie stain.

### 3.3 Discussion

The aim of the work presented in this Chapter was to engineer and isolate SFD TIMP-3 mutants for use in subsequent in vitro biochemical and cell-based assays. To this end, I successfully generated pCEP4 plasmid vectors encoding C-terminally FLAG-tagged E162K, H181R, Y191C and S204C TIMP-3 using the Agilent QuikChange II XL Site-Directed Mutagenesis Kit (**Figure 3.1**). pCEP4 is a large plasmid of 10.4 kb, so use of this kit was appropriate as it is optimised for use with large plasmids. Previous experiments in Dr Linda Troeberg's group found that following the Agilent QuikChange protocol guidelines resulted in low colony numbers, but that higher colony numbers were obtained when the amount of template was increased from 10 to 100 ng and when amounts of forward and reverse primers were decreased (Doherty et al., 2016). I followed this modified protocol (**Table 2.13 & Table 2.14**) with good success.

As outlined above (**3.1**), only one group has purified an SFD TIMP-3 mutant, S179C TIMP-3, by expression in *E. coli* and subsequent re-folding on a metal affinity chromatography column (Fogarasi et al., 2008). Using this particular expression system poses a major issue because *E. coli* are unable to properly form proteins that contain complex disulfide bonds and are also unable to perform post-translational modifications (Mamipour et al., 2017). Given that the structure of TIMP-3 is stabilised by 6 intramolecular disulfide bonds (Brew & Nagase, 2010), purification and subsequent refolding from *E. coli* may result in an improperly folded protein that may not truly reflect how these SFD TIMP-3 mutants would fold and function natively. However, Fogarasi and colleagues did show that their refolded TIMP-3 proteins were active when titrated against MMP-13, indicating correct folding of the inhibitory ridge of TIMP-3. I transfected mammalian cells (HEK-293 cells) with the pCEP4 vectors encoding different TIMP-3 constructs as these cells contain the necessary molecular chaperones needed for correct disulfide bond formation (Hendershot et al., 2023) and so were more likely to generate proteins reflecting the properties of TIMP-3 mutants in SFD patients.

In initial optimisation experiments with  $n = 1$ , transfection of HEK-293 cells with 3  $\mu$ g of pCEP4 vector encoding WT TIMP-3 gave the lowest fold-change in *TIMP3* mRNA expression but the highest fold-change in TIMP-3 protein expression compared with Y191C and S204C TIMP-3 used at the same concentrations (**Figure 3.2**). Firm conclusions cannot be drawn from  $n = 1$ , but these data suggest that for Y191C and

S204C TIMP-3, large increases in *TIMP3* mRNA expression (~ 600-fold), do not necessarily correspond with a large increase in protein expression. The imbalance between mRNA and protein expression of the different SFD TIMP-3 mutants is interesting and suggests that further post-transcriptional and post-translational mechanisms may be in place, however there is a lack of documented evidence to support this. It is possible that a decreased amount of Y191C and S204C detectable in the conditioned media (**Figure 3.2**) is due to impaired secretion of these SFD TIMP-3 proteins, as has been observed previously (Hongisto et al., 2020). Thus, it would have been beneficial to western blot the cell layer of transfected HEK-293 cells to determine whether there is a correlation between intracellular TIMP-3 protein and mRNA level. Alternatively, these SFD TIMP-3 proteins may be detrimental to cell health. WT TIMP-3 has been shown to induce apoptosis in a variety of cell types (Baker et al., 1999; Majid et al., 2002), and Y191C and S204C have been shown to induce apoptosis of RPE cells more than WT TIMP-3 (Majid et al., 2002). Therefore, I hypothesise that these SFD TIMP-3 mutants may cause apoptosis of HEK-293 cells to a greater degree, resulting in fewer viable cells and an overall lower protein expression in the conditioned medium.

Isolation of WT, H181R, Y191C and S204C TIMP-3 was successful with strong staining for bands at the expected molecular mass of ~ 25 kDa in elution fractions in both TNC-B and SF DMEM (**Figure 3.4**, **Figure 3.5** & **Figure 3.8**). Isolation of E162K TIMP-3 in TNC-B also appeared to be successful, but bands at ~ 25 kDa were very weak (**Figure 3.6 A**), in comparison with known amounts of WT TIMP-3 (**Figure 3.6 B**). HEK-293 cells transfected with this mutant may have expressed very little of the E162K protein, or it may be particularly toxic to cells. Due to time constraints, this mutant was not analysed further in the current study, but these preliminary data suggest that investigation of the relative toxicity of this mutant may be an interesting area for future study.

Isolation of WT, E162K, H181R, Y191C and S204C TIMP-3 predominantly gave a major species at ~ 25 kDa in elution samples (**Figure 3.4**, **Figure 3.5**, **Figure 3.6** & **Figure 3.8**). WT TIMP-3 is seen in many cell types as 2 bands, with unglycosylated TIMP-3 migrating at 24 kDa and N-glycosylation of TIMP-3 at position Asn184 near the carboxyl terminus resulting in a ~ 27 kDa form (Apte et al., 1994b; Langton et al., 1998; Leco et al., 1994). Analysis of crude conditioned media (**Figure 3.2**) shows that HEK-293 cells express mostly glycosylated TIMP-3 (WT, S204C, Y191C) with

small amounts of non-glycosylated TIMP-3. As has been observed previously (Doherty et al., 2016; Troeberg et al., 2009), non-glycosylated TIMP-3 was lost during isolation, due to its lower abundance and possibly elevated ‘stickiness’.

When isolation of WT TIMP-3 (**Figure 3.4**), as well as E162K, H181R, Y191C and S204C TIMP-3 was analysed using the anti-FLAG M2 antibody, no bands were seen in the unbound fractions, indicating that all detectable FLAG-tagged TIMP-3 was isolated by the resin. Analysis of these samples with the anti-TIMP-3 AB6000 antibody (**Figure 3.4** & data not shown) shows that bands at ~ 25 kDa are present in the unbound fraction. These most likely correspond to endogenously produced TIMP-3 that lacks a FLAG tag, although proteolytic loss of the FLAG tag during culture has been reported (Kashiwagi et al., 2004; Troeberg et al., 2009).

Silver staining was performed on eluted samples of WT, H181R, Y191C and S204C TIMP-3 in TNC-B to determine their purity (**Figure 3.7**). All preparations contained an abundant band at ~ 25 kDa, as expected for monomeric TIMP-3, and additionally contained less abundant bands at higher molecular masses. These higher molecular weight bands were particularly abundant in the Y191C preparations (**Figure 3.7 B**). Due to the lower yield of S204C, this necessitated TCA precipitation, possibly resulting in an apparent relative increase in the strong bands observed at higher molecular weights. These high molecular weight species may correspond to multimers of SFD TIMP-3 variants, but this is unlikely because these bands are more abundant on the silver stains than on TIMP-3 immunoblots. WT, H181R, Y191C, and S204C TIMP-3 may form complexes with other proteins such as ECM components, resulting in the observation of these high molecular weight species. Alternatively, these proteins may bind non-specifically to M2 resin, or have remained despite the extensive washing steps employed before elution. Previous analyses in our group showed that the yield of TIMP-3 drops substantially with every purification step (Troeberg et al., 2009), so I decided to proceed with the mutants at this level of purity, since further purification would have greatly reduced yield and the number and scope of experiments that could be undertaken.

Pro-MMP-1 was also successfully isolated from the conditioned medium of HEK-293 cells, followed by activation using 1 mM AMPA (**Figure 3.10**). The mechanism by which APMA induces this activation is not entirely clear (Chen et al., 1993; Galazka et al., 1996), although it involves disruption of a cysteine switch

(Fernandez-Patron et al., 2002). A known concentration of active MMP-1 was then titrated against doubling dilutions of WT, H181R, Y191C or S204C TIMP-3 to determine their active concentrations. E162K TIMP-3 was not titrated due to its low yield (**Figure 3.6**). Titrations consistently revealed highest active concentrations for WT TIMP-3 in TNC-B or SF DMEM compared to the SFD TIMP-3 mutants, which were always less than half the concentration of WT TIMP-3. There are several factors that could contribute to this, including higher expression of WT TIMP-3 in transfected HEK-293 cells (**Figure 3.2 & Figure 3.3**) or greater loss of the mutants during isolation on the anti-FLAG M2 resin. Furthermore, the age of the HEK-293 cells that conditioned medium was collected from would also affect yield, as over time the cell population loses the pCEP4 vector resulting in an overall lower expression in the conditioned medium. H181R, Y191C and S204C TIMP-3 all inhibited MMP-1 effectively, indicating the mutations had not significantly altered the structure of TIMP-3 and affected their ability to form high-affinity complexes with this enzyme. The H181R and Y191C mutations are located away from the active ridge of TIMP-3, so are unlikely to affect the ability of these mutants to bind to MMPs, and indeed Y191C has been reported to have unaffected inhibition of MMP-2 and MMP-9 (Arris et al., 2003; Langton et al., 1998, 2005; Yeow et al., 2002), however data for H181R is lacking. It is difficult to determine where the S204C mutation occurs in the TIMP-3 structure due to its close proximity to the flexible C-terminus of TIMP-3, so its impact on TIMP-3 structure is particularly difficult to predict, however S204C has been reported to have unaffected inhibition of MMP-2 and MMP-9 (Arris et al., 2003; Langton et al., 1998, 2005; Yeow et al., 2002). Additionally, attempts at predicting the structure of H181R, Y191C and S204C TIMP-3 using AlphaFold (data not shown) suggested that the inhibitory ridge of TIMP-3 was unaffected by these mutations. Collectively previous reports in combination with my observations indicate that H181R, Y191C and S204C retain the ability to bind and inhibit at least some, but the kinetics of these interactions requires further investigation.

As discussed previously (**3.1**), there is a general consensus that SFD TIMP-3 mutants form dimers, multimers and higher molecular weight complexes (Betts & Troeberg, 2024) and the presence of these dimers have been observed by multiple investigators in several cell types (Arris et al., 2003; Langton et al., 2000, 2005; Weber et al., 2002; Yeow et al., 2002). Dimers are widely considered to form through intermolecular disulfide bonds, but even mutants lacking an unpaired cysteine, (e.g., E162K and H181R) have been shown to form dimers (Alsaffar et al., 2022; Saihan

et al., 2009). Anti-FLAG M2 blots of HEK-293 transfection experiments (**Figure 3.2 & Figure 3.3**) and isolations (**Figure 3.5, Figure 3.6 & Figure 3.8**) revealed the presence of potential dimeric species at ~ 55 kDa for WT and SFD mutants, corroborating previous observations (Alsaffar et al., 2022; Langton et al., 2005; Saihan et al., 2009). However, these bands were weak, and in some cases (e.g., **Figure 3.2 Figure 3.5 A & Figure 3.8 B**) absent. Another group have reported an absence of dimer observation for a different SFD mutant, S179C TIMP-3 (J. H. Qi et al., 2002), and it was suggested by other investigators (Langton et al., 2005) that the C-terminal FLAG tag used by Qi et al 2002, impeded the formation of dimeric species. This could also be the case for my SFD mutants (H181R, Y191C and S204C) due to the presence of a FLAG tag at the C-terminus. Dimeric species were also observed in HEK-293 cells expressing WT TIMP-3 (**Figure 3.3**) and dimeric species of WT TIMP-3 have been observed previously (Langton et al., 2005; Yeow et al., 2002), indicating that dimer formation is not exclusive to SFD TIMP-3 mutants.

Higher molecular weight species (above 100 kDa) were also consistently observed in isolation blots (**Figure 3.4, Figure 3.5 & Figure 3.6**) for WT TIMP-3 and all of the SFD TIMP-3 mutants. As discussed these species may arise from identical monomers, or SFD TIMP-3 proteins could also form dimeric and multimeric species with WT TIMP-3 expressed endogenously by HEK-293 cells. Alternatively, higher molecular weight species may arise from binding of WT or SFD TIMP-3 proteins to components of the ECM or by binding to other proteins non-specifically bound to the M2 resin.

The overwhelming hypothesis is that dimers and multimers arise from intermolecular disulfide bond formation between SFD TIMP-3 monomers that have a free cysteine introduced by mutation. Multiple groups have shown by immunoblot analysis that reduction of SFD TIMP-3 mutants results in disappearance of a dimeric band and a concurrent increase in the intensity of monomeric bands (Alsaffar et al., 2022; Arris et al., 2003; Langton et al., 2000, 2005), indicating that SFD dimers are a product of intermolecular disulfide bond formation. Therefore, I performed reduction and alkylation experiments on WT, H181R, Y191C and S204C TIMP-3 in TNC-B and SF DMEM to determine if I could reproduce these findings (**Figure 3.9**). Immunoblotting with an anti-FLAG M2 antibody revealed strong bands at ~ 25 kDa for WT, H181R, Y191C and S204C TIMP-3, in TNC-B and SF DMEM, that shifted upwards upon reduction. This is indicative of the presence of disulfide bonds in the recombinant

monomeric proteins. Also, for the Y191C TIMP-3 variant in TNC-B (**Figure 3.9 A & B**), a high molecular weight band, above 130 kDa, present in the non-reducing sample disappeared under reducing conditions, indicating that this did involve aberrant disulfide bond formation. However, most of the ‘multimer’ bands were more visible and had an upwards shift in reducing conditions compared to non-reducing conditions, suggesting that these are not a product of intermolecular disulfide bonding. For example, bands corresponding to the molecular weight reported for SFD TIMP-3 dimers (Alsaffar et al., 2022; Arris et al., 2003; Langton et al., 2005) migrated at ~ 55 kDa in WT, H181R, Y191C and S204C TIMP-3, in TNC-B and SF DMEM, under reducing conditions (**Figure 3.9 A & C**), but could not be seen in non-reducing lanes, unless immunoblots were overexposed (**Figure 3.9 B & D**). Bands appeared more strongly at ~ 55 kDa under reducing conditions and this was also the case for ~ 25 kDa bands, suggesting that reduction resulted in a change in protein structure that exposed the FLAG epitope more allowing for greater antibody detection. In addition, Y191C, as well as S204C TIMP-3 had strong staining at very high molecular weights that appeared to remain at the same molecular weight even when run under reducing conditions, with this particularly noticeable for those isolated in SF DMEM, which lacks the 0.05 % Brij detergent included in the TNC-B buffer.

Overall, the consistency and abundance with which dimers were detected in my experiments appear to be considerably reduced compared to that reported by other investigators. Furthermore, my reduction and alkylation experiments suggest that dimeric species can form without intermolecular disulfide bond formation for H181R, Y191C and S204C TIMP-3, indicating that both TIMP-3 mutants with and without free cysteine residues can form dimers via a disulfide bond-independent mechanism. It is important to consider that my experiments were performed in HEK-293 cells, thus it is possible that the SFD mutants do not behave in the same way they would when expressed natively in cells of the retina. However, it is interesting to consider whether disulfide bond-independent multimers could form in SFD. Perhaps these could be non-disulfide bonded aggregates, like those that have been reported for amyloid beta plaques that are resistant to reduction (Pedrero-Prieto et al., 2019). Alternatively, these disulfide bond-independent multimers could be an artefact of SDS-PAGE, with SDS inducing an unfolded state that favours aggregation. Analyses such as gel filtration chromatography and static light

scattering could be used to address the issue of whether these species occur in solution.

A potential reason for the considerably decreased detection of SFD mutant dimers in this study compared to other investigators may be due the different detection methods used. In general, previous experiments have used reverse zymography or chemiluminescent immunoblot methods without reporting linear ranges of detection, which could result in overexposure and an apparent 'increased' abundance of dimer (Betts & Troeberg, 2024). Light scattering approaches or circular dichroism could also prove useful in quantifying relative abundance of monomers and dimers/multimers in preparations of SFD TIMP-3 mutants (Betts & Troeberg, 2024). Alternatively, these differences may be due to the cell type expressing the proteins, with SFD mutant dimer formation being reported in human fibroblasts, ARPE-19, BHK, COS-7, mouse RPE, hiPSC-RPE, porcine aortic endothelial cells and HEK-293 cells (Alsaffar et al., 2022; Arris et al., 2003; Guan et al., 2022; Hongisto et al., 2020; Langton et al., 1998, 2000, 2005; Lin et al., 2006; Naessens et al., 2019; Qi & Anand-Apte, 2022; Saihan et al., 2009; Weber et al., 2002; Yeow et al., 2002). Only L10H and G12R have been reported to form dimeric species in transfected HEK-293 cells (Guan et al., 2022). It may be that SFD mutants may have a higher propensity to form dimeric/multimeric species when expressed in specific cell types other than HEK-293 cells, given the low level of dimeric/multimeric species observed in the experiments presented above (**Figure 3.2, Figure 3.3, Figure 3.5, Figure 3.6, Figure 3.8 & Figure 3.9**). Formation of SFD mutant dimeric species will be revisited in **Chapter 4**.

Increasing numbers of studies aim to examine the global effect of SFD TIMP-3 mutants on RPE cells (Engel et al., 2022; Grenell et al., 2024; Hongisto et al., 2020), so the next chapter investigated whether SFD TIMP-3 mutants induce changes in gene expression in ARPE-19 cells or promote apoptosis.

## **Chapter 4: What are the effects of SFD TIMP-3 mutants on RPE gene expression and health?**

## 4.1 Introduction

TIMP-3 is a multifunctional protein that was originally classified as an inhibitor of matrix metalloproteinases but can also inhibit other metalloproteinases including ADAMs and ADAMTSs (Brew & Nagase, 2010). TIMP-3 is also a potent inhibitor of angiogenesis, by competitively blocking VEGF binding to VEGFR2 (Anand-Apte et al., 1997; Qi et al., 2003). Rightly so, the pathology of SFD has largely been studied by looking at how SFD mutations in TIMP-3 affect these aforementioned functions of the protein and how this may consequently cause pathology. For instance, the ability of SFD TIMP-3 mutants to inhibit MMPs and angiogenesis has been extensively studied (Betts & Troeberg, 2024).

More recently, there have been an increasing number of studies that have taken more agnostic approaches in examining how mutations in TIMP-3 lead to SFD pathology. These studies have investigated the global effect of SFD TIMP-3 proteins on RPE cells in terms of metabolism and protein expression, rather than looking at how individual functions of TIMP-3 may be altered by SFD mutations. Such approaches include mass spectrometry to profile both proteomic changes (Hongisto et al., 2020) and metabolomic effects (Engel et al., 2022; Grenell et al., 2024). An additional study sought to determine whether SFD TIMP-3 mutants cause apoptosis of RPE cells (Majid et al., 2002), however this area has not received much follow-up.

Thus, the aim of this chapter was to investigate some of the broader impacts of the SFD TIMP-3 mutants, H181R, Y191C and S204C by looking at their impact on RPE gene expression and health. To this end, ARPE-19 cells were transfected with WT, H181R, Y191C or S204C TIMP-3 and the expression of LRP family receptors, metalloproteinases, proteoglycans, cytokines and oxidative stress enzymes was investigated at the mRNA level (**4.2.2 & 4.2.3**). Furthermore, it was examined whether H181R or S204C TIMP-3 induced apoptosis of RPE cells to a greater degree than WT TIMP-3 (**4.2.4**).

## 4.2 Results

### 4.2.1 Optimisation of ARPE-19 cell transfection with pCEP4 plasmids encoding WT and SFD TIMP-3 mutants

ARPE-19 cells were chosen as they are a highly characterised RPE cell line capable of forming a polarised epithelial layer with apical and basolateral specialisation and polarised secretion, as well as exhibiting phagocytic capacity and expression of characteristic proteins such as RPE65, CRALBP and MerTK (Ahmado et al., 2011; Dunn et al., 1996; Lynn et al., 2017). Additionally, ARPE-19 cells also exhibit classical cobblestone morphology of RPE cells and have been used widely in the literature in thousands of reports over the last 20-30 years (Lynn et al., 2018).

ARPE-19 cells were transfected with several amounts of pCEP4 vector encoding C-terminally FLAG-tagged WT, Y191C or S204C TIMP-3 or an empty pCEP4 vector which was used as a negative control. Two different transfection reagents, jetPRIME or Lipofectamine 3000, were compared to ascertain which enabled the higher expression of WT, Y191C and S204C TIMP-3 in the conditioned media. Plasmid amounts were chosen based on recommendations from the transfection reagents manufacturers. After 48 h, conditioned media and RNA samples were collected to quantify TIMP-3 expression at the protein and mRNA levels using immunoblotting and RT-qPCR, respectively (**Figure 4.1 A, B, C & D**).

Using an anti-TIMP-3 AB6000 antibody (**Figure 4.1 A**) and an anti-FLAG M2 antibody (**Figure 4.1 B**), expression of WT, Y191C and S204C TIMP-3 in the conditioned medium of transfected ARPE-19 cells was observed when jetPRIME or Lipofectamine 3000 was used. The AB6000 immunoblot showed that cells transfected with the empty pCEP4 vector expressed a protein at  $\sim$  25 kDa, corresponding to the molecular weight of TIMP-3, but these bands were not observed in the anti-FLAG M2 blot, hence this indicates endogenously expressed WT TIMP-3 (**Figure 4.1 A & B**). Conditioned media from HEK-293 cells transfected with WT TIMP-3 was included as a positive control, and this sample showed two distinct bands just above and below  $\sim$  25 kDa, indicative of a glycosylated and non-glycosylated form of TIMP-3. ARPE-19 cells transfected with jetPRIME reagent exhibited a strong band for WT TIMP-3, which was much stronger than the bands for cells transfected with the same amount of plasmids encoding Y191C and S204C TIMP-3 (**Figure 4.1 A & B**). Similarly, ARPE-19 cells transfected using

Lipofectamine 3000 exhibited much stronger staining at ~ 25 kDa for WT TIMP-3 than Y191C and S204C TIMP-3 at the same plasmid amounts, and 5 µg of plasmid gave higher WT TIMP-3 expression than 2.5 µg of plasmid (**Figure 4.1 A & B**). It was hard to distinguish two separate TIMP-3 bands in transfected ARPE-19 conditioned media, compared to the transfected HEK-293 sample, suggesting that there is altered glycosylation in the two cell types. Additional bands between 40 and 55 kDa were observed for WT, Y191C and S204C in ARPE-19 cells transfected using jetPRIME; these bands were also seen when ARPE-19 cells were transfected using Lipofectamine 3000, although they were much weaker than bands at ~ 25 kDa (**Figure 4.1 A & B**). Furthermore, higher molecular weight bands above the molecular weight markers were also observed, although these were also much weaker than bands at ~ 25 kDa. Quantification of ~ 25 kDa bands from the anti-FLAG M2 blot revealed that ARPE-19 cells transfected with 2.5 µg of each plasmid using jetPRIME had greater expression of WT, Y191C and S204C TIMP-3 in the conditioned media than when Lipofectamine 3000 was used and either 2.5 or 5 µg of plasmid (**Figure 4.1 C**). This did not correlate with mRNA expression, as highest fold mRNA changes were observed when Lipofectamine 3000 and 5 µg of plasmid were used (**Figure 4.1 D**).

jetPRIME was then tested against Lipofectamine LTX (**Figure 4.1 E & F**) which has been reported to have high transfection efficiency in ARPE-19 cells (Shaw & Lipinski, 2021). ARPE-19 cells were transfected with 2 µg of each plasmid, using either jetPRIME or Lipofectamine LTX. Anti-FLAG M2 immunoblotting revealed stronger bands for WT, Y191C and S204C TIMP-3 when Lipofectamine LTX was used compared to jetPRIME (**Figure 4.1 E**). Quantification of the bands, demonstrated that protein expression of WT, Y191C and S204C TIMP-3 were all higher when Lipofectamine LTX was used compared to jetPRIME and that WT TIMP-3 expression was higher than Y191C and S204C TIMP-3 expression (**Figure 4.1 F**). Despite this being an n = 1 experiment, Lipofectamine LTX was chosen as the transfection reagent for subsequent ARPE-19 cell transfections.

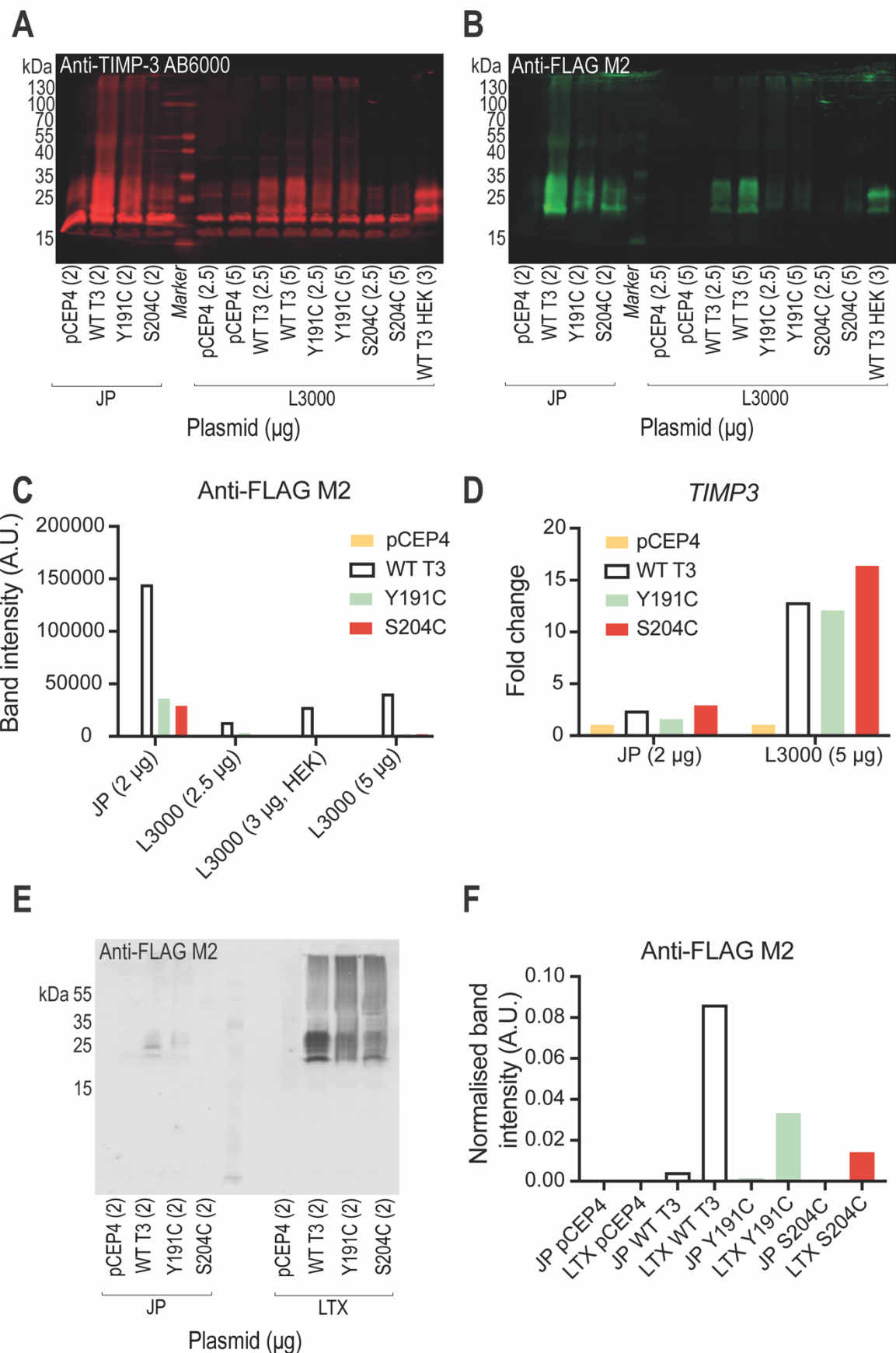


**Figure 4.1: Optimisation of ARPE-19 transfection with pCEP4 plasmids encoding WT, Y191C and S204C TIMP-3 with jetPRIME, Lipofectamine 3000, or Lipofectamine LTX transfection reagents.**

ARPE-19 cells (500 000 per well in a 6-well plate) were cultured overnight in growth DMEM (2 ml). On the day of transfection, media were replaced with fresh growth DMEM (2 ml) for jetPRIME reagents or replaced with Opti-MEM (2 ml) for Lipofectamine 3000 and Lipofectamine LTX. Cells were transfected with jetPRIME, Lipofectamine 3000, or Lipofectamine LTX and the indicated

plasmid amounts following the manufacturer's instructions. After 24 h, media were changed to SF DMEM (2 ml) and cells cultured for a further 24 h. (A-B) Conditioned media were then collected, TCA precipitated, and resuspended in 2x non-reducing SDS-PAGE sample buffer (50  $\mu$ l). Resuspended samples (15  $\mu$ l) from jetPRIME and Lipofectamine 3000 transfections were analysed by immunoblotting using an anti-FLAG M2 (A) or anti-TIMP-3 AB6000 (B) antibody, followed by detection with a fluorescent anti-mouse or anti-rabbit IgG secondary antibody, respectively. (C) Bands on the anti-FLAG M2 immunoblot were quantified. (D) RNA was extracted, cDNA synthesised and mRNA expression of *TIMP3* measured by RT-qPCR. Using the  $\Delta\Delta CT$  method, data were normalised against the housekeeper gene *GAPDH*, and expressed relative to HEK-293 cells transfected with an empty pCEP4 vector. n=1 replicate. (E-F) Resuspended samples (15  $\mu$ l) from jetPRIME and Lipofectamine LTX transfections were analysed by immunoblotting using an anti-FLAG M2 (E) antibody, followed by detection with a fluorescent anti-mouse IgG secondary antibody. (F) Bands on the anti-FLAG M2 immunoblot were quantified and normalised to total protein stain in each lane (data not shown). n=1 replicate. JP denotes jetPRIME; L3000 denotes Lipofectamine 3000; LTX denotes Lipofectamine LTX.

After selecting a transfection reagent, it was next determined what a suitable amount of plasmid was to use in order to achieve similar protein expression of monomeric (~ 25 kDa) WT, H181R, Y191C and S204C TIMP-3 in the conditioned media of ARPE-19 cells (**Figure 4.2**). ARPE-19 cells were transfected with 1, 5 or 9  $\mu$ g of pCEP4 vector encoding C-terminally FLAG-tagged WT, H181R, Y191C or S204C TIMP-3. ARPE-19 cells transfected with 5  $\mu$ g of an empty pCEP4 vector or treated with Lipofectamine LTX reagent alone were used as negative controls. Probing of the conditioned media with an anti-FLAG M2 antibody revealed strong bands at ~ 25 kDa for all plasmids (other than the 5  $\mu$ g pCEP4 negative control) used at each plasmid amount (**Figure 4.2 A**, black arrow). Bands were also seen in all transfected samples between 40-55 kDa (**Figure 4.2 A**, red arrow), corresponding to the dimeric molecular weight of TIMP-3, as has been reported previously for SFD TIMP-3 mutants and also WT TIMP-3 (Betts & Troeberg, 2024). Quantification of monomeric bands (25 kDa) and normalisation to a total protein stain revealed that WT TIMP-3 expression was far higher at all amounts of plasmid compared to expression of H181R, Y191C and S204C TIMP-3 (**Figure 4.2 B, left-hand side**). The expression of H181R TIMP-3 detected in the conditioned medium was similar across all amounts of plasmid used, however 5  $\mu$ g of plasmid achieved the highest detectable protein expression (**Figure 4.2 B, left-hand side**). Similarly, the amount of Y191C TIMP-3 detectable in the conditioned medium was uniform across all amounts of plasmid used (**Figure 4.2 B, left-hand side**), whereas for S204C TIMP-3 a progressive increase in protein detected was observed, with 9  $\mu$ g of plasmid achieving the highest protein expression (**Figure 4.2 B, left-hand side**). In contrast, abundance of WT TIMP-3 at its dimeric molecular weight (40-55 kDa) was lower than that for Y191C and S204C TIMP-3 a (excluding 9  $\mu$ g of Y191C) (**Figure 4.2 B, right-hand side**). From these experiments it was decided that lower amounts of

pCEP4 vector encoding WT TIMP-3 needed to be used in order to achieve a similar protein expression to the 3 SFD TIMP-3 mutants.

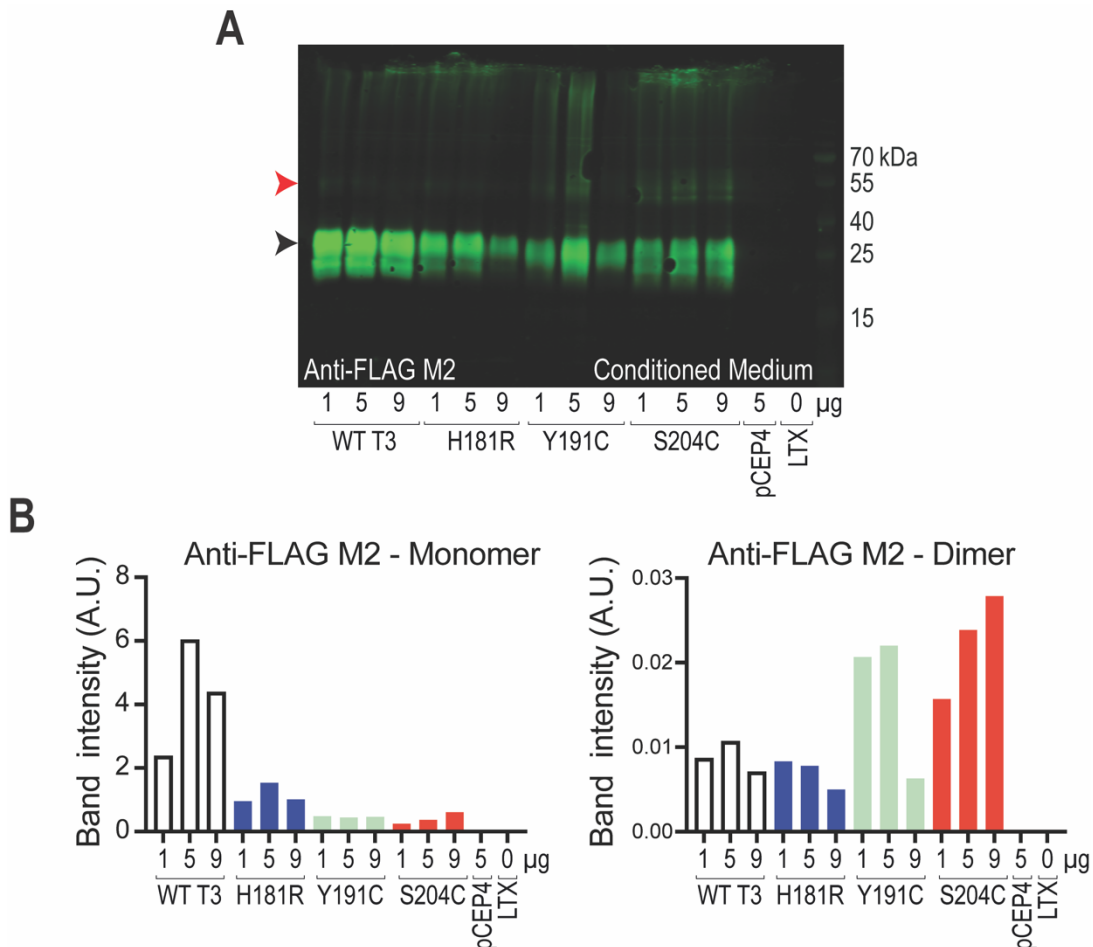


**Figure 4.2: Initial optimisation of ARPE-19 transfection with pCEP4 plasmids encoding WT T3, H181R, Y191C and S204C.**

ARPE-19 cells (250 000 per well in a 12-well plate) were cultured overnight in growth DMEM (2 ml). On the day of transfection, wells were washed in SF DMEM (3 x 2.5 ml) and media were replaced with Opti-MEM (2 ml). Cells were transfected with Lipofectamine LTX and the indicated plasmid amounts following the manufacturer's instructions. After 4 h, media were changed to SF DMEM (2 ml) supplemented with NaClO<sub>3</sub> (30 mM) and cultured for a further 20 h. Conditioned media were then collected, TCA precipitated, and resuspended in 2x non-reducing SDS-PAGE sample buffer (50  $\mu$ l). Resuspended samples (15  $\mu$ l) were analysed by immunoblotting using an anti-FLAG M2 antibody (A), followed by detection with a fluorescent anti-mouse IgG secondary antibody. (B) Bands on the anti-FLAG M2 immunoblot were quantified at the monomeric (~24 kDa, black arrow) and dimeric (~48 kDa, red arrow) molecular weights and normalised to a total protein stain in each lane (not shown). n=1 replicate. LTX denotes Lipofectamine LTX.

In further optimisation experiments, lower amounts of pCEP4 plasmid encoding WT TIMP-3 were used (0.25, 0.5, 0.75 and 1  $\mu$ g) alongside 5 and 9  $\mu$ g of SFD mutant TIMP-3 plasmids (Figure 4.3 A). Analysis using an anti-FLAG M2 antibody revealed that 0.25  $\mu$ g of pCEP4 plasmid encoding WT TIMP-3 gave similar expression of monomeric TIMP-3 as 5  $\mu$ g of pCEP4 plasmid encoding H181R, Y191C or S204C TIMP-3 (Figure 4.3 A, left-hand side). Again, bands were visible between 40-55 kDa (red arrow), corresponding to the dimeric forms of TIMP-3 proteins. Quantification and normalisation of these dimeric bands demonstrated that S204C

TIMP-3 at both plasmid amounts had a greater amount of dimer formation (**Figure 4.3 A, right-hand side**), matching previous observations (**Figure 4.2 B, right-hand side**). Dimers were only observed for H181R at 5 µg of plasmid and were weak in comparison to S204C dimers, but similar to those observed for WT TIMP-3. Y191C dimers were strong when 5 µg of plasmid were used. These results again show that generally Y191C and S204C TIMP-3 exhibited the highest amount of dimeric species in conditioned media.

In these experiments, the ECM was also probed with an anti-FLAG M2 antibody for the presence of WT and SFD TIMP-3 (**Figure 4.3 B**). Quantification and normalisation of monomeric bands (**Figure 4.3 B**, black arrow), revealed strong staining for WT TIMP-3 when 1 µg of plasmid was used, as well as H181R TIMP-3 when 5 µg was used (**Figure 4.3 B, left-hand side**). 5 and 9 µg of S204C plasmid resulted in abundant dimer detection in the ECM, with notably low abundance of monomeric species. For WT, H181R or Y191C, very low amounts of dimeric species were detected (**Figure 4.3 B, right-hand side**).

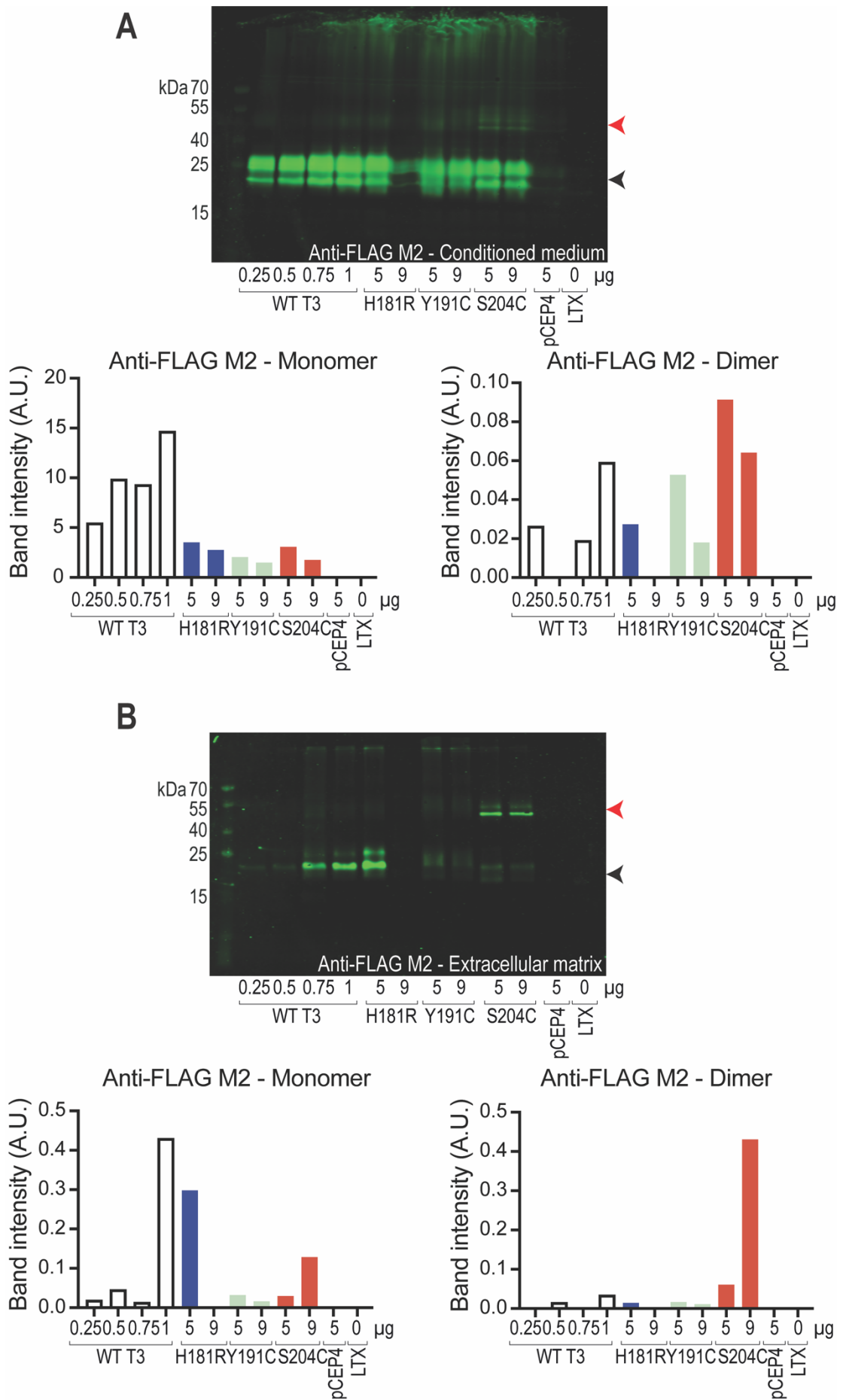


**Figure 4.3: Further optimisation of ARPE-19 transfection with pCEP4 plasmids encoding WT T3, H181R, Y191C and S204C.**

ARPE-19 cells (250 000 per well in a 12-well plate) were cultured overnight in growth DMEM (2 ml). On the day of transfection, wells were washed in SF DMEM (3 x 2.5 ml) and media were replaced with Opti-MEM (2 ml). Cells were transfected with Lipofectamine LTX and the indicated plasmid amounts following the manufacturer's instructions. After 4 h, media were changed to SF DMEM (2 ml) supplemented with NaClO<sub>3</sub> (30 mM) and cultured for a further 20 h. Conditioned media were then collected, TCA precipitated, and resuspended in 2x non-reducing SDS-PAGE sample buffer (50 µl). **(A)** Resuspended samples (15 µl) were analysed by immunoblotting using an anti-FLAG M2 antibody, followed by detection with a fluorescent anti-mouse IgG secondary antibody. Bands on the anti-FLAG M2 immunoblot were quantified at the monomeric (~24 kDa, black arrow) and dimeric (~48 kDa, red arrow) molecular weights. n=1 replicate. **(B)** After conditioned media were removed, ARPE-19 cells were collected in cell dissociation solution and discarded. 2x non-reducing SDS-PAGE sample buffer (50 µl) was used to collect ECM samples, which were subsequently boiled (100 °C, 5 min). ECM samples (15 µl) were analysed by immunoblotting using an anti-FLAG M2 antibody, followed by detection with a fluorescent anti-mouse IgG secondary antibody. Bands on the anti-FLAG M2 immunoblot were quantified at the monomeric (~24 kDa, black arrow) and dimeric (~48 kDa, red arrow) molecular weights and normalised to a total protein stain in each lane (not shown). n=1 replicate. LTX denotes Lipofectamine LTX.

#### 4.2.2 Optimised ARPE-19 cell transfection with pCEP4 plasmids encoding WT and SFD TIMP-3 mutants

Given that similar expression of monomeric TIMP-3 species was observed with 0.25 µg of WT TIMP-3 plasmid and 5 µg of H181R, Y191C and S204C TIMP-3 plasmids (**Figure 4.3**), these amounts of plasmids were used in an optimised transfection experiment with ARPE-19 cells (**Figure 4.4**). Following transfection, conditioned media were collected for immunoblot analysis (**Figure 4.4 C**), and ARPE-19 cells were collected for analysis of gene expression of *TIMP3* (**Figure 4.4 B**) and other candidate ECM-related genes (**Figure 4.5**, **Figure 4.6**, **Figure 4.7 & Figure 4.8**), as well as an MTS assay to assess cell viability (**Figure 4.4 A**).

A cell viability assay was performed to determine whether transfection with pCEP4 plasmids encoding WT, H181R, Y191C or S204C TIMP-3 affected ARPE-19 cell health (**Figure 4.4 A**). A positive control for cell death was generated by repeatedly freeze-thawing untransfected ARPE-19 cells between -80 °C and 25 °C. There was no significant difference in absorbance between ARPE-19 cells transfected with an empty pCEP4 plasmid or pCEP4 plasmids encoding WT, H181R, Y191C or S204C TIMP-3. However, the positive control for cell death had significantly decreased absorbance compared to cells transfected with the empty pCEP4 vector (**Figure 4.4 A**). This indicated that transfection with these plasmids did not have an adverse effect on ARPE-19 cell health.

RT-qPCR analysis revealed that ARPE-19 cells transfected with plasmids encoding H181R, Y191C or S204C TIMP-3 all exhibited significantly increased *TIMP3* expression relative to control cells transfected with an empty pCEP4 vector (**Figure**

**4.4 B).** *TIMP3* expression in cells transfected with a pCEP4 plasmid encoding WT TIMP-3 was not significantly different from cells transfected with the empty pCEP4 vector (**Figure 4.4 B**). This mRNA expression did not correlate with monomeric TIMP-3 protein expression in the conditioned media, as WT TIMP-3 expression was significantly higher in cells transfected with TIMP-3/pCEP4 than empty pCEP4 vector (**Figure 4.4 C**). Expression of WT TIMP-3 was also significantly higher than that of the SFD TIMP-3 mutants (significance not shown), despite previous optimisation of plasmid amounts (**Figure 4.3**).

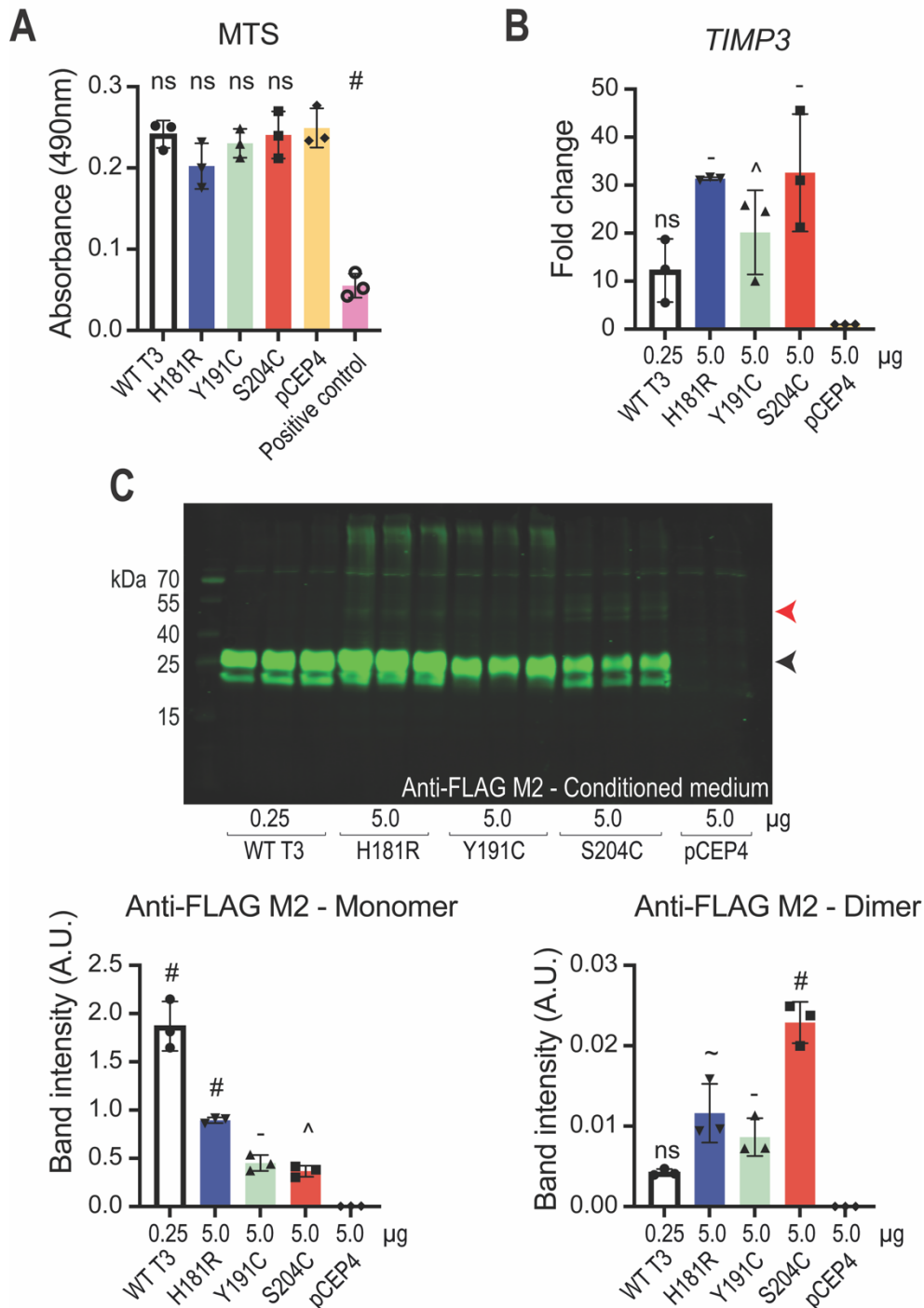


**Figure 4.4: Optimised transfection of ARPE-19 cells with pCEP4 plasmids encoding WT, H181R, Y191C and S204C TIMP-3.**

ARPE-19 cells (250 000 per well in a 12-well plate) were cultured overnight in growth DMEM (2 ml). On the day of transfection, wells were washed in SF DMEM (3 x 2.5 ml) and media were replaced with Opti-MEM (2 ml). Cells were transfected with Lipofectamine LTX and the indicated plasmid amounts following the manufacturer's instructions. After 4 h, media were changed to SF DMEM (2 ml) supplemented with NaClO<sub>3</sub> (30 mM) and cultured for a further 20 h. Conditioned media were then collected, TCA precipitated, and resuspended in 2x non-reducing SDS-PAGE sample buffer (50  $\mu$ l). **(A)** After conditioned media were removed, ARPE-19 cells were collected in cell dissociation solution, collected by centrifugation (400 RCF, 5 min), and resuspended in SF DMEM (2 ml). Cells were incubated for 90 min [37 °C, 5 % (v/v) CO<sub>2</sub>] with MTS reagent and absorbance at 490 nm quantified using a SPECTROstar Omega plate reader. Data are presented as mean  $\pm$  SD (n = 3), with normality assessed with Shapiro-Wilks test and analysed for significance relative to the pCEP4 cells with one-way ANOVA and corrected for multiple comparisons with Dunnett's multiple comparisons test ( $\sim$  = p  $\leq$  0.001, # = p  $\leq$  0.0001). **(B)** RNA was extracted, cDNA synthesised and mRNA expression of *TIMP3* measured by RT-qPCR. Using the  $\Delta\Delta CT$  method, data were normalised against the housekeeper gene *GAPDH* and expressed relative to a pCEP4 control. *TIMP3* expression (mean  $\pm$  SD, n = 3 per condition) was compared with data assessed for normality using Shapiro-Wilks test, and analysed for significance with a one-way ANOVA and corrected for comparisons with Dunnett's multiple comparisons test (ns = not significant,  $^{\wedge}$  = p  $\leq$  0.05, - = p  $\geq$  0.001). **(C)** Resuspended samples (15  $\mu$ l) were analysed by immunoblotting using an anti-FLAG M2 antibody, followed by detection with a fluorescent anti-mouse IgG secondary antibody. TIMP-3 bands (mean  $\pm$  SD, n = 3 per condition) on the anti-FLAG M2 immunoblot were quantified at the monomeric (~24 kDa, black arrow) and dimeric (~48 kDa, red arrow) molecular weights and normalised to total protein stain in each lane (not shown). Data were assessed for normality with Shapiro-Wilks test and analysed for significance. The graphs display significance relative to the pCEP4 control with one-way ANOVA and corrected for multiple comparisons with Tukey's multiple comparisons test (ns = not significant,  $^{\wedge}$  = p  $\leq$  0.05, - = p  $\geq$  0.001,  $\sim$  = p  $\leq$  0.001, # = p  $\leq$  0.0001).

Similar to previous observations, ARPE-19 cells transfected with S204C TIMP-3 displayed significantly more dimeric TIMP-3 compared to an empty pCEP4 vector (**Figure 4.4 C**), as well as WT, H181R and Y191C TIMP-3 (significance not shown). ARPE-19 cells transfected with a pCEP4 vector encoding WT TIMP-3 had the lowest abundance of dimers in the conditioned media (**Figure 4.4 C**).

#### **4.2.3 Expression of LRP, metalloproteinase, proteoglycan, cytokines and oxidative stress genes induced by ARPE-19 transfection with WT and SFD TIMP-3**

ARPE-19 cells collected from the transfection performed in **Figure 4.4** were also analysed for changes in expression of candidate ECM-related and oxidative stress genes, to investigate whether expression of these proteins had transcriptional effects on cells.

LRP1 has been shown to endocytose TIMP-3 in other cell types, including chondrocytes and macrophages (Doherty et al., 2016; Schubert et al., 2019; Scilabria et al., 2013), thus changes in *LRP* gene expression were measured following ARPE-19 transfection with pCEP4 plasmid vectors encoding WT, H181R, Y191C and S204C TIMP-3 (**Figure 4.5**). Transfection with an empty pCEP4 vector was used as a negative control and all changes in gene expression were measured relative to this. Fold changes in expression of *LRP1*, *LRP1B*, *LRP2*, *LRP4*, *LRP5*, *LRP6*, *LRP8*, *LRP10*, *LRP11*, *LRP12*, *LDLR*, *VLDLR*, *LDLRAD3* and *SORL1* were minimal and not significant in ARPE-19 cells transfected with WT or SFD TIMP-3 compared to those transfected with an empty pCEP4 vector (**Figure 4.5**). A lot of variation was observed amongst biological replicates for several genes (*LRP1*, *LRP1b*, *LRP4*, *LRP6*, *LRP8*, *LRP12*, *LDLR* and *vLDLR*), particularly for cells transfected with S204C TIMP-3. There was also some variability between biological replicates for cells transfected with H181R for the genes *LRP1b*, *LRP2* and *LRP4* (**Figure 4.5**).

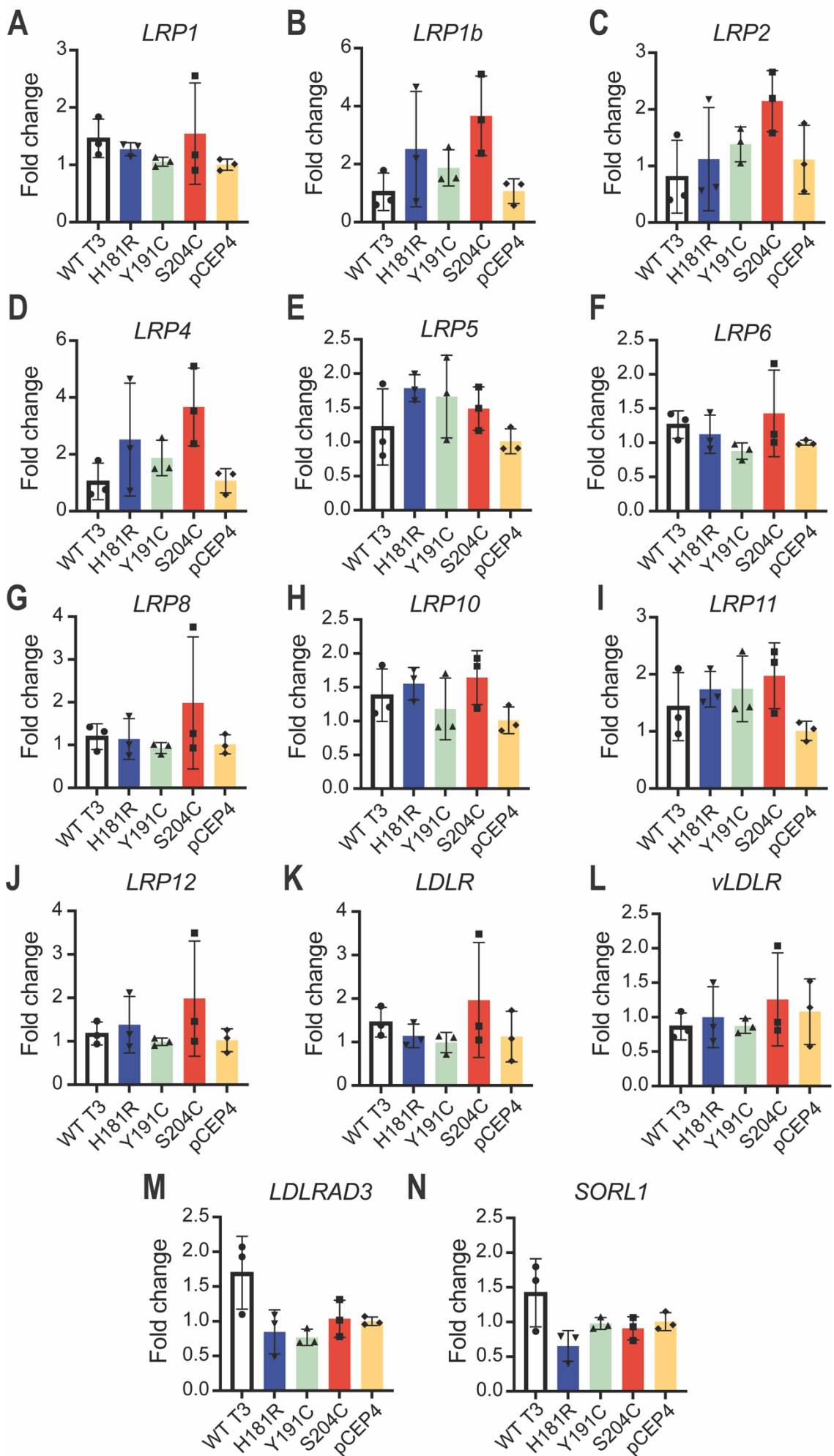


**Figure 4.5: Transfection of ARPE-19 cells with pCEP4 plasmids encoding WT, H181R, Y191C and S204C TIMP-3 did not change LRP-receptor mRNA expression.**

ARPE-19 cells (250 000 per well in a 12-well plate) were cultured overnight in growth DMEM (2 ml). On the day of transfection, wells were washed in SF DMEM (3 x 2.5 ml) and media were replaced with Opti-MEM (2 ml). Cells were transfected with Lipofectamine LTX and 0.25 µg of WT TIMP-3 (T3) plasmid or 5 µg of H181R, Y191C, S204C TIMP-3 or pCEP4 plasmid. After 4 h, media were changed to SF DMEM (2 ml) supplemented with NaClO<sub>3</sub> (30 mM) and cultured for a further 20 h. RNA was extracted, cDNA synthesised and mRNA expression of *LRP1* (**A**), *LRP1b* (**B**), *LRP2* (**C**), *LRP4* (**D**), *LRP5* (**E**), *LRP6* (**F**), *LRP8* (**G**), *LRP10* (**H**), *LRP11* (**I**), *LRP12* (**J**), *LDLR* (**K**), *vLDLR* (**L**), *LDLRAD3* (**M**), or *SORL1* (**N**) were measured by RT-qPCR. Using the  $\Delta\Delta CT$  method, data were normalised against the housekeeper gene *GAPDH* and expressed relative to a pCEP4 control. The expression of each gene (mean  $\pm$  SD, n = 3 per condition) was compared to the pCEP4 control with data assessed for normality using Shapiro-Wilks test, analysed for significance with a one-way ANOVA and corrected for comparisons with Dunnett's multiple comparisons test. Statistical comparisons for all genes were non-significant and are not labelled on the graph.

Genes encoding metalloproteinases including *MMP1*, *MMP2*, *MMP3*, *MMP8*, *MMP9*, *MMP13*, *MMP14*, *ADAM8*, *ADAM10* and *ADAM17* were also measured following ARPE-19 transfection. These genes have previously been reported to be expressed by RPE cells (Alexander et al., 1990; Bevitt et al., 2003; Campbell et al., 2019; De Groef et al., 2015). Expression of all of these genes again was again not significantly changed by transfection of ARPE-19 cells with plasmids encoding WT or SFD TIMP-3 relative to ARPE-19 cells transfected with an empty pCEP4 vector (**Figure 4.6**). Biological replicates transfected with S204C TIMP-3 showed variation in the expression of several genes, including *MMP9*, *MMP14* and *ADAM8*. A high amount of variation was also seen for certain genes in cells transfected with WT TIMP-3, including *ADAM8*, *ADAM10* and *ADAM17* (**Figure 4.6**).

Several proteoglycans are known to be present in the retinal BrM, including aggrecan, versican, agrin and perlecan (Keenan et al., 2012), thus fold changes in the expression of genes encoding these proteoglycans was investigated following ARPE-19 transfection with WT and SFD TIMP-3 (**Figure 4.7**). There was no significant difference in expression of *ACAN*, *VCAN*, *AGRN* and *HSPG2* in ARPE-19 cells transfected with plasmids encoding WT or SFD TIMP-3 compared to ARPE-19 cells transfected with an empty pCEP4 vector (**Figure 4.7**).

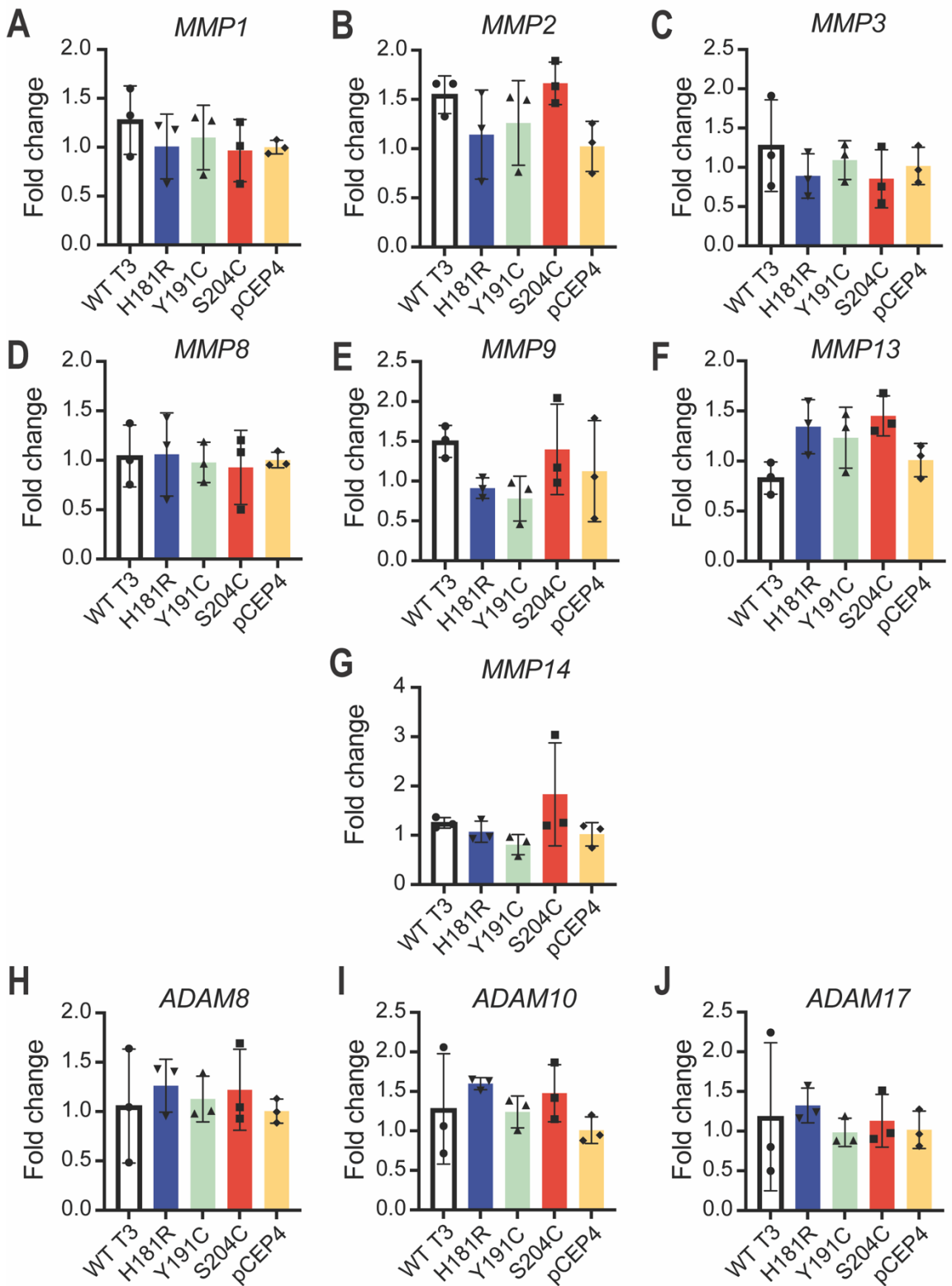


**Figure 4.6: Transfection of ARPE-19 cells with pCEP4 plasmids encoding WT, H181R, Y191C and S204C TIMP-3 did not change MMP or ADAM mRNA expression.**

ARPE-19 cells (250 000 per well in a 12-well plate) were cultured overnight in growth DMEM (2 ml). On the day of transfection, wells were washed in SF DMEM (3 x 2.5 ml) and media were replaced with Opti-MEM (2 ml). Cells were transfected with Lipofectamine LTX and 0.25 µg of WT TIMP-3 (T3) plasmid or 5 µg of H181R, Y191C, S204C TIMP-3 or pCEP4 plasmid. After 4 h, media were changed to SF DMEM (2 ml) supplemented with NaClO<sub>3</sub> (30 mM) and cultured for a further 20 h. RNA was extracted, cDNA synthesised and mRNA expression of MMP1 (A), MMP2 (B), MMP3 (C), MMP8 (D), MMP9 (E), MMP13 (F), MMP14 (G), ADAM8 (H), ADAM10 (I), ADAM17 (J) were measured by RT-qPCR. Using the  $\Delta\Delta CT$  method, data were normalised against the housekeeper gene GAPDH and expressed relative to a pCEP4 control. The expression of each gene (mean  $\pm$  SD, n = 3 per condition) was compared to the pCEP4 control with data assessed for normality using Shapiro-Wilks test, analysed for significance with a one-way ANOVA and corrected for comparisons with Dunnett's

multiple comparisons test. Statistical comparisons for all genes were non-significant and are not labelled on the graph.

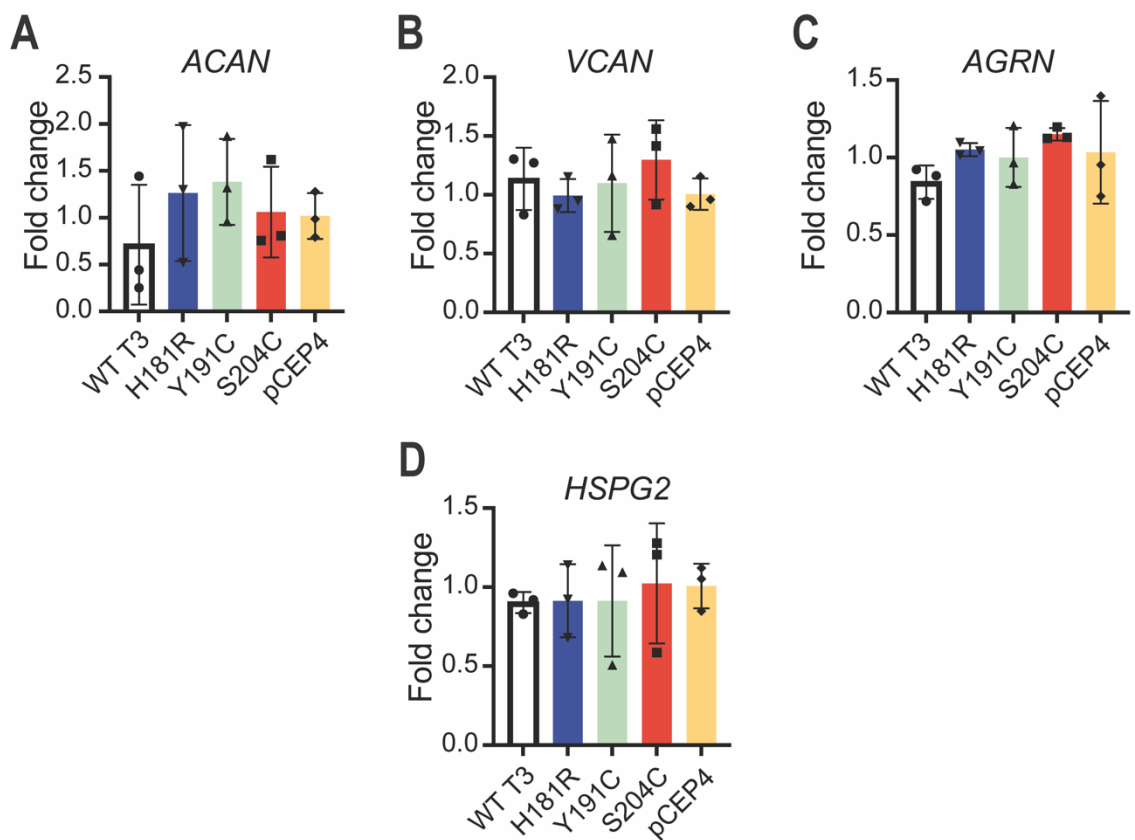


**Figure 4.7: Transfection of ARPE-19 cells with pCEP4 plasmids encoding WT, H181R, Y191C and S204C TIMP-3 did not change proteoglycan mRNA expression.**

ARPE-19 cells (250 000 per well in a 12-well plate) were cultured overnight in growth DMEM (2 ml). On the day of transfection, wells were washed in SF DMEM (3 x 2.5 ml) and media were replaced with Opti-MEM (2 ml). Cells were transfected with Lipofectamine LTX and 0.25 µg of WT TIMP-3 (T3) plasmid or 5 µg of H181R, Y191C, S204C TIMP-3 or pCEP4 plasmid. After 4 h, media were changed to SF DMEM (2 ml) supplemented with NaClO<sub>3</sub> (30 mM) and cultured for a further 20 h. RNA was extracted, cDNA synthesised and mRNA expression of *ACAN* (A), *VCAN* (B), *AGRN* (C), *HSPG2* (D) were measured by RT-qPCR. Using the  $\Delta\Delta CT$  method, data were normalised against the housekeeper gene *GAPDH* and expressed relative to a pCEP4 control. The expression of each gene (mean  $\pm$  SD, n = 3 per condition) was compared to the pCEP4 control with data assessed for normality using Shapiro-Wilks test, analysed for significance with a one-way ANOVA and corrected for comparisons with Dunnett's multiple comparisons test. Statistical comparisons for all genes were non-significant and are not labelled on the graph.

Finally, the expression of genes encoding some pro-inflammatory cytokines was analysed, along with antioxidant genes (Figure 4.8), as oxidative stress has been proposed to be involved in SFD pathogenesis (Engel et al., 2022; Wolk et al., 2020). Again, there was no significant difference in expression of *TNF*, *IL6*, *GPX1*, *GSS*, *SOD1* or *SOD2* in ARPE-19 cells transfected with plasmids encoding WT or SFD TIMP-3 compared to ARPE-19 cells transfected with an empty pCEP4 vector (Figure 4.8)

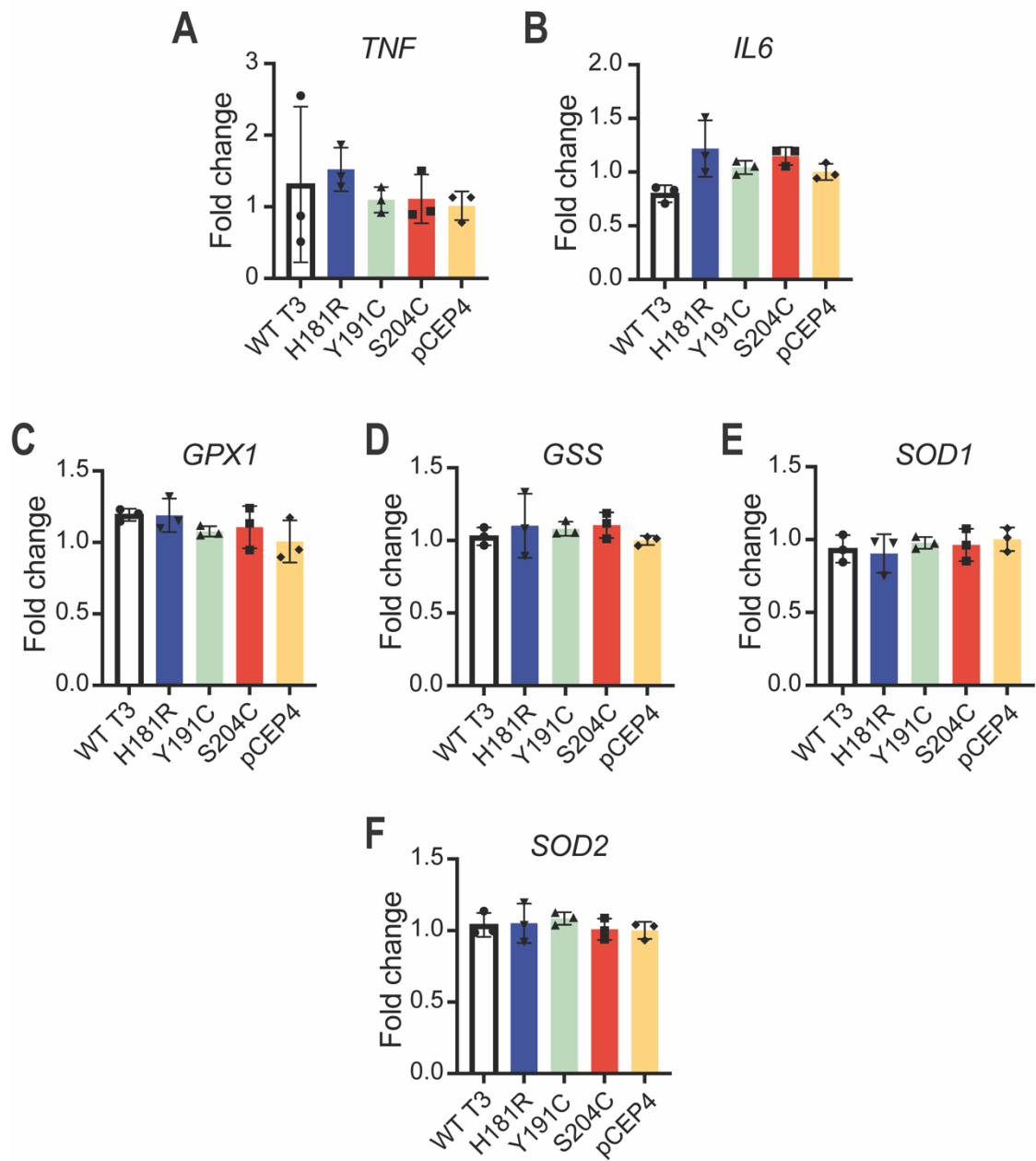


**Figure 4.8: Transfection of ARPE-19 cells with pCEP4 plasmids encoding WT, H181R, Y191C and S204C TIMP-3 did not change cytokine or oxidative stress gene mRNA expression.**

ARPE-19 cells (250 000 per well in a 12-well plate) were cultured overnight in growth DMEM (2 ml). On the day of transfection, wells were washed in SF DMEM (3 x 2.5 ml) and media were replaced with Opti-MEM (2 ml). Cells were transfected with Lipofectamine LTX and 0.25 µg of WT TIMP-3 (T3) plasmid or 5 µg of H181R, Y191C, S204C TIMP-3 or pCEP4 plasmid. After 4 h, media were changed to SF DMEM (2 ml) supplemented with NaClO<sub>3</sub> (30 mM) and cultured for a further 20 h. RNA was extracted, cDNA synthesised and mRNA expression of *TNF* (A), *IL6* (B), *GPX1* (C), *GSS* (D), *SOD1* (E) and *SOD2* (F) were measured by RT-qPCR. Using the  $\Delta\Delta CT$  method, data were normalised against the housekeeper gene *GAPDH* and expressed relative to a pCEP4 control. The expression of each gene (mean  $\pm$  SD, n = 3 per condition) was compared to the pCEP4 control with data assessed for normality using Shapiro-Wilks test, analysed for significance with a one-way ANOVA and corrected for comparisons with Dunnett's multiple comparisons test. Statistical comparisons for all genes were non-significant and are not labelled on the graph.

#### 4.2.4 Effect of WT, H181R and S204C TIMP-3 on ARPE-19 apoptosis

WT TIMP-3 is known to cause apoptosis in a variety of cell types including HeLa cells (Baker et al., 1999) and primary RPE cells (Majid et al., 2002). Previously, the SFD TIMP-3 mutants, S179C, G190C, Y191C and S204C have been observed to cause a significant increase in apoptosis compared to WT TIMP-3 in primary RPE cells transfected with plasmids encoding these proteins (Majid et al., 2002). I therefore examined whether addition of exogenous recombinant WT, H181R and S204C to the conditioned medium of ARPE-19 cells caused apoptosis and whether SFD TIMP-3 mutants caused apoptosis to a greater degree (**Figure 4.9 & Figure 4.10**).

Apoptosis was assessed by flow cytometry with fluorescently-labelled Annexin V (FITC, excitation of 488 nm and an emission max of 525 nm) and propidium iodide (excitation of 488 nm but has an emission max of 610 nm). Annexin V binds to phosphatidylserine, which translocates to the outer leaflet of the cell membrane in apoptotic cells (Fadok et al., 1998). Propidium iodide is commonly used as a live/dead stain and is cell membrane impermeant, but if a cell membrane is compromised, propidium iodide intercalates between DNA bases. Propidium iodide staining was thus taken an indicator of late-stage apoptosis.

**Figure 4.9 A** summarises the gating strategy used to analyse single ARPE-19 cells. **Figure 4.9 B** demonstrates where gates were drawn to control for the autofluorescence of cells (left-hand side). The propidium iodide fluorescence minus one (FMO) (**Figure 4.9 B, middle**) shows a mix of untreated ARPE-19 cells stained with only Annexin V, whilst for the Annexin V FMO (**Figure 4.9, right-hand side**), cells were stained with propidium iodide only. These FMOs determined the gating for propidium iodide and Annexin V staining and control for bleed-through between fluorophores to prevent falsely measuring Annexin V staining in the propidium iodide channel and vice versa.

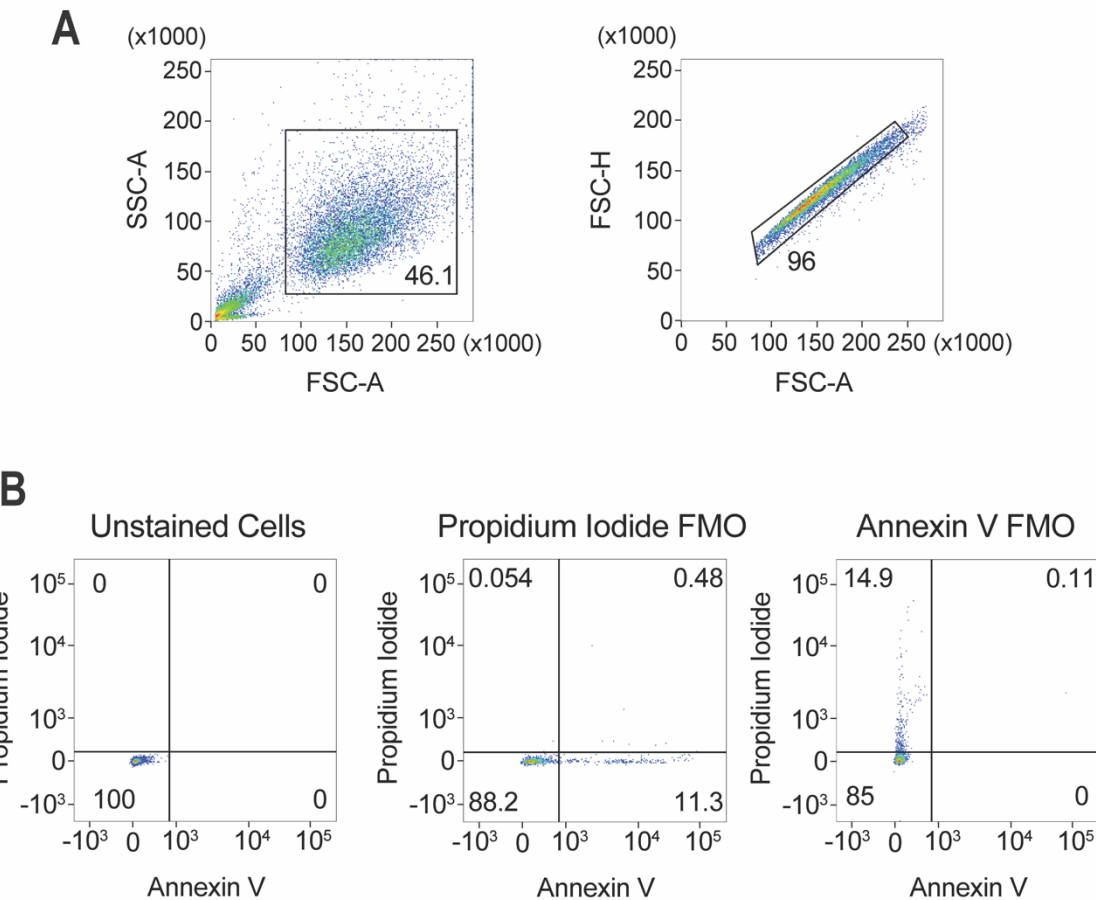


**Figure 4.9: Gating strategy and FMO controls for Annexin V and propidium iodide.**

ARPE-19 cells (250 000 per well in a 12-well plate) were cultured overnight in growth DMEM (2 ml). The following morning, wells were washed in SF DMEM (3 x 2.5 ml) and media were replaced with SF DMEM (2 ml) containing WT, H181R or S204C TIMP-3 (all in SF DMEM, 100 nM final concentration) or no TIMP-3. A positive control for cell death was generated by repeated freeze-thawing at – 80 °C and room temperature. Cells were stained with Annexin V and propidium iodide and analysed by flow cytometry. As fluorescence minus one (FMO) controls, cells were stained with Annexin V or propidium iodide alone. (A) Representative flow plots and gating strategy used for ARPE-19 cells. SSC-A, side scatter area; FSC-A, forward scatter area; FSC-H, forward scatter height. (B) Representative flow plots in which ARPE-19 cells were unstained or individually stained with propidium iodide or Annexin V to exclude auto- and background fluorescence and ensure correct gating. 10 000 events were recorded for unstained cells, and 2 000 events were recorded for each FMO.

To examine the effect of exogenous recombinant WT, H181R and S204C TIMP-3 on RPE apoptosis, ARPE-19 cells were incubated with 100 nM of each protein for 16 h (Figure 4.10). A positive control was generated by repeatedly freeze-thawing cells between -80 °C and 25 °C. This significantly increased the percentage of cells staining positive for propidium iodide/annexin V compared to untreated cells or cells treated with 100 nM WT, H181R or S204C TIMP-3, indicating a greater degree of apoptosis (Figure 4.10 B, statistics not shown). Furthermore, untreated cells or cells treated with WT, H181R or S204C TIMP-3 showed no significant difference in the percentage of cells staining positive for propidium iodide/annexin V (Figure 4.10 B, statistics not shown), indicating that treatment with WT or SFD TIMP-3 did not significantly increase apoptosis.

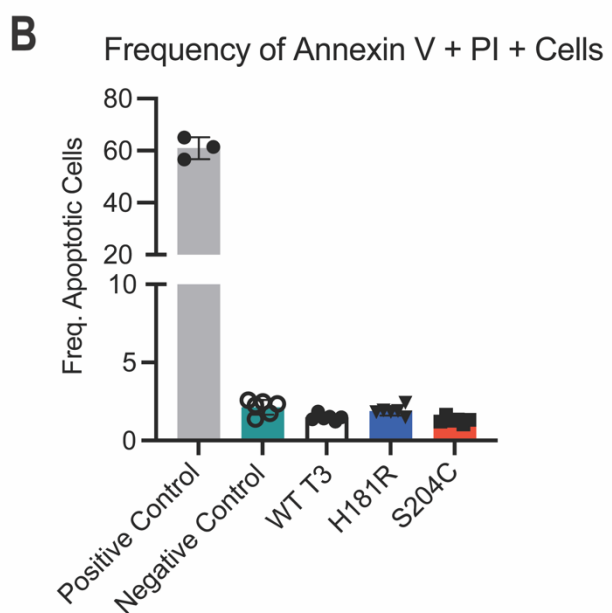
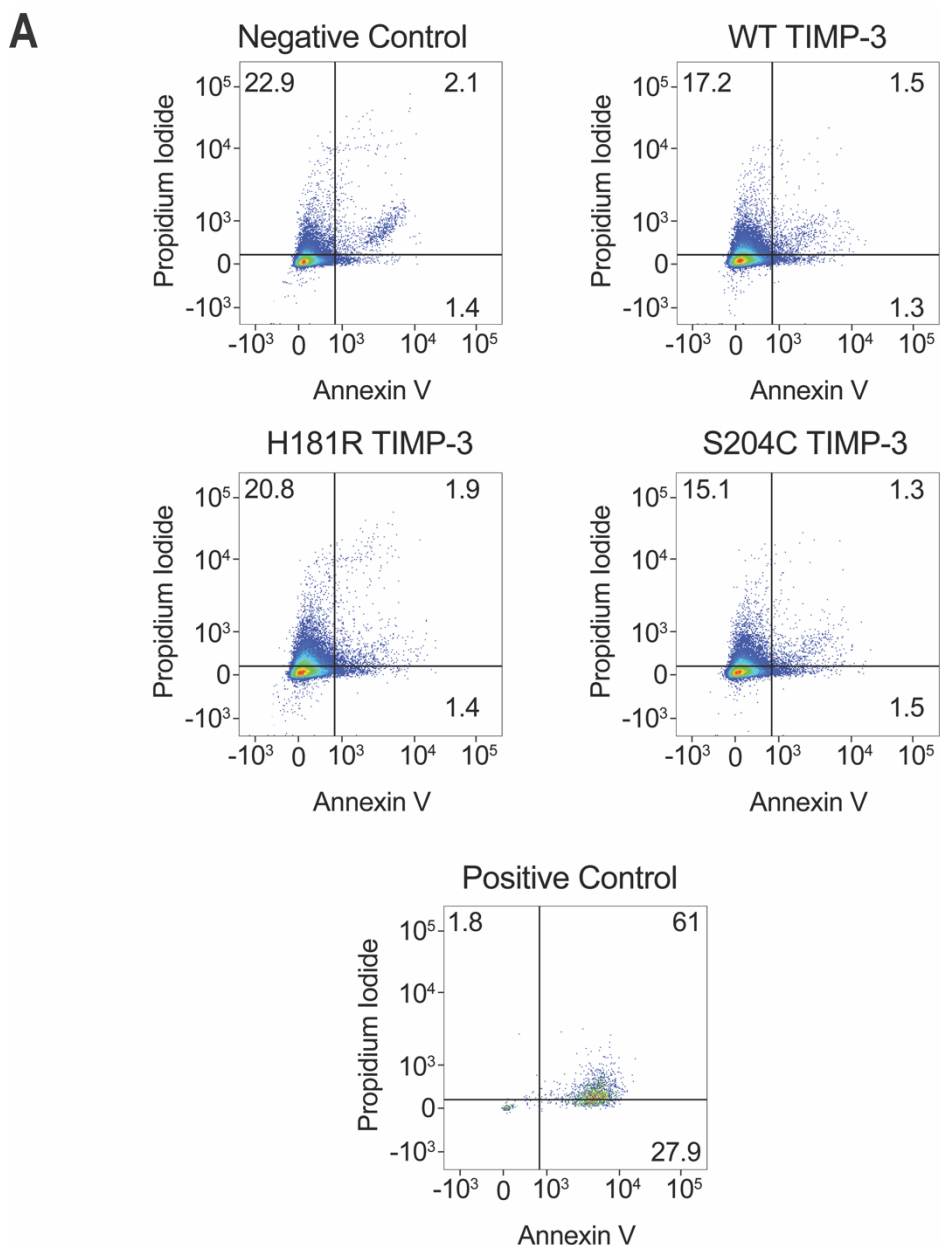


**Figure 4.10: Treatment of ARPE-19 cells with WT, H181R and S204C TIMP-3 did not induce apoptosis.**

ARPE-19 cells (250 000 per well in a 12-well plate) were cultured overnight in growth DMEM (2 ml). The following morning, wells were washed in SF DMEM (3 x 2.5 ml) and media were replaced with SF DMEM (2 ml) containing WT, H181R or S204C TIMP-3 (all in SF DMEM, 100 nM final concentration) or no TIMP-3 (negative control). A positive control for cell death was generated by repeated freeze-thawing at – 80 °C and room temperature. After 16 h, cells were collected and stained with Annexin V and propidium iodide and analysed using flow cytometry. **(A)** Representative flow plots for negative control cells (no TIMP-3), WT, H181R and S204C TIMP-3 or positive control cells. The number in each quadrant indicates the percentage of cells in that area (n = 6 for negative control, WT, H181R and S204C TIMP-3; n = 3 for positive control) 20 000 events were recorded for the negative control, WT, H181R and S204C TIMP-3, whilst 5 000 events were recorded for the positive control cells. **(B)** The percentage of cells staining positive for Annexin V and propidium iodide was compared between groups, with data assessed for normality using Shapiro-Wilks test, analysed for significance with a one-way ANOVA and corrected for comparisons with Tukey's multiple comparisons test. The positive control was significantly different to all other groups (\*\*\*\* = p ≤ 0.0001), and all other statistical comparisons were non-significant (not labelled on the graph).

### 4.3 Discussion

In initial optimisation experiments (n = 1), ARPE-19 cells were transfected with pCEP4 vectors encoding C-terminally FLAG-tagged WT, Y191C or S204C TIMP-3. Various transfection reagents (jetPRIME, Lipofectamine 3000 or Lipofectamine LTX) were compared, to determine which resulted in the highest expression of TIMP-3 protein detectable in the conditioned media (**Figure 4.1**). Interestingly, higher amounts of WT, Y191C and S204C TIMP-3 were detectable in the conditioned media when jetPRIME was used compared to Lipofectamine 3000, despite using less plasmid (2 µg, **Figure 4.1 A, B, C**) and achieving lower fold changes in WT, Y191C and S204C *TIMP3* mRNA expression than with Lipofectamine 3000 (**Figure 4.1 D**). Lipofectamine LTX has previously been reported as an effective transfection reagent for use with ARPE-19 cells (Shaw & Lipinski, 2021) and here use of Lipofectamine LTX achieved much higher expression of WT, Y191C and S204C TIMP-3 proteins in the conditioned media compared to jetPRIME (**Figure 4.1 E & F**). Although only an n = 1 experiment, Lipofectamine LTX was selected for further transfections of ARPE-19 cells in this Chapter and **Chapter 6**.

Previous studies in which RPE cells have been transfected with SFD TIMP-3 mutants have not attempted to control or match the amount of protein expression from different plasmids, making it difficult to dissect the different effects WT and SFD TIMP-3 have on RPE cells (Langton et al., 2005). Hence, a series of further optimisation experiments were performed in which a range of amounts of pCEP4 vectors encoding C-terminally FLAG-tagged WT, H181R, Y191C or S204C TIMP-3 were compared, with the aim of achieving equal amounts of monomeric (~25 kDa) TIMP-3 expression in the conditioned media (**Figure 4.2 & Figure 4.3**). Transfection of ARPE-19 cells with 1, 5 or 9 µg of pCEP4 vector encoding WT TIMP-3 gave the

highest monomeric protein expression when compared to pCEP4 vectors encoding H181R, Y191C or S204C TIMP-3 at all plasmid amounts, with 1  $\mu$ g of WT TIMP-3 plasmid being the most effective (**Figure 4.2 A & B**). Interestingly high monomeric protein expression did not correlate with dimeric protein expression, as cells expressing WT TIMP-3 had much less dimeric protein expression in the conditioned medium than cells expressing Y191C or S204C TIMP-3 at all plasmid amounts other than 9  $\mu$ g of Y191C (**Figure 4.2 A & B**). This initial transfection indicated that pCEP4 vectors encoding the SFD mutants achieved similar amounts of monomeric protein expression in the conditioned medium at all plasmid amounts, but that expression of WT TIMP-3 was considerably higher, even at lower plasmid amounts. This was consistent with previous observations from transfections in HEK-293 cells (). By lowering the amount of pCEP4 vector encoding WT TIMP-3 to 0.25  $\mu$ g, a roughly similar amount of monomeric TIMP-3 protein was detectable in the conditioned media as when 5  $\mu$ g of plasmid encoding H181R, Y191C or S204C was used (**Figure 4.3 A**). Again, there was considerably more dimeric species present in the conditioned media of cells transfected with Y191C or S204C TIMP-3 compared to WT TIMP-3 (**Figure 4.3 A**), suggesting that these SFD TIMP-3 mutants have a higher propensity to form dimers, in agreement with previously published literature (Alsaffar et al., 2022; Langton et al., 2005). However, the dimeric bands in this study were weak as was also observed in HEK-293 cells (**Figure 3.2**). Blotting the ECM revealed strong monomeric bands (black arrow) for WT TIMP-3 (at 0.75 and 1  $\mu$ g of plasmid) and H181R TIMP-3 (5  $\mu$ g of plasmid) (**Figure 4.3 B**). There were weak monomeric bands for both Y191C and S204C, with cells transfected with S204C plasmid displaying strong dimers in comparison to WT, H181R and Y191C TIMP-3 in the ECM (**Figure 4.3 B**). This is also consistent with what has been observed by other investigators, with S204C previously found to have high propensity to dimerise (Langton et al., 2005; Soboleva et al., 2003; Weber et al., 2002; Yeow et al., 2002).

Based on initial optimisation experiments (**Figure 4.3 A**), transfection was performed with 0.25  $\mu$ g of plasmid encoding WT TIMP-3 used alongside 5  $\mu$ g of plasmid encoding H181R, Y191C or S204C TIMP-3 (**Figure 4.4**). In an MTS assay, there was no significant difference in absorbance values between ARPE-19 cells transfected with an empty pCEP4 vector or pCEP4 vectors encoding WT, H181R, Y191C or S204C TIMP-3, but positive cell death controls had significantly lower absorbance values compared to empty pCEP4 vectors (**Figure 4.4 A**). This indicated that cell viability was unaffected by transfection. Despite optimisation, WT

TIMP-3 monomeric protein expression was significantly higher than all the SFD TIMP-3 mutants (**Figure 4.4 C**), indicating that accurate standardisation of TIMP-3 protein expression following transfection was challenging. Despite the high WT TIMP-3 protein expression, these transfected cells had the lowest fold change in *TIMP3* mRNA expression (**Figure 4.4 B**), consistent with what was observed in **Chapter 3** for HEK-293 cells expressing WT TIMP-3. In **Chapter 3** I hypothesised that the lower expression of SFD TIMP-3 mutants may be due to fewer viable cells, however the MTS assay conducted in this Chapter indicates that this is not the case (**Figure 4.4 A**). Perhaps reduced expression of SFD TIMP-3 proteins in the conditioned media corresponds to increased intracellular protein expression and impaired secretion of these proteins, as has previously been reported (Hongisto et al., 2020). As suggested in **Chapter 3** it would have been interesting to perform western blot of the ARPE-19 cell layer and correlate mRNA expression with intracellular protein expression. Alternatively, it is possible that SFD TIMP-3 proteins may be recognised as misfolded proteins and sent for proteasomal degradation, resulting in decreased apparent expression. ARPE-19 cells transfected with S204C TIMP-3 showed significantly higher expression of dimers in the conditioned medium (**Figure 4.4 C**), as was observed in optimisation experiments, supporting the conclusion that S204C TIMP-3 has a high propensity to dimerise. S204C TIMP-3 dimers were particularly noticeable in the ECM (**Figure 4.3 B**). It would have been interesting to investigate whether these S204C dimers involved disulfide bond formation, but ECM samples were collected by adding SDS sample buffer to culture plates after removal of cells, and in our hands, reduction and alkylation was ineffective in SDS sample buffer (results not shown). Future experiments could explore preparing ECM samples in another way, for example, using chaotropic agents such as urea. Dimeric species were also observed in ARPE-19 cells expressing WT TIMP-3, corroborating results in HEK-293 cells (**Figure 3.2 & Figure 3.3**) as well as previously published literature (Langton et al., 2005; Yeow et al., 2002). H181R and Y191C showed increased dimer expression compared to WT TIMP-3 (only significant for H181R), so it seems that SFD TIMP-3 proteins do have a higher propensity to form dimers, agreeing with previous literature (Alsaffar et al., 2022; Langton et al., 2005). Higher molecular weight complexes were also observed, particularly for cells expressing H181R and Y191C TIMP-3 (**Figure 4.4 C**), similar to those observed in **Chapter 3**. These could be multimers SFD TIMP-3 proteins, or monomeric forms of the proteins in SDS-stable complexes with other protein components.

Given that TIMP-3 is known to bind HS (Troebert et al., 2014), perhaps binding of SFD TIMP-3 mutants to HS chains in the ECM brings two monomers into such close proximity that they have a higher chance of forming dimers. Despite dimeric bands being present for all of the SFD TIMP-3 mutants in transfected ARPE-19 cells, they were relatively weak in comparison to what has been published by other investigators (Alsaffar et al., 2022; Langton et al., 2005), and consistent with observations in HEK-293 cells (**Chapter 3**). This may relate to the method of detection used, with inadvertent overexposure of chemiluminescent methods leading to overestimation of dimer abundance. Interestingly, dimeric species were also observed in ARPE-19 cells expressing WT TIMP-3, corroborating with results in **Chapter 3** and previously published literature (Langton et al., 2005; Yeow et al., 2002).

TIMP-3 has been shown to induce changes in gene expression, through a PI3 kinase pathway (Xia et al., 2023). In this study neonatal rat ventricular myocytes were cultured with 100 ng/ml (equivalent to 4 nM) recombinant TIMP-3 for 24 h, and it was observed that expression of genes such as *ADAM12*, *ADAM17*, *ADAMTS7*, *IL1 $\beta$* , *IL6*, *MMP2*, *MMP3* and *MMP9* were upregulated in these cells compared to untreated controls (Xia et al., 2023). Furthermore, TIMP-3 is a known ligand of LRP1 (Scilabria et al., 2013), and LRP1 has been implicated in signalling and modulating signalling pathways such as ERK (Langlois et al., 2010) and the mitogen-activated protein kinase pathway (Muratoglu et al., 2010). MMP-9 is also a known ligand of LRP1 (Hahn-Dantona et al., 2001) and recently it was shown that a peptide fragment of MMP-9 can bind to LRP1 and activate ERK1/2 signalling (Kim et al., 2024), suggesting that other ligands of LRP1 may also be able to induce LRP1-dependent signalling and potentially induce changes in gene expression. RPE cells express LRP1 (Hollborn et al., 2004a), so perhaps TIMP-3 binding to LRP1 may also result in changes in gene expression. Alternatively, TIMP-3 may induce changes in gene expression in RPE cells in an LRP1-independent mechanism. To investigate these possibilities, ARPE-19 cells were transfected with WT, H181R, Y191C or S204C TIMP-3 (**Figure 4.4**) and mRNA expression of LRP receptors, metalloproteinases, proteoglycans, cytokines, and oxidative stress components was examined by RT-qPCR (**Figure 4.5**, **Figure 4.6**, **Figure 4.7 & Figure 4.8**). These analyses found no significant change in expression of any of the candidate target genes in transfected cells (**Figure 4.5**, **Figure 4.6**, **Figure 4.7 & Figure 4.8**). There was a large amount

of variation between biological replicates for some genes, particularly for cells expressing S204C TIMP-3. Some of these genes included *TIMP3*, *LRP1b*, *LRP1*, *LRP6*, *LRP8* and *LRP12* (**Figure 4.4 & Figure 4.5**). Attempts were made to correlate the *TIMP3* mRNA levels of individual replicates expressing S204C with the mRNA levels of other genes such as *LRP1b* and *LRP8*, however these comparisons revealed no such correlations.

This is likely to indicate that WT and mutant TIMP-3 do not induce changes in gene expression in RPE cells, but may also reflect limitations in the experimental design. Firstly, only one timepoint was analysed, with RNA isolated 24 h after transfection. Perhaps this was not long enough for TIMP-3 proteins to cause any biologically significant effect on gene expression in this cell type, even though it has been shown to induce changes in rat ventricular myocytes at this timepoint (Xia et al., 2023). ARPE-19 cells were grown in a monolayer for simplicity, but in future experiments polarisation of these cells on Transwell inserts (Ahmado et al., 2011; Lynn et al., 2017; Lynn et al., 2018) would be more physiologically appropriate for investigating effects of SFD TIMP-3 proteins on RPE cell health and gene expression. Additionally, results in this Chapter showed that transfection of ARPE-19 cells proved fairly difficult, and an improved transfection efficiency could have caused changes in gene expression. ARPE-19 transfection will be revisited in **Chapter 6**. However, WT and SFD TIMP-3 proteins were expressed from pCEP4 vectors, which are driven by a viral promoter, and can result in non-physiologically high expression of proteins. It may be more relevant to perform transcriptomic studies on transgenic hiPSC-RPE models that endogenously express SFD TIMP-3 mutants. Engel et al. (2022) generated a hiPSC-RPE model expressing S204C TIMP-3 and also used CRISPR-Cas9 to generate an isogenic control expressing WT TIMP-3 - this would be the ideal model for such transcriptomic analysis. However, it is also highly plausible that WT and SFD TIMP-3 do not result in changes in gene expression. There is only limited evidence from previous studies that TIMP-3 can alter gene expression, with the aforementioned study by Xia et al. (2023) being one of the few to show this. Although they demonstrated that TIMP-3 changed expression of several cytokine and metalloproteinase genes, with 1-2-fold change in expression of some (e.g., *ADAM12*, *ADAM17*, *ADAMTS7*) but up to 90-fold change in others (e.g., *IL1 $\beta$* , *MMP9*). However, their source of recombinant TIMP-3 is not fully described. For example, if this recombinant TIMP-3 was expressed in *E. coli*, it may contain LPS that could be responsible for the observed changes in gene expression,

especially as many of the upregulated genes such as *IL1 $\beta$* , are inflammatory genes known to be upregulated in response to LPS. To control for this possibility, TLR4 antagonists like polymyxin B could be included during stimulation.

Given TIMP-3's activity as a metalloprotease inhibitor, it is likely that WT, H181R, Y191C and S204C TIMP-3 result in changes in the cellular proteome. It would be particularly interesting to look for differences in potential shed ligands of ADAM10 or ADAM17, which may indicate an altered ability of SFD TIMP-3 proteins to inhibit these metalloproteases. An agnostic approach was attempted to examine differences in shed ligands by performing mass spectrometry on conditioned media of ARPE-19 cells that had been treated with recombinant WT and SFD TIMP-3 proteins (data not shown). A similar approach has been used previously to identify changes in ADAM10 substrates in HEK-293 cells overexpressing WT TIMP-3 (Scilabre et al., 2018). However, in the present study no significant differences in shed ligands were detected due to an insufficient concentration of proteins present and/or detectable proteins being below the false discovery rate. An attempt was also made to explore the ability of SFD TIMP-3 proteins to inhibit ADAM17 by looking at levels of a candidate ADAM17 substrate, TNF, which may play a role in SFD pathogenesis (Spaide, 2021). Briefly, polarised M1 macrophages were treated with LPS in the presence or absence of WT or SFD TIMP-3 proteins and the amount of shed TNF was measured by ELISA (data not shown). However, this experimental approach was unsuccessful due to widespread cell death induced by the Brij contained the in TIMP-3 protein preparations used.

An increasing number of proteomic approaches have been used to study the effect of SFD TIMP-3 proteins on RPE cells. For instance, Hongisto et al. (2020) performed proteomics on cell lysates of hiPSC-RPE cells expressing S204C TIMP-3, and found a significant increase in ECM and ECM-remodelling proteins such as collagen  $\alpha$ 1, laminin subunit gamma 1, and nidogen 2 compared to control hiPSC-RPE cells. They also observed upregulated fibulin-3, a binding partner of TIMP-3 (Klenotic et al., 2004), and apolipoprotein E, a known drusen component (Crabb et al., 2002), in hiPSC-RPE cells expressing S204C TIMP-3. Further pathway analysis indicated that S204C-expressing hiPSC-RPE had increased expression of angiogenic factors, including angiogenin and chemokines such as monocyte chemoattractant protein 1. Omics approaches have also been used by a few groups to study the metabolic activity of RPE cells expressing SFD TIMP-3 mutants (Engel et al., 2022; Grenell et

al., 2024). Engel et al., (2022) performed metabolomics on hiPSC-RPE cells expressing S204C TIMP-3, using liquid chromatography and mass spectrometry. The most significantly altered metabolite they detected was 4-hydroxyproline, which they suggested resulted from collagen degradation. They also detected a reduced flux from malate to pyruvate - this is an important pathway for glutathione regeneration and corresponding with this, they observed a significant reduction in glutathione in S204C-expressing cells. Their results suggest that RPE cells expressing S204C are more susceptible to oxidative stress. More recently, Grenell et al. (2024) also performed metabolomics on hiPSC-RPE cells expressing S204C TIMP-3, and detected increased intracellular lactate and pyruvate levels, indicating increased glycolytic activity compared to control cells. Furthermore, they also observed increased intracellular  $\alpha$ -ketoglutarate and glutamine levels in S204C hiPSC-RPE cells. These results do not specifically concur with those from Engel et al., (2022), but both studies highlight the importance of using agnostic approaches to investigate the wider effects of SFD TIMP-3 mutants on RPE cell health.

WT TIMP-3 is known to induce apoptosis in a variety of cell types (Baker et al., 1999), including RPE cells (Majid et al., 2002). Therefore, I investigated whether addition of isolated recombinant WT, H181R or S204C TIMP-3 to ARPE-19 cells induced apoptosis and whether the SFD TIMP-3 mutants caused apoptosis to a greater degree than WT TIMP-3 (**Figure 4.10**). 100 nM of each protein in SF DMEM was added to cells for 16 h. Y191C TIMP-3 was not used in this experiment due to limitations in the isolation of Y191C and not being able to achieve a high enough concentration of this mutant in SF DMEM. The percentage of cells positive for apoptotic markers in the untreated group was not significantly different from treatments with any of the TIMP-3 proteins (**Figure 4.10 B**), indicating that not only did WT TIMP-3 not appear to cause apoptosis, but the SFD TIMP-3 mutants also did not cause a greater degree of apoptosis than WT TIMP-3. Previously it has been shown that the SFD TIMP-3 mutants S179C, G190C, Y191C and S204C cause a greater degree of RPE apoptosis than WT TIMP-3 (Majid et al., 2002). This published experiment was performed in transfected primary RPE cells, in which it is difficult to control the levels of protein expressed. Thus, I added a known concentration (100 nM) of recombinant TIMP-3 proteins, but perhaps the amount added was not sufficient to cause apoptosis, or a 16 h timepoint was too short. It has been shown previously in porcine chondrocytes treated with WT TIMP-3 for 72 h that 1  $\mu$ M TIMP-3 was required to cause even a small increase in apoptosis

(Gendron et al., 2003). Furthermore, it is also important to consider that as ARPE-19 cells are a cell line, their death programmes are altered (Liu et al., 2018), so the authentic apoptotic pathways may not be in place.

Accumulation of SFD TIMP-3 mutants is well documented (Chong et al., 2000; Engel et al., 2022; Galloway et al., 2017; Langton et al., 2005; Majid et al., 2007; Soboleva et al., 2003; Weber et al., 2002; Yeow et al., 2002) and impaired turnover of SFD TIMP-3 mutants has been reported (Langton et al., 2005). So, in the next Chapter, I investigated whether uptake of H181R, Y191C and S204C TIMP-3 by RPE cells was different to that of WT TIMP-3.

## **Chapter 5: Turnover of TIMP-3 and SFD TIMP-3 variants by RPE cells.**

## 5.1 Introduction

A hallmark of SFD is the thickening of the Bruch's membrane and the accumulation of drusen deposits (Betts & Troeberg, 2024). These deposits are composed of lipids such as esterified cholesterol and phosphatidylcholine (Wang et al., 2010), as well as accumulated protein, which in the case of SFD is mutant TIMP-3 (Chong et al., 2000; Fariss et al., 1998). Extracellular accumulation of mutant TIMP-3 has been observed in SFD patients, as well as in cell and mouse models of SFD (Chong et al., 2000; Engel et al., 2022; Galloway et al., 2017; Langton et al., 2005; Majid et al., 2007; Soboleva et al., 2003; Weber et al., 2002; Yeow et al., 2002). Interestingly, EFEMP1, a binding partner of TIMP-3 has also been identified in SFD drusen (Galloway et al., 2017).

Langton and colleagues suggested that TIMP-3 accumulates in SFD because SFD TIMP-3 mutants, particularly dimers and multimers, are more resistant to turnover (Langton et al., 2005). They investigated removal of WT, E162X, S179C and S204C TIMP-3 from the ECM of ARPE-19 cells and observed that WT TIMP-3 was almost completely removed from the ECM over 96 h, whereas dimeric and multimeric species of E162X, S179C and S204C TIMP-3 were cleared more slowly with ~ 20-30 % detectable in the ECM after 96 h, indicating that turnover of SFD TIMP-3 mutants was impaired. Turnover of monomeric forms of these proteins (excluding E162X) was not investigated in this study. Soboleva and colleagues (2003) investigated turnover of monomeric S179C from the ECM of fibroblasts and found that the turnover of this mutant was the same as WT TIMP-3 over a 48 h time-course.

Due to their essential role in the phagocytosis of photoreceptor outer segments (POS), RPEs are highly proteolytically active and they have a very dynamic endosomal-lysosomal system (Kwon & Freeman, 2020; Mazzoni et al., 2014). WT TIMP-3 is known to be endocytosed and undergo lysosomal degradation in a range of other cell types including chondrocytes and macrophages (Doherty et al., 2016; Schubert et al., 2019; Scilabria et al., 2013). Thus, in this chapter endocytosis of monomeric (~25 kDa) WT, H181R, Y191C and S204C TIMP-3 (isolated in Chapter 3) by RPE cells was investigated. Immunoblotting analysis was used to follow clearance of exogenously added WT, H181R, Y191C and S204C TIMP-3 from conditioned media of cells, and immunofluorescent microscopy was used to visualise endocytosed TIMP-3 inside RPE cells.

## 5.2 Results

### 5.2.1 Evaluating the effect of TNC-B on ARPE-19 and hTERT RPE-1 cell viability

WT, H181R, Y191C and S204C TIMP-3 were originally isolated in TNC-B buffer (**Figure 3.4 & Figure 3.5**) as this has been done previously in our laboratory (Troeberg et al., 2009). The ‘stickiness’ of TIMP-3, results in considerable loss even when the protein is stored in Protein LoBind tubes (Eppendorf), so 0.05 % Brij was added to help retain TIMP-3 in solution. However, Brij is a strong membrane solubiliser (Casadei et al., 2018), causing the formation of membrane pores and subsequent cell lysis. Therefore the viability of ARPE-19 (**Figure 5.1**) and hTERT RPE-1 (**Figure 5.2**) cells after the addition of TNC-B and TNC was investigated using the CellTiter 96 Aqueous One Solution Cell Proliferation Assay (Promega) as described in **2.2.10**. Briefly, the production of a coloured formazan product can be measured by quantifying absorbance at 490 nm and this is directly proportional to the metabolic activity of the cells and thus the number of live cells.

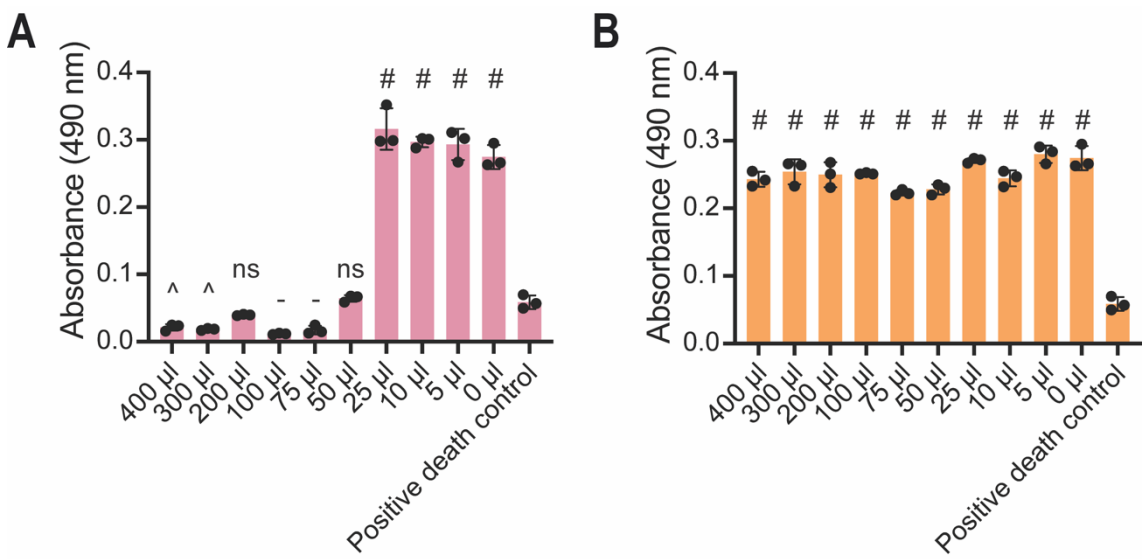


**Figure 5.1: TNC-B at high volumes caused ARPE-19 cell death, whereas TNC alone did not.**

ARPE-19 cells (250 000 per well in a 12-well plate) were cultured overnight in growth DMEM (2 ml) and washed in SF DMEM (3 x 2.5 ml). TNC-B (A) or TNC (B) was added at the indicated volumes to ARPE-19 cells in 2 ml SF DMEM for 24 h. For negative controls, the buffers were omitted, while for positive controls, cells were repeatedly (3 times) frozen ( $-80^{\circ}\text{C}$ ) and thawed ( $25^{\circ}\text{C}$ ) to induce cell death. Conditioned media were removed, and cells collected in cell dissociation solution. Cells were centrifuged (400 RCF, 5 min), and resuspended in SF DMEM (2 ml). An aliquot (80  $\mu\text{l}$ , equating to 10 000 cells) was diluted to 100  $\mu\text{l}$  (with 20  $\mu\text{l}$  SF DMEM) and mixed with 20  $\mu\text{l}$  CellTiter 96 Aqueous One Solution Cell Proliferation Assay in a 96-well plate. Cells were incubated for 90 min [ $37^{\circ}\text{C}$ , 5 % (v/v)  $\text{CO}_2$ ] and absorbance at 490 nm, quantified on a SPECTROstar Omega plate reader. Data are presented as mean  $\pm$  SD ( $n = 3$ ), with normality assessed with Shapiro-Wilks test and significance relative to the positive death control analysed with one-way ANOVA and corrected for multiple comparisons with Dunnett’s multiple comparisons test (ns = not significant,  $^{\wedge} = p \leq 0.05$ ,  $- = p \geq 0.001$ ,  $\# = p \leq 0.0001$ ).

**Figure 5.1 A** shows a comparison of ARPE-19 cell number after treatment with different volumes of TNC-B in SF DMEM (2 ml final volume) in a single well of a 12-well plate. Repeated freeze-thawing was used as a positive control for cell death, and these samples had absorbance values at 490 nm of ~ 0.05. Untreated cells (0  $\mu$ l buffer) acted as a negative control and had an absorbance reading of ~ 0.3, which was significantly increased compared to the positive cell death control. Treatment with a volume of TNC-B between 50 to 400  $\mu$ l resulted in absorbance values significantly lower than or not significantly different from the positive death control, indicating cell death when these volumes of TNC-B were used. Conversely, a volume of TNC-B between 5-25  $\mu$ l resulted in an absorbance value that was significantly larger than the positive cell death control and similar to the negative control (0  $\mu$ l TNC-B), showing that these volumes of TNC-B had no effect on ARPE-19 cell viability. Furthermore, the same experiment was repeated with addition of TNC alone with no Brij present (**Figure 5.1 B**), and all of the added volumes of TNC resulted in an absorbance significantly greater ( $p \leq 0.0001$ ) than the positive cell death control. These results demonstrate that the addition of TNC alone does not decrease cell viability. The addition of more than 25  $\mu$ l of TNC-B did decrease cell viability, indicating that Brij is responsible for the observed decrease in ARPE-19 cell viability in TNC-B buffer. It is important to note that these cell viability experiments were conducted using a specific volume of SF DMEM (2 ml final volume) per well of a 12-well plate. Therefore, moving forwards for endocytosis assays involving ARPE-19 cells, it was ensured that the same well size and media volume were used and that the volume of isolated WT, H181R, Y191C or S204C TIMP-3 in TNC-B added did not exceed 25  $\mu$ l.

**Figure 5.2 A** shows a comparison of hTERT RPE-1 cell number after treatment with different volumes of TNC-B in SF DMEM (2 ml final volume) per well of a 12-well plate. Similar to cell viability assays conducted with ARPE-19 cells, a positive control for cell death was generated by repeated freeze-thawing of hTERT RPE-1 cells, and this gave an absorbance at 490 nm of less than 0.05. Untreated cells (0  $\mu$ l buffer) acted as a negative control and gave an absorbance reading of ~ 0.03, which was significantly higher than the positive death control. When 25  $\mu$ l or more of TNC-B was added to cells, absorbance values were low (~ 0.05) and not significantly different from the positive death control, indicating that these volumes of TNC-B decreased hTERT RPE-1 cell viability. Interestingly, viability of ARPE-19 cells was unaffected by 25  $\mu$ l of TNC-B (**Figure 5.1 A**), suggesting that ARPE-19 cells are

more tolerant to TNC-B than hTERT RPE-1 cells. When 5 or 10  $\mu$ l of TNC-B was added to hTERT RPE-1 cells, absorbance values were significantly higher than the positive control for cell death. As with ARPE-19 cells, all volumes tested of TNC alone (without Brij) gave absorbance values significantly higher than the positive control for cell death (**Figure 5.2 B**). This confirms that the decrease in cell viability induced by TNC-B can be attributed to the presence of Brij. Therefore, moving forwards for endocytosis assays involving hTERT RPE-1 cells, it was ensured that the same well size and media volume were used, and that isolated WT, H181R, Y191C or S204C TIMP-3 were added in no more than 10  $\mu$ l of TNC-B.

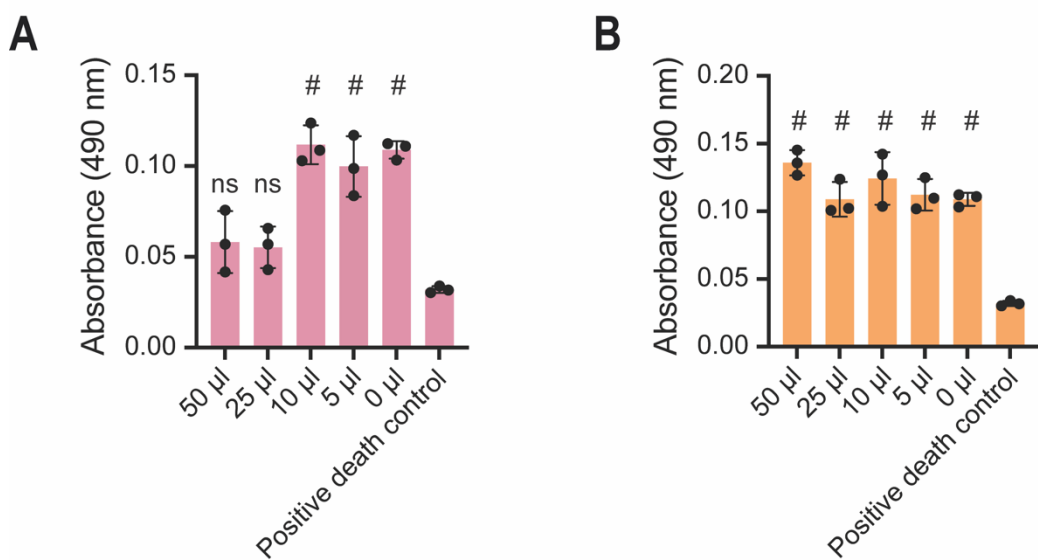


**Figure 5.2: TNC-B at high volumes caused hTERT RPE-1 cell death, whereas TNC alone did not.**

hTERT RPE-1 (250 000 cells per well in a 12-well plate) were cultured overnight in growth DMEM (2 ml) and washed in SF DMEM (3 x 2.5 ml). TNC-B (**A**) or TNC (**B**) were added at the indicated volumes to ARPE-19 cells in 2 ml SF DMEM for 24 h. For negative controls, the buffers were omitted, while for positive controls, cells were repeatedly frozen ( $-80^{\circ}\text{C}$ ) and thawed ( $25^{\circ}\text{C}$ ) to induce cell death. Conditioned media were removed, and cells collected in cell dissociation solution. Cells were centrifuged (400 RCF, 5 min), and resuspended in SF DMEM (2 ml). An aliquot (80  $\mu$ l, equating to 10 000 cells) was diluted to 100  $\mu$ l (with 20  $\mu$ l SF DMEM) and mixed with 20  $\mu$ l CellTiter 96 Aqueous One Solution Cell Proliferation Assay in a 96-well plate. Cells were incubated for 90 min ( $37^{\circ}\text{C}$ , 5 % (v/v)  $\text{CO}_2$ ) and absorbance at 490 nm, quantified by reading on a BioTek Cytation 7 plate reader. Data are presented as mean  $\pm$  SD ( $n = 3$ ), with normality assessed with Shapiro-Wilks test and significance relative to the positive death control analysed with one-way ANOVA and corrected for multiple comparisons with Dunnett's multiple comparisons test (ns = not significant, # =  $p \leq 0.0001$ ).

## 5.2.2 Endocytosis of WT, H181R, Y191C and S204C TIMP-3 by ARPE-19 cells

Endocytosis of monomeric (~ 25 kDa) WT TIMP-3 was investigated using an experimental design that has been optimised within our laboratory previously (C. M. Doherty et al., 2016) (**Figure 5.3**). Recombinant isolated WT TIMP-3 (2.5 nM) was added to the conditioned media of ARPE-19 cells and its disappearance from the media monitored over a time-course of 24 h by immunoblotting. **Figure 5.3 A** shows a representative total protein stain performed before incubation of the blot with antibodies, for an individual WT TIMP-3 endocytosis assay. The bands present between 55 and 70 kDa in all lanes corresponds to the molecular weight of BSA, as 0.2 % FBS was added to the conditioned media to seed TCA precipitation. Quantification of the total protein stain was used as a loading control to normalise bands of interest on the immunoblot for all endocytosis assays.

Using an anti-FLAG M2 antibody, the abundance of monomeric WT TIMP-3 at ~ 25 kDa in the conditioned media was measured over a time-course of 24 h (Figure 4.3 B). Some initial optimisation experiments were performed in which several 0 h timepoints were used, including WT TIMP-3 in conditioned media that had been added on to ARPE-19 cells and immediately removed, or WT TIMP-3 in conditioned media that has not been added to cells (indicated as 'Not on Cells' in **Figure 5.3**). I observed that WT TIMP-3 'Not on Cells' had a weaker signal than WT TIMP-3 that was added to cells for 0 h. Therefore, moving forward, I used a 0 h timepoint in which TIMP-3 was added to ARPE-19 cells and immediately removed and TCA precipitated.

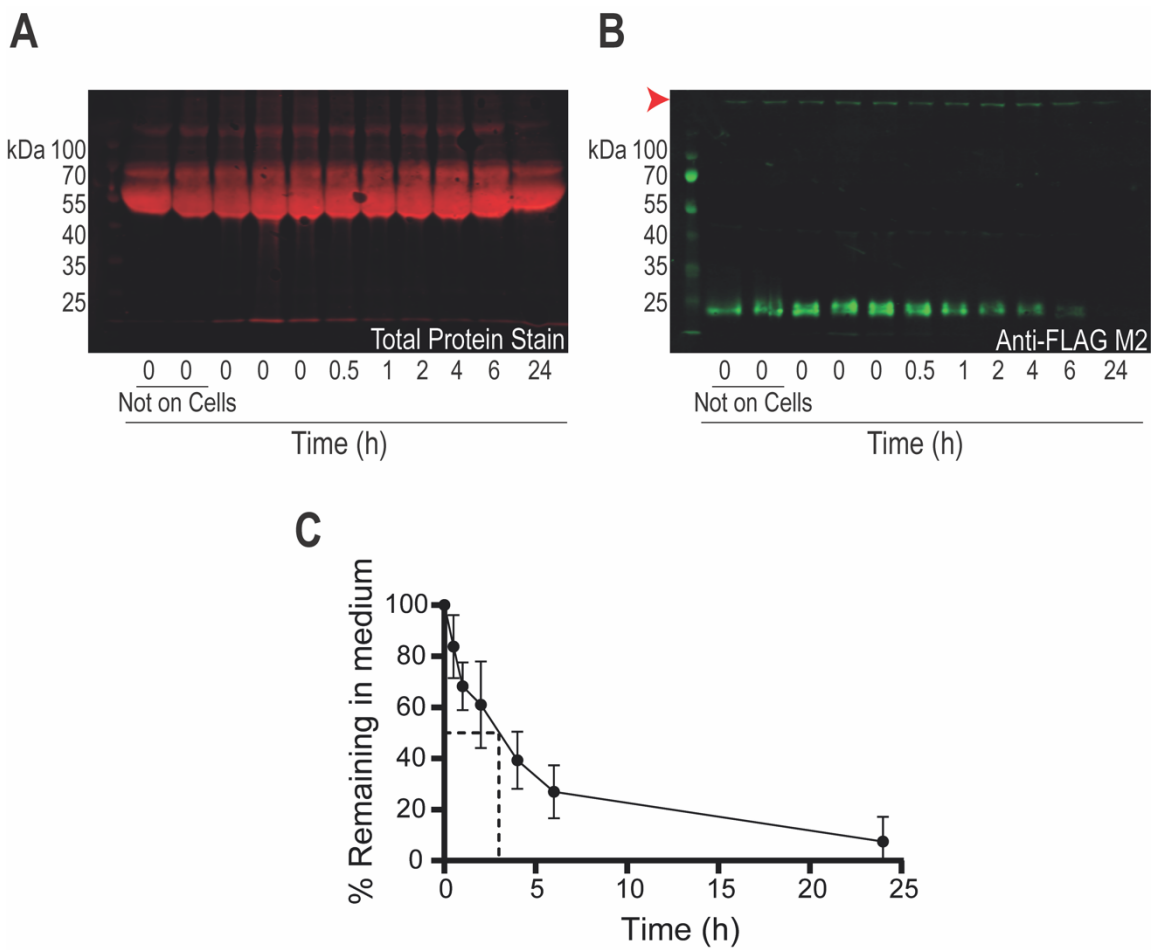
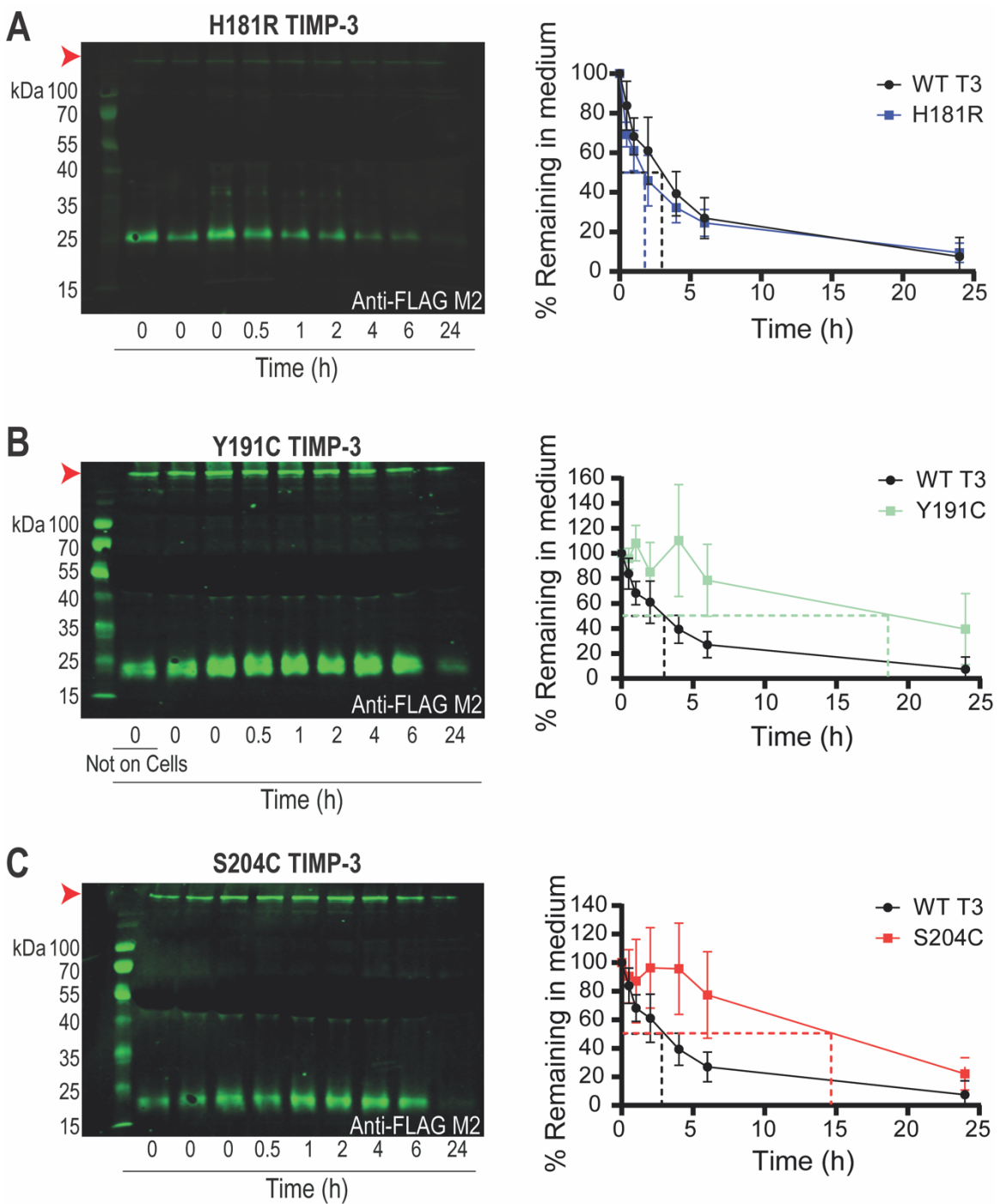


**Figure 5.3: WT TIMP-3 was endocytosed by ARPE-19 cells.**

ARPE-19 (250 000 cells per well in a 12-well plate) were plated overnight in growth DMEM and washed in SF DMEM (3 x 2.5 ml). Isolated WT TIMP-3 (2.5 nM in TNC-B) was added to the cells in 2 ml DMEM containing 0.2 % (v/v) FBS. Samples were collected at the indicated times, TCA precipitated, and resuspended in 2x SDS-PAGE sample buffer (50  $\mu$ l). (A) Resuspended samples (15  $\mu$ l) were electrophoresed and blotted onto a PVDF membrane. Total protein staining was performed using Revert Total Protein Stain (LiCOR). (B) The blot was then blocked, and TIMP-3 abundance probed using an anti-FLAG M2 antibody, followed by detection with a fluorescent anti-mouse IgG secondary antibody. Bands were imaged using LiCOR Odyssey CLx and quantified in Image Studio software. The red arrow indicates higher molecular weight species above the molecular weight markers. (C) TIMP-3 signal was normalised to total protein staining in each lane, and normalised band intensity expressed as a percentage of that at time = 0. A plot of normalised TIMP-3 abundance versus time, showed that WT TIMP-3 ( $n = 6$ ) readily disappeared from ARPE-19 conditioned medium over time and had a  $t_{1/2}$  of  $\sim 3$  h.

Over a time-course of 24 h, monomeric WT TIMP-3 ( $\sim 25$  kDa) progressively disappeared from the conditioned media until at 24 h there was virtually no TIMP-3 detectable in the conditioned medium (Figure 5.3 B), indicative of monomeric TIMP-3 uptake by ARPE-19 cells. TIMP-3 abundance in the media was plotted as a % against time (Figure 5.3 C) and a half-life of  $\sim 3$  h estimated. Higher molecular weight species above 100 kDa were observed (Figure 5.3 B, denoted by red arrow) and the abundance of these species was further examined in Figure 5.6.

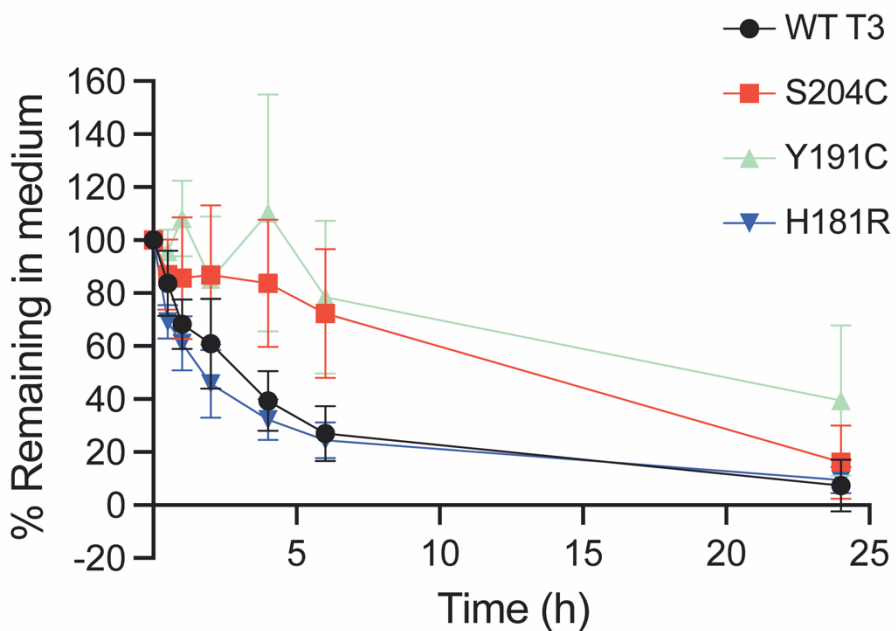
Endocytosis of monomeric (~ 25 kDa) H181R, Y191C and S204C TIMP-3 was investigated by adding isolated recombinant preparations of these mutants (2.5 nM) to the conditioned media of ARPE-19 cells and monitoring their disappearance from conditioned media over a time-course of 24 h by immunoblotting (**Figure 5.4**). Probing with an anti-FLAG M2 antibody revealed that monomeric H181R (~ 25 kDa) was taken up in a similar manner to WT TIMP-3, reflected by its progressive disappearance from the conditioned media over 24 h (**Figure 5.4 A**). A half-life of ~ 2 h was estimated for H181R. Conversely, uptake of monomeric Y191C (~ 25 kDa, **Figure 5.4 B**) and monomeric S204C (~ 25 kDa, **Figure 5.4 C**) was impaired in comparison to monomeric WT TIMP-3, as at 6 h there was still ~ 80 % of these proteins remaining in the conditioned media compared to ~ 25 % of WT TIMP-3 at this timepoint. By 24 h the amount of Y191C and S204C detectable in the conditioned media was greatly diminished, indicating that ARPE-19 cells had taken up these proteins. Half-lives for Y191C and S204C were estimated to be ~ 18 h and ~ 15 h, respectively, both considerably slower than the half-life for WT TIMP-3. Higher molecular weight species above 100 kDa were observed for H181R, Y191C and S204C (**Figure 5.4 A, B & C**, as denoted by the red arrow). The turnover of these was assessed in **Figure 5.6**.



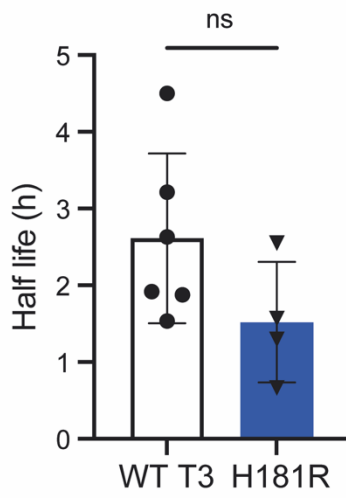
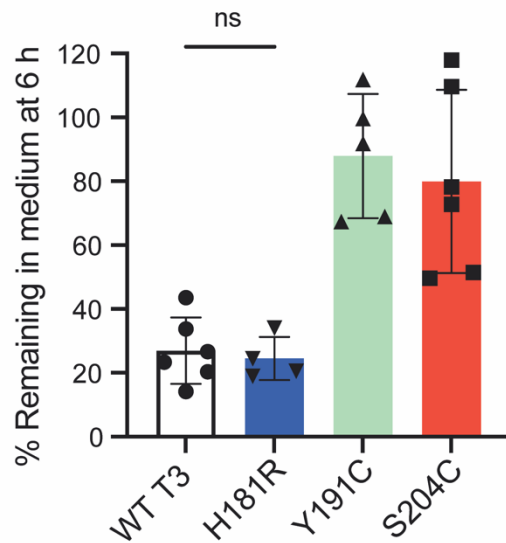
**Figure 5.4: H181R TIMP-3 was endocytosed at a similar rate to WT TIMP-3, but endocytosis of Y191C and S204C TIMP-3 by ARPE-19 cells was slower.**

ARPE-19 (250 000 cells per well in a 12-well plate) were plated overnight in growth DMEM and washed in SF DMEM (3 x 2.5 ml). Isolated H181R, Y191C or S204C TIMP-3 (2.5 nM in TNC-B) was added to the cells in 2 ml DMEM containing 0.2 % (v/v) FBS in (A), (B) and (C), respectively. Samples were collected at the indicated times, TCA precipitated, and resuspended in 2x SDS-PAGE sample buffer (50  $\mu$ l). Resuspended samples (15  $\mu$ l) were electrophoresed and blotted onto a PVDF membrane. Total protein staining was performed using Revert Total Protein Stain (LiCOR). The blot was then blocked, and H181R, Y191C or S204C TIMP-3 abundance probed using an anti-FLAG M2 antibody, followed by detection with a fluorescent anti-mouse IgG secondary antibody. Bands were imaged using LiCOR Odyssey CLx and quantified in Image Studio software. The red arrows in (A), (B) and (C) indicate higher molecular weight species above the molecular weight markers. H181R, Y191C and S204C TIMP-3 signal was normalised to total protein staining (not shown), and normalised band intensity expressed as a percentage of that at time = 0. A plot of normalised H181R, Y191C or S204C TIMP-3 abundance versus time showed that H181R TIMP-3 ( $n = 4$ ,  $t_{1/2} \approx 2$  h) readily disappeared from ARPE-19 conditioned medium, whereas Y191C TIMP-3 ( $n = 5$ ,  $t_{1/2} \approx 18$  h) and S204C TIMP-3 ( $n = 6$ ,  $t_{1/2} \approx 15$  h) had delayed endocytosis.

**Figure 5.5 A** shows summary data for the endocytosis assays performed for WT, H181R, Y191C and S204C TIMP-3 in ARPE-19 cells. Data from each time course experiment were fitted to a one-phase exponential decay model to calculate half-lives. The kinetics of WT and H181R TIMP-3 uptake by ARPE-19 cells were very similar and half-lives of  $2.6 \pm 1.1$  h and  $1.5 \pm 0.8$  h, respectively were calculated, with these not being significantly different from each (**Figure 5.5 B**). Furthermore, the amount of WT and H181R TIMP-3 remaining in the conditioned media after 6 h was almost identical at  $\sim 20\%$  (**Figure 5.5 C**). Conversely, uptake of Y191C and S204C was impaired in comparison to WT TIMP-3, particularly at 4 and 6 h timepoints, however, by 24 h Y191C and S204C TIMP-3 had disappeared from the conditioned media, indicating uptake by ARPE-19 cells (**Figure 5.5 A**). Fitting a one-phase exponential decay model for calculation of half-lives was not possible for Y191C and S204C, as their levels in conditioned media didn't always go below 50 % and there were not enough timepoints between 6 and 24 h to calculate accurate half-lives. Rather the amount of these proteins remaining in the conditioned media after 6 h was compared to that of WT TIMP-3 (**Figure 5.5 C**). This revealed that significantly more Y191C and S204C ( $p \leq 0.001$ ) remained in the conditioned media after 6 h compared to WT TIMP-3.

**A**

\*\*\*

**B****C**

**Figure 5.5: WT TIMP-3 and H181R TIMP-3 were readily endocytosed by ARPE-19 cells, but endocytosis of Y191C and S204C TIMP-3 was significantly delayed.**

ARPE-19 (250 000 cells) were plated overnight in growth DMEM (2 ml) and washed in SF DMEM (3 x 2.5 ml). Isolated WT TIMP-3, H181R TIMP-3, Y191C TIMP-3 or S204C TIMP-3 (all 2.5 nM in TNC-B) was added to cells in 2 ml DMEM containing 0.2 % (v/v) FBS. TIMP-3 abundance was quantified by immunoblotting with an anti-FLAG M2 antibody, and normalised to total protein staining of the blot. (A) Normalised TIMP-3 intensity was expressed as a percentage of abundance at time = 0, and plotted over time for WT TIMP-3 (n = 6), H181R TIMP-3 (n = 4), Y191C TIMP-3 (n = 5) and S204C TIMP-3 (n = 6). (B) Half-lives for WT and H181R TIMP-3 were calculated by fitting a one-phase exponential decay model to each individual endocytosis time-course experiment. For WT TIMP-3 (n = 6), a half-life of 2.6 h ± 1.1 h was calculated, while for H181R TIMP-3 (n = 4), a half-life of 1.5 ± 0.8 h was calculated. Data were assessed for normality with Shapiro-Wilks test and subsequently analysed for significance with an unpaired t-test (ns = not significant). (C) For Y191C and S204C TIMP-3 half-lives could not be calculated over the 24 h time-course, so the amount (mean ± SD) of these mutants remaining in the medium at 6 h was compared to WT TIMP-3. Data were assessed for normality with Shapiro-Wilks test, analysed for significance relative to WT TIMP-3 with one-way ANOVA and corrected for multiple comparisons with Tukey's multiple comparisons test (ns = not significant, \*\*\* p ≤ 0.001).

Higher molecular weight species above 100 kDa were identified in endocytosis assays for WT, H181R, Y191C and S204C TIMP-3 as denoted by the red arrows (**Figure 5.3 & Figure 5.4**). These higher molecular weight bands were quantified and normalised to total protein staining in each lane and the % remaining in the medium plotted against time (**Figure 5.6**). There was a lot of variation amongst experiments, particularly for the S204C TIMP-3 variant, indicating that in some instances higher molecular weight species did disappear from the medium and in other replicates the amount increased or remained constant. On average, the amount of higher molecular weight species for WT and the 3 SFD mutants remained fairly constant over the 24 h timecourse, indicating that they are not taken up by ARPE-19 cells.

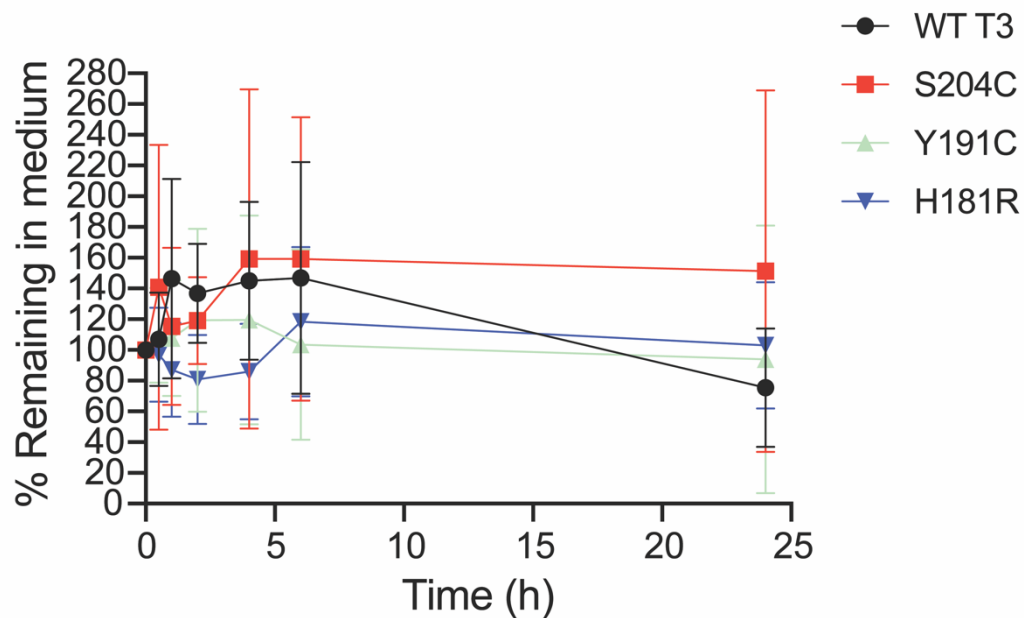
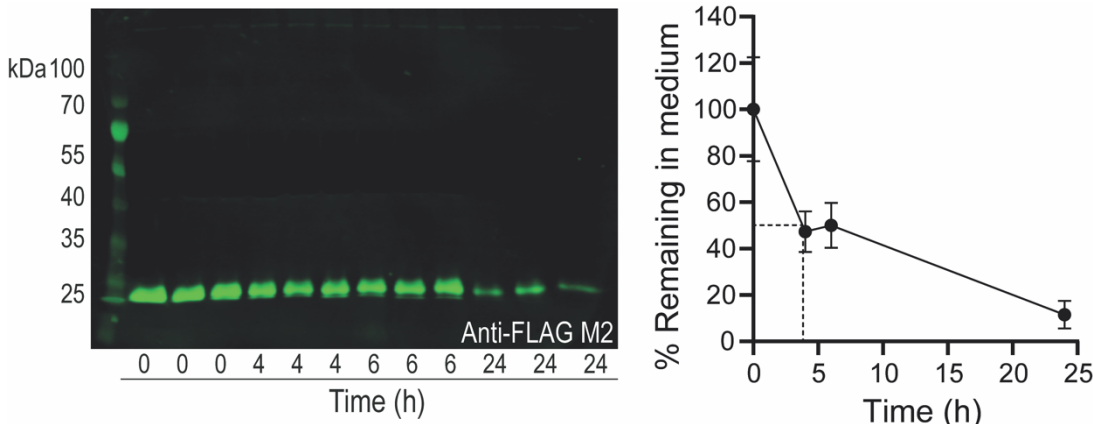


**Figure 5.6: Higher molecular weight species were not endocytosed by ARPE-19 cells.**  
 ARPE-19 (250 000 cells) were plated overnight in growth DMEM (2 ml) and washed in SF DMEM (3 x 2.5 ml). Isolated WT TIMP-3, H181R TIMP-3, Y191C TIMP-3 or S204C TIMP-3 (all 2.5 nM in TNC-B) was added to cells in 2 ml DMEM containing 0.2 % (v/v) FBS. Abundance of higher molecular weight species was quantified by immunoblotting with an anti-FLAG M2 antibody, and normalised to total protein staining in each lane. Normalised band intensity was expressed as a percentage of that at time = 0, and plotted over time for WT TIMP-3 (n = 4), H181R TIMP-3 (n = 4), Y191C TIMP-3 (n = 5) and S204C TIMP-3 (n = 5).

### 5.2.3 Endocytosis of WT, H181R, Y191C and S204C by hTERT RPE-1 cells

Endocytosis of monomeric (~ 25 kDa) WT, H181R, Y191C and S204C TIMP-3 was investigated in another RPE cell line, hTERT RPE-1 cells (**Figure 5.7 & Figure 5.8**) to confirm observations made in ARPE-19 cells (**Figure 5.3, Figure 5.4 & Figure 5.5**). hTERT RPE-1 cells were subject to the same experimental setup, in which isolated recombinant WT, H181R, Y191C and S204C TIMP-3 was added to the conditioned medium and their disappearance monitored over a timecourse of 24 h. Fewer timepoints (0, 4, 6 and 24 h) were collected for hTERT RPE-1 cells as this was a confirmatory experiment.

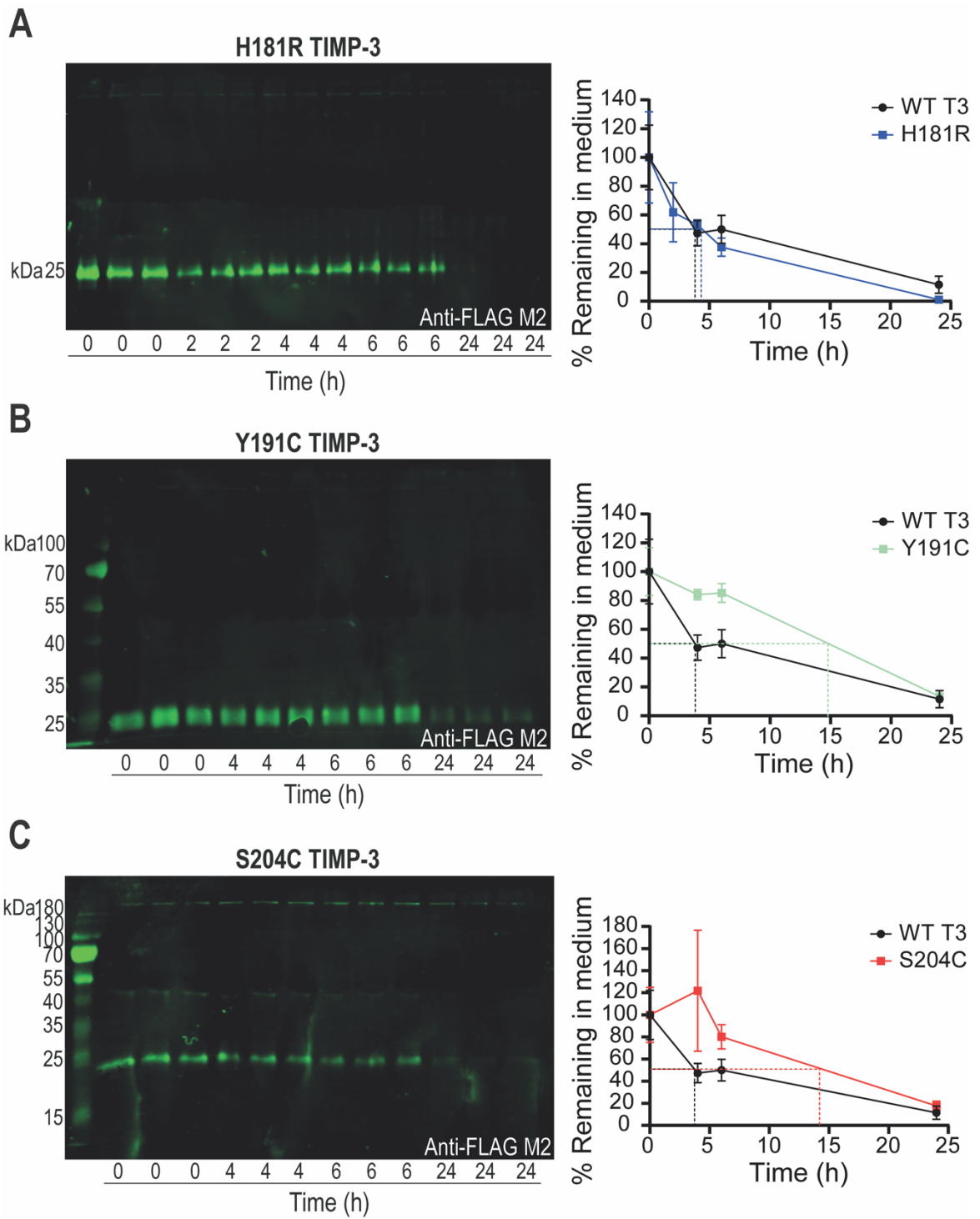
Using an anti-FLAG M2 antibody, monomeric WT TIMP-3 at ~ 25 kDa was observed to progressively disappear from conditioned media, until at 24 h most of the TIMP-3 had disappeared (**Figure 5.7**). This indicated that monomeric TIMP-3 was taken up by hTERT RPE-1 cells. TIMP-3 abundance was plotted as a % against time and a half-life of ~ 4 h estimated for WT TIMP-3. This was slightly slower than that for ARPE-19 cells.



**Figure 5.7: WT TIMP-3 was endocytosed by hTERT RPE-1 cells.**

hTERT RPE-1 (250 000 cells per well in a 12-well plate) were plated overnight in growth DMEM and washed in SF DMEM (3 x 2.5 ml). Isolated WT TIMP-3 (2.5 nM in TNC-B) was added to the cells in 2 ml DMEM containing 0.2 % (v/v) FBS. Samples were collected at the indicated times, TCA precipitated, and resuspended in 2x non-reducing SDS-PAGE sample buffer (50  $\mu$ l). Resuspended samples (15  $\mu$ l) were electrophoresed and blotted onto a PVDF membrane. Total protein staining was performed using Revert Total Protein Stain (LiCOR). The blot was then blocked, and TIMP-3 abundance probed using an anti-FLAG M2 antibody, followed by detection with a fluorescent anti-mouse IgG secondary antibody. Bands were imaged using LiCOR Odyssey CLx and quantified in Image Studio software. TIMP-3 signal was normalised to total protein staining in each lane, and normalised band intensity expressed as a percentage of that at time = 0. A plot of normalised TIMP-3 abundance versus time, showed that WT TIMP-3 (n = 3) readily disappeared from hTERT RPE-1 conditioned medium over time and had a  $t_{1/2}$  of ~ 4 h.

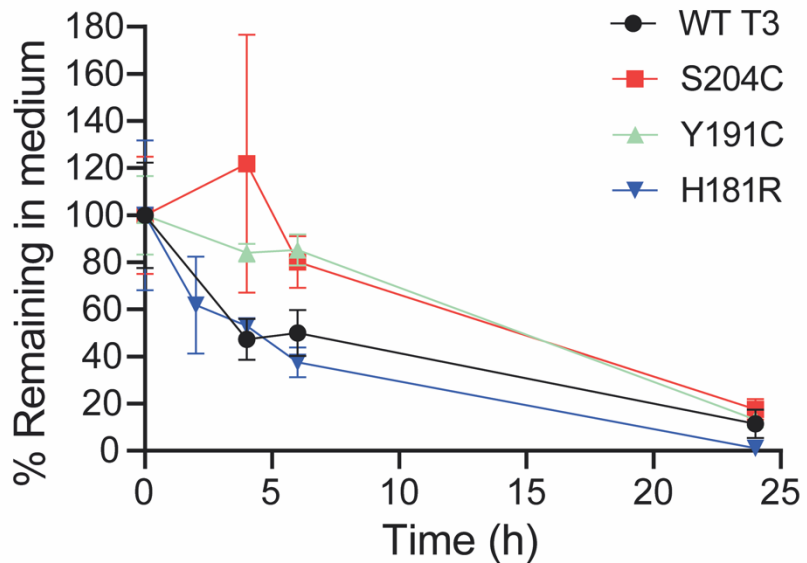
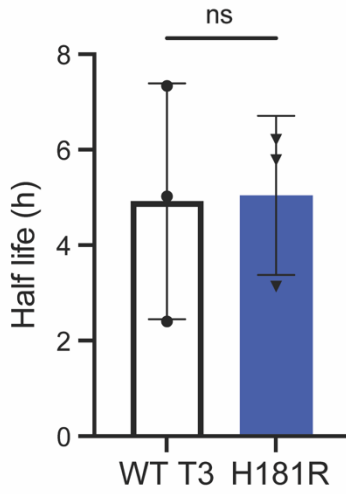
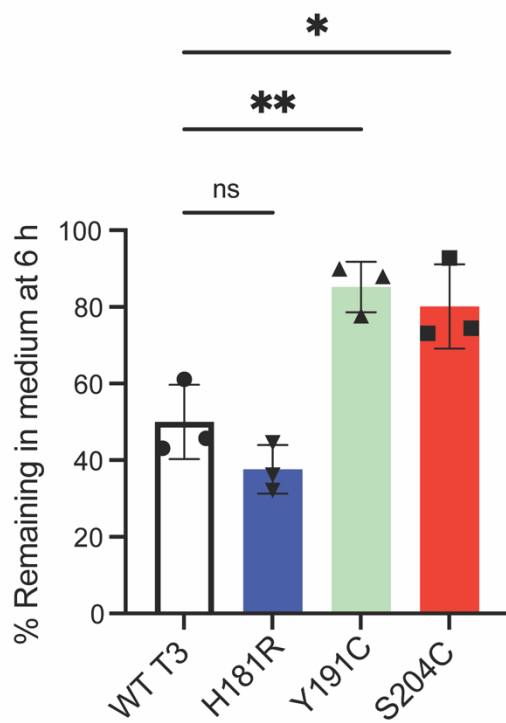
Endocytosis of monomeric (~ 25 kDa) H181R, Y191C and S204C TIMP-3 was investigated by adding recombinant isolated preparations of these mutants (2.5 nM) to the conditioned media of hTERT RPE-1 cells and monitoring their disappearance from conditioned media over 24 h by immunoblotting (**Figure 5.8**). Probing with an anti-FLAG M2 antibody revealed that monomeric H181R (~ 25 kDa) was taken up in a similar manner to WT TIMP-3, reflected by its progressive disappearance from the conditioned media over a 24 h time-course (**Figure 5.8 A**), corroborating with observations of H181R TIMP-3 uptake in ARPE-19 cells. An approximate half-life of ~ 4 h was calculated for H181R. Conversely, uptake of monomeric Y191C (~ 25 kDa, **Figure 5.8 B**) and monomeric S204C (~ 25 kDa, **Figure 5.8 C**) was impaired in comparison to monomeric WT TIMP-3, with consistently higher amounts of Y191C and S204C TIMP-3 detected in conditioned media at 4 and 6 h compared to WT TIMP-3 levels at this time. At 6 h there was still between 80-90 % of these proteins remaining in the conditioned media compared to between 40-50 % of WT TIMP-3 at this timepoint. By 24 h the amount of Y191C and S204C detectable in the conditioned media was greatly diminished, indicating that hTERT RPE-1 cells had taken up these proteins. Estimated half-lives for Y191C and S204C from the plotted graphs were ~ 15 h and ~ 14 h, respectively, which is considerably slower than for WT TIMP-3.



**Figure 5.8: H181R TIMP-3 was endocytosed at a similar rate to WT TIMP-3, but endocytosis of Y191C and S204C TIMP-3 by hTERT RPE-1 cells was slower.**

hTERT RPE-1 (250 000 cells per well in a 12-well plate) were plated overnight in growth DMEM and washed in SF DMEM (3 x 2.5 ml). Isolated H181R, Y191C or S204C TIMP-3 (2.5 nM in TNC-B) was added to the cells in 2 ml DMEM containing 0.2 % (v/v) FBS in (A), (B) and (C), respectively. Samples were collected at the indicated times, TCA precipitated, and resuspended in 2x SDS-PAGE sample buffer (50  $\mu$ l). Resuspended samples (15  $\mu$ l) were electrophoresed and blotted onto a PVDF membrane. Total protein staining was performed using Revert Total Protein Stain (LiCOR). The blot was then blocked, and H181R, Y191C or S204C TIMP-3 abundance probed using an anti-FLAG M2 antibody, followed by detection with a fluorescent anti-mouse IgG secondary antibody. Bands were imaged using LiCOR Odyssey CLx and quantified in Image Studio software. H181R, Y191C and S204C TIMP-3 signal was normalised to total protein staining in each lane, and normalised band intensity expressed as a percentage of that at time = 0. A plot of normalised H181R, Y191C or S204C TIMP-3 abundance versus time, showed that H181R TIMP-3 (n = 3) readily disappeared from hTERT RPE-1 conditioned medium, whereas Y191C TIMP-3 (n = 3) and S204C TIMP-3 (n = 3) had delayed endocytosis.

**Figure 5.9 A** shows summary data for all of the endocytosis assays performed for WT, H181R, Y191C and S204C TIMP-3 in hTERT RPE-1 cells. The kinetics of WT and H181R TIMP-3 uptake by hTERT RPE-1 cells were very similar. When data were fitted to a one-phase exponential decay model, half-lives of  $4.9 \pm 2.5$  h and  $5.0 \pm 1.7$  h were calculated for WT and H181R TIMP-3 respectively, with there being no significant difference in these calculated values (**Figure 5.9 B**). Furthermore, the amount of WT and H181R TIMP-3 remaining in conditioned media after 6 h was not significantly different at  $\sim 50\%$  and  $\sim 40\%$ , respectively (**Figure 5.9 C**). Conversely, uptake of Y191C and S204C was impaired in comparison to WT TIMP-3, particularly at 4 and 6 h timepoints, although by 24 h Y191C and S204C TIMP-3 had disappeared from the conditioned media, indicating these proteins had been taken up by hTERT RPE-1 cells, albeit more slowly (**Figure 5.9 A**). It was not possible to fit the data to a one-phase exponential decay model for calculation of half-lives for Y191C and S204C, as there were not enough timepoints between 6 and 24 h to calculate accurate half-lives. Rather the amount of these proteins remaining in conditioned media after 6 h was compared to that of WT TIMP-3 (**Figure 5.9 C**). These comparisons revealed that there was significantly more of both Y191C and S204C ( $p = 0.0047$  and  $p = 0.0117$ , respectively) remaining in conditioned media after 6 h compared to WT TIMP-3.

**A****B****C**

**Figure 5.9: WT TIMP-3 and H181R TIMP-3 were readily endocytosed by hTERT RPE-1 cells, but endocytosis of Y191C and S204C TIMP-3 was significantly delayed.**

hTERT RPE-1 (250 000 cells) were plated overnight in growth DMEM (2 ml) and were washed in SF DMEM (3 x 2.5 ml). Isolated WT TIMP-3, H181R TIMP-3, Y191C TIMP-3 or S204C TIMP-3 (all 2.5 nM in TNC-B) was added to cells in 2 ml DMEM containing 0.2 % (v/v) FBS. TIMP-3 abundance was quantified by immunoblotting with an anti-FLAG M2 antibody, and normalised to total protein staining in each lane. (A) Normalised TIMP-3 intensity was expressed as a percentage of that at time = 0, and plotted over time for WT TIMP-3 (n = 3), H181R TIMP-3 (n = 3), Y191C TIMP-3 (n = 3) and S204C TIMP-3 (n = 3). (B) Half-lives for WT and H181R TIMP-3 were calculated by fitting a one-phase exponential decay model to each individual endocytosis time-course experiment. For WT TIMP-3 (n = 3), a half-life of  $4.9 \pm 2.5$  h was calculated, while for H181R TIMP-3 (n = 3), a half-life of  $5.0 \pm 1.7$  h was calculated. Data were assessed for normality with Shapiro-Wilks test and subsequently analysed for significance with an unpaired t-test (ns = not significant). (C) For Y191C and S204C TIMP-3 half-lives could not be calculated over the 24 h time-course, so the amount (mean  $\pm$  SD) of these mutants remaining in the medium at 6 h was compared to WT TIMP-3. Data were assessed for normality with Shapiro-Wilks test, analysed for significance relative to WT TIMP-3 with one-way ANOVA and corrected for multiple comparisons with Tukey's multiple comparisons test (ns = not significant, \* p  $\leq$  0.05, \*\* p  $\geq$  0.001).

## 5.2.4 WT, H181R, Y191C and S204C TIMP-3 were not degraded in conditioned media

A potential alternative explanation for the disappearance of WT and mutant TIMP-3 from conditioned media is that the proteins may stick to plasticware, or may be degraded by proteases secreted by RPE cells or present as contaminants in the TIMP-3 preparations. Therefore, a series of experiments were performed to investigate the stability of WT, H181R, Y191C and S204C TIMP-3 incubated in conditioned media alone with no cells (**Figure 5.10**). To do this, ARPE-19 cells were incubated in SF DMEM for 0, 6 and 24 h. Conditioned media were collected, and incubated with WT and mutant TIMP-3 in low protein-binding microcentrifuge tubes for 6 h (WT and H181R TIMP-3) or 24 h (Y191C and S204C TIMP-3).

### 5.2.4.1 WT and mutant TIMP-3 were stable in conditioned media collected from ARPE-19 cells after 0 h

Media harvested from ARPE-19 cells after 0 h had no significant effect on WT and H181R TIMP-3 abundance over a further 6 h (**Figure 5.10 A & B, left-hand side**). Similarly, media harvested from ARPE-19 cells after 0 h had no significant effect on Y191C and S204C TIMP-3 abundance over 24 h (**Figure 5.10 C & D, left-hand side**). It is worth noting that there was considerable variation of the amount of Y191C and S204C TIMP-3 detectable at 0 h and 24 h which suggested that these proteins may have a high tendency to aggregate and ‘stick’.

### 5.2.4.2 WT and mutant TIMP-3 were stable in conditioned media collected from ARPE-19 cells after 6 or 24 h

Media harvested from ARPE-19 cells after 6 h had no significant effect on WT and H181R TIMP-3 abundance over a further 6 h (**Figure 5.10 A & B, right-hand side**). Similarly, media harvested from ARPE-19 cells after 24 h had no significant effect on Y191C and S204C TIMP-3 abundance over a further 24 h (**Figure 5.10, C & D, right-hand side**). Again, there was considerable variation particularly for the 0 h timepoint for S204C TIMP-3 (**Figure 5.10 D, right-hand side**).

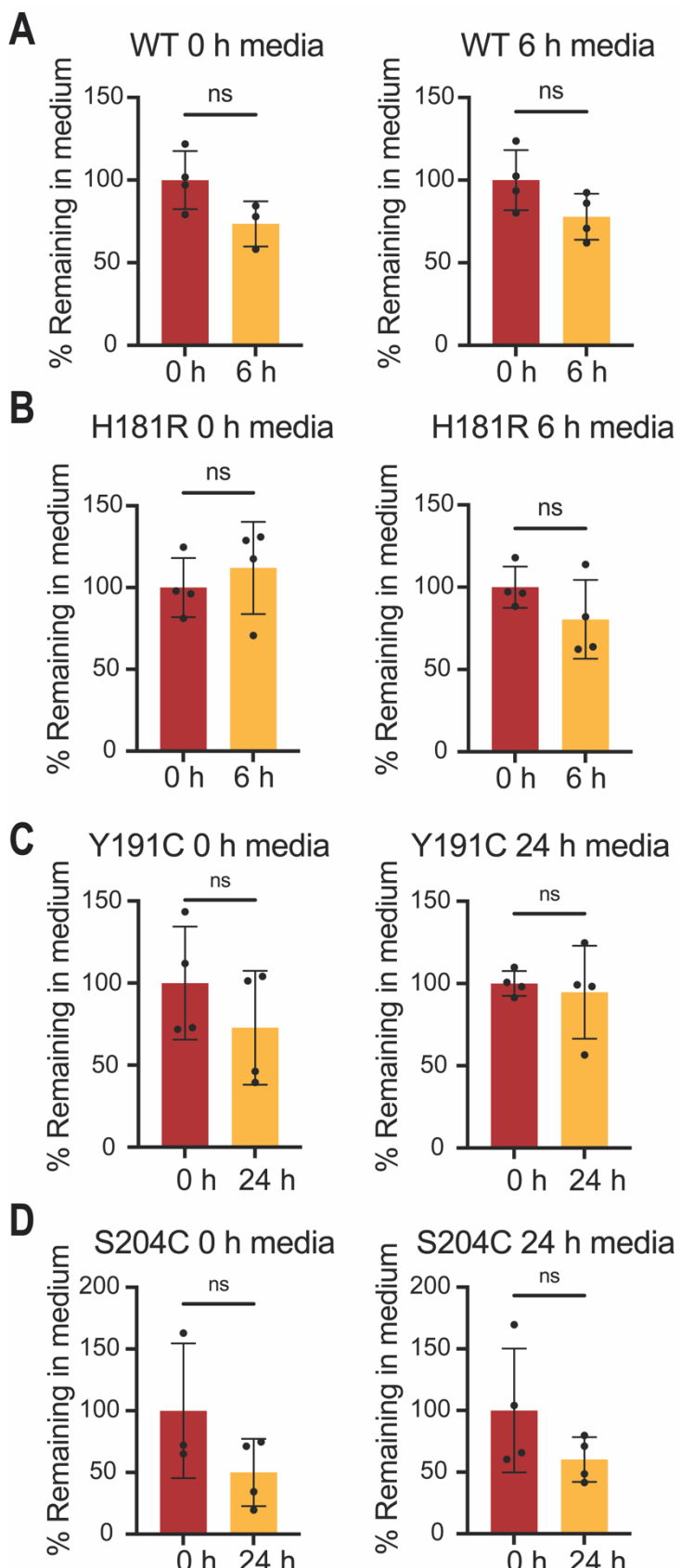


**Figure 5.10: Conditioned media alone did not cause significant loss of WT, H181R, Y191C and S204C TIMP-3.**

ARPE-19 (250 000 cells) were plated overnight in growth DMEM (2 ml) and were washed in SF DMEM (3 x 2.5 ml). The cells were then incubated with SF DMEM (2ml) containing 0.2 % (v/v) FBS for 0, 6 or 24 h and the conditioned media harvested. (A) Isolated WT TIMP-3 (2.5 nM in TNC-B) was incubated in a LoBind microcentrifuge tube for 0 h or 6 h in 1 ml of media harvested at 0 or 6 h as indicated. (B) Isolated H181R TIMP-3 (2.5 nM in TNC-B) was incubated in a LoBind microcentrifuge tube for 0 h or 6 h in 1 ml of media harvested at 0 or 6 h as indicated. (C) Isolated Y191C TIMP-3 (2.5 nM in TNC-B) was incubated in a LoBind microcentrifuge tube for 0 h or 24 h in

1 ml of media harvested at 0 or 24 h as indicated. (D) Isolated S204C TIMP-3 (2.5 nM in TNC-B) was incubated in a LoBind microcentrifuge tube for 0 h or 24 h in 1 ml of media harvested at 0 or 24 h as indicated. TIMP-3 abundance in conditioned media was quantified by immunoblotting with an anti-FLAG M2 antibody. TIMP-3 intensity was expressed as a percentage of abundance at time = 0. Data were assessed for normality with Shapiro-Wilks test and subsequently analysed for significance with Welch's unpaired t-test (ns = not significant). Data are presented as mean  $\pm$  SD, n = 3.

### 5.2.5 Visualisation of WT, H181R, Y191C and S204C TIMP-3 endocytosis by immunofluorescent microscopy

To visualise internalisation of WT, H181R, Y191C and S204C TIMP-3 by RPE cells, ARPE-19 cells were cultured on glass coverslips (16 mm diameter) coated with gelatin (10 mg/ml). Based on previously optimised conditioned in our laboratory (Scilabra et al., 2013), 40 nM of recombinant FLAG-tagged WT, H181R, Y191C or S204C TIMP-3 were added to cells. To achieve this concentration, proteins isolated in SF DMEM (**Figure 3.8**) were used to avoid TNC-B-induced effects on ARPE-19 cell viability (**Figure 5.1**).

A timepoint of 2 h was selected to visualise internalisation of WT and H181R TIMP-3 (**Figure 5.11**), as considerable amounts of both has been lost from conditioned media at this time (**Figure 5.5**). Using the anti-FLAG M2 antibody, intense punctate staining was observed around the nucleus of cells incubated with WT or H181R TIMP-3 (**Figure 5.11**).

A timepoint of 18 h was used to visualise internalisation of Y191C and S204C TIMP-3 (**Figure 5.12**), as a considerable amount of these proteins has been lost from conditioned media by this time (**Figure 5.5**). Again, strong punctate staining was observed using the anti-FLAG M2 antibody in cells incubated with Y191C or S204C TIMP-3 (**Figure 5.12**).

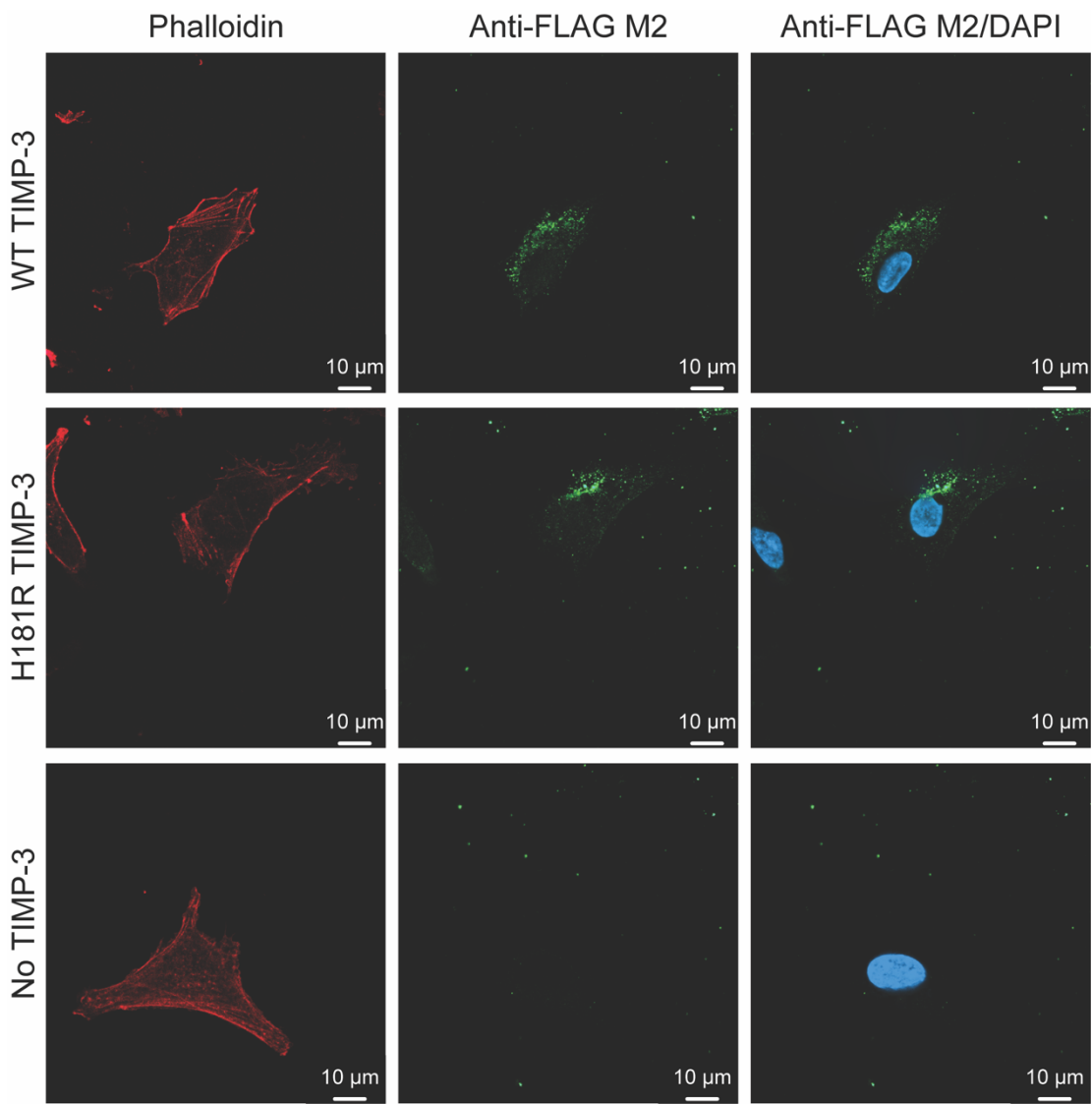


**Figure 5.11: WT and H181R TIMP-3 were endocytosed by ARPE-19 cells.**

ARPE-19 (100 000 cells) were plated on gelatin-coated coverslips for 24 h in growth DMEM (2 ml) and washed in SF DMEM (3 x 2.5 ml). Isolated WT TIMP-3 and H181R TIMP-3 (both 40 nM in SF DMEM) or no TIMP-3 was added to cells in 1 ml DMEM containing 0.2 % (v/v) FBS and cells incubated for 2 h. Cells were permeabilised and stained with an anti-FLAG M2 primary antibody, followed by detection with an Alexa Fluor-488-conjugated goat anti-mouse IgG. The actin cytoskeleton was visualised with Alexa Fluor-647-conjugated phalloidin and nuclei were visualised with DAPI staining. Cells were visualised with a Zeiss LSM 800 confocal microscope on a 60x objective lens.

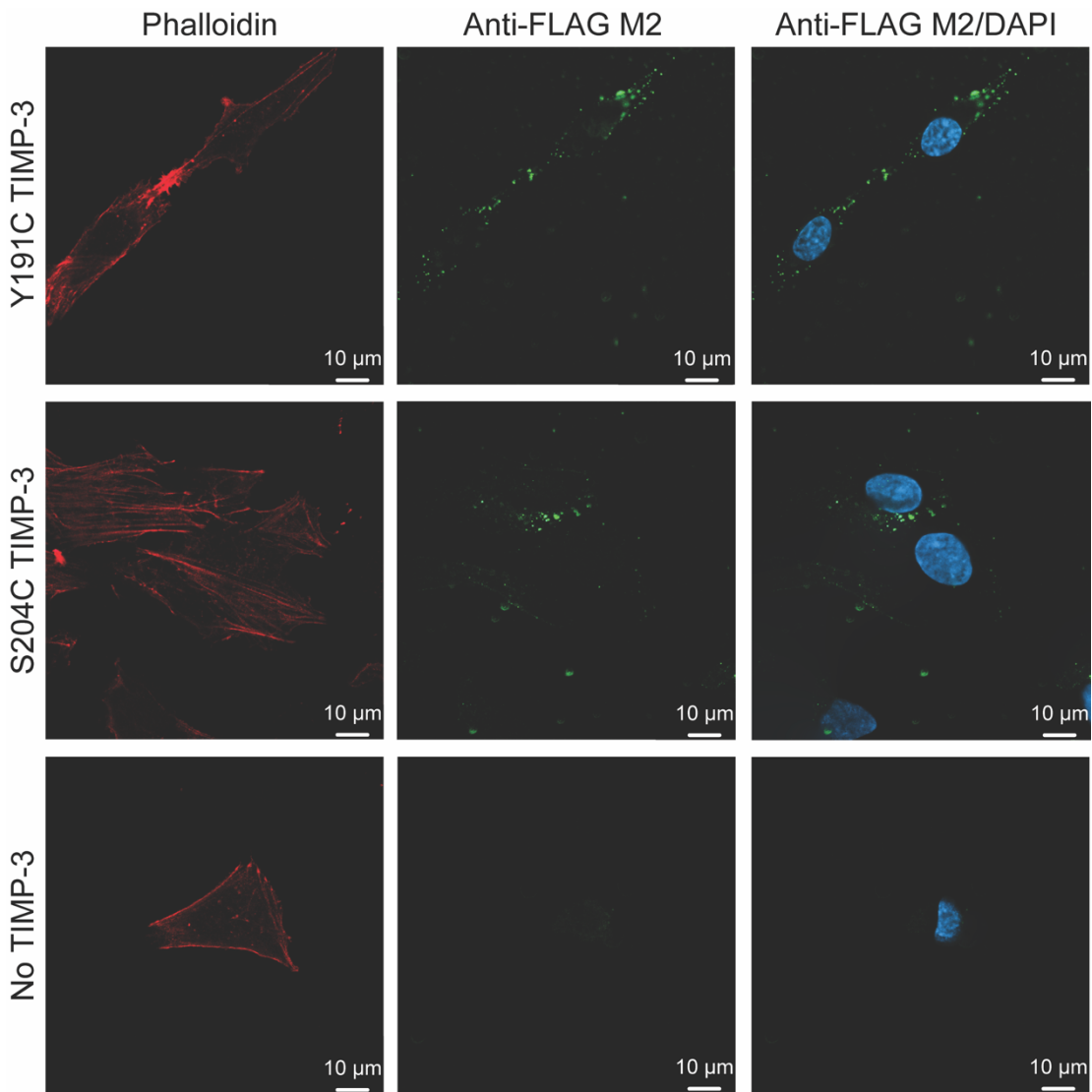


**Figure 5.12: Y191C and S204C TIMP-3 were endocytosed by ARPE-19 cells.**

ARPE-19 (100 000 cells) were plated on gelatin-coated coverslips for 24 h in growth DMEM (2 ml) and washed in SF DMEM (3 x 2.5 ml). Isolated Y191C TIMP-3 and S204C TIMP-3 (both 40 nM in SF DMEM) or no TIMP-3 was added to cells in 1 ml DMEM containing 0.2 % (v/v) FBS and cells incubated for 18 h. Cells were permeabilised and stained with an anti-FLAG M2 primary antibody, followed by detection with an Alexa Fluor-488-conjugated goat anti-mouse IgG. The actin cytoskeleton was visualised with Alexa Fluor-647-conjugated phalloidin and nuclei were visualised with DAPI staining. Cells were visualised with a Zeiss LSM 800 confocal microscope on a 60x objective lens.

### 5.2.6 WT and H181R TIMP-3 bound to heparin-Sepharose beads

WT and H181R TIMP-3 demonstrated very similar endocytic kinetics and half-lives in both ARPE-19 and hTERT RPE-1 cells (**Figure 5.5 & Figure 5.9**), raising the question of how H181R TIMP-3 accumulates in SFD if it is taken up at the same rate as WT TIMP-3. Given that WT TIMP-3 binds to HS (Troeberg et al., 2014), it was investigated whether H181R TIMP-3 binds more tightly than WT TIMP-3 to heparin, a more highly sulfated version of HS synthesised by mast cells. WT and H181R TIMP-3 were incubated with heparin-Sepharose beads before being eluted

with increasing concentrations of NaCl, and the abundance of WT or H181R TIMP-3 in eluted NaCl fractions measured by immunoblotting (**Figure 5.13**).

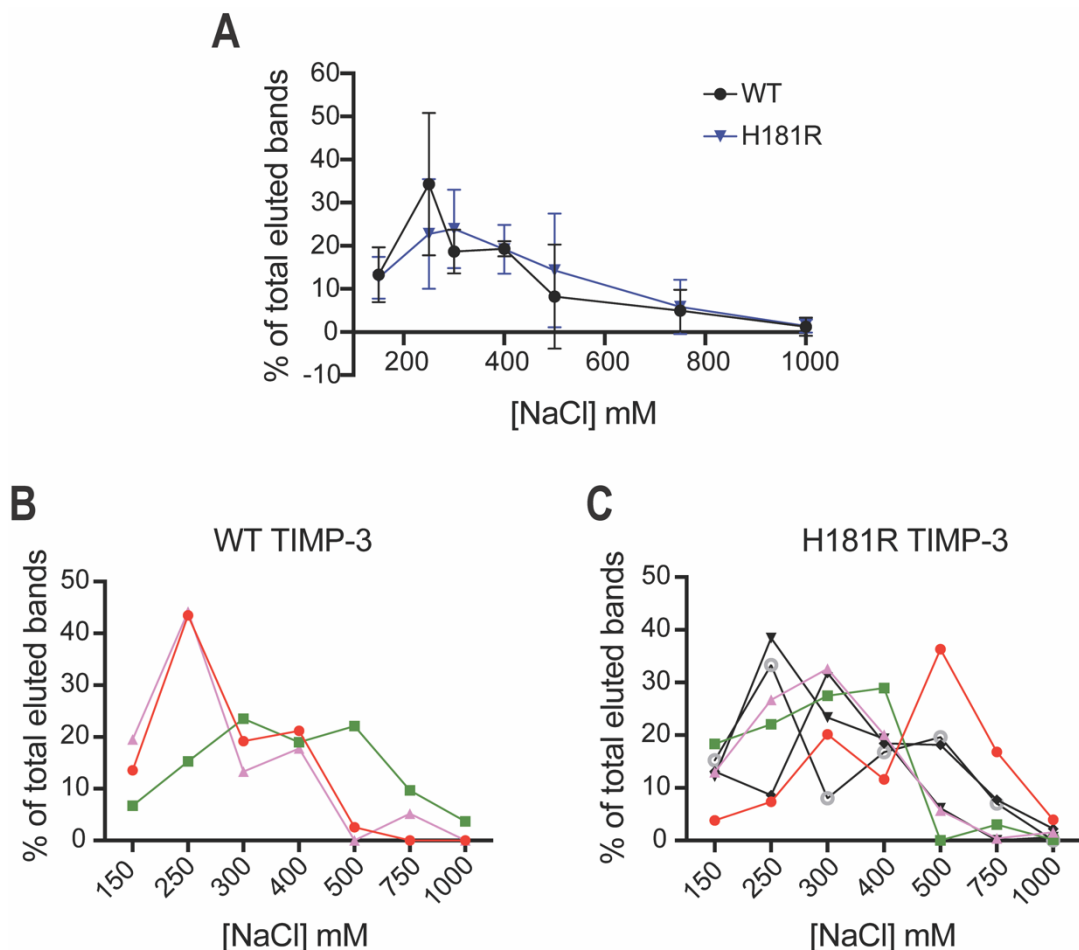


**Figure 5.13: There was no discernible difference in WT and H181R TIMP-3 binding to heparin-Sepharose beads.**

WT or H181R TIMP-3 (10 nM, in 100  $\mu$ l TNC-B) was incubated with heparin-Sepharose resin equilibrated in TNC-B (100  $\mu$ l resin in a final volume of 200  $\mu$ l of TNC-B) overnight at 4 °C in a LoBind microcentrifuge tube. Heparin-Sepharose beads were incubated with TNC-B containing sequentially increasing [NaCl] as indicated, for 15 min at each [NaCl] with gentle vortexing. Between each [NaCl], microcentrifuge tubes were centrifuged at 200 RCF (1 min) and the supernatant collected, before heparin-Sepharose beads were mixed with the next [NaCl]. Each supernatant was TCA precipitated and resuspended in 2x SDS-PAGE sample buffer (30  $\mu$ l). Resuspended samples (15  $\mu$ l) were electrophoresed and blotted onto a PVDF membrane, with WT or H181R TIMP-3 abundance in each [NaCl] fraction being quantified by immunoblotting with an anti-FLAG M2 antibody. TIMP-3 abundance per fraction was expressed as a percentage of the total eluted TIMP-3. (A) Summary data for WT (mean  $\pm$  SD, n = 3) and H181R (mean  $\pm$  SD, n = 6) TIMP-3. Individual replicate experiments are shown for WT (B) and H181R (C) TIMP-3.

Summary data (**Figure 5.13 A**) demonstrates extensive overlap between elution of WT and H181R TIMP-3, with both eluting maximally at 250 mM NaCl. There was no clear difference in WT and H181R TIMP-3 elution from heparin-Sepharose. Considerable variation was observed amongst individual experiments for both WT (**Figure 5.13 B**) and H181R (**Figure 5.13 C**) TIMP-3, with variation particularly pronounced for H181R TIMP-3.

### 5.3 Discussion

As discussed in **5.1**, extracellular accumulation of mutant TIMP-3 protein (e.g., E162X, S179C, Y191C and S204C) have been observed in SFD patients, and cell and mouse models of SFD (Chong et al., 2000; Engel et al., 2022; Galloway et al., 2017; Langton et al., 2005; Majid et al., 2007; Soboleva et al., 2003; Weber et al., 2002; Yeow et al., 2002). Interestingly, mRNA expression of *TIMP3* is not increased in SFD patients (Chong et al., 2003), suggesting that altered post-translational regulation of TIMP-3 leads to its accumulation extracellularly in the BrM (Betts & Troeberg, 2024). In other cell types, protein levels of TIMP-3 are known to be regulated by the balance between its endocytosis via the scavenger receptor LRP1 (Scilabra et al., 2013) and its binding to sulfated glycosaminoglycans (mainly HS) in the ECM (Troeberg et al., 2014). Therefore, the work presented in this Chapter investigated whether WT and SFD TIMP-3 proteins, generated in **Chapter 3**, are endocytosed by RPE cells and whether H181R, Y191C and S204C TIMP-3 are endocytosed more slowly than WT TIMP-3, which may explain why they accumulate.

WT, H181R, Y191C and S204C TIMP-3 were initially isolated in TNC-B buffer for planned in vitro analyses, but Brij-35 is a membrane solubiliser. Thus, the effect of TNC-B on viability of ARPE-19 and hTERT RPE-1 cells was investigated by adding different volumes of the buffer to cells (**Figure 5.1 & Figure 5.2**). Cell viability assays were performed using the CellTiter 96 Aqueous One Solution Cell Proliferation Assay (Promega), which reflects the metabolic activity of cells in culture and hence is an indirect measurement of live cells. This revealed that viability of ARPE-19 cells was significantly reduced when more than 25 µl of TNC-B was added to 2 ml of SF DMEM (equivalent to 0.0006 % Brij 35). Viability of hTERT RPE-1 cells was significantly reduced when more than 10 µl of TNC-B was added to 2 ml of SF DMEM (equivalent to 0.00025 % Brij 35). When TNC alone (without Brij) was added to the conditioned media of ARPE-19 or hTERT RPE-1 cells, cell viability was not significantly reduced, indicating that the toxicity was attributable to the Brij. Thus for endocytosis experiments, it was ensured that no more than 25 µl or 10 µl of isolated WT, H181R, Y191C or S204C in TNC-B was added to ARPE-19 or hTERT RPE-1 cells, respectively.

Endocytosis of monomeric WT TIMP-3 was investigated using conditions previously optimised in our laboratory (Doherty et al., 2016), with isolated recombinant WT

TIMP-3 added to conditioned media of ARPE-19 or hTERT RPE-1 cells and its disappearance from the conditioned media monitored over time (**Figure 5.3 & Figure 5.7**). In both cell types, WT TIMP-3 progressively disappeared from the conditioned media over 24 h (**Figure 5.3 B & C & Figure 5.7**). For ARPE-19 cells, a half-life of  $2.6 \pm 1.1$  h calculated (**Figure 5.5 B**), whilst in hTERT RPE-1 cells, the half-life was calculated as  $4.9 \pm 2.4$  h (**Figure 5.9 B**). The difference in half-lives calculated may relate to the fewer timepoints recorded in hTERT RPE-1 cells or may indicate that hTERT RPE-1 cells have slower endocytic machinery than that of ARPE-19 cells. These half-lives are consistent with that reported in HTB94 cells, which was  $3.6 \pm 0.3$  h (Doherty et al., 2016).

Y191C and S204C TIMP-3 had significantly delayed disappearances from the conditioned media of ARPE-19 and hTERT RPE-1 cells (**Figure 5.4 B & C, Figure 5.8 B & C**). Calculations of half-lives for these 2 mutants was not possible because more than 50 % remained at the end of several individual assays and/or there were not enough timepoints between 6 and 24 h for accurate calculation of half-lives (**Figure 5.5 A**). Therefore, the amount of Y191C and S204C TIMP-3 remaining in the conditioned medium after 6 h was compared to WT TIMP-3 in ARPE-19 (**Figure 5.5 C**) and hTERT RPE-1 cells (**Figure 5.9 C**). This revealed that there was significantly more Y191C and S204C TIMP-3 than WT TIMP-3 present in the conditioned media at 6 h, indicating that Y191C and S204C have impaired endocytosis, which could possibly explain why they accumulate in the BrM of SFD patients. These results are consistent with previous observations that S204C has 'resistance to turnover' (Langton et al., 2005).

Conversely, H181R TIMP-3 disappeared from the conditioned media of ARPE-19 and hTERT RPE-1 cells with very similar kinetics to that of WT TIMP-3 (**Figure 5.4 A & Figure 5.8 A**). Half-lives of  $1.5 \pm 0.8$  h and  $5.0 \pm 1.7$  h were calculated in ARPE-19 (**Figure 5.5 B**) and hTERT RPE-1 cells (**Figure 5.9 B**), respectively. As for WT TIMP-3, the differences in half-lives calculated may relate to the fewer timepoints recorded in hTERT RPE-1 cells, or be due to differences in kinetics of the endocytic machinery in ARPE-19 and hTERT RPE-1 cells. There was no significant difference in the half-lives calculated for WT TIMP-3 and H181R TIMP-3 in both ARPE-19 cells (**Figure 5.5 B**) and hTERT RPE-1 cells (**Figure 5.9 B**). This suggested that H181R TIMP-3 does not accumulate extracellularly due to impaired endocytosis. To my

knowledge, this is the first SFD TIMP-3 mutant that has been shown to have normal turnover akin to that of WT T3.

Based on the experiment in **Figure 5.5**, I performed some power calculations to determine the differences in endocytosis rate that could be detected using the disappearance assay in this Chapter (**Table 5.1**). Averaging the standard deviations achieved with WT, H181R, Y191C, S204C indicates an average standard deviation of 20 %. I calculated that a sample size of 4 per group would give 95 % power to detect a 60 % difference in means, but that a sample size of 400 per group would be required to give 95 % power to detect a 5 % difference in means. This showed that the variation of the assay is too great to reasonably enable detection of small differences in endocytosis rates. Therefore, this assay is unable to detect whether some SFD mutants (e.g., H181R) may cause a small delay in the uptake of TIMP-3, which may be biologically significant over a few decades and lead to TIMP-3 accumulation. This is an important consideration when examining the data presented in this Chapter.

**Table 5.1: Sample number required to detect various differences in the means of endocytosis disappearance assays at a power of 95 %.**

Difference in means (%)	5	10	20	30	40	50	60
Sample size	400	100	25	12	7	5	4

The turnover of TIMP-3 SFD TIMP-3 variants has been investigated previously by Langton et al. (2005) who suggested that SFD mutant TIMP-3 dimers and multimers are 'resistant to turnover'. They transfected ARPE-19 cells with E162X, S179C, S204C or WT TIMP-3 and grew cells to confluence. They removed and replaced transfected cells with untransfected ARPE-19 cells and monitored the loss of WT and SFD TIMP-3 mutants from the ECM by immunoblotting. After 96 h, it was observed that only ~ 1 % of WT TIMP-3 remained in the ECM, however up to 30 % of the SFD mutants remained, despite their initial fast clearance in the first 48 h. These results demonstrate that SFD TIMP-3 mutants, including one studied in this Chapter (S204C), have impaired cellular uptake and turnover. Although Langton and colleagues observed impaired uptake of SFD mutants, they reported multimeric forms of these proteins were taken up by ARPE-19 cells, which is different to what was observed in experiments conducted in this Chapter (**Figure 5.6**). Their calculated half-life for WT TIMP-3 turnover by ARPE-19 cells was 9.5 h, which is

considerably longer than the half-life of  $2.6 \pm 1.1$  h calculated in experiments presented in this Chapter (**Figure 5.5 B**). This discrepancy in calculated half-lives is most likely due to a different experimental setup, with Langton et al. (2005) looking at TIMP-3 bound to the ECM. Their experiment thus, measures the competition between TIMP-3 binding to HS in the BrM and its endocytosis by RPE cells, whereas the experiments in this Chapter are less influenced by ECM binding since the ECM is not ‘pre-loaded’ with TIMP-3. Furthermore, Langton et al. (2005) examined the turnover of dimeric and multimeric species to calculate their half-life, whereas experiments conducted here quantified the monomeric form of TIMP-3. Possible reasons for the low amount of dimer observed were discussed in **Chapter 3**. Lastly, whilst transfection is a useful method for studying cells expressing WT and SFD TIMP-3 mutants, variation in transfection efficiency makes it difficult to standardise expression between the different TIMP-3 proteins, whereas the approach used in this Chapter of adding exogenous TIMP-3 allows for accurate control of concentrations.

Higher molecular weight species (above 100 kDa) were observed with both the anti-FLAG M2 antibody (**Figure 5.3 & Figure 5.4**, marked by red arrows) and a polyclonal rabbit (AB6000) antibody (data not shown). Similar bands have been reported by others (Doherty et al., 2016; Scilabria et al., 2013). The molecular make-up of these species has not been defined, and they form a small proportion of the total TIMP-3 signal ( $\sim \leq 5\%$ ), but it is interesting to consider their make-up and endocytosis. While there was considerable variation between experimental replicates, the amount of higher molecular weight species did not appreciably reduce over the 24 h timecourse for WT and SFD TIMP-3 mutants incubated on ARPE-19 cells (**Figure 5.6**). This suggested that ARPE-19 cells are unable to endocytose and break down these higher molecular weight species. This may indicate they are complexes with shed LRP1 (Scilabria et al., 2013), although it is unclear why such complexes would not dissociate in SDS sample buffer. H181R, Y191C and S204C TIMP-3 are reported to form dimers and multimers (Alsaffar et al., 2022; Arris et al., 2003; Langton et al., 2000, 2005; Weber et al., 2002; Yeow et al., 2002), so for these SFD mutants, the higher molecular weight species could be higher-order multimers. Multimerisation could obscure regions of the proteins that interact with endocytic receptors and so block endocytosis. Thirdly, these bands could be artefacts arising from the addition of SDS, which unfolds proteins and so

could induce some aggregation via exposed hydrophobic residues, so these results warrant a cautious interpretation.

Measuring the rate of disappearance of TIMP-3 from conditioned media by immunoblotting as an indicator of endocytosis poses several questions, including:

- 1) How can one be sure that contaminating proteases within the TIMP-3 preparations are not responsible for the breakdown and disappearance of TIMP-3?
- 2) How can one be sure that proteases released from cells are not responsible for the breakdown and disappearance of the TIMP-3 proteins?
- 3) How can one be sure that these TIMP-3 proteins are taken up by RPE cells?

Similar immunoblotting techniques have been used to analyse TIMP-3 endocytosis by HTB94 cells previously, with results corroborated using confocal microscopy and inhibition of endocytosis using cytochalasin D (Doherty et al., 2016; Troeberg et al., 2008). Furthermore, Scilabria et al. (2013) examined uptake of radiolabelled FLAG-tagged [<sup>35</sup>S]TIMP-3 by HTB94 cells, and by measuring the radioactivity of the cell layer and conditioned medium, they demonstrated that radiolabelled TIMP-3 bound to the cell surface, was endocytosed and degraded by cells, with peptide fragments released back into the media. These results showed that TIMP-3 is indeed endocytosed by cells when exogenously added to the conditioned media, and indicated that immunoblotting is a reliable method for analysing this process.

To investigate whether proteases within the TIMP-3 preparations or released from RPE cells could be responsible for the disappearance of TIMP-3 proteins, several control experiments were also performed in the current study (**Figure 5.10**). These revealed that WT, H181R, Y191C and S204C TIMP-3 were stable in SF DMEM over 6 or 24 h, ruling out breakdown by contaminants in the protein preparations. WT, H181R, Y191C and S204C TIMP-3 were also stable in SF DMEM that had been cultured on ARPE-19 cells for 6 or 24 h, ruling out a role for ARPE-19-derived proteases in degradation of the proteins. Taken together, these data support the conclusion that WT and mutant TIMP-3 were not degraded in a cell-independent manner. This conclusion could be further strengthened by radiolabelling experiments such as those conducted by Scilabria et al. (2013) but this was beyond the scope of the current project.

Further evidence for WT, H181R, Y191C and S204C TIMP-3 endocytosis by RPE cells was provided by immunofluorescence confocal microscopy experiments (**Figure 5.11 & Figure 5.12**), which showed strong punctate staining inside ARPE-19 cells incubated with WT, H181R, Y191C and S204C TIMP-3, but not inside cells to which no TIMP-3 was added (**Figure 5.11 & Figure 5.12**).

The significantly impaired endocytosis of Y191C and S204C compared to WT TIMP-3 (**Figure 5.5 & Figure 5.9**), could be a mechanism by which they accumulate extracellularly in the BrM of SFD patients. It is particularly interesting that H181R has an indistinguishable endocytic rate from WT TIMP-3 (**Figure 5.5 B & Figure 5.9 B**), raising the question of how H181R accumulates extracellularly. The basic region of TIMP-3 mediates its binding to sulfated glycosaminoglycans, mainly HS, in the ECM (Lee et al., 2007) and binding of TIMP-3 to the ECM has been shown to prevent its endocytosis and degradation (Troeberg et al., 2014). HS chains are found covalently attached to core proteins to form proteoglycans, with the HSPGs perlecan and agrin being abundant in the human retina. Thus, perhaps H181R TIMP-3 accumulates extracellularly because it has a greater affinity for HS. This seems plausible given that the H181R mutation introduces an additional basic residue to the basic region on TIMP-3. However, binding of WT and H181R TIMP-3 to heparin-Sepharose beads revealed no discernible differences, with extensive overlap between WT and H181R TIMP-3 elution at all concentrations of NaCl (**Figure 5.13**). There was a huge amount of variation amongst individual replicates for both WT and H181R TIMP-3, particularly at [NaCl] of 250 and 500 mM (**Figure 5.13 A**). Plotting of individual replicates for WT (**Figure 5.13 B**) and H181R TIMP-3 (**Figure 5.13 C**), demonstrated clear inconsistencies, especially for H181R TIMP-3. This rather crude method of analysis could give rise to variation at several points, including initial binding to the heparin-Sepharose beads and in NaCl concentrations achieved at each elution step. Utilising a surface plasmon resonance approach (e.g., Carterra LSA platform) would provide much greater precision to reduce experimental variation, and provide the opportunity to interrogate WT and SFD TIMP-3 binding to a range of HS structures and sulfation patterns. This approach would give far greater detail on how SFD TIMP-3 mutations may alter TIMP-3 binding to HS, including specific binding kinetics.

Another important consideration is the age of onset of patients with the H181R, Y191C and S204C mutations. Y191C and S204C TIMP-3 have been reported to

present as early as 30 years of age (Christensen et al., 2017) and their markedly impaired endocytic rate may result in early-onset macular damage. However, for patients with the H181R mutation, presentation of disease occurs at the earliest at 50 years of age (Christensen et al., 2017). While only 3 of the 21 known SFD mutations (Betts & Troeberg, 2024) were analysed in the current study, the data suggest, there may be an inverse correlation between endocytic rate and age of onset. To establish whether this is indeed the case, more SFD mutants need to be studied. It would be interesting to investigate Y174C, G190C and S193C, which have been reported to present from 30 years of age, and E162X, S179C or Y195C which have reported ages of onset from 20 years of age (Christensen et al., 2017). Additionally, studying Y177C and Y182C could prove useful as they have an older age of onset after 50 years of age (Christensen et al., 2017), and so would provide data across a broad age range.

Patients with the H181R mutation have one of the latest ages of onset for SFD patients, similar to the age of onset for those affected by AMD (Fleckenstein et al., 2024). There is considerable clinical overlap between AMD and SFD (Gourier & Chong, 2015), with late-onset SFD diagnosed on the basis of mutations in TIMP-3. Given that H181R has unimpaired endocytosis (**Figure 5.5 & Figure 5.9**) and presents at a similar age to AMD, perhaps in these patients accumulation of H181R TIMP-3 is a consequence of the ageing processes rather than an inherent pathological property of the protein itself. Similar processes would lead to accumulation of WT TIMP-3 in AMD, where TIMP-3 is known to be one of the many components that accumulate in extracellular drusen (Crabb et al., 2002). Lipofuscin accumulation is a classical feature of ageing observed in RPE cells, and it is composed predominantly of incompletely digested photoreceptor outer segments and chemically-modified lipids and proteins (Călin et al., 2021; Kennedy et al., 1995; Sparrow & Boulton, 2005). Lipofuscin is known to disrupt normal phagocytic function of RPE cells by impairing lysosomal proteases, affecting acidification of lysosomal compartments by interfering with vATPase as well as causing leakage of lysosomal contents into the cytosol (Keeling et al., 2018; N et al., 2000; Sundelin et al., 1998). Lipofuscin can cause modification of lipids, resulting in the formation of high molecular weight molecules that remain stable in lysosomes (Brunk et al., 1995; Brunk & Terman, 2002; Keeling et al., 2018). Furthermore, lipid peroxidation of lipofuscin results in the formation of malondialdehyde and 4-hydroxynonenal which can form covalent bonds with proteins resulting in complexes that accumulate within

the lysosomal system (Esterbauer et al., 1991; Keeling et al., 2018). Ageing results in severe disruption of the endosomal-lysosomal system in RPE cells, thus it is possible that the ageing process could underly accumulation of later-onset SFD TIMP-3 variants such as H181R TIMP-3.

Interestingly, some SFD TIMP-3 mutants including S204C (Hongisto et al., 2020), have been observed to accumulated intracellularly (Guan et al., 2022). Two of these mutations (L10H and G12R) occur in the signal peptide (Guan et al., 2022), so it is likely that these mutants are not exocytosed from cells, however intracellular accumulation of S204C TIMP-3 could indicate that it is taken up by RPE cells, but that the cells struggle to degrade the S204C variant, leading to its intracellular accumulation.

As previously mentioned LRP1 is known to mediate endocytosis of WT TIMP-3 in various cell types, including HTB94 cells, MEFs and primary human macrophages (Doherty et al., 2016; Schubert et al., 2019; Scilabria et al., 2013), therefore the next Chapter investigated the role of LRP1 in mediating the endocytosis of WT and SFD TIMP-3 in RPE cells.

## **Chapter 6: Establishing the role of LRP1 in the endocytosis of TIMP-3 in RPE cells.**

## 6.1 Introduction

Extracellular protein levels of TIMP-3 can be regulated by endocytic uptake via the scavenger receptor LRP1 (Scilabria et al., 2013). Scilabria and colleagues used PEA-13 cells (an LRP1 knockout cell line) to demonstrate that TIMP-3 is predominantly endocytosed by LRP1 in mouse embryonic fibroblasts, with a smaller portion of TIMP-3 endocytosis mediated by an LRP-independent mechanism (Scilabria et al., 2013). LRP1-mediated endocytosis of TIMP-3 has also been shown in HTB94 cells, as well as primary human macrophages (Doherty et al., 2016; Schubert et al., 2019; Scilabria et al., 2013).

Data presented in **Chapter 5** indicated that WT TIMP-3 as well as the SFD mutants H181R, Y191C and S204C TIMP-3 are endocytosed by RPE cells. Primary human RPE cells express LRP1 (Hollborn, et al., 2004b) (**6.2.2**) and given that LRP1 is known to mediate WT TIMP-3 uptake (Doherty et al., 2016; Schubert et al., 2019; Yamamoto et al., 2013), this chapter investigates whether LRP1 is responsible for mediating the uptake of WT TIMP-3 and H181R, Y191C and S204C TIMP-3 in RPE cells. To do this, endocytosis assays were performed in the presence of RAP, an antagonist of ligand binding to members of the LRP family (Lee et al., 2007), to determine whether endocytosis of WT and/or the 3 SFD TIMP-3 mutants is an LRP-dependent process (**6.2.3**). To look more specifically at the role of LRP1 in endocytosis by RPE cells, siRNA knockdown of LRP1 was conducted and uptake of WT TIMP-3 monitored (**6.2.4**).

Previous mutagenesis studies revealed that lysine residues ~21 angstroms apart (e.g., K26/K45 or K42/K110) in a highly basic region of TIMP-3 are responsible for its binding to LRP1 (Doherty et al., 2016). The H181R and Y191C mutations are predicted to occur within close proximity of this basic patch and the effect of the S204C mutation on the basic patch of TIMP-3 is difficult to predict due to its occurrence near the C-terminus. It is possible that these mutations may disrupt the basic patch of TIMP-3, resulting in altered interactions with LRP1, thus endocytosis of WT and mutant TIMP-3 by PEA-13 cells (LRP1 knockout line) or WT mouse embryonic fibroblasts was also investigated to interrogate this possibility (**6.2.1**).

## 6.2 Results

### 6.2.1 Endocytosis of WT, H181R, Y191C and S204C TIMP-3 by mouse embryonic fibroblast and PEA-13 cells

LRP1 has been shown to mediate TIMP-3 uptake in other cells such as chondrocytes and macrophages (Doherty et al., 2016; Schubert et al., 2019; Scilabria et al., 2013). Uptake of TIMP-3 has also been investigated using PEA-13 cells, an LRP1-null cell line (Willnow & Herz, 1994), and their wild-type counterpart, MEF cells (Scilabria et al., 2013). Therefore, using this established PEA-13 and MEF cell system, initial experiments investigated differences in the uptake of WT, H181R, Y191C and S204C TIMP-3 in these cell types.

**Figure 6.1** shows results of endocytosis assays performed for WT TIMP-3 in MEF and PEA-13 cells. Endocytosis of monomeric (~ 25 kDa) WT TIMP-3 was investigated by adding isolated recombinant WT TIMP-3 (2.5 nM) to the conditioned media of PEA-13 and MEF cells and monitoring its disappearance from conditioned media over 8 h (**Figure 6.1 C**). Immunoblotting using an anti-FLAG M2 antibody and subsequent quantification showed that abundance of WT TIMP-3 in the conditioned media of MEF cells progressively decreased over time (**Figure 6.1 A & C**), indicative of uptake by MEF cells. The intensity of staining for WT TIMP-3 bands in the conditioned media of PEA-13 cells remained much more consistent over the 8 h time-course with only a small decrease from the amount detected at 0 h (**Figure 6.1 A & D**), indicating decreased or impaired uptake of WT TIMP-3 by these cells. Comparison of the amount of WT TIMP-3 remaining in the conditioned media at 8 h revealed that significantly more WT TIMP-3 was detectable in conditioned media of PEA-13 cells than MEF cells ( $p = 0.0384$ , **Figure 6.1 D**). These results suggest that the uptake of WT TIMP-3 in mouse embryonic fibroblasts is LRP1-dependent, consistent with previous conclusions (Doherty et al., 2016; Scilabria et al., 2013).

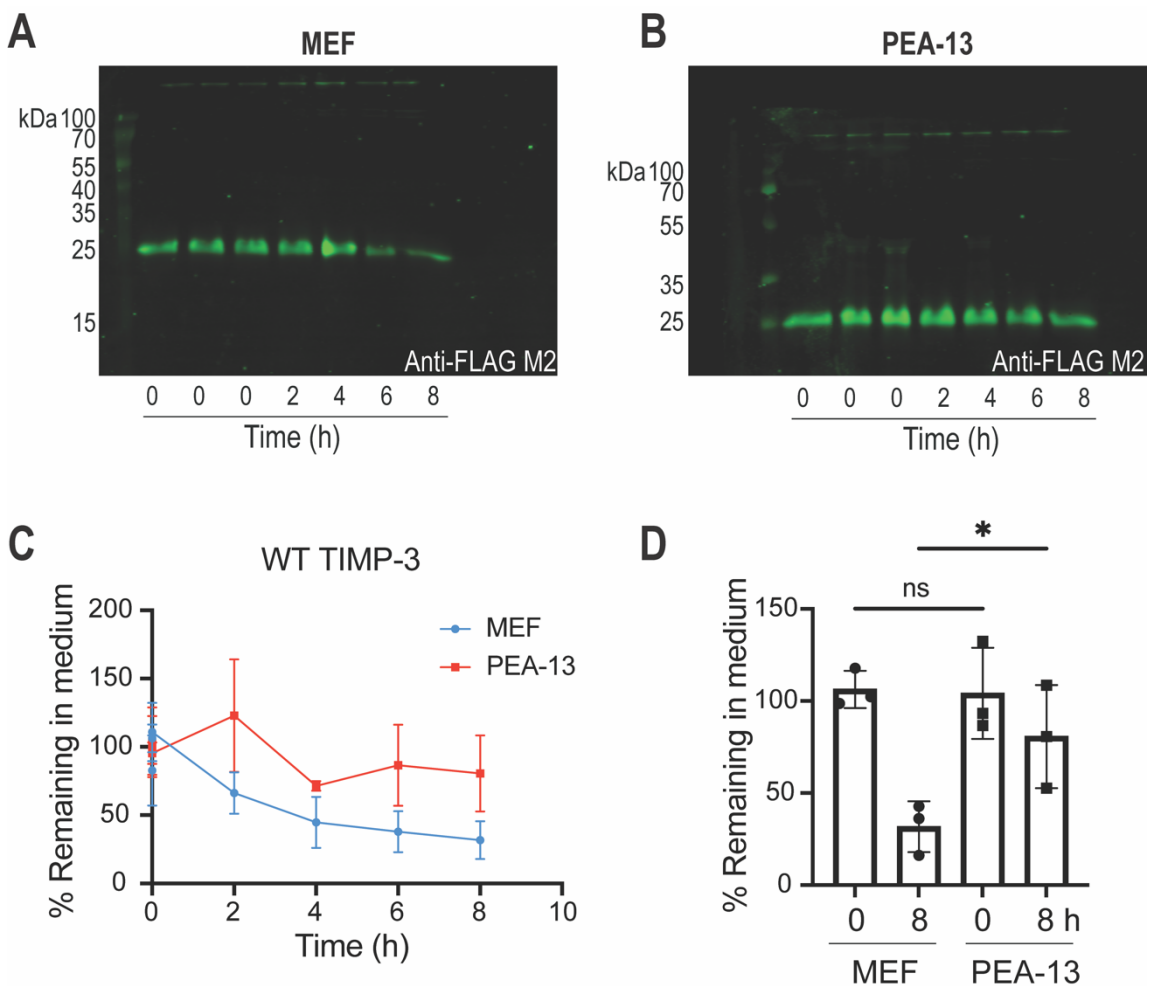
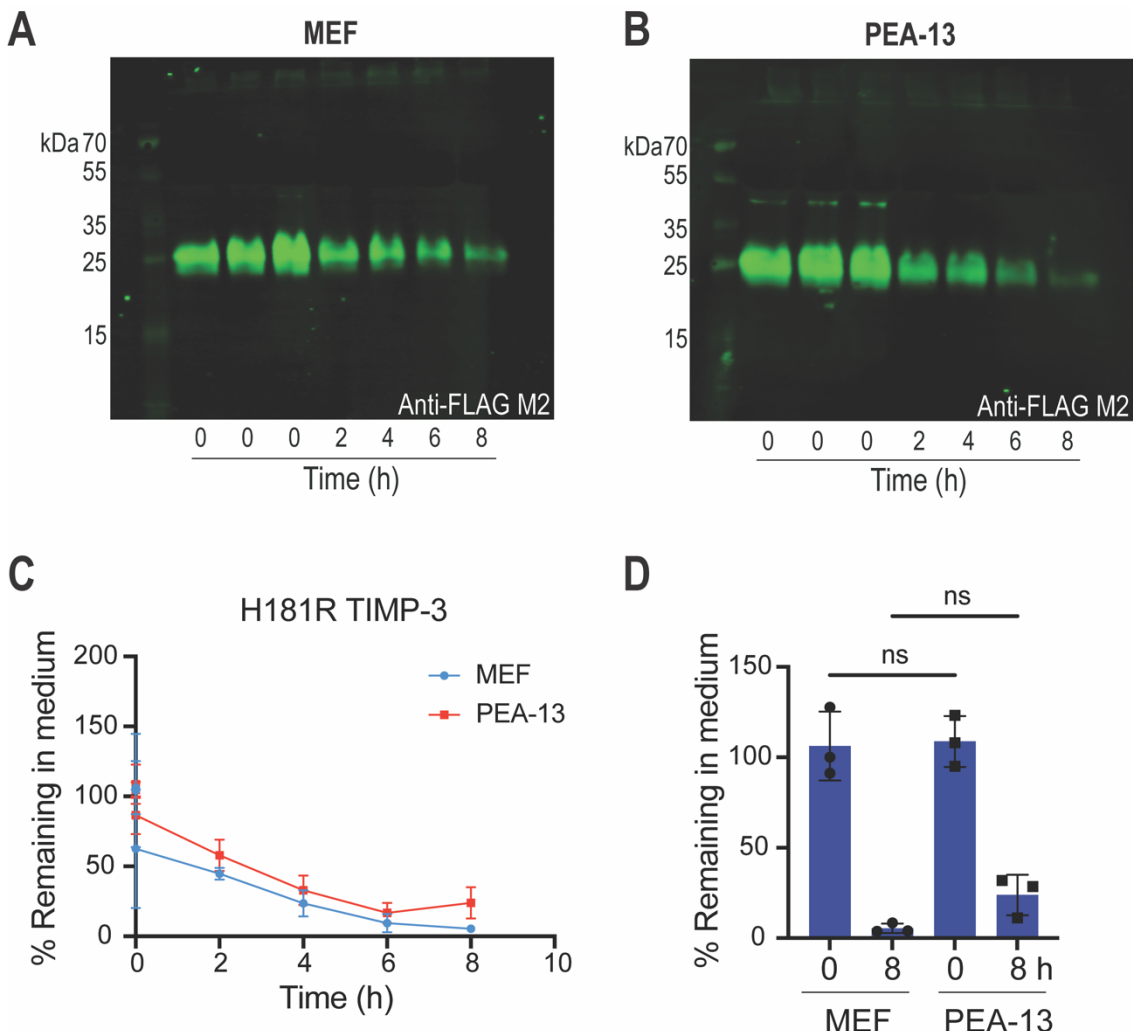


**Figure 6.1: LRP1-null PEA-13 cells had reduced uptake of WT TIMP-3 compared to WT MEF cells.**

MEF or PEA-13 cells (500 000 cells per well in a 12-well plate,  $n = 3$  per condition) were incubated overnight in 2 ml growth DMEM and were washed 3 times in SF DMEM (2.5 ml) the following morning. Isolated WT TIMP-3 (2.5 nM in TNC-B) in SF DMEM was added for 0 or 8 h, before media were TCA precipitated and resuspended in 2x SDS-PAGE sample buffer (50  $\mu$ l). Resuspended samples (15  $\mu$ l) were analysed by immunoblotting using an anti-FLAG M2 antibody, followed by detection with a fluorescent anti-mouse IgG secondary antibody. Bands were imaged using LI-COR Odyssey CLx, quantified in Image Studio software and normalised to total protein stain in each lane. (A) and (B) show immunoblots for MEF cells and PEA-13 cells, respectively. (C) Normalised band intensity was expressed as a percentage of band intensity at time = 0 h and plotted over time. (D) TIMP-3 in the medium (mean  $\pm$  SD) of MEF and PEA-13 cells at 0 and 8 h was compared, with data assessed for normality with Shapiro-Wilks test, analysed for significance with one-way ANOVA and corrected for multiple comparisons with Sidak's multiple comparisons test (ns = not significant, \*  $p \leq 0.05$ ).

**Figure 6.2** shows analysis of H181R endocytosis in MEF and PEA-13 cells. Endocytosis of monomeric (~ 25 kDa) H181R TIMP-3 was investigated by adding isolated recombinant H181R TIMP-3 (2.5 nM) to the conditioned media of PEA-13 and MEF cells and monitoring its disappearance over 8 h (**Figure 6.2 C**). Immunoblotting using an anti-FLAG M2 antibody and subsequent quantification showed that the amount of H181R TIMP-3 in the conditioned media of MEF cells progressively decreased over time until almost none was detectable (**Figure 6.2 A & C**), indicative of uptake by MEF cells. In a very similar fashion, the intensity of H181R TIMP-3 bands in the conditioned media of PEA-13 cells progressively

decreased over 8 h (**Figure 6.2 A & D**), indicating uptake of H181R TIMP-3 by these cells as well. There was not a significant difference of the amount of H181R TIMP-3 detectable in the conditioned media of PEA-13 cells compared to MEF cells at 8 h ( $p = 0.2339$ , **Figure 6.2 D**). However, there was a small numerical difference in means, with ~20 % H181R TIMP-3 detectable in the conditioned media of PEA-13 cells compared with ~5 % in MEF cells (**Figure 6.2 D**). These results suggest that the uptake of H181R TIMP-3 by mouse embryonic fibroblasts is largely independent of LRP1, although the slight numerical difference in uptake at 8 h suggests that a small fraction of the uptake of H181R TIMP-3 is mediated by LRP1.

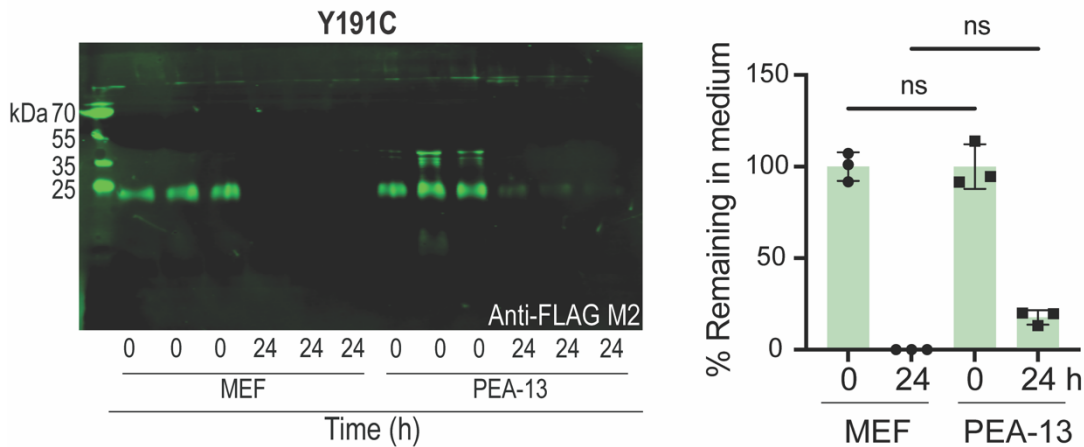
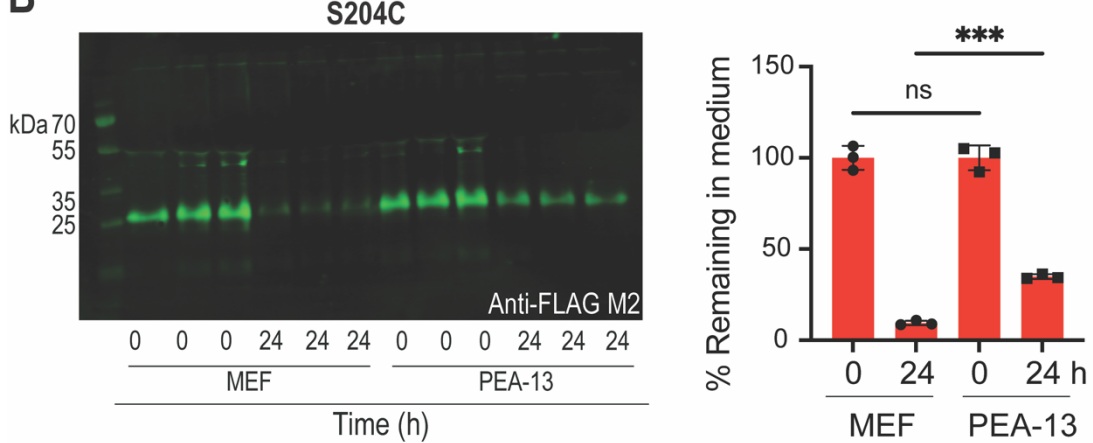


**Figure 6.2: Endocytosis of H181R TIMP-3 was not reduced in LRP1-null PEA-13 cells.** MEF or PEA-13 cells (500 000 cells per well in a 12-well plate,  $n = 3$  per condition) were incubated overnight in 2 ml growth DMEM and were washed 3 times in SF DMEM (2.5 ml) the following morning. Isolated H181R TIMP-3 (2.5 nM in TNC-B) in SF DMEM was added for 0 or 8 h, before media were TCA precipitated and resuspended in 2x SDS-PAGE sample buffer (50  $\mu$ l). Resuspended samples (15  $\mu$ l) were analysed by immunoblotting using an anti-FLAG M2 antibody, followed by detection with a fluorescent anti-mouse IgG secondary antibody. Bands were imaged using LI-COR Odyssey CLx, quantified in Image Studio software and normalised to total protein stain in each lane. (**A**) and (**B**) show immunoblots for MEF cells and PEA-13 cells, respectively. (**C**) Normalised band intensity was expressed as a percentage of band intensity at time = 0 h and plotted over time (**D**) H181R TIMP-3 in the medium (mean  $\pm$  SD) of MEF and PEA-13 cells at 0 and 8 h was compared, with data assessed for normality with Shapiro-Wilks test, analysed for significance with one-way ANOVA and corrected for multiple comparisons with Sidak's multiple comparisons test (ns = not significant).

Endocytosis of monomeric (~ 25 kDa) Y191C and S204C TIMP-3 was investigated by adding isolated recombinant Y191C and S204C TIMP-3 (2.5 nM) to PEA-13 and MEF cells and monitoring their disappearance over 24 h (**Figure 6.3**). 24 h was chosen as a suitable timepoint for Y191C and S204C TIMP-3 because previous data (**Figure 5.5**) indicated that uptake of both of these proteins by ARPE-19 cells was not appreciable at 6 or 8 h.

Immunoblotting of MEF conditioned media using an anti-FLAG M2 antibody showed that Y191C was clearly detectable at 0 h, but had disappeared from the media by 24 h (**Figure 6.3 A**). Similarly, strong bands corresponding to monomeric Y191C TIMP-3 were detectable in the conditioned media of PEA-13 cells at 0 and 24 h, although bands at 24 h were stronger than those detected in conditioned media of MEF cells at this time (**Figure 6.3 A**). Quantification of these data showed there was no significant difference in the amount of Y191C TIMP-3 detectable at 24 h in conditioned media of MEF and PEA-13 cells ( $p = 0.0666$ , **Figure 6.3 A**), although mean signal was numerically higher in conditioned media of PEA-13 cells. These results suggest that the uptake of Y191C TIMP-3 in mouse embryonic fibroblasts is largely independent of LRP1, although the slight numerical difference in means at 24 h suggests that a small fraction of Y191C uptake is mediated by LRP1.

Similarly, S204C was readily taken up from the conditioned media of both MEF and PEA-13 cells (**Figure 6.3 B**). Only weak bands were visible at 24 h, but these were significantly stronger in the conditioned media of PEA-13 cells ( $p = 0.0004$ , **Figure 6.3 B**). These results suggest that the uptake of S204C TIMP-3 in mouse embryonic fibroblasts depends in part on LRP1, although a large proportion of S204C uptake is independent of LRP1.

**A****B**

**Figure 6.3: Y191C and S204C TIMP-3 were endocytosed by LRP1-null PEA-13 and WT MEF cells.**

MEF or PEA-13 cells (500 000 cells per well in a 12-well plate) were incubated overnight in 2 ml growth DMEM and washed 3 times in SF DMEM (2.5 ml) the following morning. Isolated Y191C TIMP-3 (**A**) or S204C TIMP-3 (**B**) (2.5 nM in TNC-B) in SF DMEM were added for 0 and 24 h, before media were TCA precipitated and resuspended in 2x SDS-PAGE sample buffer (50  $\mu$ l). Resuspended samples (15  $\mu$ l) were analysed by immunoblotting using an anti-FLAG M2 antibody, followed by detection with a fluorescent anti-mouse IgG secondary antibody. Bands were imaged using LI-COR Odyssey CLx and quantified in Image Studio software and normalised to total protein stain in each lane. (**A**) and (**B**) show the immunoblots for Y191C and S204C uptake by MEF cells and PEA-13 cells, respectively. Normalised band intensity was expressed as a percentage of band intensity at time = 0 h and plotted. The amount of mutant TIMP-3 (mean  $\pm$  SD) remaining in the media at 0 and 24 h was compared for Y191C (**A**) and S204C (**B**), with data assessed for normality with Shapiro-Wilks test and analysed for significance with one-way ANOVA and corrected for multiple comparisons with Sidak's multiple comparisons test (ns = not significant, \*\*\*  $p \leq 0.001$ ).

## 6.2.2 LRP1 is expressed by retinal pigment epithelial cell lines and in primary retinal tissue

LRP1 protein expression in ARPE-19 cells was investigated by immunoblotting conditioned media samples, collected from cells after 6 and 24 h of culture, with an anti-LRP1 (8G1) antibody (**Figure 6.4, left-hand side**). In 6 h samples, very faint bands were visible at 70 kDa, 100 kDa, as well as at ~35 and ~40 kDa. All of these bands were stronger at 24 h, and additional bands were detectable at 130 kDa and 180 kDa. Use of this antibody previously within our group showed similar bands in conditioned media of HTB94 cells (Scilabra et al., 2013), and was considered to reflect protease-mediated degradation of LRP1 in media.

The mRNA expression of *LRP1* in ARPE-19 and hTERT RPE-1 cells was investigated by RT-qPCR (**Figure 6.4, right-hand side**). The CT values were normalised against a housekeeper gene, *GAPDH*, and this revealed fairly high expression in both ARPE-19 and hTERT RPE-1 cells, with *LRP1* detected ~4 cycles after *GAPDH* in both cell lines.

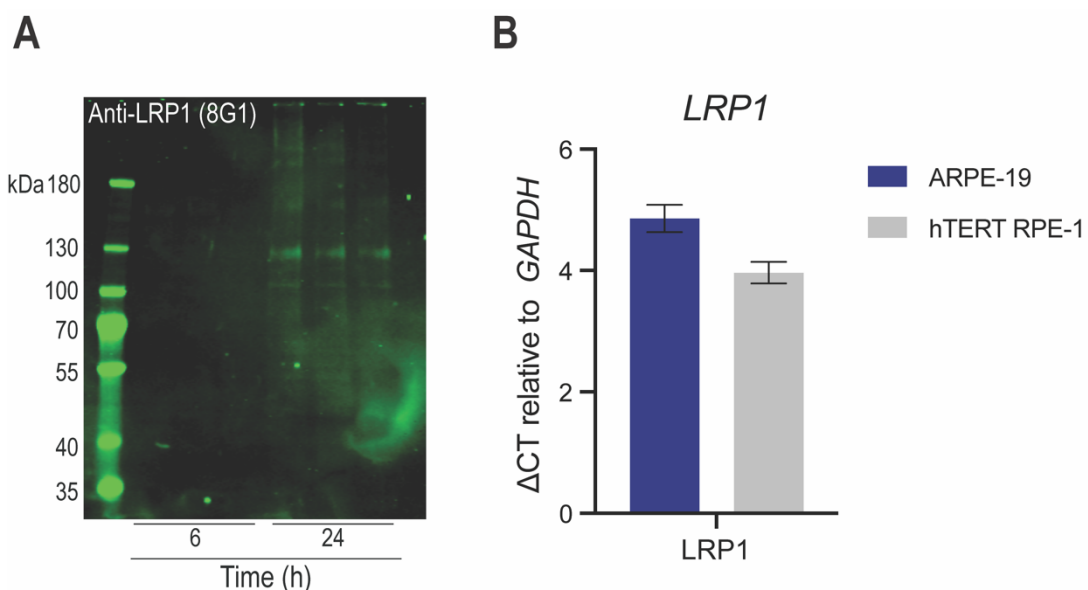


**Figure 6.4: LRP1 is expressed by ARPE-19 and hTERT RPE-1 cell lines.**

(A) ARPE-19 cells (250 000 in a 12-well plate) were plated overnight in growth DMEM (2 ml) and washed 3 times in SF DMEM (2.5 ml) the following day. Cells were incubated in SF DMEM (2 ml) for 6 and 24 h, and conditioned media collected, TCA precipitated [4 °C, 5 % (v/v), overnight] and resuspended in 2x SDS-PAGE sample buffer (50 µl). Samples (15 µl) were run on 4-15 % gels (Bio-Rad) and analysed by immunoblotting using an anti-LRP1 8G1 antibody, followed by detection with a fluorescent anti-mouse IgG secondary antibody. Bands were imaged using LI-COR Odyssey CLx. (B) ARPE-19 and hTERT RPE-1 cells (250 000 in a 12-well plate) were plated in growth DMEM (2 ml). After 24 h, RNA was extracted, cDNA synthesised and mRNA expression of *LRP1* measured by RT-qPCR. Data were normalised against the housekeeper gene *GAPDH*, using the  $\Delta\text{CT}$  method. Data are presented as mean  $\pm$  SD ( $n = 3$ ).

Given that LRP1 expression was detected at the mRNA and protein level in two RPE cell lines, it was important to ascertain whether *LRP1* and *TIMP3* were expressed at the mRNA level in primary macular tissue (**Figure 6.5**). RNAscope is a novel method of RNA in situ hybridisation and to my knowledge, this was the first study to use this approach to detect *LRP1* and *TIMP3* mRNA in primary macular tissue. Primary macular tissue was obtained, via the Manchester Eye Tissue Repository, from four donors: an 86-year-old male, a 51-year-old female a 39-year-old female and another 51-year-old female, all of whom had no reported retinal dystrophies at the time of death. RNAscope analysis was performed by Dr Sheona Drummond (University of Manchester) on sections from all four donors by incubating them with colorimetric probes specific for human *LRP1* (red) and human *TIMP3* (blue/green). However, retinal sections from two of the donors (39-year-old female and one 51-year-old female) did not survive the staining process and only the data for the 86-year-old male (M14557D) and a 51-year-old female (M14578C) were included.

Labelling for *TIMP3* was performed in three retinal sections (2 from the male donor and 1 from the female) and high *TIMP3* expression was observed throughout the sclera (**Figure 6.5 A, B & C**). It was difficult to observe *TIMP3* expression in RPE cells and also the choroid due to the endogenous production of the brown pigment melanin by RPE cells (Tian et al., 2021). Detection of *TIMP3* in the BrM was also difficult due to its thin nature, however upon close inspection of **Figure 6.5 A**, blue/green spots indicative of *TIMP3* expression can be observed in the BrM.

In sections labelled for *LRP1*, signal was abundant throughout the choroid and sclera in both donors (**Figure 6.5 A & B**), however it was difficult to determine *LRP1* expression in RPE cells, again due to the endogenous production of melanin by RPE cells. Furthermore, *LRP1* was highly expressed in the inner nuclear layer and ganglion cell layer (**Figure 6.5 B**) of the 86-year old male donor, but these layers were not present in the *LRP1* stained section of the 51-year old female donor (**Figure 6.5 A**), so staining could not be ascertained. **Figure 6.5 C** serves as a useful negative control for *LRP1* staining, since a specific colorimetric probe for *LRP1* was not used on this section and hence no *LRP1* staining was detected.

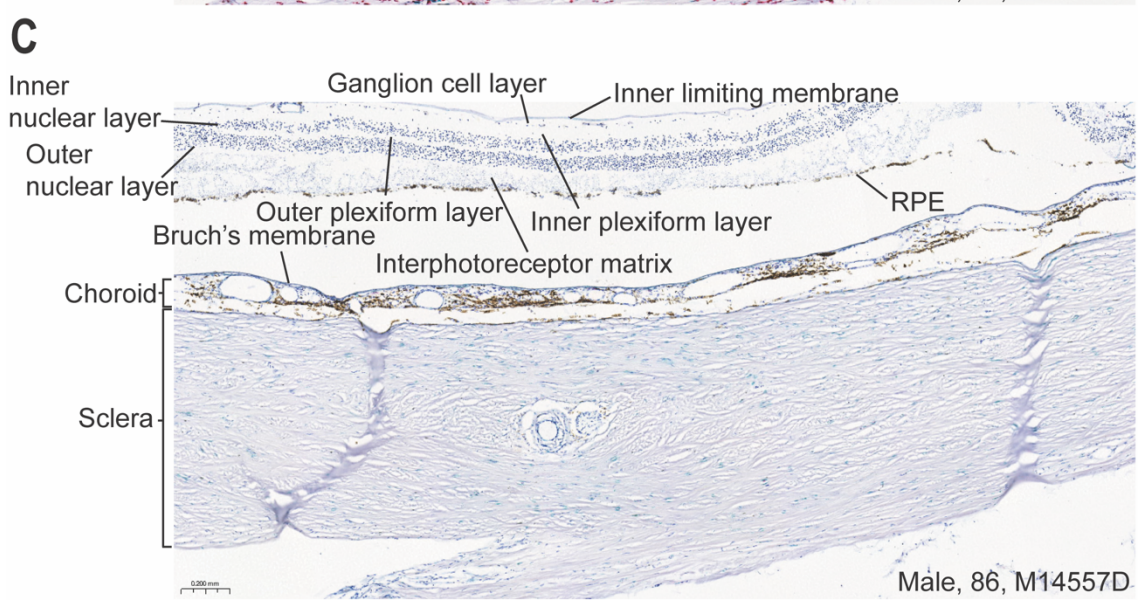
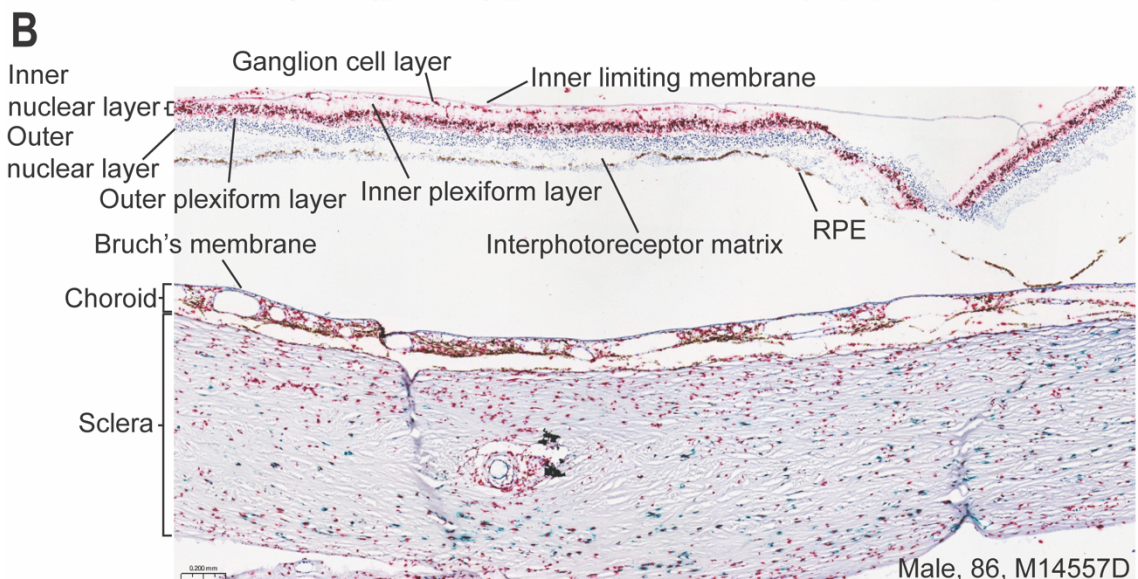
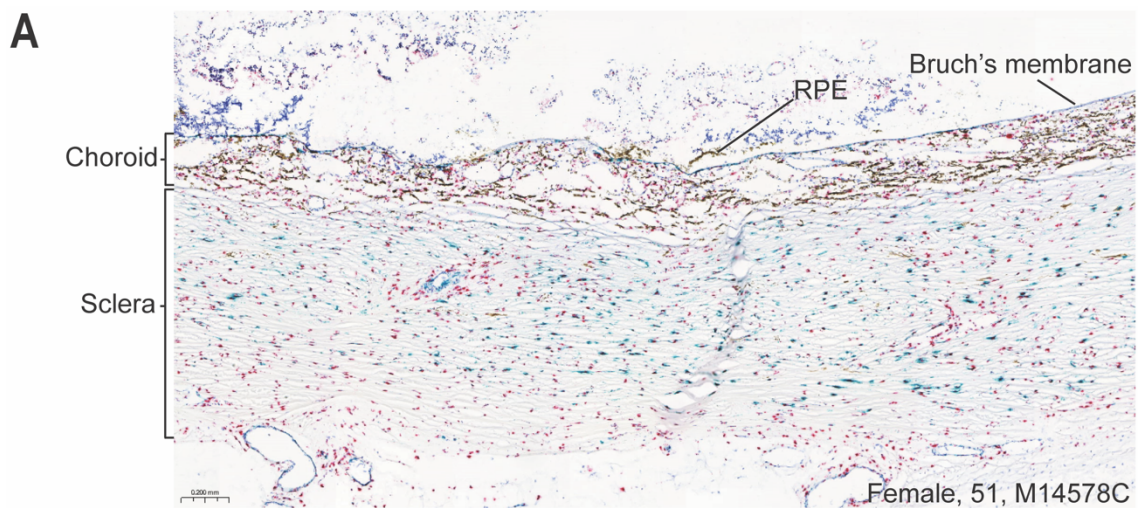


**Figure 6.5: RNAscope analysis of human retinal tissue sections revealed widespread mRNA expression of *LRP1* and *TIMP3*.**

Primary human retinal sections (from donors with no reported visual pathology) were incubated and visualised (3D Histech Pannoramic P250 digital slide scanner, 4.9 x) with colorimetric probes specific for human *LRP1* (red) and human *TIMP3* (blue/green). Both *LRP1* and *TIMP3* were visualised on a retinal section from, M14578C, a 51-year-old female (A) and M14557D, an 86-year-old male (B) while just *TIMP3* alone was visualised in a retinal section from the same 86-year-old male donor (C). *LRP1* and *TIMP3* expression was present throughout layers of the retina but was particularly abundant in the choroid and sclera. Scale bar represents 0.2 mm.

### 6.2.3 Endocytosis of WT, H181R, Y191C and S204C TIMP-3 was blocked by RAP

To investigate whether members of the LRP family mediated TIMP-3 uptake in the RPE, cells were incubated with RAP, an antagonist of ligand binding to this family of endocytic receptors (Lee et al., 2007). Firstly, the bioactivity of recombinant RAP was confirmed by incubating ARPE-19 cells with 0  $\mu$ M or 2  $\mu$ M RAP for 6 h (Figure 6.6). A total protein stain (Figure 6.6 A), showed the presence of a strong band at  $\sim$ 39 kDa, the reported molecular weight for RAP (Jensen et al., 2009) in RAP-treated but not control lanes. Bands were also visible between 55 and 70 kDa, corresponding to the molecular weight of BSA (Carter & Ho, 1994), reflecting the 0.2 % FBS added to the conditioned media during culture. The blot was then incubated with an anti-TIMP-3 AB6000 antibody to detect accumulation of endogenous TIMP-3. Bands were observed at  $\sim$ 24 kDa and  $\sim$ 27 kDa, in accordance with the reported molecular weights of unglycosylated and glycosylated TIMP-3 (Apte et al., 1994b; Langton et al., 1998; Leco et al., 1994) (Figure 6.6 B). These TIMP-3 bands were 4-fold stronger in samples from ARPE-19 cells that had been treated with 2  $\mu$ M RAP (Figure 6.6 B-C), indicating that treatment with RAP resulted in TIMP-3 accumulation in the conditioned media, and that the recombinant RAP preparation had the expected biological activity (Troeberg et al., 2008).

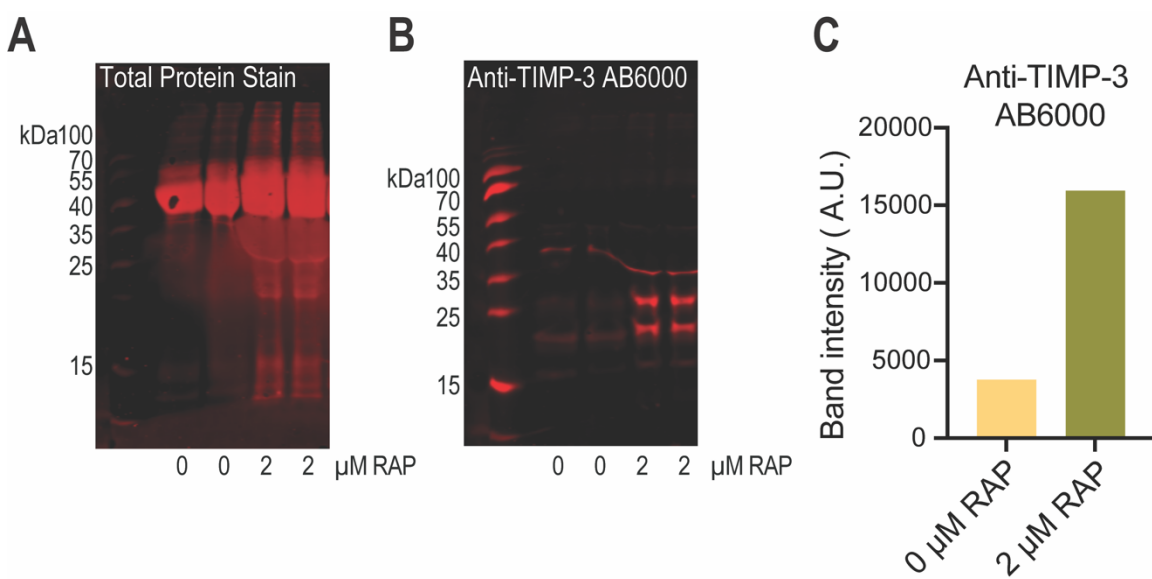


**Figure 6.6: Addition of RAP to the conditioned medium of ARPE-19 cells resulted in TIMP-3 accumulation in the conditioned medium.**

ARPE-19 cells (250 000 cells per well in a 12-well plate) were incubated overnight in growth DMEM (2 ml) and were washed 3 times in SF DMEM (2.5 ml) the following day. Cells were then treated either with 0  $\mu$ M RAP (n = 2) or 2  $\mu$ M RAP (n = 2) in SF DMEM (2 ml, 6 h). Conditioned media were collected, TCA precipitated and resuspended in 2x SDS-PAGE sample buffer (50  $\mu$ l). (A) After electrophoresis (15  $\mu$ l of sample) and blotting to PVDF membrane, a total protein stain was performed using LI-COR Revert Total Protein Stain. RAP ( $\sim$ 38 kDa) was visible in treated samples (B) The blot was incubated with an anti-TIMP-3 AB6000 antibody, followed by detection with a

fluorescent anti-rabbit IgG secondary antibody. (C) TIMP-3 bands were imaged using LI-COR Odyssey CLx and quantified in Image Studio software.

After establishing that RAP treatment resulted in accumulation of endogenous TIMP-3 in the conditioned media of ARPE-19 cells, it was next determined whether RAP treatment could block uptake of exogenously added WT TIMP-3 in ARPE-19 and hTERT RPE-1 cells (**Figure 6.7**).

ARPE-19 and hTERT RPE-1 cells were preincubated with 0 or 1  $\mu$ M RAP for 1 h before the addition of isolated recombinant WT TIMP-3 to the conditioned media. Using an anti-FLAG M2 antibody, the abundance of monomeric WT TIMP-3 (~25 kDa) in the conditioned media was measured over a time-course of 6 or 4 h in ARPE-19 and hTERT RPE-1 cells, respectively (**Figure 6.7 A & B**). At 6 h, WT TIMP-3 levels in the conditioned media of ARPE-19 cells that had not been treated with RAP decreased significantly to ~ 35 % ( $p = 0.0034$ , **Figure 6.7 A**), consistent with previous observations of WT TIMP-3 endocytosis in ARPE-19 cells in **Chapter 5**. Conversely, levels of WT TIMP-3 at 6 h in conditioned media of RAP-treated ARPE-19 cells was not significantly different at 0 and 6 h ( $p = 0.2151$ , **Figure 6.7 A**). These results demonstrated that addition of RAP blocked the uptake of exogenously added WT TIMP-3 in ARPE-19 cells.

Similar observations were made in hTERT RPE-1 cells, with TIMP-3 levels in the conditioned media decreasing significantly after 4 h in cells not treated with RAP ( $p = 0.0151$ , **Figure 6.7 B**), again consistent with previous observations in **Chapter 5**. However, TIMP-3 levels in the conditioned media were not significantly different at 0 and 4 h in hTERT RPE-1 cells treated with 1  $\mu$ M RAP ( $p = 0.6517$ , **Figure 6.7 B**). These results in hTERT RPE-1 cells corroborated the observations made in **Figure 6.7 A**, in showing that RAP blocked the uptake of exogenously added WT TIMP-3.

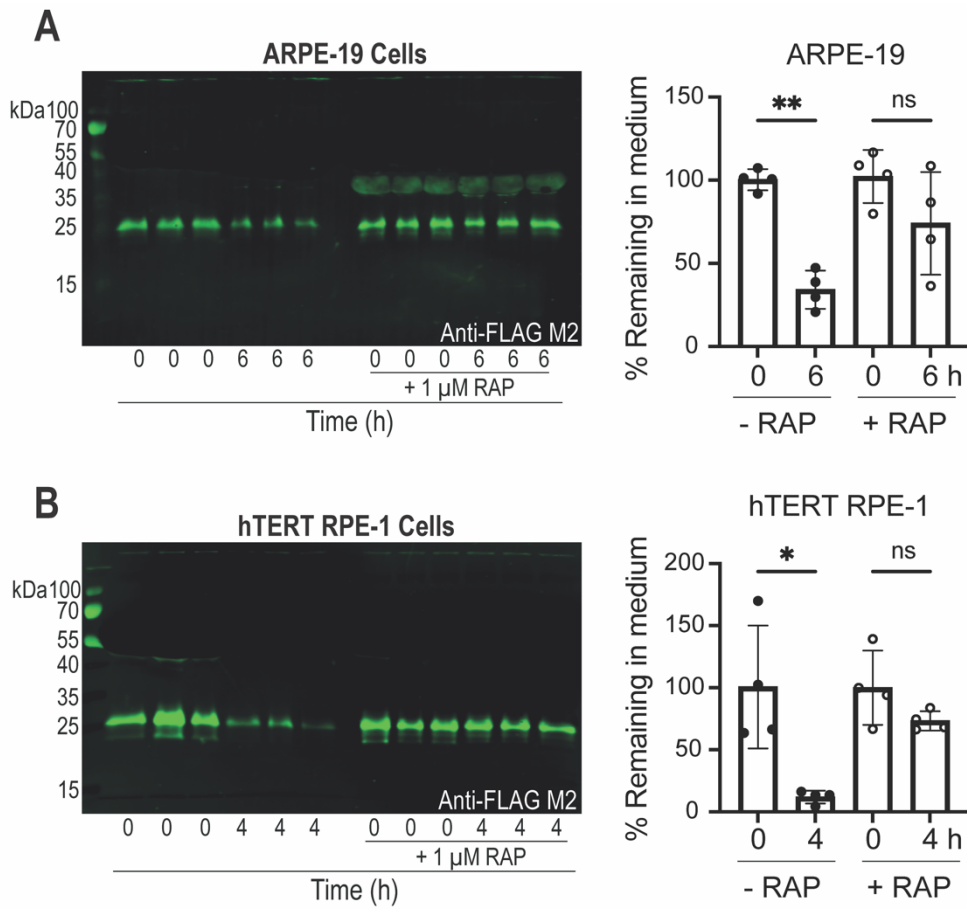


**Figure 6.7: Addition of RAP to the conditioned medium of ARPE-19 and hTERT RPE-1 cells inhibited WT TIMP-3 endocytosis.**

ARPE-19 cells (A) or hTERT RPE-1 cells (B) (250 000 cells per well in a 12-well plate) were incubated overnight in growth DMEM (2 ml) and washed 3 times in SF DMEM (2.5 ml) the following morning. Cells were treated with 0 or 1  $\mu$ M RAP ( $n = 4$  per condition) in DMEM containing 0.2 % FBS (2 ml, 1 h). Isolated WT TIMP-3 (2.5 nM in TNC-B) was then added to the conditioned medium of ARPE-19 or hTERT RPE-1 cells and conditioned media were collected at 0, 4 and 6 h, TCA precipitated and resuspended in 2x SDS-PAGE sample buffer (50  $\mu$ l). Resuspended samples (15  $\mu$ l) were analysed by immunoblotting using an anti-FLAG M2 antibody, followed by detection with a fluorescent anti-mouse IgG secondary antibody. Bands were imaged using LI-COR Odyssey CLx and quantified in Image Studio software and normalised to total protein stain in each lane. Normalised band intensity was expressed as a percentage of band intensity at time = 0 h within RAP treatment groups. Data for ARPE-19 cells (A) and hTERT RPE-1 cells (B) were assessed for normality with Shapiro-Wilks test and subsequently analysed for significance relative to 0 h within RAP treatment groups with two-way ANOVA and corrected for multiple comparisons with Tukey's multiple comparisons test (ns = not significant, \*  $p \leq 0.05$ , \*\*  $p \geq 0.001$ )

It was next investigated whether pre-incubation of ARPE-19 cells with RAP blocked the uptake of exogenously added SFD mutants: H181R, Y191C and S204C TIMP-3 (Figure 6.8 A, B & C). Using an anti-FLAG M2 antibody, the abundance of monomeric H181R, Y191C and S204C TIMP-3 was observed in conditioned media of ARPE-19 cells incubated with 0 or 1  $\mu$ M of RAP for 6 or 24 h. For comparison with WT TIMP-3, Figure 6.8 A shows the same data presented in Figure 6.7 A.

Over 6 h, H181R TIMP-3 levels in the conditioned media of cells not treated with RAP decreased significantly to ~ 35 % (p = 0.0019, **Figure 6.8 B**), consistent with previous observations of H181R TIMP-3 endocytosis in ARPE-19 cells (**Figure 5.4 & Figure 5.5**). Conversely, H181R TIMP-3 levels in conditioned media of cells treated with 1  $\mu$ M RAP were not significantly different at 0 and 6 h (p = 0.1651, **Figure 6.8 B**). These results demonstrated that addition of RAP blocked the uptake of exogenously added H181R TIMP-3 in ARPE-19 cells.

**Chapter 5** showed that at 6 h ~80 % of Y191C and S204C TIMP-3 remained in the media, indicating that 6 h was not a suitable timepoint for RAP experiments, because neither of these proteins is appreciably taken up at this timepoint. Both Y191C and S204C TIMP-3 were taken up by 24 h (**Figure 5.4 & Figure 5.5**), so this was selected as a suitable timepoint for analysing the effect of RAP.

At 24 h, Y191C and S204C TIMP-3 levels in the conditioned media of cells not treated with RAP decreased significantly to ~25 % (p = 0.0301, **Figure 6.8 C**) and ~10 % (p = 0.0283, **Figure 6.8 D**), respectively. These results were consistent with previous observations of Y191C and S204C TIMP-3 endocytosis in ARPE-19 cells at 24 h (**Figure 5.4 & Figure 5.5**). In contrast, Y191C and S204C TIMP-3 levels in conditioned media of cells treated with 1  $\mu$ M RAP were not significantly different at 0 and 24 h (p = 0.9998, **Figure 6.8 C** and p = 0.9976, **Figure 6.8 D**, respectively). This showed that addition of RAP blocked the uptake of exogenously added Y191C and S204C TIMP-3 in ARPE-19 cells.

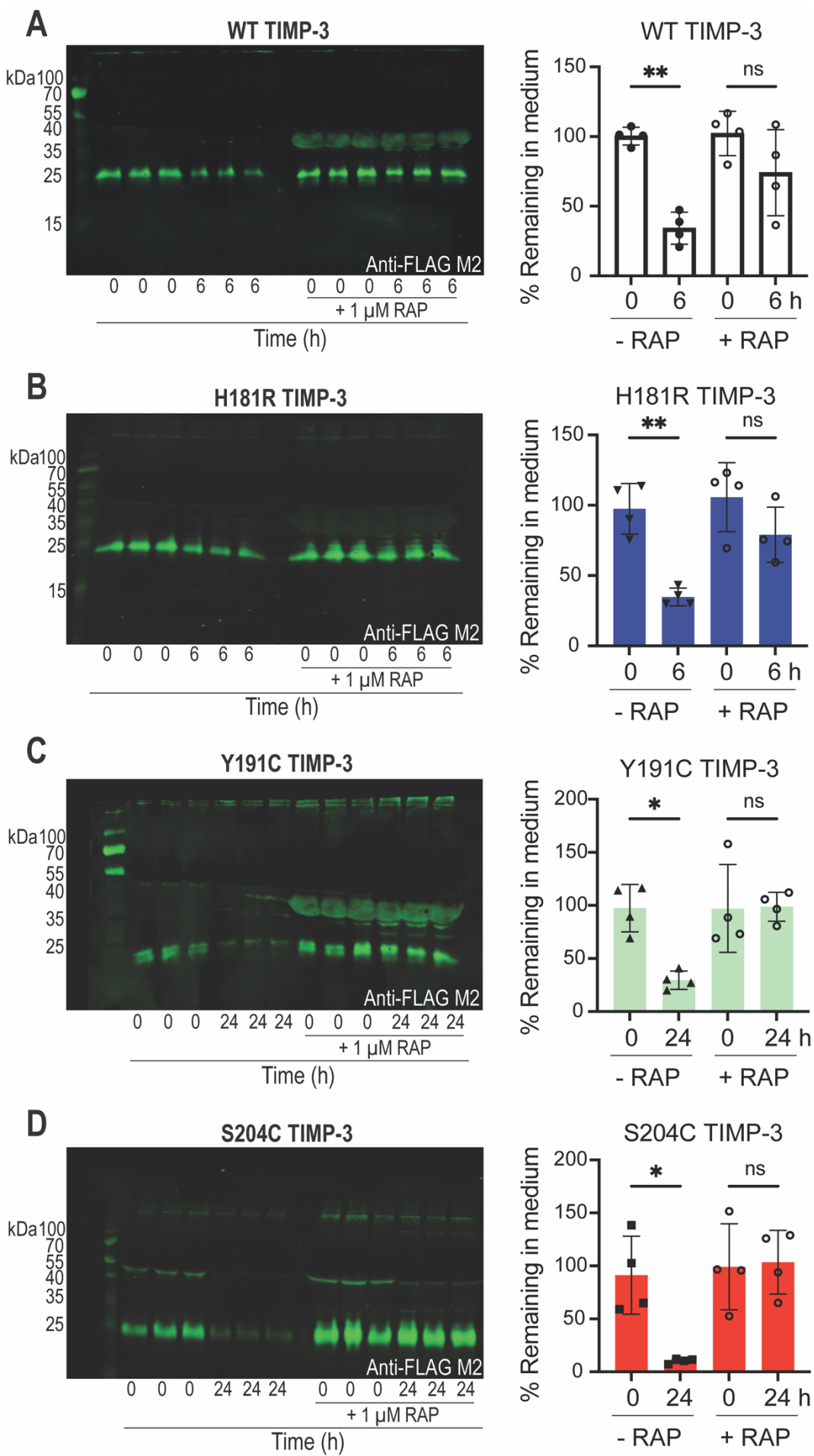


**Figure 6.8: RAP inhibited endocytosis of WT TIMP-3, H181R TIMP-3, Y191C TIMP-3 and S204C TIMP-3 by ARPE-19 cells.**

ARPE-19 cells (250 000 cells per well in a 12-well plate) were incubated overnight in growth DMEM (2 ml) and washed 3 times in SF DMEM (2.5 ml) the following morning. Cells were treated with 0 or 1  $\mu$ M RAP (n = 4 per condition) in DMEM containing 0.2 % FBS (2 ml, 1 h). Isolated WT (**A**), H181R (**B**), Y191C (**C**) or S204C (**D**) TIMP-3 (2.5 nM in TNC-B) were then added to the conditioned medium for 0, 6 and 24 h, after which media were TCA precipitated and resuspended in 2x SDS-PAGE sample buffer (50  $\mu$ l). Resuspended sample (15  $\mu$ l) were analysed by immunoblotting using an anti-FLAG M2 antibody, followed by detection with a fluorescent anti-mouse IgG secondary antibody. Bands were imaged using LI-COR Odyssey CLx and quantified in Image Studio software and normalised to total protein stain in each lane. Normalised band intensity was expressed as a percentage of band intensity at time = 0 h within RAP treatment groups. Data for WT TIMP-3 (**A**), H181R TIMP-3 (**B**), Y191C TIMP-3 (**C**) and S204C TIMP-3 (**D**) was plotted as mean  $\pm$  SD and assessed for normality with Shapiro-Wilks test. Subsequently they were analysed for significance relative to 0 h within each RAP treatment group two-way ANOVA and corrected for multiple comparisons with Tukey's multiple comparisons test (ns = not significant, \* p  $\leq$  0.05, \*\* p  $\geq$  0.001).

## 6.2.4 Effect of siRNA knockdown of LRP1 on endocytosis of WT TIMP-3 in RPE cells

### 6.2.4.1 siRNA knockdown of LRP1 in ARPE-19 cells using ThermoFisher siRNA

siRNA knockdown of LRP1 in ARPE-19 cells was performed with a view to ascertaining whether LRP1 is responsible for mediating uptake of WT TIMP-3 in RPE cells (**Figure 6.9**). Initial experiments were performed in which siRNA targeting *LRP1* and an appropriate negative control siRNA purchased from ThermoFisher (**2.2.13**) were transfected into ARPE-19 cells as indicated in **Figure 6.9 A**. The level of *LRP1* expression in ARPE-19 cells was determined at the beginning (labelled as '0 h') and end ('6 h') of the subsequent endocytosis assay by RT-qPCR. *LRP1* expression was significantly reduced in ARPE-19 cells transfected with *LRP1* siRNA compared to a non-targeting siRNA control, by ~30 % and ~40 % at 0 h ( $p = 0.0109$ ) and 6 h ( $p = 0.0065$ ), respectively (**Figure 6.9 B**).

A cell viability assay was carried out (**2.2.10**) at both 0 and 6 h to determine whether transfection with a non-targeting or *LRP1*-targeting siRNA affected ARPE-19 cell health (**Figure 6.9 C**). Untreated cells cultured in the same media but not transfected were included as a negative control. At 0 h there was no significant difference in absorbance values between untreated cells or cells transfected with either the non-targeting siRNA or *LRP1*-targeting siRNA (**Figure 6.9 C, left-hand side**). This indicated that transfection with either siRNA construct did not affect overall cellular metabolism and hence cell viability. Moreover, at 6 h there was also no significant difference in absorbance values between untreated cells and cells transfected with either siRNA construct (**Figure 6.9 C, right-hand side**). There was large variation in cells transfected with siRNA targeting *LRP1* due to cell death in one biological replicate (**Figure 6.9 C, right hand-side**).

After observing that *LRP1* expression was significantly reduced, an endocytosis assay was performed with isolated recombinant WT TIMP (2.5 nM) (**Figure 6.9 D**). At 6 h, WT TIMP-3 levels in the conditioned media of ARPE-19 cells transfected with control siRNA decreased to ~35 % of initial levels. WT TIMP-3 abundance in cells transfected with *LRP1* siRNA decreased to ~20 % at 6 h, with no statistically significant difference between cells treated with non-targeting and *LRP1*-targeting siRNA (**Figure 6.9 D**). These results demonstrate that knockdown of *LRP1* had no significant effect on WT TIMP-3 uptake by ARPE-19 cells.

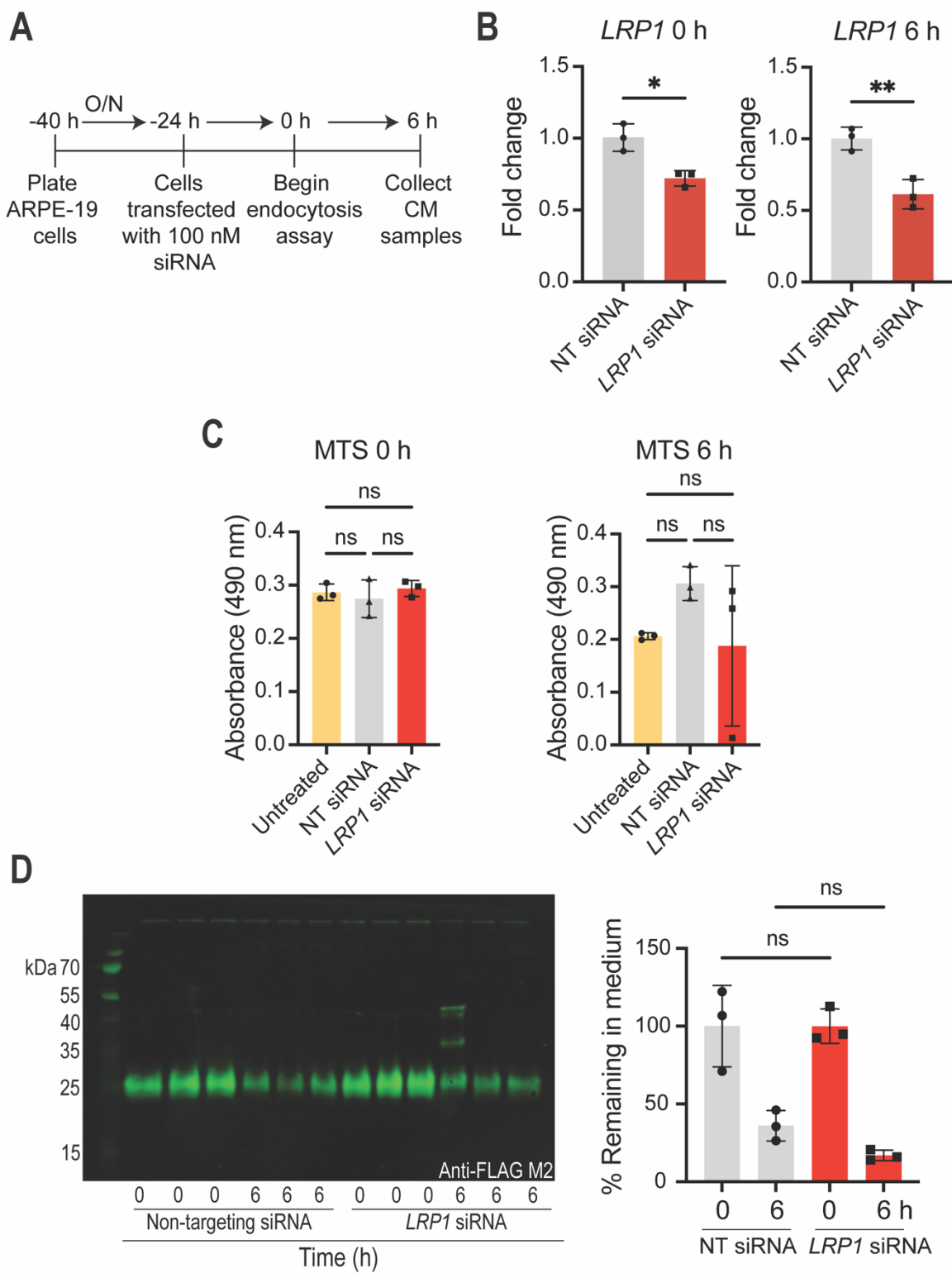


**Figure 6.9: Expression of *LRP1* was reduced by ThermoFisher siRNA knockdown, but this had no effect on TIMP-3 uptake by ARPE-19 cells.**

(A) ARPE-19 cells were plated (250 000 per well in a 12-well plate) overnight in growth DMEM (2 ml) and washed 3 times in SF DMEM (2.5 ml) the following morning. Media were replaced with Opti-MEM (1 ml) and cells were transfected with 100 nM siRNA targeting *LRP1* or a non-targeting control siRNA using Lipofectamine LTX following the manufacturer's instructions. Cells were incubated for 24 h and then washed 3 times in SF DMEM (2.5 ml). Isolated WT TIMP-3, (2.5 nM in TNC-B) was added to cells in DMEM (2 ml) containing 0.2 % FBS. Conditioned media were collected at 0 and 6 h, TCA precipitated and resuspended in 2x SDS-PAGE sample buffer (50  $\mu$ l). (B) RNA was extracted, cDNA synthesised and mRNA expression of *LRP1* measured by RT-qPCR. Using the  $\Delta\Delta CT$  method, data were normalised against the housekeeper gene *GAPDH* and expressed relative to non-targeting siRNA controls at 0 and 6 h. *LRP1* expression (mean  $\pm$  SD, n = 3 per condition) was compared with

data assessed for normality using Shapiro-Wilks test, and analysed for significance with an unpaired t-test (\*  $p \leq 0.05$ , \*\*  $p \geq 0.001$ ). **(C)** After conditioned media were removed, ARPE-19 cells were collected in cell dissociation solution, collected by centrifugation (400 RCF, 5 min), and resuspended in SF DMEM (2 ml). Cells were incubated for 90 min [37 °C, 5 % (v/v) CO<sub>2</sub>] with MTS reagent and absorbance at 490 nm quantified using a SPECTROstar Omega plate reader. Data are presented as mean  $\pm$  SD ( $n = 3$ ), with normality assessed with Shapiro-Wilks test and analysed for significance relative to the positive death control with one-way ANOVA and corrected for multiple comparisons with Tukey's multiple comparisons test (ns = not significant). **(D)** Resuspended samples (15  $\mu$ l) were analysed by immunoblotting using an anti-FLAG M2 antibody, followed by detection with a fluorescent anti-mouse IgG secondary antibody. Bands were imaged using LI-COR Odyssey CLx and quantified in Image Studio software and normalised to total protein stain in each lane (not shown). Normalised band intensity was expressed as a percentage of band intensity at time = 0 within siRNA treatment groups, and plotted as amount remaining in the medium. The amount of TIMP-3 (mean  $\pm$  SD,  $n = 3$ ) remaining in the medium at 0 and 6 h was compared with data assessed for normality using Shapiro-Wilks test, analysed for significance with one-way ANOVA and corrected for multiple comparisons with Sidak's multiple comparisons test (ns = not significant, \*\*\*  $p \leq 0.001$ ).

#### 6.2.4.2 siRNA knockdown of LRP1 using Dharmacon siRNA in ARPE-19 cells

The knockdown achieved using the ThermoFisher siRNA targeting *LRP1* was relatively poor, with only 30-40 % knockdown (**Figure 6.9 B**). Therefore, a different siRNA targeting *LRP1* was purchased from Dharmacon (**2.2.13**), as this siRNA sequence has been shown to achieve up to ~90 % knockdown in human chondrocytes (Yamamoto et al., 2013).

Initial optimisation experiments were performed as outlined in **Figure 6.10 A**, with ARPE-19 cells plated and transfected in Opti-MEM media with a range of concentrations of a non-targeting control siRNA or siRNA targeting *LRP1* (**Figure 6.10 B**). For some experiments, media were changed to growth DMEM after 6 h to aid in cell recovery after transfection. Cells were left for a further 18 h before being washed into SF DMEM, followed by RNA extraction and RT-qPCR to measure mRNA expression of *LRP1*. For each concentration of siRNA tested ( $n = 1$ ), *LRP1* expression in non-targeting control samples was calculated as 1.0, with the fold-change of *LRP1* expression in *LRP1*-targeting siRNA-transfected cells being calculated relative to respective controls at the same concentration. Data were analysed for ARPE-19 cells that were maintained in Opti-MEM media (**Figure 6.10 B, left-hand side**) and also ARPE-19 cells which were switched to growth DMEM for enhanced cell recovery (**Figure 6.10 B, right hand-side**). Greatest *LRP1* knockdown was achieved with 25 nM siRNA (~50 % or ~80 % knockdown, in Opti-MEM and growth DMEM, respectively **Figure 6.10 B**). Therefore, subsequent experiments were carried out with 25 nM siRNA, with media changed to growth DMEM 6 h post-transfection.

Further optimisation experiments were performed to confirm the reproducibility of *LRP1* knockdown when 25 nM *LRP1*-targeting siRNA was used (n = 3, **Figure 6.10 C & D**). Briefly, ARPE-19 cells were transfected with 25 nM of *LRP1*-targeting siRNA or control siRNA and media changed at 6 h to growth DMEM. Cells were then washed into SF DMEM 24 h post-transfection, with some cells collected and RNA extracted, and other cells left for 48 h post-transfection before RNA extraction (**Figure 6.10 C**). Analysis of *LRP1* expression revealed that cells transfected with *LRP1*-targeting siRNA had significantly less *LRP1* expression compared to non-targeting control siRNA 24 h post-transfection ( $p = 0.032$ ), with knockdown of ~ 50 % (**Figure 6.10 D, left-hand side**). Knockdown of *LRP1* at 48 h post-transfection was also measured because endocytosis assays following siRNA knockdown were planned to reach this timepoint post-transfection. There was also significantly less *LRP1* expression in cells transfected with *LRP1*-targeting siRNA versus non-targeting control siRNA 48 h post-transfection ( $p = 0.0078$ ) with knockdown of again 50 % (**Figure 6.10 D, right-hand side**). These experiments did not achieve the same amount *LRP1* knockdown as in the initial n = 1 optimisation experiments (**Figure 6.10 B, right-hand side**), however the amount of *LRP1* knockdown of ~ 50 % remained consistent over both timepoints (**Figure 6.10 D**).

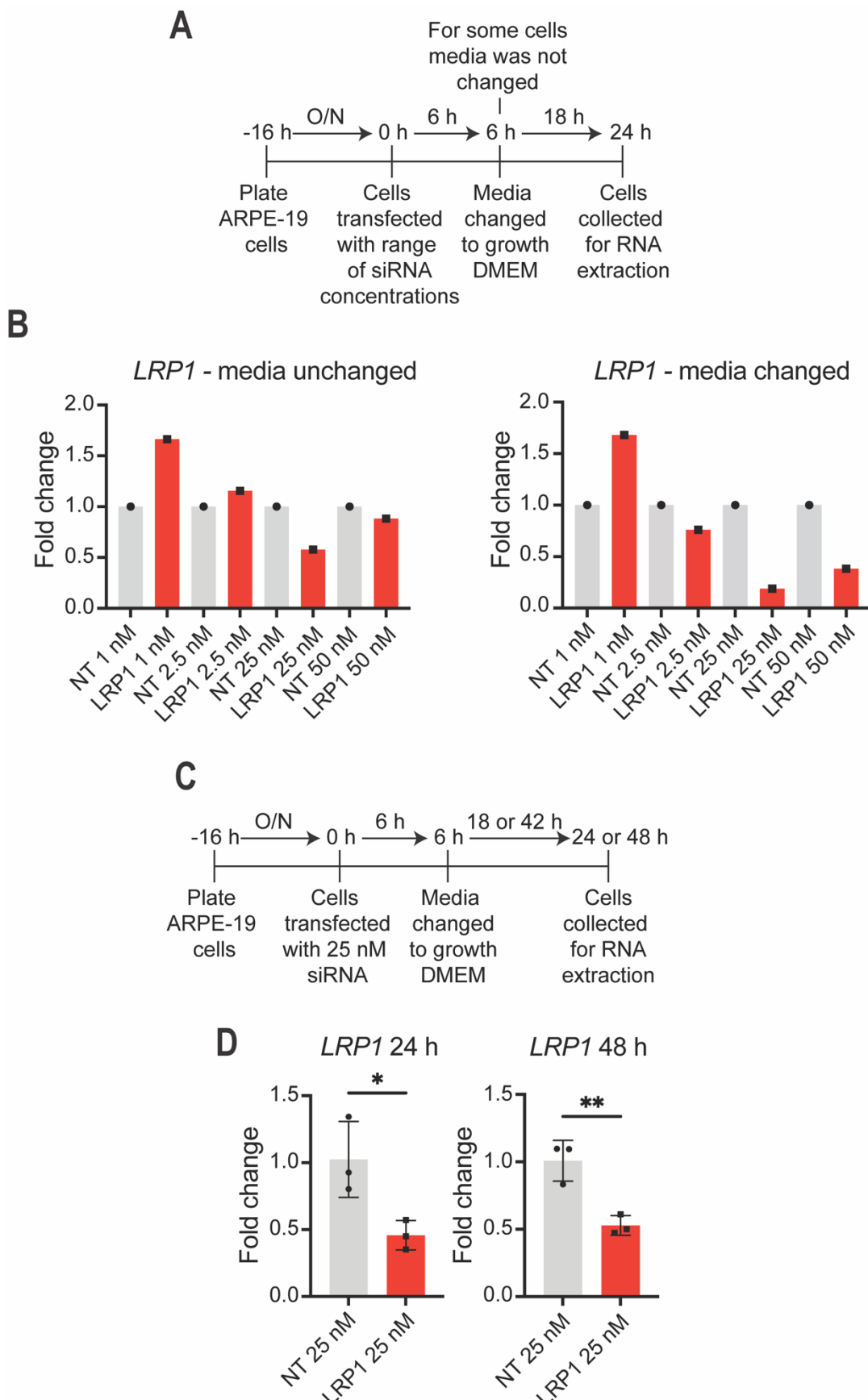


**Figure 6.10: Optimisation of Dhamacon siRNA knockdown of *LRP1* in ARPE-19 cells.**

(A) ARPE-19 cells were plated (250 000 cells per well in a 12-well plate) in growth DMEM overnight and washed 3 times in SF DMEM (2.5 ml) the following morning. Media were replaced with Opti-MEM (1 ml) and cells transfected with the concentrations of *LRP1* or non-targeting siRNA in (B) using Lipofectamine LTX following the manufacturer's instructions. Cells were incubated for 24 h in Opti-MEM or switched after 6 h to growth DMEM for a further 18 h. RNA was extracted and cDNA synthesised. (B) mRNA expression of *LRP1* (n = 1 per concentration) was measured by RT-qPCR.

Using the  $\Delta\Delta CT$  method, data were normalised against the housekeeper gene *GAPDH*, and expressed relative to non-targeting siRNA controls at each concentration. (C) ARPE-19 cells were transfected as in (A) with 25 nM non-targeting or *LRP1*-targeting siRNA, with media changed 6 h after transfection to growth DMEM for a further 18 h. Cells were washed 3 times in SF DMEM (2.5 ml) and incubated in 2 ml SF DMEM for 24 or 48 h. Cells were collected for analysis of *LRP1* mRNA expression. (D) *LRP1* expression was quantified as in (B). Data were assessed for normality using the Shapiro-Wilks test, and analysed for significance with an unpaired t-test ( $n = 3$ , mean  $\pm$  SD, \*  $p \leq 0.05$ , \*\*  $p \geq 0.001$ ).

To analyse the effect of the Dhamacon *LRP1* siRNA on TIMP-3 endocytosis, ARPE-19 cells were transfected with 25 nM negative control and *LRP1*-targeting siRNA as indicated in **Figure 6.11 A**. *LRP1* expression in ARPE-19 cells was determined at the beginning (labelled as '0 h') and end ('6 h') of the endocytosis assay by RT-qPCR. *LRP1* expression was significantly reduced in ARPE-19 cells transfected with *LRP1*-targeting siRNA compared to a non-targeting siRNA control, by  $\sim 50\%$  and  $\sim 30\%$  at 0 h ( $p \leq 0.0001$ ) and 6 h ( $p = 0.0311$ ), respectively (**Figure 6.11 B**).

A cell viability assay was conducted (**2.2.10**) at both 0 and 6 h to determine whether transfection with either siRNA affected ARPE-19 cell health (**Figure 6.11 C**). A positive control for cell death was included in which cells were repeatedly freeze-thawed between  $-80\text{ }^{\circ}\text{C}$  and  $25\text{ }^{\circ}\text{C}$ . At the start of the endocytosis assay (0 h), ARPE-19 cells transfected with either siRNA had absorbance values of  $\sim 0.4$ , which were not significantly different from each other but were significantly higher than the absorbance values of the positive death control (**Figure 6.11 C, left-hand side**). Similarly, at 6 h there was no difference in viability between ARPE-19 cells transfected with non-targeting or *LRP1*-targeting siRNA and viability in both conditions was significantly higher than the positive death control (**Figure 6.11 C, right-hand side**). These results indicated that transfection with either siRNA did not cause significant cell death at either timepoint.

An endocytosis assay using isolated recombinant WT TIMP (2.5 nM) was performed after knockdown with Dhamacon *LRP1*-targeting siRNA (**Figure 6.11 D**). At 6 h, WT TIMP-3 levels in the conditioned media of ARPE-19 cells transfected with the control siRNA decreased to  $\sim 50\%$  of the original amount detected. This decrease is markedly less than the 80 % decrease previously observed at 6 h (**Figure 5.3 & Figure 5.5**). At 6 h WT TIMP-3 abundance was significantly higher in media of ARPE-19 cells transfected with *LRP1*-targeting siRNA compared to non-targeting siRNA ( $p = 0.0391$ , **Figure 6.11 D**), indicating that *LRP1* knockdown significantly reduced WT TIMP-3 endocytosis by ARPE-19 cells. However, the difference in mean uptake was only  $\sim 20\%$  and overall uptake of WT TIMP-3 by ARPE-19 cells

was far less than the ~75 % previously observed at this timepoint (**Figure 5.3 & Figure 5.5**).

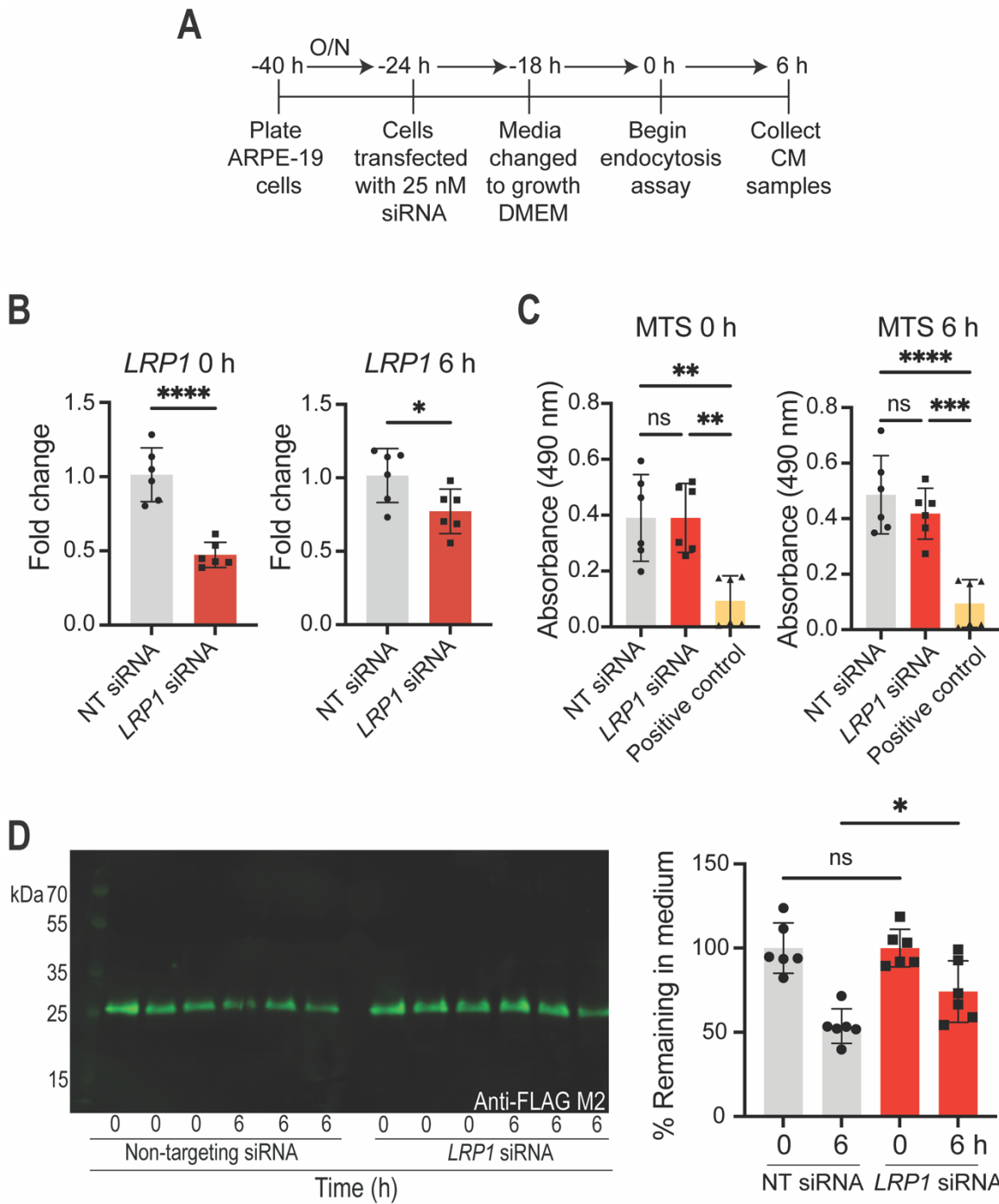


**Figure 6.11: Expression of *LRP1* was reduced by Dharmacon siRNA knockdown and this reduced TIMP-3 uptake by ARPE-19 cells.**

(A) ARPE-19 cells were plated (250 000 per well in a 12-well plate) overnight in growth DMEM (2 ml) and washed 3 times in SF DMEM (2.5 ml) the following morning. Media were changed to Opti-MEM (1 ml) and cells were transfected with 25 nM siRNA targeting *LRP1* or a non-targeting control siRNA using Lipofectamine LTX following the manufacturer's instructions. Cells were incubated for 6 h and then media were changed to growth DMEM for a further 18 h before cells were washed 3 times in SF DMEM (2.5 ml). Isolated WT TIMP-3 (2.5 nM in TNC-B) was added to cells in DMEM (2 ml) containing 0.2 % FBS. Conditioned media were collected at 0 and 6 h, TCA precipitated and resuspended in 2x SDS-PAGE sample buffer (50  $\mu$ l). (B) RNA was extracted, cDNA synthesised and mRNA expression of *LRP1* measured by RT-qPCR. Using the  $\Delta\Delta CT$  method, data were normalised against the housekeeper gene *GAPDH* and expressed relative to non-targeted siRNA controls at 0 and 6 h. *LRP1* expression (mean  $\pm$  SD, n = 6) was compared, with data assessed for normality using Shapiro-Wilks test and analysed for significance with an unpaired t-test (\* p  $\leq$  0.05, \*\*\*\* p  $\leq$  0.0001). (C) After conditioned media were removed, ARPE-19 cells were collected in cell dissociation solution,

centrifuged (400 RCF, 5 min), and resuspended in SF DMEM (2 ml). Cells were incubated for 90 min [37 °C, 5 % (v/v) CO<sub>2</sub>] with MTS reagent and absorbance at 490 nm, quantified using a SPECTROstar Omega plate reader. Data are presented as mean  $\pm$  SD (n = 6), with normality assessed with Shapiro-Wilks test and analysed for significance relative to the positive death control with one-way ANOVA and corrected for multiple comparisons with Tukey's multiple comparisons test (ns = not significant, \*\* p  $\geq$  0.001, \*\*\* p  $\leq$  0.001, \*\*\*\* p  $\leq$  0.0001). (D) Resuspended samples (15  $\mu$ l) were analysed by immunoblotting using an anti-FLAG M2 antibody, followed by detection with a fluorescent anti-mouse IgG secondary antibody. Bands were imaged using LI-COR Odyssey CLx and quantified in Image Studio software and normalised to total protein stain in each lane (not shown). Normalised band intensity was expressed as a percentage of band intensity at time = 0 within different siRNA treatment groups and plotted as % remaining in the medium. TIMP-3 levels in media (mean  $\pm$  SD, n = 6) at 0 and 6 h was compared, with data assessed for normality with Shapiro-Wilks test and analysed for significance with one-way ANOVA and corrected for multiple comparisons with Sidak's multiple comparisons test (ns = not significant, \* p  $\leq$  0.05).

#### 6.2.4.3 siRNA knockdown of LRP1 using Dharmacon siRNA in hTERT RPE-1 cells

LRP1 knockdown achieved in initial optimisation experiments in ARPE-19 cells was promising (up to  $\sim$  80 % **Figure 6.10 B, right-hand side**), but this decreased to  $\sim$  40-50 % in repeat experiments (**Figure 6.10 D & Figure 6.11 B**). Thus, knockdown of LRP1 was also investigated in hTERT RPE-1 cells, to determine if a greater level of LRP1 knockdown could be achieved (**Figure 6.12 & Figure 6.13**).

Initial optimisation experiments were performed as shown in **Figure 6.12 A**, in with hTERT RPE-1 cells plated and transfected in Opti-MEM media with a range of concentrations of a non-targeting control or LRP1-targeting siRNA (**Figure 6.12 B**). After 6 h, cells were left in Opti-MEM or changed to growth DMEM to aid in cell recovery after transfection. To mimic endocytosis assays, hTERT RPE-1 cells were incubated for a further 18 h before being washed into SF DMEM, followed by RNA extraction and RT-qPCR to measure mRNA expression of LRP1. For each concentration of siRNA used (n = 1), the LRP1 expression in non-targeting control samples was calculated as 1.0, with the fold-change of LRP1 expression in cells transfected with LRP1-targeting siRNA calculated relative to respective controls at the same concentration. Maximal knockdown of  $\sim$ 60 % was achieved with 25 nM LRP1-targeting siRNA in both Opti-MEM and growth DMEM conditions (**Figure 6.12 B**). These observations were the same as those previously seen in ARPE-19 cells. For subsequent experiments in hTERT RPE-1 cells, 25 nM siRNA was used, with media changed to growth DMEM 6 h post-transfection.

Further optimisation experiments were conducted to confirm the reproducibility of LRP1 knockdown with 25 nM LRP1-targeting siRNA (n = 3, **Figure 6.12 C & D**). Quantification of LRP1 expression revealed that hTERT RPE-1 cells transfected

with *LRP1*-targeting siRNA had significantly less *LRP1* expression compared to cells transfected with non-targeting control siRNA 24 h post-transfection ( $p = 0.005$ ), with knockdown of ~ 60 % (**Figure 6.12 D, left-hand side**). Knockdown of *LRP1* at 48 h post-transfection was also measured to mimic conditions for planned endocytosis assays. There was also significantly less *LRP1* expression in cells transfected with *LRP1*-targeting siRNA versus non-targeting control siRNA 48 h post-transfection ( $p = 0.0046$ ) with knockdown of ~ 80 % (**Figure 6.12 D, right-hand side**). These experiments achieved the same or a greater amount of *LRP1* knockdown compared to the initial  $n = 1$  optimisation experiments (**Figure 6.12 B, right-hand side**) and also much greater knockdown of *LRP1* compared to that achieved in ARPE-19 cells (**Figure 6.10 D**).

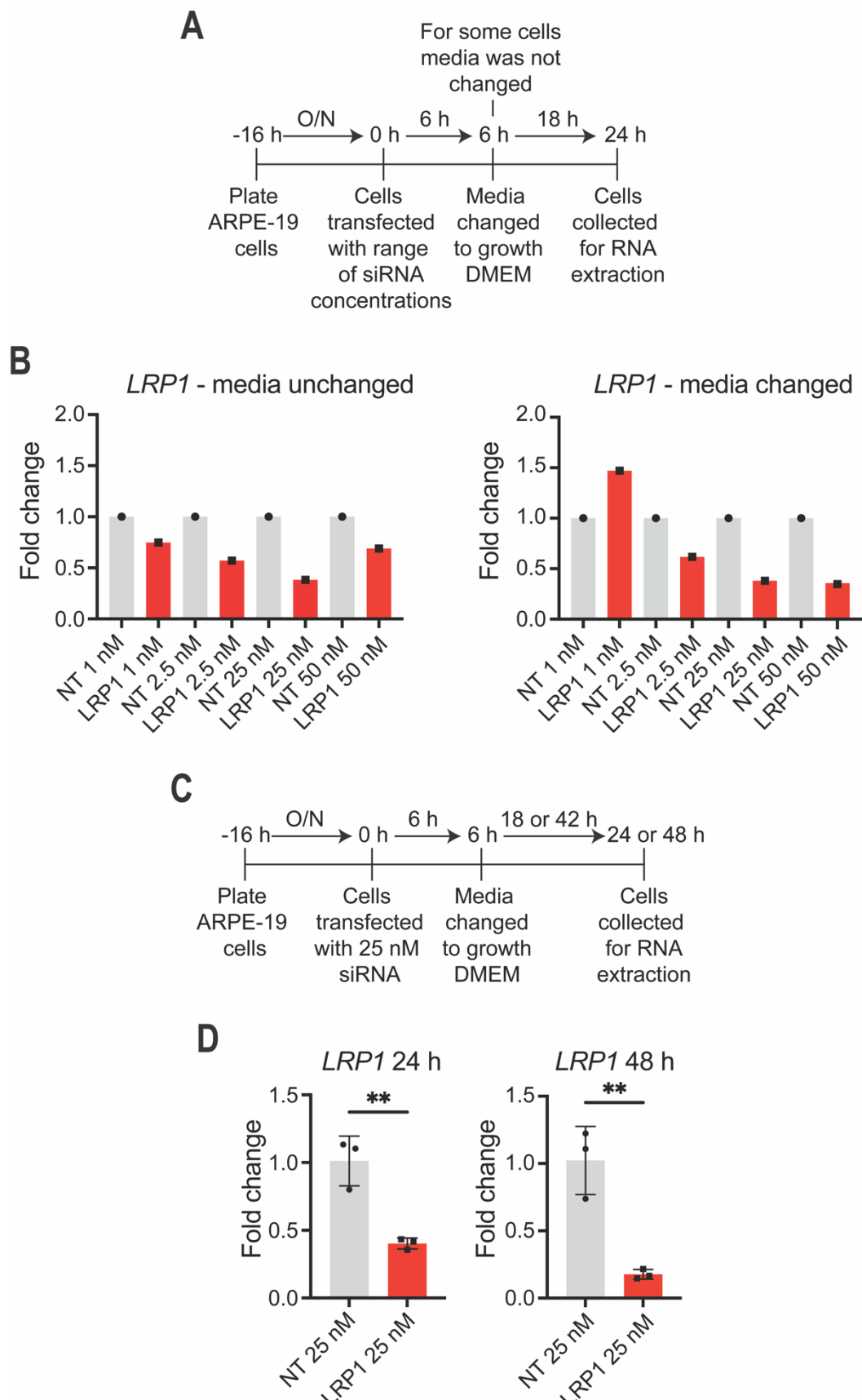


**Figure 6.12: Optimisation of Dharmacon siRNA knockdown of *LRP1* in hTERT RPE-1 cells.**

(A) hTERT RPE-1 cells were plated (250 000 cells per well in a 12-well plate) in growth DMEM overnight and washed 3 times in SF DMEM (2.5 ml) the following morning. Media were changed to Opti-MEM (1 ml) and cells were transfected with the concentrations of siRNA indicated in (B) (n = 1 per concentration) using Lipofectamine LTX following the manufacturer's instructions. Cells were incubated for 24 h in Opti-MEM, or media changed to growth DMEM after 6 h for a further 18 h. RNA

was extracted and cDNA synthesised. **(B)** mRNA expression of *LRP1* was measured by RT-qPCR. Using the  $\Delta\Delta CT$  method, data were normalised against the housekeeper gene *GAPDH*, and expressed relative to non-targeting siRNA controls at each concentration. **(C)** ARPE-19 cells were transfected as in **(A)** with 25 nM non-targeting or *LRP1*-targeting siRNA, with media changed to growth DMEM 6 h after transfection and left for a further 18 h. Cells were washed 3 times in SF DMEM (2.5 ml) and incubated in 2 ml SF DMEM for 24 or 48 h before analysis of *LRP1* mRNA expression. **(D)** *LRP1* expression was quantified as in **(B)**. Data were assessed for normality using the Shapiro-Wilks test, and analysed for significance with an unpaired t-test ( $n = 3$ , mean  $\pm$  SD, \*\*  $p \geq 0.001$ ).

To analyse the effect of *LRP1* knockdown on TIMP-3 endocytosis, experiments were performed using 25 nM *LRP1*-targeting or control siRNA to transfect hTERT RPE-1 cells, as optimised (**Figure 6.12**) and as indicated in **Figure 6.13 A**. An end timepoint of 4 h was selected for the endocytosis assays, as opposed to the 6 h timepoint chosen for ARPE-19 cells, to ensure consistency with the conditions used to analyse effects of RAP in hTERT RPE-1 cells (**Figure 6.7 B**). *LRP1* expression was determined at the beginning (labelled as '0 h') and end ('4 h') of the endocytosis assay by RT-qPCR. This showed that *LRP1* expression was significantly reduced in hTERT RPE-1 cells transfected with *LRP1*-targeting siRNA compared to the non-targeting siRNA control, with ~75 % reduction at both 0 h ( $p = 0.0005$ ) and 4 h ( $p = 0.0056$ ), respectively (**Figure 6.13 B**).

A cell viability assay was conducted (**2.2.10**) at both 0 and 4 h to ascertain whether transfection with either siRNA affected hTERT RPE-1 cell health (**Figure 6.13 C**). A positive control for cell death was included in which cells were repeatedly freeze-thawed between – 80 °C and 25 °C. At 0 h, viability of hTERT RPE-1 cells transfected with the non-targeting siRNA and *LRP1*-targeting siRNA were not significantly different from each other. Absorbance values for cells transfected with non-targeting siRNA were significantly higher than those of the positive death control. There was no significant difference in absorbance values for cells transfected with *LRP1*-targeting siRNA compared to the positive control (**Figure 6.13 C, left-hand side**). At 4 h, the siRNA transfected groups were not significantly different from each other, and both were significantly higher than the positive death control (**Figure 6.13 C, right-hand side**). This indicated that transfection with either siRNA did not cause significant cell death.

An endocytosis assay using isolated recombinant WT TIMP (2.5 nM) was performed in hTERT RPE-1 cells after *LRP1* knock down (**Figure 6.13 D**). At 4 h, WT TIMP-3 levels in conditioned media of hTERT RPE-1 cells transfected with control siRNA decreased to ~25 % of initial levels. WT TIMP-3 abundance in cells transfected with

*LRP1*-targeting siRNA decreased similarly, with no significant difference ( $p = 0.9895$ ,

**Figure 6.13 D).** This demonstrates that knockdown of *LRP1* in hTERT RPE-1 cells did not reduce WT TIMP-3 uptake.

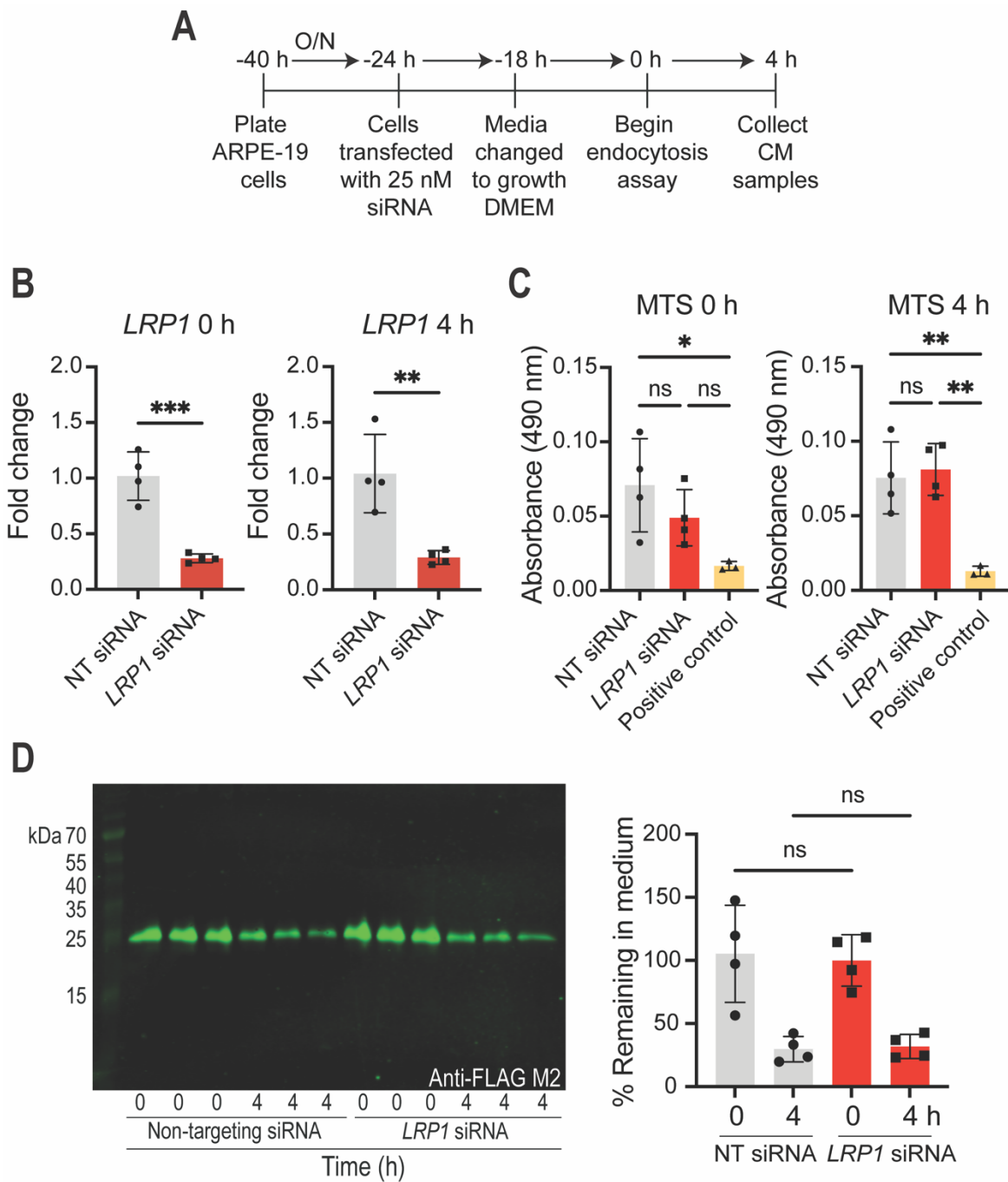


**Figure 6.13: Expression of *LRP1* in hTERT RPE-1 cells was reduced by Dharmaca siRNA knockdown, but this had no effect on TIMP-3 endocytosis.**

**(A)** hTERT RPE-1 cells were plated (250 000 per well in a 12-well plate) overnight in growth DMEM (2 ml) and washed 3 times in SF DMEM (2.5 ml) the following morning. Media were changed to Opti-MEM (1 ml) and cells were transfected with 25 nM siRNA targeting *LRP1* or a non-targeting control siRNA using Lipofectamine LTX following the manufacturer's instructions. Cells were incubated for 6 h and then media were changed to growth DMEM for a further 18 h before cells were washed 3 times in SF DMEM (2.5 ml). Isolated WT TIMP-3 (2.5 nM in TNC-B) was added to cells in DMEM (2 ml) containing 0.2 % FBS. Conditioned media were collected at 0 and 4 h, TCA precipitated and resuspended in 2x SDS-PAGE sample buffer (50  $\mu$ l). **(B)** RNA was extracted, cDNA synthesised and mRNA expression of *LRP1* measured by RT-qPCR. Using the  $\Delta\Delta CT$  method, data were normalised against the housekeeper gene *GAPDH* and expressed relative to non-targeted siRNA controls at 0 and 4 h. *LRP1* expression (mean  $\pm$  SD,  $n = 4$ ) was compared, with data assessed for normality using Shapiro-Wilks test and analysed for significance with an unpaired t-test (\*\*  $p \geq 0.001$ , \*\*\*  $p \leq 0.001$ ).

**(C)** After conditioned media were removed, hTERT RPE-1 cells were collected in cell dissociation solution, centrifuged (400 RCF, 5 min), and resuspended in SF DMEM (2 ml). Cells were then incubated with MTS reagent for 90 min (37 °C, 5 % (v/v) CO<sub>2</sub>) and absorbance at 490 nm, quantified using a SPECTROstar Omega plate reader. Data are presented as mean ± SD (n = 6), with normality assessed with Shapiro-Wilks test, analysed for significance relative to the positive death control with one-way ANOVA and corrected for multiple comparisons with Tukey's multiple comparisons test (ns = not significant, \* p ≤ 0.05, \*\* p ≥ 0.001) **(D)** Resuspended samples (15 µl) were analysed by immunoblotting using an anti-FLAG M2 antibody, followed by detection with a fluorescent anti-mouse IgG secondary antibody. Bands were imaged using LI-COR Odyssey CLx, quantified in Image Studio software and normalised to total protein stain in each lane (not shown). Normalised band intensity was expressed as a percentage of band intensity at time = 0 within siRNA treatment groups and plotted as % remaining in the medium. The amount of TIMP-3 (mean ± SD, n = 4) remaining in the medium at 0 and 4 h was compared, with data assessed for normality with Shapiro-Wilks test, analysed for significance with one-way ANOVA, and corrected for multiple comparisons with Sidak's multiple comparisons test (ns = not significant).

### 6.2.5 mRNA expression of LRP-related receptors in ARPE-19 and hTERT RPE-1 cells

Previous data showed that uptake of WT, H181R, Y191C and S204C in ARPE-19 and hTERT RPE-1 cells was blocked by RAP (**Figure 6.7 & Figure 6.8**) but that LRP1 plays a minimal role. Therefore, RT-qPCR was used to investigate mRNA expression of LRP-related receptors that can be blocked by RAP in ARPE-19 and hTERT RPE-1 cells (**Figure 6.14**). Both ARPE-19 and hTERT RPE-1 cells expressed a range of LRP receptors, including *LRP1*, *LRP1b*, *LRP2*, *LRP3* (although not detectable in ARPE-19 cells), *LRP4*, *LRP5*, *LRP6*, *LRP8*, *LRP10*, *LRP11* and *LRP12*. Both cells also expressed lipid transporting LDL receptors such as, *LDLR*, *vLDLR*, as well as other LRP-related receptors that can be blocked by RAP (Jacobsen et al., 1996; Ranganathan et al., 2011), including *LDLRAD1*, *LDLRAD2*, *LDLRAD3* and *SORL1*. CT values were normalised against the housekeeper gene *GAPDH*, and this demonstrated high expression (all within 10 cycles of *GAPDH*) of *LRP1*, *LRP4*, *LRP5*, *LRP6*, *LRP8*, *LRP10*, *LRP11*, *LRP12*, *LDLR*, *vLDLR* and *LDLRAD3* in both cell lines. *LRP1b*, *LRP2* and *LDLRAD1* were expressed to a reasonable degree (~10 cycles later after *GAPDH*) whereas *LDLRAD2* and *SORL1* came up considerably later (~ 15 cycles after *GAPDH*).

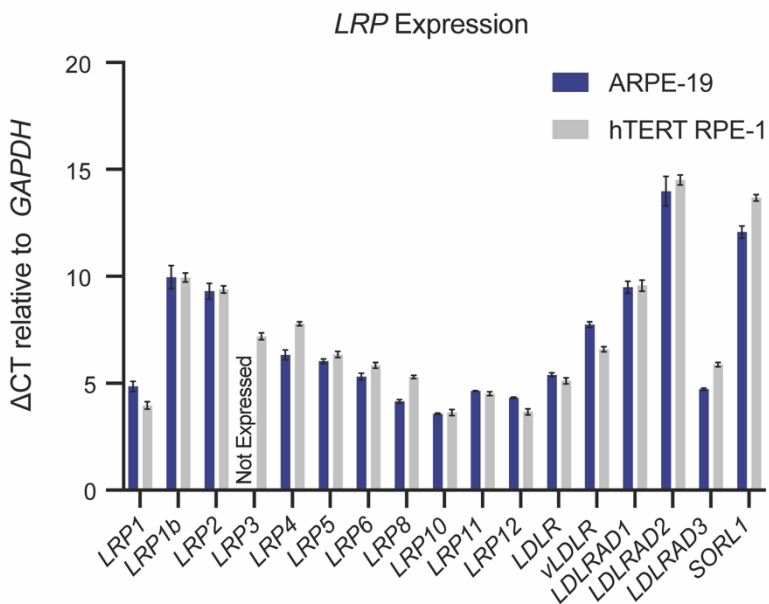


**Figure 6.14: ARPE-19 and hTERT RPE-1 cells expressed a range of LRP-related receptors at the mRNA level.**

ARPE-19 and hTERT RPE-1 cells were plated (500 000 cells per well in a 6-well plate) and incubated overnight in growth DMEM (2 ml). RNA was extracted, cDNA synthesised and mRNA expression of LRP-related receptors measured by RT-qPCR. Data were normalised against the housekeeper gene GAPDH, using the  $\Delta\text{CT}$  method (mean  $\pm$  SD, n = 3).

### 6.3 Discussion

LRP1 has previously been shown to mediate the endocytosis of WT TIMP-3 in various cell types including mouse embryonic fibroblasts, HTB94 chondrosarcoma cells and primary human macrophages (Doherty et al., 2016; Schubert et al., 2019; Scilabria et al., 2013). Thus, the aim of the work presented in this Chapter was to determine whether LRP1 is also responsible for mediating the endocytosis of WT TIMP-3, as well as the SFD mutants H181R, Y191C and S204C TIMP-3, in RPE cells. To this end, initial experiments used LRP1-null PEA-13 cells and WT MEF cells to investigate whether H181R, Y191C and S204C TIMP-3 can interact with LRP1 in the same manner as WT TIMP-3. Further experiments were performed in which RAP was pre-incubated with ARPE-19 and hTERT RPE-1 cells and uptake of WT, H181R, Y191C and S204C TIMP-3 monitored to determine if their uptake in RPE cells was dependent on the LRP family of receptors, which are all antagonised by this protein. Finally, siRNA knockdown of *LRP1* in ARPE-19 and hTERT RPE-1 cells was used to investigate the role of LRP1 in WT TIMP-3 uptake in RPE cells.

Previously published data using PEA-13 cells, an LRP1-null cell line (Willnow & Herz, 1994), have demonstrated that WT TIMP-3 endocytosis is mediated primarily

by LRP1 (Scilabra et al., 2013). Therefore, initial experiments were conducted to analyse whether H181R, Y191C and S204C interact with LRP1 in the same manner as WT TIMP-3, using PEA-13 cells in conjunction with WT MEF cells (**Figure 6.1**, **Figure 6.2 & Figure 6.3**). Endocytosis of WT TIMP-3 was significantly decreased in PEA-13 cells compared to WT MEFs (**Figure 6.1**) which is consistent with what has previously been observed for WT TIMP-3 (Scilabra et al., 2013). These results demonstrate that a large proportion of TIMP-3 endocytosis is mediated by LRP1 in this cell type. However, as observed by Scilabra et al. (2013) there was still some residual TIMP-3 endocytosis in PEA-13 cells, indicating that an LRP1-independent pathway also accounts for a small proportion of TIMP-3 uptake (**Figure 6.1 B**).

For H181R and Y191C TIMP-3, there was no significant difference in levels of these mutants remaining in the media of LRP1-null PEA-13 cells compared to MEF cells, indicating that LRP1 did not contribute significantly to their endocytosis. However, mean amounts of H181R and Y191C TIMP-3 were numerically slightly higher in media of PEA-13 cells than MEF cells (**Figure 6.2 & Figure 6.3 A**), indicating that a small proportion of their endocytosis may be mediated by LRP1. A higher sample size would help clarify whether this contribution of significant or not. It is possible that the H181R and Y191C mutations impair binding to LRP1, so that their endocytosis is primarily mediated in an LRP1-independent manner. Alternatively, these proteins may have a much-increased affinity for an alternative LRP receptor(s) and so do not rely on LRP1 to mediate their uptake.

Significantly less S204C TIMP-3 was taken up by PEA-13 cells, indicating this mutant is able to interact with and be endocytosed by LRP1. However, the numerical difference in means (**Figure 6.3 B**) was fairly small and not as large as that observed for WT TIMP-3 (**Figure 6.1 B**). Like H181R and Y191C, these data suggest that S204C TIMP-3 is able to interact with and be endocytosed by LRP1 to some extent, but that LRP1-independent routes accounts for most of the uptake.

It is highly likely that PEA-13 cells also express other LRPs, given that they are only genetically deficient in LRP1 (Willnow & Herz, 1994), therefore the LRP1-independent uptake observed for WT, H181R, Y191C and S204C TIMP-3 by PEA-13 cells could be mediated by other LRPs. For instance, TIMP-2 can be endocytosed by LRP1 either in complex with proMMP-2 or as a free inhibitor (Emonard et al., 2004), and more recently has been shown to be endocytosed by

LRP2 as a complex with proMMP2 (Johanns et al., 2017). Thus, it seems plausible to suggest that LRP2 could be responsible for mediating the LRP1-independent endocytosis observed. This could be clarified by using an LRP2 ELISA, siRNA knockdown of LRP2 or even a CRISPR Cas-9 knockout of LRP2.

Whilst data from the MEF and PEA-13 cells indicates that H181R and Y191C (and to a lesser extent S204C) have reduced affinity for LRP1, performing an LRP1 ELISA would be a useful method to confirm differences in interaction of these proteins with LRP1. LRP1 is a huge protein (>500 kDa) that is difficult to express recombinantly, and previously available commercial suppliers no longer sell the isolated protein. WT TIMP-3 is known to bind to ligand-binding cluster II of LRP1 (Scilabria et al., 2017), so an ELISA could be devised in which recombinant ligand-binding cluster II of LRP1 was immobilised on a plate and binding of WT and the 3 SFD mutants could be investigated. Even low affinity for LRP1 may be biologically important, because shed LRP1 has been shown to bind and prevent the endocytosis of WT TIMP-3 (Scilabria et al., 2013). So perhaps the reservoir of LRP1 in the choroid and inner retina (**Figure 6.5 A & B** (Barcelona et al., 2010; Sánchez et al., 2006)) could, once shed, bind to SFD TIMP-3 variants in the Bruch's membrane and prevent their endocytosis, leading to their accumulation.

LRP1 is reportedly expressed by primary human RPE cells (Hollborn et al., 2004b) and RT-qPCR confirmed that *LRP1* was highly expressed at the mRNA level in both ARPE-19 and hTERT RPE-1 cells (**Figure 6.4**). Immunoblotting was also used to confirm LRP1 protein expression in conditioned media from ARPE-19 cells using the anti-LRP1 8G1 antibody (**Figure 6.4**). LRP1 exists as a 515 kDa alpha and an 85 kDa beta chain, with cleavage of the beta chain result in shedding of the ectodomain from the cell membrane into conditioned media by a variety of cells (Brifault et al., 2017; Gorovoy et al., 2010; Lillis et al., 2008; Liu et al., 2009; Panezai et al., 2017; Scilabria et al., 2013; Yamamoto et al., 2018). The 8G1 antibody used recognises an epitope in the alpha chain of LRP1, so a band of 515 kDa was expected. However, considerable degradation of the LRP1 alpha chain has been observed by others, with bands of much lower molecular weight visible with the 8G1 antibody (Scilabria et al., 2013). This is thought to be mediated by proteases secreted by the cells. In conditioned media of ARPE-19 cells, bands were observed between 70-100 kDa, at ~100 kDa and between 130-180 kDa after 6 h of culture (**Figure 6.4, left-hand side**). The intensity of these bands increased at 24 h,

indicating a time-dependent increase in LRP1 shedding in ARPE-19 cells, as has also been observed in HTB94 cells (Scilabre et al., 2013). Additional bands were visible at 24 h, including discrete bands at ~35 and ~40 kDa and ~130 kDa. A smear was also present above 180 kDa. The strong staining above 180 kDa ran towards the top of the 4-15 % polyacrylamide gel indicating a very high molecular weight, which may correspond to the full-length alpha chain, with the bands at lower molecular weights (e.g., ~130 kDa, ~100 kDa, 70-100 kDa and 35-40 kDa) likely being proteolytic breakdown products of the LRP1 alpha chain (**Figure 6.4, left-hand side**). These largely correspond to bands previously observed in conditioned media from HTB94 cells (Scilabre et al., 2013), but the bands at ~35 and ~40 kDa have not been reported previously and may reflect cell-specific processing of LRP1 in ARPE-19 cells. Exploring the expression of transmembrane LRP1 at the cellular level using the 5A6 antibody would have also been beneficial in conjunction with the detection of the shed 515 kDa alpha chain in the conditioned media (**Figure 6.4**).

RNAScope analysis was performed on primary from two donors with no reported retinal pathology to ascertain the levels of *LRP1* expression in retinal layers. To my knowledge, this is the first report of *LRP1* mRNA expression in retinal layers using this approach. RNAScope analysis revealed expression of *LRP1* throughout layers of the retina, including the ganglion cell layer, the inner nuclear layer and particularly high abundance in the choroid and sclera (**Figure 6.5**). LRP1 is known to be expressed at the protein level by Müller glial cells (Sánchez et al., 2006) and due to the radial extension of Müller glial cells throughout the retina from the inner limiting membrane to the outer limiting membrane (separating the internal and external parts of photoreceptors) (Kobat & Turgut, 2020), it is plausible that Müller glial cells may be responsible for the *LRP1* expression observed in the inner nuclear layer and ganglion cell layer (**Figure 6.5 B**). Further studies support abundant LRP1 protein expression throughout the inner retina, including the ganglion cell layer, the inner and outer nuclear layers, as well as the RPE and choroidal layer (Barcelona et al., 2010). These authors also reported abluminal expression of LRP1 and suggested that vascular smooth muscle cells and astrocytes are likely to express LRP1 in vascular areas of the retina, rather than the endothelial cells (Barcelona et al., 2010). This supports what was observed in the RNA Scope experiments in the current study, with *LRP1* expression localised to blood vessels in the choroid and sclera appearing to be abluminal (**Figure 6.5 A & B**). Barcelona and colleagues report that LRP1 expression in retinas from diabetic and sickle cell donors was higher than in

control, suggesting that comorbidities could increase LRP1 expression in the retina further. Outside of the retina, LRP1 is also highly expressed in the cornea (Mogensen et al., 2022), and in many other cell types of the body.

Unfortunately, expression of *LRP1* in RPE cells was difficult to determine from the RNAScope analysis, due to endogenous production of the brown pigment melanin by RPE cells (Tian et al., 2021). However, LRP1 has been shown to be expressed at the protein level by RPE cells in multiple studies (Barcelona et al., 2010; Hollborn et al., 2004b).

RNAScope analysis was also used to visualise *TIMP3* expression in the retina, again to my knowledge the first time such an approach has been used to profile *TIMP3* mRNA expression in the retina (**Figure 6.5 C**). This revealed expression throughout the sclera and also the choroid. Additionally, *TIMP3* expression was observed in the BrM. TIMP-3 protein is known to be a constitutive component in the BrM (Fariss et al., 1997), that increases with age (Kamei & Hollyfield, 1999), however the mRNA expression of *TIMP3* has been shown not to change with age (Bailey et al., 2001).

Data presented in this Chapter in conjunction with previously published data demonstrated that LRP1 is expressed by RPE cells. Next it was important to determine whether LRP1 functions as the endocytic receptor for WT, H181R, Y191C and S204C TIMP-3 in RPE cells. A summary of the experiments performed are presented in **Table 6.1**. To this end, initial experiments were performed in ARPE-19 cells or hTERT RPE-1 cells were preincubated with RAP before endocytosis assays were performed (**Figure 6.6**, **Figure 6.7** & **Figure 6.8**). RAP normally functions as a molecular chaperone that binds to LDL receptor family members with high affinity inside cells and facilitates their transport between the endoplasmic reticulum and Golgi apparatus (Lee et al., 2007) and their delivery to the cell surface (D. Lee et al., 2007). As a result of its high affinity for LRP receptors, RAP competitively inhibits the interaction of LRPs with their ligands, so recombinant RAP can be used experimentally as an antagonist of ligand binding to LDL receptors (Troeberg et al., 2008). It should be noted that RAP is not selective for LRP1, but rather can be used to diagnose involvement of the broader LRP family in an endocytic process. For example, addition of RAP to the conditioned media of HTB94 cells resulted in the accumulation of TIMP-3 in the conditioned media (Doherty et al., 2016; Scilabria et

al., 2013; Troeberg et al., 2008), indicating that LRP<sub>s</sub> are responsible for mediating TIMP-3 uptake in these cells. Similarly, preincubation of ARPE-19 cells with RAP resulted in accumulation of endogenously-expressed WT TIMP-3 in the conditioned media (**Figure 6.6**) and RAP also significantly impaired uptake of exogenously-added WT TIMP-3 (**Figure 6.7**), indicating a member of the LRP family is responsible for TIMP-3 uptake in these cells. A similar result was observed in hTERT RPE-1 cells (**Figure 6.7**).

Preincubation with RAP also significantly reduced the uptake of the 3 SFD TIMP-3 mutants, H181R, Y191C and S204C in ARPE-19 cells (**Figure 6.8**), indicating that their uptake by RPE cells is also LRP-dependent. High molecular weight species migrating above the highest molecular weight marker were observed in immunoblots for WT, H181R, Y191C and S204C TIMP-3 (**Figure 6.8**), with particularly high abundance in Y191C and S204C TIMP-3 immunoblots (**Figure 6.8 C & D**). This is consistent with observations in **Chapter 3**, with Y191C and S204C TIMP-3 tending to form more of these higher molecular weight species. For Y191C TIMP-3, these higher molecular weight species remained constant over the time-course and were more abundant in those cells treated with RAP. Perhaps treatment with RAP favours formation of multimers by increasing the concentration of monomers in the media, shifting the monomer/multimer equilibrium.

It is also noteworthy that some endocytosis still occurred despite the presence of RAP. This was particularly evident for WT and H181R TIMP-3, with ~20 % of these proteins still taken up by 6 h in RAP-treated cells (**Figure 6.8 A & B**). This was also noticeable for some individual replicates of Y191C and S204C TIMP-3 (**Figure 6.8 C & D**). These observations indicate that WT, H181R, Y191C and S204C can also be internalised by RPE cells in an LRP-independent (i.e. RAP-insensitive) manner, and indeed LRP-independent mechanisms of TIMP-3 endocytosis have been observed in other cell types (Doherty et al., 2016; Scilabria et al., 2013). HSPGs are capable of binding and internalising LDL/LRP ligands including ApoE (Mahley & Huang, 2007) and have been implicated in endocytic processes in RPE cells (Storm et al., 2020). Thus, one could speculate that HSPGs may be responsible for this LRP-independent uptake of WT TIMP-3 and the 3 SFD mutants. However, data from CHO-K1 (WT cells) and CHO-745 cells [which lack HS and CS chains because of a mutation in xylotransferase (Esko et al., 1985)] indicates that HSPGs and CSPGs are not involved in TIMP-3 internalisation (Scilabria et al., 2013), although this effect

could be cell-dependent. Interestingly, the addition of sodium chlorate to the conditioned media of various cell types, including RPE cells in this study (**Figure 4.2, Figure 4.3 & Figure 4.4**) results in TIMP-3 accumulation in the conditioned media. Sodium chlorate is known to inhibit overall O-sulfation of HS, including 2-O- and 6-O-sulfation (Safaiyan et al., 1999), which would reduce TIMP-3 binding to HS chains. Perhaps HSPGs act as a co-receptor for TIMP-3 endocytosis in RPE cells, as has been suggested for other ligands (Storm et al., 2020), and that by reducing HS sulfation this prevents TIMP-3 endocytosis.

Alternatively, receptors belonging to the macrophage mannose receptor family may be possible candidates, including urokinase plasminogen activator receptor-associated protein, which is expressed by RPE cells (Elner, 2002) and is known to participate in the endocytosis of LRP1 ligands such as collagen (Engelholm et al., 2003; Kjøller et al., 2004). RPE cells are also known to express other scavenger receptors such as stabilin-1 and stabilin-2, as well as scavenger receptors BI and BII, although these receptors are implicated in RPE endocytosis of photoreceptor outer segments and lipids and not protein uptake (Duncan et al., 2002; Li et al., 2007). Approaches such as crosslinking and affinity chromatography or using a proximity labelling domain could be used to investigate receptors involved in TIMP-3 internalisation by RPE cells. For example, a biotin-based proximity labelling technique such as APEX could be employed to identify binding interactions of TIMP-3 to receptors within 20 nm (Trinkle-Mulcahy, 2019), however validation experiments such as an ELISA should be performed to confirm such interactions.

Given that LRP1 is known to mediate endocytosis of WT TIMP-3 in various cell types (Doherty et al., 2016; Schubert et al., 2019; Scilabria et al., 2013), it is plausible to hypothesise that LRP1 is responsible for the endocytosis of WT TIMP-3 in RPE cells and that SFD mutations may impair the ability of TIMP-3 to bind to and be endocytosed by LRP1. Mutagenesis studies revealed that pairs of lysine residues ~ 21 angstroms apart (e.g., K26A/K45A or K42A/K110A) on a highly basic region of TIMP-3 are responsible for its binding to LRP1, and that non-naturally occurring mutations in TIMP-3 impair its ability to bind to LRP1 and be endocytosed (C. M. Doherty et al., 2016). H181R and Y191C mutations are located near to the basic region of TIMP-3. The H181R mutation introduces an additional basic residue, so this could further drive H181R binding to LRP1, which could account for the slightly increased endocytic rate observed (**Figure 5.5 & Figure 5.9**). The additional

cysteine residue introduced by the Y191C mutation could disrupt the basic patch of TIMP-3 by affecting the native 6 intramolecular disulfide bonds in TIMP-3 (Brew & Nagase, 2010), thereby altering the three-dimensional structure of TIMP-3 and so decreasing its binding to LRP1 and hence its rate of endocytosis (**Figure 5.5 & Figure 5.9**). It is difficult to predict the impact of the S204C mutation as it occurs towards the end of the C-terminus, which is unresolved in the crystal structure (Doherty et al., 2016; Wisniewska et al., 2008), but again it is possible that the S204C mutation could affect the native 6 intramolecular disulfide bonds in TIMP-3, disrupting the basic patch and resulting in decreased binding to and endocytosis via LRP1. Attempts to predict changes in TIMP-3 protein structure as a result of H181R, Y191C or S204C mutations were performed using AlphaFold (data not shown). This analysis revealed that there were not considerable changes in TIMP-3 protein structure, suggesting that the basic patch of TIMP-3 is not likely to be substantially affected by these 3 SFD mutations.

A series of siRNA knockdown experiments were performed (**Figure 6.9, Figure 6.10, Figure 6.11, Figure 6.12 & Figure 6.13**) to investigate whether LRP1 is responsible for mediating the uptake of WT TIMP-3 in RPE cells, as has been shown in HTB94 cells (Doherty et al., 2016; Scilabria et al., 2013) and primary macrophages (Schubert et al., 2019). Knockdown of *LRP1* was measured at the mRNA level in this study, however it would have been useful to confirm this at the protein level by using the 5A6 antibody to measure transmembrane LRP1 levels. Initial attempts using an siRNA sequence purchased from ThermoFisher, achieved between 30-40 % *LRP1* knockdown in ARPE-19 cells (**Figure 6.9 B**) and had no significant effect on endocytosis of WT TIMP-3 (**Figure 6.9 D**). However the knockdown achieved was relatively poor, so optimisation experiments in both ARPE-19 and hTERT RPE-1 cells were performed with an siRNA sequence purchased from Dharmacon (**Figure 6.10 & Figure 6.12**), which has been shown to achieve ~90 % knockdown in human chondrocytes (Yamamoto et al., 2013). The greatest *LRP1* knockdown was observed when ARPE-19 cells and hTERT RPE-1 cells were transfected with 25 nM of this siRNA and media changed to growth DMEM 6 h post-transfection (**Figure 6.10 & Figure 6.12**), so these conditions were used in subsequent experiments. However, in repeat experiments on ARPE-19 cells, the degree of knockdown achieved reduced to 40-50 % (**Figure 6.11 B**). The reason for this change was not obvious but there was a degree of variation around knockdown achieved in optimisation and final experiments and it may also indicate that overall

cell health between experiments was changed, possibly due to prolonged culture. ARPE-19 cells were somewhat difficult to transfect, as two siRNA sequences achieved relatively poor knockdown, although the transfection efficiency was not measured. This degree of knockdown led to a significant reduction in endocytosis of WT TIMP-3 in ARPE-19 cells, but the effect size was small and so the biological significance of this is questionable (**Figure 6.11 D**). Furthermore, uptake of WT TIMP-3 in ARPE-19 cells transfected with control siRNA was only 50 % (**Figure 6.11 D**), which is considerably less than the previously observed uptake for WT TIMP-3 by ARPE-19 cells at this timepoint previously (**Figure 5.3 & Figure 5.5**). Perhaps ARPE-19 cells were 'stressed' due to transfection, which impaired their uptake of WT TIMP-3, although MTS assays indicated that cell viability was not affected by transfection (**Figure 6.11 C**).

Given the poor knockdown achieved in ARPE-19 cells and the drop in WT TIMP-3 uptake with transfection (**Figure 6.11 D**), the effect of *LRP1* knockdown on WT TIMP-3 uptake was also investigated using hTERT RPE-1 cells (**Figure 6.13**). The knockdown of *LRP1* achieved in hTERT RPE-1 cells was far greater than in ARPE-19 cells with 70-80 % knockdown achieved (**Figure 6.13 B**). This indicates that hTERT RPE-1 cells have higher transfectability than ARPE-19 cells. Uptake of WT TIMP-3 by hTERT RPE-1 cells transfected with *LRP1*-targeting siRNA was almost identical to that in control siRNA-transfected cells, at ~75 % uptake (**Figure 6.13 D**). This demonstrated that in hTERT RPE-1 cells, *LRP1* is not responsible for mediating the uptake of WT TIMP-3 and when taken in conjunction with the RAP data (**Figure 6.7 B**), this suggests that the uptake of WT TIMP-3 is majorly mediated by another member of the LRP family in this cell type.

Collectively, the findings in this Chapter indicate that WT TIMP-3 is taken up by RPE cells primarily by an LRP other than LRP1 (i.e. an LRP-dependent but LRP1-independent process **Figure 6.7, Figure 6.11 & Figure 6.13**). While, WT TIMP-3 is capable of interacting with LRP1 (**Figure 6.1**), this receptor does not seem to play the major role in its endocytosis by RPE cells. Given that LRP1 is expressed at a reasonable level (based on mRNA analysis), it is unclear why RPE differ from chondrocytes and macrophages in this regard. It would be useful to investigate LRP1 protein expression and shedding to confirm functionality of the receptor in RPE. The data indicate that H181R, Y191C and S204C TIMP-3 are also taken up by RPE cells in an LRP-dependent process (**Figure 6.8 B, C & D**), and whilst

endocytosis assays for these SFD mutants were not performed with *LRP1* knockdown, data from the MEF and PEA-13 cell experiments suggest that these proteins interact less with *LRP1* (**Figure 6.2 & Figure 6.3**), than WT TIMP-3 does (**Figure 6.1**), so it is likely that their endocytosis in RPE is also largely independent of *LRP1*.

**Table 6.1: Summary of LRP-dependence of WT, H181R, Y191C and S204C TIMP-3 endocytosis in MEF and RPE cells.**

TIMP-3	MEF/PEA-13	RAP Sensitivity	siRNA Knockdown of <i>LRP1</i>	Conclusion
<b>WT</b>	Uptake significantly different between MEF (WT) and PEA-13 (LRP1 null) cells ( <b>Figure 6.1</b> ).	Uptake was highly RAP sensitive in ARPE-19 and hTERT RPE-1 cells ( <b>Figure 6.7</b> ).	Uptake significantly decreased by <i>LRP1</i> siRNA in ARPE-19 cells ( <b>Figure 6.11</b> ).  Uptake not significantly changed by <i>LRP1</i> siRNA in hTERT RPE-1 cells ( <b>Figure 6.13</b> ).	1. LRP1 can mediate uptake (e.g., in MEF cells). 2. In RPE cells, uptake is largely LRP-dependent but distinct from LRP1. LRP1 may mediate a small degree of endocytosis.
<b>H181R</b>	Uptake not significantly different between MEF (WT) and PEA-13 (LRP1 null) cells, but small numerical difference in means ( <b>Figure 6.2</b> ).	Uptake was highly RAP sensitive in ARPE-19 cells ( <b>Figure 6.8</b> ).	Not performed.	Uptake in RPE cells is LRP-dependent, but likely to be distinct from LRP1.
<b>Y191C</b>	Uptake not significantly different between MEF (WT) and PEA-13 (LRP1 null) cells, but small numerical difference in means ( <b>Figure 6.3</b> ).	Uptake was completely RAP sensitive in ARPE-19 cells ( <b>Figure 6.8</b> ).	Not performed.	Uptake in RPE cells is LRP-dependent, but likely to be distinct from LRP1.
<b>S204C</b>	Uptake significantly different between MEF (WT) and PEA-13 (LRP1 null) cells ( <b>Figure 6.3</b> ).	Uptake was completely RAP sensitive in ARPE-19 cells ( <b>Figure 6.8</b> ).	Not performed.	Uptake in RPE cells is LRP-dependent, and likely to involve both LRP1-independent (major) and -dependent (minor) routes.

These observations all point to other members of the LRP family being responsible for the bulk of endocytosis of WT, H181R, Y191C and S204C TIMP-3 in RPE cells. Therefore, mRNA expression of LRPs and other RAP-sensitive receptors in ARPE-19 and hTERT RPE-1 cells was measured by RT-qPCR (**Figure 6.14**) to identify possible candidates. Whilst LDLR and vLDLR are classical endocytic receptors (Goldstein & Brown, 1974; Takahashi et al., 1992) and are known to be expressed by RPE cells (Gordiyenko et al., 2004; Hayes et al., 1989; Hu et al., 2008; Sreekumar et al., 2023), to my knowledge there is a lack of evidence for their involvement in the endocytosis of proteins including proteases and inhibitors of proteases, thus these may not be plausible candidates. Receptors that are particularly interesting to consider include LRP1b, LRP2 and LDLRAD3, which were all expressed at the mRNA level in RPE cells, with *LDLRAD3* having the highest mRNA expression (**Figure 6.14**). LDLRAD3 has been reported to have endocytic capacity (Ranganathan et al., 2011), whilst LRP1b is known to mediate endocytosis of many of the same ligands as LRP1 (Haas et al., 2011; Liu et al., 2001), albeit more slowly (Knisely et al., 2007). LRP2 is also an interesting candidate, as it is expressed by RPE cells (Storm et al., 2014) and has been shown to endocytose protease and protease-inhibitor complexes, including TIMP-2: proMMP-2 complexes (Johanns et al., 2017).

Despite *LRP5* and *LRP6* being highly expressed at the mRNA level, they have no reported endocytic function and are well documented to be involved in canonical Wnt signalling (Ren et al., 2021), thus it is unlikely that they mediate the LRP-dependent endocytosis observed in this Chapter. Unfortunately, the endocytic capacity of many of these other LRP receptors has been minimally studied, making it difficult to postulate whether they are potentially involved in endocytosis of WT, H181R, Y191C and S204C TIMP-3 by RPE cells. However, LRP1b, LDLRAD3 and particularly LRP2 are interesting candidates that require further investigation. An approach using siRNA targeting *LRP1b*, *LDLRAD3* and *LRP2* could be used to screen each of these receptors in turn, or knockout of the genes encoding for each of these receptors by CRISPR Cas-9 could help to dissect the individual contribution of these receptors. These approaches could be labour intensive so blocking antibodies directed against each receptor could be used. Alternatively, pharmacological blocking agents could be used, for example Cilastatin has been shown to block LRP2 (Hori et al., 2017), although there is a lack of drugs available for other receptors.

## **Chapter 7: Discussion**

## 7.1 Key findings

SFD is known to be caused by mutations in the *TIMP3* gene, and to be associated with extracellular accumulation of mutant TIMP-3 proteins in the BrM (Chong et al., 2000; Fariss et al., 1998). However, molecular mechanism(s) by which SFD TIMP-3 proteins accumulate are unknown and molecular mechanism(s) by which they contribute/result in CNV and geographic atrophy are not fully characterised.

In this thesis, I aimed to determine how SFD TIMP-3 proteins accumulate extracellularly. More specifically, I investigated whether RPE cells endocytose WT TIMP-3 and if this process is LRP1-dependent. I also investigated whether endocytosis of three SFD variants (H181R, Y191C and S204C TIMP-3) differed from that of WT TIMP-3.

Key findings of the work show here are that:

- WT TIMP-3 is endocytosed by ARPE-19 and hTERT RPE-1 cells by an LRP other than LRP1. RPE cells are thus the first reported cell type in which TIMP-3 uptake is not mediated by LRP1.
- Y191C and S204C TIMP-3 are also endocytosed by ARPE-19 and hTERT RPE-1 cells, but their endocytosis is significantly slower than WT TIMP-3, possibly due to reduced affinity for the endocytic LRP receptor. This is likely to be a key mechanism by which they accumulate in the BrM of SFD patients.
- H181R TIMP-3 is endocytosed by ARPE-19 and hTERT RPE-1 cells as fast as WT TIMP-3, indicating that SFD is a heterogenous disease, and that different SFD mutants accumulate via different molecular mechanisms.

Implications and limitations of these findings, as well as future areas for research are discussed in this Chapter.

## 7.2 Molecular mechanisms of SFD TIMP-3 accumulation

### 7.2.1 WT TIMP-3 is taken up by RPE cells

The work presented here shows that ARPE-19 and hTERT RPE-1 cells endocytose monomeric WT TIMP-3 from conditioned media with half-lives of  $2.6 \pm 1.1$  h and  $4.9 \pm 2.4$  h, respectively, similar to the half-life of WT TIMP-3 endocytosis by chondrocytes (Doherty et al., 2016). A half-life for WT TIMP-3 uptake by RPE cells has previously been calculated by Langton et al. (2005) as 9.5 h, but these authors

monitored the disappearance of WT TIMP-3 from the ECM of transfected RPE cells, where competition with ECM binding is likely to be a significant contributing factor. Additionally, Langton et al. (2005) examined the uptake of dimers and multimers, whereas this thesis focused on uptake of monomers.

### **7.2.2 Endocytosis of Y191C and S204C TIMP-3 by RPE cells is significantly delayed**

Endocytosis of monomeric forms of the SFD TIMP-3 proteins Y191C and S204C by ARPE-19 and hTERT RPE-1 cells was significantly impaired (**Figure 5.5 & Figure 5.9**), to the extent that half-lives were not calculated (**Chapter 5**). This is likely to be a key molecular mechanism by which these mutants accumulate in the BrM of SFD patients. These findings build on observations made by Langton et al. (2005), who showed that dimers of S204C (along with S179C and E162X) have ‘resistance to turnover’, and suggest that for some SFD mutations, endocytosis of monomeric, dimeric and multimeric species by RPE cells is impaired. A highly basic region of TIMP-3 is responsible for TIMP-3 binding to LRP1 and it may be that this basic region is also critical for the binding of TIMP-3 to other LRP receptors. It is possible that this basic region is obscured by dimerisation/multimerisation of SFD TIMP-3 mutants, hence impairing cellular uptake by reducing binding to the endocytic receptor. In the case of monomeric species of SFD TIMP-3 mutants (e.g., Y191C and S204C), it is possible that the additional cysteine residue could affect the native 6 intramolecular disulfide bonds (Brew & Nagase, 2010) and so disrupt the basic patch, resulting in impaired endocytosis. Determining the crystal structure of Y191C and S204C TIMP-3 would be extremely useful to determine how intramolecular disulfide bonds may be altered and whether the structure of TIMP-3 is appreciably changed by these mutations. However, large quantities of protein are required for X-ray crystallography, and this is not achievable by the method of protein expression and isolation used in this study. Alternatively, mass spectrometry approaches could be utilised to determine intramolecular disulfide bond patterns in Y191C and S204C TIMP-3, as has been employed for other proteins (Xu et al., 2008).

### **7.2.3 Endocytosis of H181R TIMP-3 by RPE cells is unimpaired**

In contrast, endocytosis of the monomeric form of the H181R TIMP-3 variant by ARPE-19 and hTERT RPE-1 cells was unaffected, with uptake as fast or slightly quicker than WT TIMP-3 (**Figure 5.5 & Figure 5.9**). The additional basic residue introduced by the H181R mutation could promote TIMP-3 binding to LRP receptors,

since basic residues of the ligand have been shown to interact with acidic pockets on LRPs (Doherty et al., 2016; Fisher et al., 2006).

Basic residues also promote binding to GAGs, which are known to sequester TIMP-3 in the ECM and competitively inhibit TIMP-3 endocytosis via LRP1 (Lee et al., 2007; Troeberg et al., 2014; Yu et al., 2000). Thus, some preliminary studies were conducted to investigate potential differences in binding of WT and H181R TIMP-3 to heparin, a highly sulfated form of HS, to determine whether increased ECM binding of H181R could lead to its accumulation. There was no discernible difference in elution of WT and H181R TIMP-3 at all concentrations of NaCl used (**Figure 5.13**), but this methodology was extremely variable. Priority for future work would be to explore this question further using a more quantitative surface plasmon resonance approach (e.g., Carterra LSA platform), which would also allow us to profile binding of WT and SFD TIMP-3 to different HS and other GAG structures and sulfation patterns. This would provide quantitative data in the form of  $K_D$  values which we could compare with published  $K_D$  values for WT TIMP-3 (Troeberg et al., 2014). Another important area worth investigating is whether patients with SFD or other macular diseases such as AMD carry mutations in HS synthesising/modification enzymes. For example, an increase in the quantity and sulfation of HS may contribute to accumulation of TIMP-3 and other ligands in the BrM in these retinal diseases.

Analysis of the H181R mutation led to the critical conclusion that not all SFD TIMP-3 mutants accumulate by the same molecular mechanism. Furthermore, this also suggested that there may be an inverse correlation between the rate of endocytosis and the age of symptom onset, as patients carrying the H181R mutation present with visual disturbance later than those carrying the Y191C and S204C mutations. To establish this correlation, it would be useful to profile rates of endocytosis for other SFD TIMP-3 proteins. These can however be challenging to express and purify. For example, the extremely low yield of E162K TIMP-3 (**Figure 3.6**) was disappointing, as I would predict that this SFD mutant would behave in a similar manner to H181R TIMP-3 due to the introduction of a basic residue. E162K may exhibit the same rate of endocytosis as WT and H181R TIMP-3 and have a possible increase in affinity for HS, perhaps greater than H181R which would account for the later onset of patients carrying the E162K mutation.

## 7.2.4 Uptake of WT, H181R, Y191C and S204C TIMP-3 is LRP-dependent but distinct from LRP1

LRP1 is a large endocytic receptor that is known to bind to over 100 ligands (Bres & Faissner, 2019; Mogensen et al., 2022; Yamamoto et al., 2022), and shown to mediate the endocytosis of WT TIMP-3 in HTB94 cells, MEFs and primary human macrophages (Doherty et al., 2016; Schubert et al., 2019; Scilabria et al., 2013). I thus investigated whether LRP1 was responsible for the endocytosis of WT, H181R, Y191C and S204C TIMP-3 in RPE cells (**Chapter 6**).

In agreement with previously published literature (Doherty et al., 2016; Scilabria et al., 2013), my data supports the conclusion that in MEF cells, WT TIMP-3 endocytosis is significantly mediated by LRP1 (**Figure 6.1**). Surprisingly, in ARPE-19 and hTERT RPE-1 cells, endocytosis of WT TIMP-3 appeared to be mediated by an LRP other than LRP1 (**Figure 6.13**).

All three SFD mutants analysed were rapidly taken up by LRP1-null PEA-13 cells (**Figure 6.2 & Figure 6.3 A & B**), indicating they most likely have reduced affinity for LRP1 compared to WT TIMP-3. S204C TIMP-3 retained a small but significant dependence on LRP1 (**Figure 6.3 B**), although this was markedly less than for WT TIMP-3. Moving to RPE cells, RAP strongly inhibited uptake of WT, H181R, Y191C and S204C TIMP-3 (**Figure 6.8**), indicating that endocytosis of all of these by RPE cells relies predominantly on a member of the LRP family. Taken together with the MEF-PEA-13 data, this suggests that they are all endocytosed by an LRP other than LRP1 in RPE cells.

This is the first report of TIMP-3 endocytosis by a receptor other than LRP1. Perhaps RPE cells express LRP1 at lower levels than other LRPs, shifting WT and mutant TIMP-3 towards endocytosis by another LRP family member. *LRP1* was abundantly expressed at the mRNA level in ARPE-19 and hTERT RPE-1 cells (**Figure 6.14**), but this may not necessarily translate to expression of the receptor at the protein level. Examining shedding of LRP1 may be helpful, as it is possible that an increase in LRP1 shedding could reduce the amount of functional receptor available on the cell surface to mediate endocytosis of TIMP-3. The protease responsible for shedding LRP1 in RPE cells is unknown and many factors could alter the rate of shedding, e.g., inflammation, which is increasingly suggested to play a role in SFD (Galloway et al., 2017; Hongisto et al., 2020; Spaide, 2021).

Considering which LRP receptor may be responsible for endocytosis of WT, H181R, Y191C and S204C TIMP-3 by RPE cells, I profiled expression of several LRP family receptors at the mRNA level. LRP1b, LRP2 and LDLRAD3 were all expressed. LDLRAD3 has the potential to mediate endocytosis as shown by Ranganathan et al. (2011) who demonstrated that COS-1 cells transfected with LDLRAD3 with an N-terminal *myc* tag internalised an [<sup>125</sup>I]-labelled 9E10 antibody specific for the *myc* tag. Additionally, LRP1b is known to mediate endocytosis of similar ligands to LRP1 including urokinase plasminogen activator, RAP and plasminogen activator inhibitor type-1 (Haas et al., 2011; Liu et al., 2001). LRP2 would be of particular interest as it is known to be expressed by RPE cells (Qi et al., 2023; Storm et al., 2014) and endocytoses protease and protease-inhibitor complexes, including TIMP-2: proMMP-2 complexes (Johanns et al., 2017). Curiously, LRP2 has been suggested to mediate transcytosis of IGF-1 in the choroid plexus epithelium (Bolós et al., 2010; Carro et al., 2005; Storm et al., 2019), so whether or not LRP2 could mediate transcytosis of ligands, including TIMP-3, between the basal and apical faces of RPE cells would be fascinating to determine. Relatively little is known about the endocytic capacity of other LRP receptors for which I observed mRNA expression in RPE cells (**Figure 6.14**). To identify the LRP receptor responsible for uptake of WT and SFD TIMP-3 proteins, a systematic siRNA knockdown approach could be used to test candidate LRP receptors, however this would require considerable time and optimisation.

The data also indicated that an LRP-independent pathway accounts for between 10-20 % of WT, H181R, Y191C and S204C TIMP-3 uptake. As discussed in Chapter 6, candidate receptors mediating this uptake could include HSPGs or receptors belonging to the macrophage mannose receptor family. A crosslinking approach or fusion with a proximity labelling domain could enable identification of both receptors involved in the LRP-independent uptake and the LRP receptor involved.

**Figure 7.1** summarises the key findings in this thesis and proposes a mechanism for accumulation of H181R, Y191C and S204C TIMP-3 in SFD. Different TIMP-3 mutant proteins may rely on or interact with different LRP and/or other receptors to varying degrees to mediate their uptake. For example, WT and H181R TIMP-3 may interact with a certain LRP receptor that mediates a ‘fast’ uptake, whereas Y191C and S204C TIMP-3 may have impaired interaction with this LRP and/or rather rely

on another LRP receptor that mediates a slower rate of uptake. However, this is not known and would be an exciting area for future investigation. Overall, the data in this thesis points to an LRP-dependent mechanism of uptake distinct from LRP1 as being the primary means of WT and mutant TIMP-3 endocytosis in RPE cells.

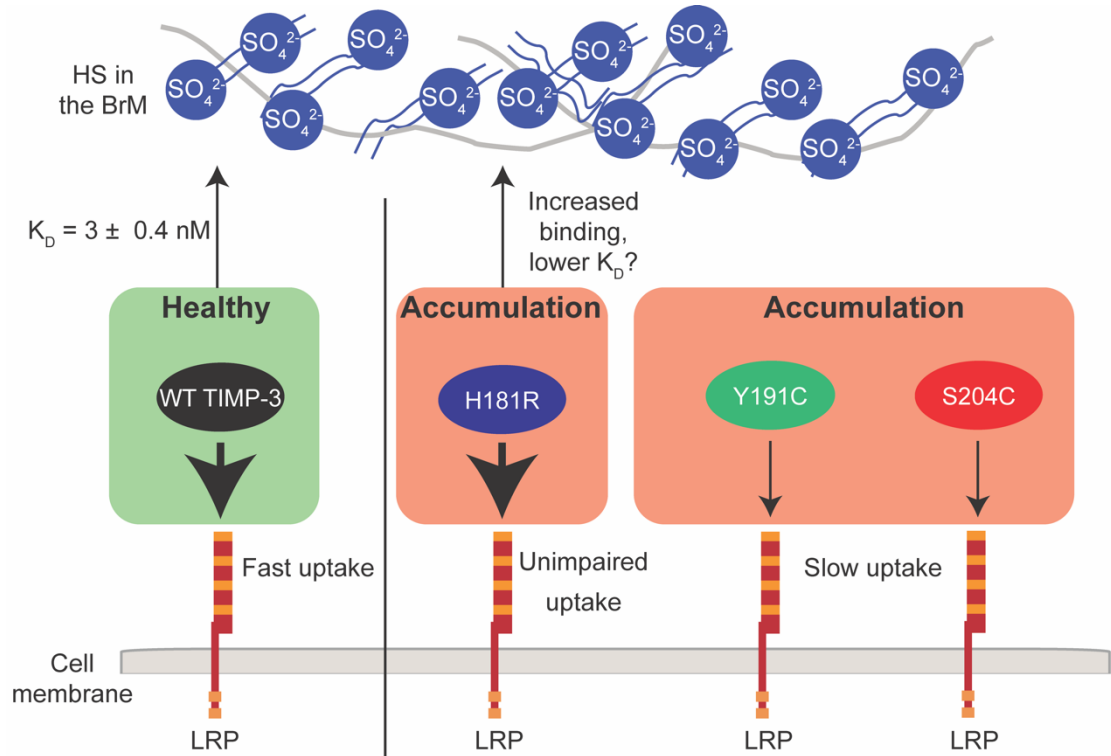


**Figure 7.1: Proposed mechanisms of SFD TIMP-3 accumulation.**

The data in this thesis support a model in which RPE cells endocytose WT TIMP-3 via an LRP other than LRP1, with Y191C and S204C TIMP-3 accumulating extracellularly due to impaired LRP-mediated endocytosis. On the other hand, endocytosis of H181R TIMP-3 is unaffected – this mutant may accumulate due to increased ECM binding, although this remains to be resolved.

## 7.2.5 Limitations and further experiments examining endocytosis

It would have been interesting to monitor in greater depth the uptake of higher molecular weight species (above 100 kDa) of WT, H181R, Y191C and S204C TIMP-3 by RPE cells. **Figure 5.6** showed that these higher molecular weight species were not endocytosed by RPE cells, although there was a considerable amount of variation amongst experiments and the molecular composition of these species is not clear (1.5.1).

It would have been informative to perform additional experiments to confirm that WT, H181R, Y191C and S204C TIMP-3 are taken up by RPE cells via clathrin-dependent endocytosis, and to rule out other endocytic pathways, such as caveolae-dependent

endocytosis. This could be done using a panel of inhibitors. For example, cytochalasin D inhibits actin polymerisation and has been used previously by our group to demonstrate TIMP-3 endocytosis by HTB94 cells (Troebert et al., 2008). Dynasore is also a commonly used inhibitor of clathrin-dependent endocytosis, which inhibits of the GTPase activity of dynamin, and so prevents intracellular release of clathrin-coated vesicles (Kirchhausen et al., 2008). Dynamin is also involved in other endocytic pathways (1.7.2), so this reagent is not strictly diagnostic of clathrin-dependent endocytosis. Other more specific inhibitors of clathrin-mediated endocytosis include Pitstop2, although it has been reported to have promiscuous selectivity and interfere with receptor expression (Guo et al., 2015), so instead inhibitors of clathrin such as bolinaquinone could be used (Margarucci et al., 2011; Szewczyk-Roszczenko et al., 2023). Inhibitors of caveolae-dependent endocytosis such as methyl- $\beta$ -cyclodextrin (Guo et al., 2015) could also be informative.

RPE cells exhibit specialised polarity with apically and basolaterally-expressed transporters, which are important for maintaining retinal homeostasis (Caceres & Rodriguez-Boulan, 2020; Lehmann et al., 2014). Therefore, a key limitation of experiments conducted in this study are that ARPE-19 and hTERT RPE-1 cells were not polarised. It would be interesting to investigate whether TIMP-3 and SFD TIMP-3 mutants are taken up at the apical or basolateral face or both of the RPE. Future experiments could be conducted in which RPE cells are grown on transwell inserts to generate a polarised monolayer and the endocytosis of WT and SFD TIMP-3 investigated at both apical and basolateral faces. Polarisation of RPE cells has previously been performed in vitro and confirmation of the formation of a polarised monolayer has been performed by measuring transepithelial electrical resistance, as well as staining for zonula occludens 1 to confirm the formation of tight junctions (Engel et al., 2022; Hongisto et al., 2020). I would hypothesise that endocytosis of WT and SFD TIMP-3 would occur predominantly at the basolateral face of RPE cells, given that is the face in contact with the extracellular BrM.

Additionally, to support the conclusion that LRP1 is not responsible for the endocytosis of TIMP-3 in RPE cells, it would have been beneficial to confirm the knockdown of LRP1 at the protein level in conjunction with the data showing knockdown at the mRNA level. This could have been done using the 5A6 antibody

which detects the 85 kDa beta transmembrane chain of LRP1 associated with the cell layer.

### 7.3 Other considerations of SFD TIMP-3 proteins

#### 7.3.1 Dimerisation status of SFD TIMP-3 proteins

In this study, dimeric species of 40-55 kDa were observed in immunoblots for all SFD TIMP-3 mutants (E162K, H181R, Y191C and S204C) in the conditioned media of transfected HEK-293 cells (**Figure 3.2 & Figure 3.3**), during isolation on anti-FLAG resins (**Figure 3.5, Figure 3.6 & Figure 3.8**), as well as in the conditioned media and ECM of transfected ARPE-19 cells (**Figure 4.3 & Figure 4.4**). My results agree with other investigators who have showed that SFD TIMP-3 mutants form dimeric species (Alsaffar et al., 2022; Langton et al., 2005; Yeow et al., 2002). S204C TIMP-3 showed much more abundant dimeric species than WT TIMP-3 and other SFD TIMP-3 mutants (**Figure 4.4**), also agreeing with previously published reports (Alsaffar et al., 2022; Langton et al., 2005). S204C TIMP-3 dimers were particularly abundant in the ECM (**Figure 4.3**), potentially suggesting that binding of S204C TIMP-3 to the ECM increases the chance of dimer formation. It is also possible that SFD TIMP-3 mutants may bind to other ECM components (e.g., fibulin-3) with different affinities compared to WT TIMP-3, or that they may bind to entirely different ECM components due to aberrant disulfide bond formation.

While dimeric/multimeric TIMP-3 species were observed in this study, they were generally less abundant than monomeric species and overall weaker than has been reported by other groups (Alsaffar et al., 2022; Langton et al., 2005; Yeow et al., 2002). I cannot rule out that this is because of inclusion of a FLAG tag at the C-terminus of my constructs, as this has been suggested by others (Langton et al., 2005) to impair dimerisation. Alternatively, I may have observed less dimerisation due to the improved linear range of the fluorescent LI-COR system I used in comparison to the chemiluminescent detection methods used by many others. This is an important point to resolve, as much pathophysiological significance has been ascribed to SFD TIMP-3 dimers.

Various investigators have shown by immunoblotting that reduction of SFD TIMP-3 proteins results in the disappearance of dimeric bands and a concurrent increase in monomeric band intensity (Alsaffar et al., 2022; Arris et al., 2003; Langton et al., 2000, 2005). I thus performed reduction and alkylation of WT and SFD TIMP-3 in TNC-B and SF DMEM using  $\beta$ -mercaptoethanol and iodoacetamide (**Figure 3.9**).

Monomeric species shifted upwards under reducing conditions, demonstrating the presence of intramolecular disulfide bonds within WT and SFD TIMP-3 proteins. Interestingly, dimeric and multimeric bands also appeared to shift upwards under reducing conditions, suggesting that these are not a product of intermolecular disulfide bond formation, going against the previously published literature (Alsaffar et al., 2022; Langton et al., 2005). A possible explanation for this observation is that SFD TIMP-3 mutants form large complexes/aggregates that are held together by a network of both disulfide bonds and disulfide-independent mechanisms, with the large size of these precluding their detection in non-reducing conditions. Reduction would reduce the molecular mass of such complexes by breaking disulfide bonds, but retention of disulfide-independent bonds would cause the TIMP-3-containing complexes to migrate with an apparent molecular mass above that of monomeric TIMP-3. Examples of disulfide-independent linkages include isopeptide bonds, which can be formed by tissue transglutaminase (Griffin et al., 2002), and ester bonds, as occur in complement proteins (Venkatesh & Levine, 1988). Various other kinds of covalent non-disulfide bonds have been demonstrated in proteins (Ravikiran & Mahalakshmi, 2014). Imaging of the stacking gel may demonstrate the presence of such high molecular weight species under non-reducing conditions. I would be curious to perform analytical ultracentrifugation or analysis utilising the UNCLE platform (Unchained Labs) on isolated TIMP-3 preparations, to shed light on the molecular mass of species present, and to establish the relative abundance of monomeric, dimeric and higher molecular weight species.

### 7.3.2 Broader effects of SFD TIMP-3 proteins on RPE cells

The global effects of SFD TIMP-3 proteins were only briefly visited in this thesis, by looking at how these proteins may affect candidate gene expression and apoptosis in RPE cells.

The data presented in **Chapter 4 (Figure 4.5, Figure 4.6, Figure 4.7 & Figure 4.8)** indicated that WT and SFD TIMP-3 proteins did not change expression of any of the candidate genes (*MMPs*, *ADAMs*, *ADAMTSs*, etc.) selected based on previous observations by Xia et al. (2023). Given the emerging body of literature showing that WT and SFD TIMP-3 mutants result in changes in the cellular proteome (Engel et al., 2022; Hongisto et al., 2020; Scilabria et al., 2018), this area requires further research using agnostic proteomic approaches.

High levels of WT TIMP-3 are pro-apoptotic and the mechanism by which this occurs is thought to be due to stabilisation of death receptors on the cell surface as a result of ADAM17 inhibition (Ahonen et al., 2003; Baker et al., 1999; Bond et al., 2002). Transfection and overexpression of WT and SFD TIMP-3 (S179C, G190C, Y191C and S204C) have been shown to induce apoptosis in RPE cells with SFD TIMP-3 proteins resulting in a higher degree of apoptosis (Majid et al., 2002). Data in **Chapter 4 (Figure 4.10)** indicated that exogenous addition of WT or SFD TIMP-3 did not cause RPE cell apoptosis, although this may have been a result of the low concentrations (100 nM) of proteins added. Higher concentrations of WT and SFD TIMP-3 could be tested, but the physiological relevance may become questionable. Physiologically relevant concentrations of SFD TIMP-3 proteins may increase the sensitivity of RPE cells to apoptotic stimuli. For example, Alsaffar (2017) demonstrated that apoptosis of serum-starved ARPE-19 cells treated with camptothecin or anti-FAS activation antibodies was higher if they expressed E162X and H181R TIMP-3 mutants than if they expressed WT TIMP-3.

### 7.3.3 Regulation of SFD TIMP-3 protein expression

Interestingly, in both transfected HEK-293 and ARPE-19 cells (**Figure 3.2, Figure 3.3, Figure 4.1 & Figure 4.4**), it was consistently observed that cells transfected with H181R, Y191C or S204C TIMP-3 had high mRNA expression of TIMP-3 but low levels of TIMP-3 protein detectable in the conditioned media, whereas cells transfected with WT TIMP-3 had low levels of TIMP-3 mRNA expression but a much higher expression of TIMP-3 protein in the conditioned media compared to cells expressing SFD TIMP-3 proteins. These observations suggest that there are possible differences in the post-transcriptional and/or post-translational regulation of these proteins. There is a lack of data to support changes in post-transcriptional regulation, but perhaps SFD TIMP-3 mRNA has altered stability and may have less translation to protein, resulting in the observed increased SFD TIMP-3 mRNA and lower protein levels. The mechanisms for this are undefined. There is evidence from SFD patients (Chong et al., 2003) and a hiPSC-RPE model of SFD (Hongisto et al., 2020) that levels of TIMP-3 mRNA are decreased or unchanged compared to cells expressing WT TIMP-3. This indicates there are altered transcriptional and post-transcriptional mechanisms of SFD TIMP-3 mRNA; however this is reverse effect to that observed in this study. One has to take into consideration the artificial nature of this expression system, with very high mRNA expression being driven by a viral promoter.

The decreased amount of SFD TIMP-3 protein detectable in the conditioned media may occur at a post-translational level due to impaired secretion of SFD TIMP-3 proteins as has been observed for hiPSC-RPE cells expressing S204C TIMP-3 (Hongisto et al., 2020). It would have been beneficial to western blot the cell layer to explore intracellular levels of TIMP-3 in these transfected cells. Lastly, the post-translational regulation of TIMP-3 in terms of its endocytosis and turnover may also be influenced by the availability of the endocytic receptor. Whilst the specific endocytic receptor responsible for TIMP-3 uptake in RPE cells remains unknown, this study indicates that it is predominantly LRP driven, thus regulation of the LRP receptor(s) on the cell surface by proteolytic shedding may also contribute to the different levels of SFD and WT TIMP-3 proteins detectable in the conditioned media.

## 7.4 Additional areas for future investigation

Working with WT and SFD TIMP-3 proteins is considerably limited by the yield of these recombinant proteins achievable in this and other studies. This may be due to low levels of expression in HEK-293 cells due to a potential apoptotic effect, or due to elevated ‘stickiness’ of these proteins resulting in a large loss during purification on the M2 FLAG column. Expression of TIMP-3 proteins in a bacterial expression system would result in a much greater yield, however these proteins may not be correctly folded complicating conclusions about the structure and dimerisation state of proteins. Thus, optimisation of a method enabling large production of recombinant TIMP-3 proteins would be vastly beneficial.

The ability of SFD TIMP-3 proteins to inhibit MMPs has not been extensively profiled, with MMP-2 and MMP-9 being the only MMPs broadly studied, and this largely being done by reverse zymography. More studies are required to investigate the ability of SFD TIMP-3 mutants to inhibit a broader range of MMPs such as MMP-1, MMP-3 and MMP-14, as these MMPs are also expressed by RPE cells. Furthermore, methods other than reverse zymography (e.g., fluorescent enzymatic kinetic assays) would allow determination of specific kinetics such as the  $K_i$  of SFD TIMP-3-MMP interactions, indicating more subtle changes in affinity that would not be detected by zymographic methods. Arguably more interesting would be to examine the ability of SFD TIMP-3 proteins to inhibit ADAMs and ADAMTSs, as there is very limited evidence for this. Of particular importance would be to determine inhibition of ADAM17, as decreased affinity for this enzyme could

promote inflammation in SFD (Hongisto et al., 2020; Spaide, 2021). Spaide (2021) reports effective use of an anti-TNF biologic in an SFD patient carrying the S204C mutation, but it is unknown if this therapeutic approach would be effective for all SFD TIMP-3 mutants, so profiling the ability of SFD TIMP-3 mutants to inhibit ADAM17 is important for personalised medicine approaches. Alsaffar (2017) postulated that SFD TIMP-3 dimers may stabilise the dimeric form of ADAM17, keeping it in a state of inhibition. This may result in stabilisation of death receptors and an increase in cellular apoptosis, so investigating the interaction of SFD TIMP-3 dimers with ADAM17 would also be an interesting avenue to explore. However, isolation of dimeric species of SFD TIMP-3 proteins would be technically challenging.

Given that TIMP-3 is widely expressed with reported high expression in the lung adipose tissue and synovium (Apte et al., 1994a; Leco et al., 1994), one would expect SFD patients to present with pathology in other tissues. For example, given that there is evidence that SFD TIMP-3 proteins accumulate extracellularly in the BrM, perhaps these mutants also accumulate in the ECM of other tissues, such as the lung. Pathological effects of SFD TIMP-3 proteins such as increased apoptosis and aberrant angiogenesis would be expected to be observed in other tissues. Thus far, reports on extraocular pathologies in SFD patients are sparse with conflicting results (Meunier et al., 2016; Tsokolas et al., 2018). Broader examinations of other tissues in SFD patients would be beneficial and it is possible that different SFD mutations may result in different severities of pathology in other tissues. Alternatively, it would be interesting to determine whether SFD TIMP-3 mutants confer a protective effect in osteoarthritis, where a decrease in TIMP-3 (Morris et al., 2010) is thought to lead to unregulated MMP-13 and ADAMTS-5 activity. Assuming extracellularly accumulated SFD TIMP-3 mutants retain inhibition of MMPs and ADAMTSs (which requires further investigation), then these mutants may confer increased protection against osteoarthritis. Generating mouse models carrying SFD mutations, in addition to the previously published S179C model (Weber et al., 2002), would be beneficial for examining such extraocular effects.

## 7.5 Therapeutic implications

Treatments currently in use for SFD include anti-VEGF therapy (1.1) which targets CNV occurring in late-stage SFD. This aims to stop progression of the disease without treating the underlying cause and is also not effective in SFD patients experiencing geographic atrophy. Drugs targeting the complement system may be

of use for geographic atrophy, as has been approved for use in AMD, although the involvement of complement in SFD pathogenesis is not clearly established. Rather treating the underlying cause of SFD, i.e., correcting the mutations in the *TIMP3* gene appear to be the best action to take, as suggested by Elsayed et al. (2022). This would be a preventative method, but would need to be employed early enough to avoid significant accumulation of SFD TIMP-3 protein in the BrM. Therefore, early identification and genotyping of SFD patients is critical.

Approaches for clearing accumulated TIMP-3 would also be desirable as these would reduce the pathological mechanisms (e.g., apoptosis, unregulated angiogenesis, inflammation, alterations in metabolism) induced by these proteins. A key finding of this thesis is that SFD is a heterogenous disease in terms of the molecular mechanisms by which mutant TIMP-3 proteins accumulate, so approaches which clear some SFD TIMP-3 mutants may be ineffective for clearing others. Genotyping of patients is thus critical for personalised medicine approaches to later-stage disease as well.

In light of the data presented in this study, for the Y191C and S204C TIMP-3 variants, a possible approach may be to aim to stimulate faster endocytosis of these proteins in order to clear them from the extracellular environment. However, achieving a selective increase in endocytosis of these ligands alone would be almost impossible. Data in **Chapter 6** indicates that an LRP or LRPs mediates uptake of these SFD TIMP-3 proteins. If these LRPs are negatively regulated by proteolytic shedding of their ectodomains, then targeting their sheddases may be a viable approach as has been tested for LRP1 in chondrocytes (Yamamoto et al., 2017). However, identification of the specific LRP receptor(s) and subsequently the responsible sheddase would require extensive experimental investigation. Given that LRP receptors such as LRP1b and LRP2 are known to mediate the endocytic uptake of a range of ligands, stimulating their endocytic activity would have many off-target effects and considerably impact the extracellular levels of many other ligands. An increase in endocytic rate may also overwhelm the endosomal trafficking system, resulting in increased intracellular accumulation and cell death.

H181R (and possible other SFD TIMP-3 mutants) has unimpaired endocytic uptake by RPE cells (**Chapter 5, Figure 5.4**), and so must accumulate by a different mechanism to Y191C and S204C. This mechanism may be increased ECM binding,

although this remains to be determined. Thus, blocking the binding of SFD TIMP-3 mutants to the ECM may be an alternative approach. Surfen, an antagonist of binding to HS (Schuksz et al., 2008), may block ECM binding of H181R TIMP-3, allowing for its endocytic uptake. Of course, this would not work as effectively for the Y191C and S204C mutants as even if their binding to HS is blocked, their impaired endocytic uptake would still result in extracellular accumulation. Again, there would be many off-target effects with this approach given that HS is known to bind over 400 ligands (Ori et al., 2011; Vallet et al., 2022). It is also possible that SFD TIMP-3 proteins bind with higher affinity to other ECM components such as fibulin-3, a known binding partner of TIMP-3 (Klenotic et al., 2004). Developing drugs to target this association may also be useful, although more experimental evidence is required for this association.

Stimulating endocytosis or blocking HS has many off-target effects and would be hard to achieve, so clearing aggregated TIMP-3 proteins by the addition of monoclonal antibodies could be an alternative. This approach is being investigated for the treatment of Alzheimer's disease, with monoclonal antibodies (e.g., aducanumab, lecanemab, donaenemab and remternetug) directed against amyloid  $\beta$  plaques acting as opsonisation signals to attract activated microglia to phagocytose and degrade amyloid  $\beta$  (Arndt et al., 2018; Cummings et al., 2024; Söderberg et al., 2023). Given that the eye is an immune privileged site, injection of monoclonal antibodies directed against SFD TIMP-3 and subsequent clearance by retinal glial cells may be a viable approach.

Even though SFD is a relatively rare disease, with an estimated prevalence of 1 in 220 000 (Christensen et al., 2017), it shares many similarities with other retinal diseases including AMD. Thus, SFD may be a good model for studying mechanisms of disease common to other retinal dystrophies and approaches to modulate endocytosis and/or ECM binding of TIMP-3 may also provide novel strategies for treating AMD, where proteins other than TIMP-3 accumulate in drusen. Continued research on this rare macular degeneration is thus warranted.

# Bibliography

*Age-related macular degeneration - Macular Society.* Retrieved March 3, 2022, from <https://www.macularsociety.org/macular-disease/macular-conditions/age-related-macular-degeneration/>

Ahmado, A., Carr, A. J., Vugler, A. A., Gias, C., Lawrence, J. M., Chen, L. L., ... & Coffey, P. J. (2011). Induction of differentiation by pyruvate and DMEM in the human retinal pigment epithelium cell line ARPE-19. *Investigative Ophthalmology & Visual Science*, 52(10), 7148-7159.

Ahonen, M., Poukkula, M., Baker, A. H., Kashiwagi, M., Nagase, H., Eriksson, J. E., & Kähäri, V. M. (2003). Tissue inhibitor of metalloproteinases-3 induces apoptosis in melanoma cells by stabilization of death receptors. *Oncogene*, 22(14), 2121-2134.

Alexander, J. P., Bradley, J. M., Gabourel, J. D., & Acott, T. S. (1990). Expression of matrix metalloproteinases and inhibitor by human retinal pigment epithelium. *Investigative Ophthalmology & Visual Science*, 31(12), 2520-2528.

Alsaffar, F. (2017). *The molecular characterisation of TIMP3 mutations responsible for Sorsby's Fundus Dystrophy: is there a link to age-related macular degeneration.*

Alsaffar, F. A., Mujamammi, A. H., Aldughaim, M. S., Nicklin, M. J., & Barker, M. D. (2023). Evidence that all Sorsby's fundus dystrophy mutations cause TIMP3 dimerization resulting in impaired inhibition of VEGFR2. *Genes & Diseases*, 10(1), 45.

Amour, A., Slocombe, P. M., Webster, A., Butler, M., Knight, C. G., Smith, B. J., ... & Murphy, G. (1998). TNF- $\alpha$  converting enzyme (TACE) is inhibited by TIMP-3. *FEBS Letters*, 435(1), 39-44.

Anand-Apte, B., Pepper, M. S., Voest, E., Montesano, R., Olsen, B., Murphy, G., ... & Zetter, B. (1997). Inhibition of angiogenesis by tissue inhibitor of metalloproteinase-3. *Investigative Ophthalmology & Visual Science*, 38(5), 817-823.

Annaval, T., Wild, R., Crétinon, Y., Sadir, R., Vivès, R. R., & Lortat-Jacob, H. (2020). Heparan sulfate proteoglycans biosynthesis and post synthesis mechanisms combine few enzymes and few core proteins to generate extensive structural and functional diversity. *Molecules*, 25(18), 4215.

Apte, S. S., Hayashi, K., Seldin, M. F., Mattei, M. G., Hayashi, M., & Olsen, B. R. (1994a). Gene encoding a novel murine tissue inhibitor of metalloproteinases (TIMP), TIMP-3, is expressed in developing mouse epithelia, cartilage, and muscle, and is located on mouse chromosome 10. *Developmental Dynamics*, 200(3), 177-197.

Apte, S. S., Mattei, M. G., & Olsen, B. R. (1994b). Cloning of the cDNA encoding human tissue inhibitor of metalloproteinases-3 (TIMP-3) and mapping of the TIMP3 gene to chromosome 22. *Genomics*, 19(1), 86-90.

Ardeljan, D., & Chan, C. C. (2013). Aging is not a disease: distinguishing age-related macular degeneration from aging. *Progress in Retinal and Eye Research*, 37, 68-89.

Arndt, J. W., Qian, F., Smith, B. A., Quan, C., Kilambi, K. P., Bush, M. W., ... & Weinreb, P. H. (2018). Structural and kinetic basis for the selectivity of aducanumab for aggregated forms of amyloid- $\beta$ . *Scientific Reports*, 8(1), 6412.

Arris, C. E., Bevitt, D. J., Mohamed, J., Li, Z., Langton, K. P., Barker, M. D., ... & McKie, N. (2003). Expression of mutant and wild-type TIMP3 in primary gingival fibroblasts from Sorsby's fundus dystrophy patients. *Biochimica et Biophysica Acta (BBA)-Molecular Basis of Disease*, 1638(1), 20-28.

Bailey, T. A., Alexander, R. A., Dubovy, S. R., Luthert, P. J., & Chong, N. V. (2001). Measurement of TIMP-3 expression and Bruch's membrane thickness in human macula. *Experimental Eye Research*, 73(6), 851-858.

Bainbridge, J. W., Smith, A. J., Barker, S. S., Robbie, S., Henderson, R., Balaggan, K., ... & Ali, R. R. (2008). Effect of gene therapy on visual function in Leber's congenital amaurosis. *New England Journal of Medicine*, 358(21), 2231-2239.

Bakall, B., Sohn, E. H., Riley, J., Brack, D., & Stone, E. M. (2014). Novel mutations and change of nomenclature for pathogenic variants in the TIMP3 gene causing Sorsby fundus dystrophy. *Investigative Ophthalmology & Visual Science*, 55(13), 3290-3290.

Baker, A. H., George, S. J., Zaltsman, A. B., Murphy, G., & Newby, A. C. (1999). Inhibition of invasion and induction of apoptotic cell death of cancer cell lines by overexpression of TIMP-3. *British Journal of Cancer*, 79(9), 1347-1355.

Balaskas, K., Hovan, M., Mahmood, S., & Bishop, P. (2013). Ranibizumab for the management of Sorsby fundus dystrophy. *Eye*, 27(1), 101-102.

Barbazetto, I. A., Hayashi, M., Klais, C. M., Yannuzzi, L. A., & Allikmets, R. (2005). A novel TIMP3 mutation associated with Sorsby fundus dystrophy. *Archives of Ophthalmology*, 123(4), 542-543.

Barcelona, P. F., Luna, J. D., Chiabrando, G. A., Juarez, C. P., Bhutto, I. A., Baba, T., ... & Lutty, G. A. (2010). Immunohistochemical localization of low density lipoprotein receptor-related protein 1 and  $\alpha$ 2-Macroglobulin in retinal and choroidal tissue of proliferative retinopathies. *Experimental Eye Research*, 91(2), 264-272.

Barnes, H., Larsen, B., Tyers, M., & van der Geer, P. (2001). Tyrosine-phosphorylated low density lipoprotein receptor-related protein 1 (Lrp1) associates with the adaptor protein SHC in SRC-transformed cells. *Journal of Biological Chemistry*, 276(22), 19119-19125.

Betts, J. H., & Troeberg, L. (2024). Mechanisms of TIMP-3 accumulation and pathogenesis in Sorsby fundus dystrophy. *Molecular Vision*, 30, 74.

Bevitt, D. J., Mohamed, J., Catterall, J. B., Li, Z., Arris, C. E., Hiscott, P., ... & McKie, N. (2003). Expression of ADAMTS metalloproteinases in the retinal pigment epithelium derived cell line ARPE-19: transcriptional regulation by TNF $\alpha$ . *Biochimica et Biophysica Acta (BBA)-Gene Structure and Expression*, 1626(1-3), 83-91.

Black, R. A., Rauch, C. T., Kozlosky, C. J., Peschon, J. J., Slack, J. L., Wolfson, M. F., ... & Cerretti, D. P. (1997). A metalloproteinase disintegrin that releases tumour-necrosis factor- $\alpha$  from cells. *Nature*, 385(6618), 729-733.

Blobel, C. P., & Apte, S. (2022). ADAMs and ADAMTSs. *Encyclopedia of Respiratory Medicine*, 568.

Bolós, M., Fernandez, S., & Torres-Aleman, I. (2010). Oral administration of a GSK3 inhibitor increases brain insulin-like growth factor 1 levels. *Journal of Biological Chemistry*, 285(23), 17693-17700.

Bond, M., Murphy, G., Bennett, M. R., Newby, A. C., & Baker, A. H. (2002). Tissue inhibitor of metalloproteinase-3 induces a Fas-associated death domain-dependent type II apoptotic pathway. *Journal of Biological Chemistry*, 277(16), 13787-13795.

Booij, J. C., Baas, D. C., Beisekeeva, J., Gorgels, T. G., & Bergen, A. A. (2010). The dynamic nature of Bruch's membrane. *Progress in Retinal and Eye Research*, 29(1), 1-18.

Bres, E. E., & Faissner, A. (2019). Low density receptor-related protein 1 interactions with the extracellular matrix: more than meets the eye. *Frontiers in Cell and Developmental Biology*, 7, 31.

Brew, K., & Nagase, H. (2010). The tissue inhibitors of metalloproteinases (TIMPs): an ancient family with structural and functional diversity. *Biochimica et Biophysica Acta (BBA)-Molecular Cell Research*, 1803(1), 55-71.

Brifault, C., Gilder, A. S., Laudati, E., Banki, M., & Gonias, S. L. (2017). Shedding of membrane-associated LDL receptor-related protein-1 from microglia amplifies and sustains neuroinflammation. *Journal of Biological Chemistry*, 292(45), 18699-18712.

Brunk, U. T., & Terman, A. (2002). Lipofuscin: mechanisms of age-related accumulation and influence on cell function. *Free Radical Biology and Medicine*, 33(5), 611-619.

Brunk, U., Wihlmark, U., Wrigstad, A., Roberg, K., & Nilsson, S. E. (1995). Accumulation of lipofuscin within retinal pigment epithelial cells results in enhanced sensitivity to photo-oxidation. *Gerontology-Basel*, 41, 201-212.

Caban, M., Owczarek, K., & Lewandowska, U. (2022). The role of metalloproteinases and their tissue inhibitors on ocular diseases: focusing on potential mechanisms. *International Journal of Molecular Sciences*, 23(8), 4256.

Cabral de Guimaraes, T. A. C., Varela, M. D., Georgiou, M., & Michaelides, M. (2022). Treatments for dry age-related macular degeneration: therapeutic avenues, clinical trials and future directions. *British Journal of Ophthalmology*, 106(3), 297-304.

Cabral-Pacheco, G. A., Garza-Veloz, I., Castruita-De la Rosa, C., Ramirez-Acuña, J. M., Perez-Romero, B. A., Guerrero-Rodriguez, J. F., ... & Martinez-Fierro, M. L. (2020). The roles of matrix metalloproteinases and their inhibitors in human diseases. *International Journal of Molecular Sciences*, 21(24), 9739.

Caceres, P. S., & Rodriguez-Boulan, E. (2020). Retinal pigment epithelium polarity in health and blinding diseases. *Current Opinion in Cell Biology*, 62, 37-45.

Călin, E. F., Popescu, S. I. P., Cernat, C. C. C., Patoni, C., Popescu, M. N., & Mușat, O. (2021). Lipofuscin: a key compound in ophthalmic practice. *Romanian Journal of Ophthalmology*, 65(2), 109.

Calligaris, M., Cuffaro, D., Bonelli, S., Spanò, D. P., Rossello, A., Nuti, E., & Scilabria, S. D. (2021). Strategies to target ADAM17 in disease: from its discovery to the iRhom revolution. *Molecules*, 26(4), 944.

Campbell, M. A., Sarohia, G. S., Campbell, M., Cui, J. Z., & Matsubara, J. A. (2019). The presence of ADAMs in the eye: Exploring a promising therapeutic target for age-related macular degeneration. *Investigative Ophthalmology & Visual Science*, 60(9), 1239-1239.

Capon, M. R. C., Polkinghorne, P. J., Fitzke, F. W., & Bird, A. C. (1988). Sorsby's pseudoinflammatory macula dystrophy—Sorsby's fundus dystrophies. *Eye*, 2(1), 114-122.

Capon, M. R., Marshall, J., Krafft, J. I., Alexander, R. A., Hiscott, P. S., & Bird, A. C. (1989). Sorsby's fundus dystrophy: a light and electron microscopic study. *Ophthalmology*, 96(12), 1769-1777.

Capurro, M. I., Shi, W., & Filmus, J. (2012). LRP1 mediates Hedgehog-induced endocytosis of the GPC3–Hedgehog complex. *Journal of Cell Science*, 125(14), 3380-3389.

Carreca, A. P., Pravatà, V. M., Markham, M., Bonelli, S., Murphy, G., Nagase, H., ... & Scilabria, S. D. (2020). TIMP-3 facilitates binding of target metalloproteinases to the

endocytic receptor LRP-1 and promotes scavenging of MMP-1. *Scientific Reports*, 10(1), 12067.

Carro, E., Spuch, C., Trejo, J. L., Antequera, D., & Torres-Aleman, I. (2005). Choroid plexus megalin is involved in neuroprotection by serum insulin-like growth factor I. *Journal of Neuroscience*, 25(47), 10884-10893.

Carter, D. C., & Ho, J. X. (1994). Structure of serum albumin. *Advances in Protein Chemistry*, 45, 153-203.

Casadei, B. R., Domingues, C. C., Clop, E. M., Couto, V. M., Perillo, M. A., & de Paula, E. (2018). Molecular features of nonionic detergents involved in the binding kinetics and solubilization efficiency, as studied in model (Langmuir films) and biological (Erythrocytes) membranes. *Colloids and Surfaces B: Biointerfaces*, 166, 152-160.

Chen, L. C., Noelken, M. E., & Nagase, H. (1993). Disruption of the cysteine-75 and zinc ion coordination is not sufficient to activate the precursor of human matrix metalloproteinase 3 (stromelysin 1). *Biochemistry*, 32(39), 10289-10295.

Chen, M., Forrester, J. V., & Xu, H. (2007). Synthesis of complement factor H by retinal pigment epithelial cells is down-regulated by oxidized photoreceptor outer segments. *Experimental Eye Research*, 84(4), 635-645.

Chen, W., Stambolian, D., Edwards, A. O., Branham, K. E., Othman, M., Jakobsdottir, J., ... & Stoltz, R. A. (2010). Genetic variants near TIMP3 and high-density lipoprotein-associated loci influence susceptibility to age-related macular degeneration. *Proceedings of the National Academy of Sciences*, 107(16), 7401-7406.

Cho, H. J., Kim, G. H., Park, S. H., Hyun, J. Y., Kim, N. K., & Shin, I. (2015). Probing the effect of an inhibitor of an ATPase domain of Hsc70 on clathrin-mediated endocytosis. *Molecular BioSystems*, 11(10), 2763-2769.

Cho, W. J., Jeremic, A., & Jena, B. P. (2005). Size of supramolecular SNARE complex: membrane-directed self-assembly. *Journal of the American Chemical Society*, 127(29), 10156-10157.

Chong, N. V., Alexander, R. A., Gin, T., Bird, A. C., & Luthert, P. J. (2000). TIMP-3, collagen, and elastin immunohistochemistry and histopathology of Sorsby's fundus dystrophy. *Investigative Ophthalmology & Visual Science*, 41(3), 898-902.

Chong, N. V., Keonin, J., Luthert, P. J., Frennesson, C. I., Weingeist, D. M., Wolf, R. L., ... & Hageman, G. S. (2005). Decreased thickness and integrity of the macular elastic layer of Bruch's membrane correspond to the distribution of lesions associated with age-related macular degeneration. *The American Journal of Pathology*, 166(1), 241-251.

Chong, N. H. V., Kvanta, A., Seregard, S., Bird, A. C., Luthert, P. J., & Steen, B. (2003). TIMP-3 mRNA is not overexpressed in Sorsby fundus dystrophy. *American Journal of Ophthalmology*, 136(5), 954-955.

Christensen, D. R., Brown, F. E., Cree, A. J., Ratnayaka, J. A., & Lotery, A. J. (2017). Sorsby fundus dystrophy—a review of pathology and disease mechanisms. *Experimental Eye Research*, 165, 35-46.

Clark, S. J., Keenan, T. D., Fielder, H. L., Collinson, L. J., Holley, R. J., Merry, C. L., ... & Bishop, P. N. (2011). Mapping the differential distribution of glycosaminoglycans in the adult human retina, choroid, and sclera. *Investigative Ophthalmology & Visual Science*, 52(9), 6511-6521.

Coveney, C. R., Collins, I., Mc Fie, M., Chanalaris, A., Yamamoto, K., & Wann, A. K. (2018). Cilia protein IFT88 regulates extracellular protease activity by optimizing LRP-1-mediated endocytosis. *The FASEB Journal*, 32(12), 6771.

Crabb, J. W., Miyagi, M., Gu, X., Shadrach, K., West, K. A., Sakaguchi, H., ... & Hollyfield, J. G. (2002). Drusen proteome analysis: an approach to the etiology of age-related macular degeneration. *Proceedings of the National Academy of Sciences*, 99(23), 14682-14687.

Crane, I. J., & Liversidge, J. (2008). Mechanisms of leukocyte migration across the blood–retina barrier. In *Seminars in Immunopathology* (30) 165-177. Springer-Verlag.

Cummings, J., Osse, A. M. L., Cammann, D., Powell, J., & Chen, J. (2024). Anti-amyloid monoclonal antibodies for the treatment of Alzheimer's disease. *BioDrugs*, 38(1), 5-22.

Curcio, C. A., & Johnson, M. (2012). Structure, function, and pathology of Bruch's membrane. *Retina*, 1(Part 2), 466-481.

de Almeida, L. G., Thode, H., Eslambolchi, Y., Chopra, S., Young, D., Gill, S., ... & Dufour, A. (2022). Matrix metalloproteinases: from molecular mechanisms to physiology, pathophysiology, and pharmacology. *Pharmacological Reviews*, 74(3), 714-770.

De Groef, L., Andries, L., Lemmens, K., Van Hove, I., & Moons, L. (2015). Matrix metalloproteinases in the mouse retina: a comparative study of expression patterns and MMP antibodies. *BMC Ophthalmology*, 15, 1-16.

de Jong, P. T. V. M. (2006). Age-related macular degeneration. *The New England Journal of Medicine*, 355(14), 1474–1485.

De La Paz, M. A., Pericak-Vance, M. A., Lennon, F., Haines, J. L., & Seddon, J. M. (1997). Exclusion of TIMP3 as a candidate locus in age-related macular degeneration. *Investigative Ophthalmology & Visual Science*, 38(6), 1060-1065.

Deane, R., Sagare, A., Hamm, K., Parisi, M., Lane, S., Finn, M. B., ... & Zlokovic, B. V. (2008). apoE isoform-specific disruption of amyloid  $\beta$  peptide clearance from mouse brain. *The Journal of Clinical Investigation*, 118(12), 4002-4013.

DeBenedictis, M. J., Gindzin, Y., Glaab, E., & Anand-Apte, B. (2020). A novel TIMP3 mutation associated with a retinitis pigmentosa-like phenotype. *Ophthalmic Genetics*, 41(5), 480-484.

Della, N. G., Campochiaro, P. A., & Zack, D. J. (1996). Localization of TIMP-3 mRNA expression to the retinal pigment epithelium. *Investigative Ophthalmology & Visual Science*, 37(9), 1921–1924.

Doherty, C. M., Visse, R., Dinakarpandian, D., Strickland, D. K., Nagase, H., & Troeberg, L. (2016). Engineered tissue Inhibitor of metalloproteinases-3 variants resistant to endocytosis have prolonged chondroprotective activity. *Journal of Biological Chemistry*, 291(42), 22160.

Doherty, G. J., & McMahon, H. T. (2009). Mechanisms of endocytosis. *Annual Review of Biochemistry*, 78, 857-902.

Dolmer, K., Campos, A., & Gettins, P. G. W. (2013). Quantitative dissection of the binding contributions of ligand lysines of the receptor-associated protein (RAP) to the low density lipoprotein receptor-related protein (LRP1). *Journal of Biological Chemistry*, 288(33), 24081–24090.

Drynda, A., Quax, P. H., Neumann, M., van der Laan, W. H., Pap, G., Drynda, S., ... & Pap, T. (2005). Gene transfer of tissue inhibitor of metalloproteinases-3 reverses the inhibitory effects of TNF- $\alpha$  on Fas-induced apoptosis in rheumatoid arthritis synovial fibroblasts. *The Journal of Immunology*, 174(10), 6524-6531.

Duffy, M. J., McKiernan, E., O'Donovan, N., & McGowan, P. M. (2009). The role of ADAMs in disease pathophysiology. *Clinica Chimica Acta*, 403(1-2), 31-36.

Dumas, J. J., Merithew, E., Sudharshan, E., Rajamani, D., Hayes, S., Lawe, D., ... & Lambright, D. G. (2001). Multivalent endosome targeting by homodimeric EEA1. *Molecular Cell*, 8(5), 947-958.

Duncan, K. G., Bailey, K. R., Kane, J. P., & Schwartz, D. M. (2002). Human Retinal Pigment Epithelial Cells Express Scavenger Receptors BI and BII. *Biochemical and Biophysical Research Communications*, 292(4), 1017–1022.

Dunn, K. C., Aotaki-Keen, A. E., Putkey, F. R., & Hjelmeland, L. M. (1996). ARPE-19, a human retinal pigment epithelial cell line with differentiated properties. *Experimental Eye Research*, 62(2), 155-170.

Ebrahem, Q., Qi, J. H., Sugimoto, M., Ali, M., Sears, J. E., Cutler, A., Khokha, R., Vasanji, A., & Anand-Apte, B. (2011). Increased neovascularization in mice lacking tissue

inhibitor of metalloproteinases-3. *Investigative Ophthalmology & Visual Science*, 52(9), 6117–6123.

Edwards, A. O., Ritter, R., Abel, K. J., Manning, A., Panhuyzen, C., & Farrer, L. A. (2005). Complement factor H polymorphism and age-related macular degeneration. *Science*, 308(5720), 421–424.

Elkin, S. R., Lakoduk, A. M., & Schmid, S. L. (2016). Endocytic pathways and endosomal trafficking: a primer. *Wiener Medizinische Wochenschrift*, 166, 196-204.

Elner, S. G. (2002). Human retinal pigment epithelial lysis of extracellular matrix: functional urokinase plasminogen activator receptor, collagenase, and elastase. *Transactions of the American Ophthalmological Society*, 100, 273.

Elsayed, M. E. A., Kaukonen, M., Kiraly, P., Kapetanovic, J. C., & MacLaren, R. E. (2022). Potential CRISPR base editing therapeutic options in a Sorsby Fundus Dystrophy patient. *Genes*, 13(11), 2103.

Emonard, H., Bellon, G., Troeberg, L., Berton, A., Robinet, A., Henriet, P., ... & Courtoy, P. J. (2004). Low density lipoprotein receptor-related protein mediates endocytic clearance of pro-MMP-2·TIMP-2 complex through a thrombospondin-independent mechanism. *Journal of Biological Chemistry*, 279(52), 54944-54951.

Engel, A. L., Wang, Y., Khuu, T. H., Worrall, E., Manson, M. A., Lim, R. R., ... & Chao, J. R. (2022). Extracellular matrix dysfunction in Sorsby patient-derived retinal pigment epithelium. *Experimental Eye Research*, 215, 108899.

Engelholm, L. H., List, K., Netzel-Arnett, S., Cukierman, E., Mitola, D. J., Aaronson, H., ... & Bugge, T. H. (2003). uPARAP/Endo180 is essential for cellular uptake of collagen and promotes fibroblast collagen adhesion. *The Journal of Cell Biology*, 160(7), 1009-1015.

Esko, J. D., Stewart, T. E., & Taylor, W. H. (1985). Animal cell mutants defective in glycosaminoglycan biosynthesis. *Proceedings of the National Academy of Sciences of the United States of America*, 82(10), 3197–3201.

Esterbauer, H., Schaur, R. J., & Zollner, H. (1991). Chemistry and biochemistry of 4-hydroxynonenal, malonaldehyde and related aldehydes. *Free Radical Biology and Medicine*, 11(1), 81–128.

Fadok, V. A., Bratton, D. L., Frasch, S. C., Warner, M. L., & Henson, P. M. (1998). The role of phosphatidylserine in recognition of apoptotic cells by phagocytes. *Cell Death and Differentiation*, 5(7), 551–562.

Fan, D., & Kassiri, Z. (2020). Biology of tissue inhibitor of metalloproteinase 3 (TIMP3), and its therapeutic implications in cardiovascular pathology. *Frontiers in Physiology*, 11, 546314.

Fang, I. M., Yang, C. H., Yang, C. M., & Chen, M. S. (2009). Overexpression of integrin alpha6 and beta4 enhances adhesion and proliferation of human retinal pigment epithelial cells on layers of porcine Bruch's membrane. *Experimental Eye Research*, 88(1), 12–21.

Fariss, R. N., Apte, S. S., Luthert, P. J., Bird, A. C., & Milam, A. H. (1998). Accumulation of tissue inhibitor of metalloproteinases-3 in human eyes with Sorsby's fundus dystrophy or retinitis pigmentosa. *The British Journal of Ophthalmology*, 82(11), 1329–1334.

Fariss, R. N., Apte, S. S., Olsen, B. R., Iwata, K., & Milam, A. H. (1997). Tissue inhibitor of metalloproteinases-3 is a component of Bruch's membrane of the eye. *The American Journal of Pathology*, 150(1), 323.

Fedak, P. W., Smookler, D. S., Kassiri, Z., Ohno, N., Leco, K. J., Verma, S., ... & Khokha, R. (2004). TIMP-3 deficiency leads to dilated cardiomyopathy. *Circulation*, 110(16), 2401-2409.

Felbor, U., Benkowitz, C., Klein, M. L., Greenberg, J., Gregory, C. Y., & Weber, B. H. F. (1997). Sorsby Fundus Dystrophy: Reevaluation of variable expressivity in patients carrying a TIMP3 founder mutation. *Archives of Ophthalmology*, 115(12), 1569–1571.

Felbor, U., Stöhr, H., Amann, T., Schönherr, U., Apfelstedt-Sylla, E., & Weber, B. H. F. (1996). A second independent Tyr168Cys mutation in the tissue inhibitor of metalloproteinases-3 (TIMP3) in Sorsby's fundus dystrophy. *Journal of Medical Genetics*, 33(3), 233–236.

Felbor, U., Stöhr, H., Amann, T., Schönherr, U., & Weber, B. H. F. (1995). A novel Ser156Cys mutation in the tissue inhibitor of metalloproteinases-3 (TIMP3) in Sorsby's fundus dystrophy with unusual clinical features. *Human Molecular Genetics*, 4(12), 2415–2416.

Fernandez-Catalan, C., Bode, W., Huber, R., Turk, D., Calvete, J. J., Lichte, A., Tschesche, H., & Maskos, K. (1998). Crystal structure of the complex formed by the membrane type 1-matrix metalloproteinase with the tissue inhibitor of metalloproteinases-2, the soluble progelatinase A receptor. *The EMBO Journal*, 17(17), 5238–5248.

Fernandez-Patron, C., Zouki, C., Whittal, R. M., Chan, J. S., Davidge, S. T., & Filep, J. G. (2002). Methods for analysis of matrix metalloproteinase regulation of neutrophil-endothelial cell adhesion. *Biological Procedures Online*, 4, 38-48.

Ferris, F. L., Wilkinson, C. P., Bird, A., Chakravarthy, U., Chew, E., Csaky, K., & Sadda, S. R. (2013). Clinical classification of age-related macular degeneration. *Ophthalmology*, 120(4), 844–851.

Fisher, C., Beglova, N., & Blacklow, S. C. (2006). Structure of an LDLR-RAP complex reveals a general mode for ligand recognition by lipoprotein receptors. *Molecular Cell*, 22(2), 277–283.

Fleckenstein, M., Schmitz-Valckenberg, S., & Chakravarthy, U. (2024). Age-related macular degeneration: A review. *JAMA*, 331(2), 147-157.

Fogarasi, M., Janssen, A., Weber, B. H. F., & Stöhr, H. (2008). Molecular dissection of TIMP3 mutation S156C associated with Sorsby fundus dystrophy. *Matrix Biology*, 27(5), 381–392.

Frantz, C., Stewart, K. M., & Weaver, V. M. (2010). The extracellular matrix at a glance. *Journal of Cell Science*, 123(24), 4195-4200.

Fritsche, L. G., Igl, W., Bailey, J. N. C., Grassmann, F., Sengupta, S., Bragg-Gresham, J. L., ... & Zhang, K. (2015). A large genome-wide association study of age-related macular degeneration highlights contributions of rare and common variants. *Nature Genetics*, 48(2), 134-143.

Fung, A. T., Stöhr, H., Weber, B. H., Holz, F. G., & Yannuzzi, L. A. (2013). Atypical sorsby fundus dystrophy with a novel tyr159cys timp-3 mutation. *Retinal Cases & Brief Reports*, 7(1), 71-74.

Gabriely, G., Wurdinger, T., Kesari, S., Esau, C. C., Burchard, J., Linsley, P. S., & Krichevsky, A. M. (2008). MicroRNA 21 promotes glioma invasion by targeting matrix metalloproteinase regulators. *Molecular and Cellular Biology*, 28(17), 5369–5380.

Galazka, G., Windsor, L. J., Birkedal-Hansen, H., & Engler, J. A. (1996). APMA (4-aminophenylmercuric acetate) activation of stromelysin-1 involves protein interactions in addition to those with cysteine-75 in the propeptide. *Biochemistry*, 35(34), 11221–11227.

Galloway, C. A., Dalvi, S., Hung, S. S., MacDonald, L. A., Latchney, L. R., Wong, R. C., ... & Singh, R. (2017). Drusen in patient-derived hiPSC-RPE models of macular dystrophies. *Proceedings of the National Academy of Sciences*, 114(39), E8214–E8223.

García-Onrubia, L., Valentín-Bravo, F. J., Coco-Martin, R. M., González-Sarmiento, R., Pastor, J. C., Usategui-Martín, R., & Pastor-Idoate, S. (2020). Matrix metalloproteinases in age-related macular degeneration (AMD). *International Journal of Molecular Sciences*, 21(16), 5934.

Gehrs, K. M., Jackson, J. R., Brown, E. N., Allikmets, R., & Hageman, G. S. (2010). Complement, age-related macular degeneration and a vision of the future. *Archives of Ophthalmology*, 128(3), 349–358.

Gemenetzi, M. K., Luff, A. J., & Lotery, A. J. (2011). Successful treatment of choroidal neovascularization secondary to sorsby fundus dystrophy with intravitreal bevacizumab. *Retinal Cases and Brief Reports*, 5(2), 132–135.

Gendron, C., Kashiwagi, M., Hughes, C., Caterson, B., & Nagase, H. (2003). TIMP-3 inhibits aggrecanase-mediated glycosaminoglycan release from cartilage explants stimulated by catabolic factors. *FEBS Letters*, 555(3), 431–436.

Gill, S. E., Pape, M. C., Khokha, R., Watson, A. J., & Leco, K. J. (2003). A null mutation for Tissue Inhibitor of Metalloproteinases-3 (Timp-3) impairs murine bronchiole branching morphogenesis. *Developmental Biology*, 261(2), 313–323.

Gliem, M., Müller, P. L., Mangold, E., Holz, F. G., Bolz, H. J., Stöhr, H., ... & Issa, P. C. (2015). Sorsby fundus dystrophy: novel mutations, novel phenotypic characteristics, and treatment outcomes. *Investigative Ophthalmology & Visual Science*, 56(4), 2664–2676.

Goldberg, G. I., Wilhelm, S. M., Kronberger, A., Bauer, E. A., Grant, G. A., & Eisen, A. Z. (1986). Human fibroblast collagenase. Complete primary structure and homology to an oncogene transformation-induced rat protein. *Journal of Biological Chemistry*, 261(14), 6600–6605.

Goldstein, J. L., & Brown, M. S. (1974). Binding and degradation of low density lipoproteins by cultured human fibroblasts. *Journal of Biological Chemistry*, 249(16), 5153–5162.

Gordiyenko, N., Campos, M., Lee, J. W., Fariss, R. N., Sztein, J., & Rodriguez, I. R. (2004). RPE cells internalize low-density lipoprotein (LDL) and oxidized LDL (oxLDL) in large quantities in vitro and in vivo. *Investigative Ophthalmology & Visual Science*, 45(8), 2822–2829.

Gorovoy, M., Gaultier, A., Campana, W. M., Firestein, G. S., & Gonias, S. L. (2010). Inflammatory mediators promote production of shed LRP1/CD91, which regulates cell signaling and cytokine expression by macrophages. *Journal of Leukocyte Biology*, 88(4), 769.

Gourier, H. C., & Chong, N. V. (2015). Can novel treatment of age-related macular degeneration be developed by better understanding of sorsby's fundus dystrophy. *Journal of Clinical Medicine*, 4(5), 874–883.

Gray, T. L., Wong, H. C., & Raymond, G. L. (2012). Choroidal neovascularization secondary to sorsby fundus dystrophy treated with intravitreal bevacizumab. *Retinal Cases and Brief Reports*, 6(2), 193–196.

Grenell, A., Singh, C., Raju, M., Wolk, A., Dalvi, S., Jang, G. F., ... & Anand-Apte, B. (2024). Tissue Inhibitor of Metalloproteinase 3 (TIMP3) mutations increase glycolytic activity and dysregulate glutamine metabolism in RPE cells. *BioRxiv*, 2024-01.

Griffin, M., Casadio, R., & Bergamini, C. M. (2002). Transglutaminases: nature's biological glues. *Biochemical Journal*, 368(2), 377-396.

Guan, B., Huryn, L. A., Hughes, A. B., Li, Z., Bender, C., Blain, D., ... & Hufnagel, R. B. (2022). Early-onset TIMP3-related retinopathy associated with impaired signal peptide. *JAMA Ophthalmology*, 140(7), 730-733.

Guo, L., Hussain, A. A., Limb, G. A., & Marshall, J. (1999). Age-dependent variation in metalloproteinase activity of isolated human Bruch's membrane and choroid. *Investigative Ophthalmology & Visual Science*, 40(11), 2676-2682.

Guo, S., Zhang, X., Zheng, M., Zhang, X., Min, C., Wang, Z., ... & Kim, K. M. (2015). Selectivity of commonly used inhibitors of clathrin-mediated and caveolae-dependent endocytosis of G protein-coupled receptors. *Biochimica et Biophysica Acta (BBA)-Biomembranes*, 1848(10), 2101-2110.

Haas, J., Beer, A. G., Widschwendter, P., Oberdanner, J., Salzmann, K., Sarg, B., ... & Marschang, P. (2011). LRP1b shows restricted expression in human tissues and binds to several extracellular ligands, including fibrinogen and apoE-carrying lipoproteins. *Atherosclerosis*, 216(2), 342-347.

Hageman, G. S., Anderson, D. H., Johnson, L. V., Hancox, L. S., Taiber, A. J., Hardisty, L. I., ... & Allikmets, R. (2005). A common haplotype in the complement regulatory gene factor H (HF1/CFH) predisposes individuals to age-related macular degeneration. *Proceedings of the National Academy of Sciences*, 102(20), 7227-7232.

Hahn-Dantona, E., Ruiz, J. F., Bornstein, P., & Strickland, D. K. (2001). The low density lipoprotein receptor-related protein modulates levels of matrix metalloproteinase 9 (MMP-9) by mediating its cellular catabolism. *Journal of Biological Chemistry*, 276(18), 15498-15503.

Hall, M. L., Givens, S., Santosh, N., Iacovino, M., Kyba, M., & Ogle, B. M. (2022). Laminin 411 mediates endothelial specification via multiple signaling axes that converge on  $\beta$ -catenin. *Stem Cell Reports*, 17(3), 569-583.

Hayes, K. C., Lindsey, S., Stephan, Z. F., & Brecker, D. (1989). Retinal pigment epithelium possesses both LDL and scavenger receptor activity. *Investigative Ophthalmology & Visual Science*, 30(2), 225-232.

Hendershot, L. M., Buck, T. M., & Brodsky, J. L. (2023). The essential functions of molecular chaperones and folding enzymes in maintaining endoplasmic reticulum homeostasis. *Journal of Molecular Biology*, 168418.

Herz, J., Clouthier, D. E., & Hammer, R. E. (1992). LDL receptor-related protein internalizes and degrades uPA-PAI-1 complexes and is essential for embryo implantation. *Cell*, 71(3), 411-421.

Hewitt, A. T., Nakazawa, K., & Newsome, D. A. (1989). Analysis of newly synthesized Bruch's membrane proteoglycans. *Investigative Ophthalmology & Visual Science*, 30(3), 478-486.

Hogan, M. J. (1961). Ultrastructure of the choroid. Its role in the pathogenesis of chorioretinal disease. *Transactions of the Pacific Coast Oto-Ophthalmological Society Annual Meeting*, 42, 61-87.

Hogan, M. J., & Alvarado, J. (1967). Studies on the human macula: IV. Aging changes in Bruch's membrane. *Archives of Ophthalmology*, 77(3), 410-420.

Hollborn, M., Birkenmeier, G., Saalbach, A., Iandiev, I., Reichenbach, A., Wiedemann, P., & Kohen, L. (2004a). Expression of LRP1 in retinal pigment epithelial cells and its regulation by growth factors. *Investigative Ophthalmology & Visual Science*, 45(6), 2033-2038.

Hollborn, M., Reichenbach, A., Wiedemann, P., & Kohen, L. (2004b). Contrary effects of cytokines on mRNAs of cell cycle- and ECM-related proteins in hRPE cells in vitro. *Current Eye Research*, 28(3), 215-223.

Holtet, T. L., Nielsen, K. L., Etzerodt, M., Moestrup, S. K., Gliemann, J., Sottrup-Jensen, L., & Thøgersen, H. C. (1994). Receptor-binding domain of human  $\alpha$ 2-macroglobulin Expression, folding and biochemical characterization of a high-affinity recombinant derivative. *FEBS Letters*, 344(2-3), 242-246.

Holz, F. G., Sheraidah, G., Pauleikhoff, D., & Bird, A. C. (1994). Analysis of lipid deposits extracted from human macular and peripheral Bruch's membrane. *Archives of Ophthalmology*, 112(3), 402-406.

Hongisto, H., Dewing, J. M., Christensen, D. R., Scott, J., Cree, A. J., Nättinen, J., ... & Lotery, A. J. (2020). In vitro stem cell modelling demonstrates a proof-of-concept for excess functional mutant TIMP3 as the cause of Sorsby fundus dystrophy. *The Journal of Pathology*, 252(2), 138-150.

Hori, Y., Aoki, N., Kuwahara, S., Hosojima, M., Kaseda, R., Goto, S., ... & Saito, A. (2017). Megalin blockade with cilastatin suppresses drug-induced nephrotoxicity. *Journal of the American Society of Nephrology*, 28(6), 1783-1791.

Hoskin, A., Sehmi, K., & Bird, A. C. (1981). Sorsby's pseudoinflammatory macular dystrophy. *British Journal of Ophthalmology*, 65(12), 859-865.

Hsu, V. W., & Prekeris, R. (2010). Transport at the recycling endosome. *Current Opinion in Cell Biology*, 22(4), 528–534.

Hu, K., Yang, J., Tanaka, S., Gonias, S. L., Mars, W. M., & Liu, Y. (2006). Tissue-type plasminogen activator acts as a cytokine that triggers intracellular signal transduction and induces matrix metalloproteinase-9 gene expression. *Journal of Biological Chemistry*, 281(4), 2120–2127.

Hu, W., Jiang, A., Liang, J., Meng, H., Chang, B., Gao, H., & Qiao, X. (2008). Expression of VLDLR in the retina and evolution of subretinal neovascularization in the knockout mouse model's retinal angiomatic proliferation. *Investigative Ophthalmology & Visual Science*, 49(1), 407–415.

Huang, J. D., Curcio, C. A., & Johnson, M. (2008). Morphometric analysis of lipoprotein-like particle accumulation in aging human macular Bruch's membrane. *Investigative Ophthalmology & Visual Science*, 49(6), 2721–2727.

Huang, L., Huffman, K., Borooh, S., & Bakall, B. (2021). A novel pathogenic mutation of the TIMP3 gene in Sorsby Fundus Dystrophy. *Investigative Ophthalmology & Visual Science*, 62(8), 3052–3052.

Hunt, R. C., Fox, A., Vytautas, P., Sigel, M. M., Kosnosky, W., Choudhury, P., & Black, E. P. (1993). Cytokines cause cultured retinal pigment epithelial cells to secrete metalloproteinases and to contract collagen gels. *Investigative Ophthalmology & Visual Science*, 34(11) 3179–3186.

Hussain, A. A., Lee, Y., Zhang, J. J., & Marshall, J. (2011). Disturbed matrix metalloproteinase activity of Bruch's membrane in age-related macular degeneration. *Investigative Ophthalmology & Visual Science*, 52(7), 4459–4466.

Iyer, S., Wei, S., Brew, K., & Acharya, K. R. (2007). Crystal structure of the catalytic domain of matrix metalloproteinase-1 in complex with the inhibitory domain of tissue inhibitor of metalloproteinase-1. *Journal of Biological Chemistry*, 282(1), 364–371.

Jacobsen, L., Madsen, P., Moestrup, S. K., Lund, A. H., Tommerup, N., Nykjær, A., Sottrup-Jensen, L., Gliemann, J., & Petersen, C. M. (1996). Molecular characterization of a novel human hybrid-type receptor that binds the  $\alpha$ 2-macroglobulin receptor-associated protein. *Journal of Biological Chemistry*, 271(49), 31379–31383.

Jacobson, S. G., Cideciyan, A. V., Bennett, J., Kingsley, R. M., Sheffield, V. C., & Stone, E. M. (2002). Novel mutation in the TIMP3 gene causes Sorsby Fundus Dystrophy. *Archives of Ophthalmology*, 120(3), 376–379.

Jacobson, S. G., Cideciyan, A. V., Regunath, G., Rodriguez, F. J., Vandenberg, K., Sheffield, V. C., & Stone, E. M. (1995). Night blindness in Sorsby's fundus dystrophy reversed by vitamin A. *Nature Genetics*, 11(1), 27-32.

Janssen, A., Hoellenriegel, J., Fogarasi, M., Schrewe, H., Seeliger, M., Tamm, E., ... & Stöhr, H. (2008). Abnormal vessel formation in the choroid of mice lacking tissue inhibitor of metalloprotease-3. *Investigative Ophthalmology & Visual Science*, 49(7), 2812-2822.

Jensen, G. A., Andersen, O. M., Bonvin, A. M., Bjerrum-Bohr, I., Etzerodt, M., Thøgersen, H. C., ... & Kragelund, B. B. (2006). Binding site structure of one LRP–RAP complex: implications for a common ligand–receptor binding motif. *Journal of Molecular Biology*, 362(4), 700-716.

Jensen, J. K., Dolmer, K., Schar, C., & Gettins, P. G. (2009). Receptor-associated protein (RAP) has two high-affinity binding sites for the low-density lipoprotein receptor-related protein (LRP): consequences for the chaperone functions of RAP. *Biochemical Journal*, 421(2), 273-282.

Jensen, P. H., Moestrup, S. K., & Gliemann, J. (1989). Purification of the human placental  $\alpha$ 2-macroglobulin receptor. *FEBS Letters*, 255(2), 275–280.

Johanns, M., Lemoine, P., Janssens, V., Grieco, G., Moestrup, S. K., Nielsen, R., ... & Henriet, P. (2017). Cellular uptake of proMMP-2: TIMP-2 complexes by the endocytic receptor megalin/LRP-2. *Scientific Reports*, 7(1), 4328.

Johnson, A. A., Guziewicz, K. E., Lee, C. J., Kalathur, R. C., Pulido, J. S., Marmorstein, L. Y., & Marmorstein, A. D. (2017). Bestrophin 1 and retinal disease. *Progress in Retinal and Eye Research*, 58, 45–69.

Johnson, E. B., Hammer, R. E., & Herz, J. (2005). Abnormal development of the apical ectodermal ridge and polysyndactyly in Megf7-deficient mice. *Human Molecular Genetics*, 14(22), 3523–3538.

Johnson, L. V., Leitner, W. P., Rivest, A. J., Staples, M. K., Radeke, M. J., & Anderson, D. H. (2002). The Alzheimer's A $\beta$ -peptide is deposited at sites of complement activation in pathologic deposits associated with aging and age-related macular degeneration. *Proceedings of the National Academy of Sciences*, 99(18), 11830–11835.

Jones, S. E., Jomary, C., & Neal, M. J. (1994). Expression of TIMP3 mRNA is elevated in retinas affected by simplex retinitis pigmentosa. *FEBS Letters*, 352(2), 171–174.

Kamei, M., & Hollyfield, J. G. (1999). TIMP-3 in Bruch's membrane: Changes during aging and in age-related macular degeneration. *Investigative Ophthalmology and Visual Science*, 40(10), 2367–2375.

Kanai, Y., Wang, D., & Hirokawa, N. (2014). KIF13B enhances the endocytosis of LRP1 by recruiting LRP1 to caveolae. *Journal of Cell Biology*, 204(3), 395-408.

Kanekiyo, T., Zhang, J., Liu, Q., Liu, C. C., Zhang, L., & Bu, G. (2011). Heparan sulphate proteoglycan and the low-density lipoprotein receptor-related protein 1 constitute major pathways for neuronal amyloid-beta uptake. *The Journal of Neuroscience: The Official Journal of the Society for Neuroscience*, 31(5), 1644–1651.

Kang, K. H., Park, S. Y., Rho, S. B., & Lee, J. H. (2008). Tissue inhibitor of metalloproteinases-3 interacts with angiotensin II type 2 receptor and additively inhibits angiogenesis. *Cardiovascular Research*, 79(1), 150–160.

Kapoor, K. G., & Bakri, S. J. (2013). Intravitreal anti-vascular endothelial growth factor therapy for choroidal neovascularization due to Sorsby macular dystrophy. *Journal of Ocular Pharmacology and Therapeutics*, 29(4), 444-447.

Karamanos, N. K., Theocharis, A. D., Piperigkou, Z., Manou, D., Passi, A., Skandalis, S. S., ... & Onisto, M. (2021). A guide to the composition and functions of the extracellular matrix. *The FEBS Journal*, 288(24), 6850-6912.

Kashiwagi, M., Enghild, J. J., Gendron, C., Hughes, C., Caterson, B., Itoh, Y., & Nagase, H. (2004). Altered proteolytic activities of ADAMTS-4 expressed by C-terminal processing. *Journal of Biological Chemistry*, 279(11), 10109–10119.

Kashiwagi, M., Tortorella, M., Nagase, H., & Brew, K. (2001). TIMP-3 is a potent inhibitor of aggrecanase 1 (ADAM-TS4) and aggrecanase 2 (ADAM-TS5). *Journal of Biological Chemistry*, 276(16), 12501–12504.

Kassiri, Z., Oudit, G. Y., Kandalam, V., Awad, A., Wang, X., Ziou, X., ... & Scholey, J. W. (2009). Loss of TIMP3 enhances interstitial nephritis and fibrosis. *Journal of the American Society of Nephrology*, 20(6), 1223-1235.

Kaur, I., Rathi, S., & Chakrabarti, S. (2010). Variations in TIMP3 are associated with age-related macular degeneration. *Proceedings of the National Academy of Sciences*, 107(28), E112-E113.

Keeling, E., Lotery, A. J., Tumbarello, D. A., & Ratnayaka, J. A. (2018). Impaired cargo clearance in the retinal pigment epithelium (RPE) underlies irreversible blinding diseases. *Cells*, 7(2), 16.

Keenan, T. D., Clark, S. J., Unwin, R. D., Ridge, L. A., Day, A. J., & Bishop, P. N. (2012). Mapping the differential distribution of proteoglycan core proteins in the adult human

retina, choroid, and sclera. *Investigative Ophthalmology & Visual Science*, 53(12), 7528-7538.

Keenan, T. D., Pickford, C. E., Holley, R. J., Clark, S. J., Lin, W., Dowsey, A. W., ... & Bishop, P. N. (2014). Age-dependent changes in heparan sulfate in human Bruch's membrane: implications for age-related macular degeneration. *Investigative Ophthalmology & Visual Science*, 55(8), 5370-5379.

Kelly, O. G., Pinson, K. I., & Skarnes, W. C. (2004). The Wnt co-receptors Lrp5 and Lrp6 are essential for gastrulation in mice. *Development*, 131 (12): 2803–2815.

Kelwick, R., Desanlis, I., Wheeler, G. N., & Edwards, D. R. (2015). The ADAMTS (A Disintegrin and Metalloproteinase with Thrombospondin motifs) family. *Genome Biology*, 16(1), 1–16.

Kennedy, C. J., Rakoczy, P. E., & Constable, I. J. (1995). Lipofuscin of the retinal pigment epithelium: A review. *Eye*, 9(6), 763–771.

Kim, J. H., Shivkumar, A., Norimoto, M., Castro Lingl, S., Seitz, C., Amaro, R. E., ... & Campana, W. M. (2024). Binding and activation of LRP1-dependent cell signaling in schwann cells using a peptide derived from the hemopexin domain of MMP-9. *Biochemistry*, 63(6), 725-732.

Kinoshita, A., Shah, T., Tangredi, M. M., Strickland, D. K., & Hyman, B. T. (2003). The intracellular domain of the low density lipoprotein receptor-related protein modulates transactivation mediated by amyloid precursor protein and Fe65. *Journal of Biological Chemistry*, 278(42), 41182–41188.

Kirchhausen, T., Macia, E., & Pelish, H. E. (2008). Use of dynasore, the small molecule inhibitor of dynamin, in the regulation of endocytosis. *Methods in Enzymology*, 438, 77–93.

Kjøller, L., Engelholm, L. H., Høyer-Hansen, M., Danø, K., Bugge, T. H., & Behrendt, N. (2004). uPARAP/endo180 directs lysosomal delivery and degradation of collagen IV. *Experimental Cell Research*, 293(1), 106–116.

Klein, R. J., Zeiss, C., Chew, E. Y., Tsai, J. Y., Sackler, R. S., Haynes, C., ... & Hoh, J. (2005). Complement factor H polymorphism in age-related macular degeneration. *Science*, 308(5720), 385-389.

Klenotic, P. A., Munier, F. L., Marmorstein, L. Y., & Anand-Apte, B. (2004). Tissue inhibitor of metalloproteinases-3 (TIMP-3) Is a binding partner of epithelial growth factor-containing fibulin-like extracellular matrix protein 1 (EFEMP1): implications for macular degenerations \*. *Journal of Biological Chemistry*, 279(29), 30469–30473.

Knauer, M. F., Orlando, R. A., & Glabe, C. G. (1996). Cell surface APP751 forms complexes with protease nexin 2 ligands and is internalized via the low density lipoprotein receptor-related protein (LRP). *Brain Research*, 740(1-2), 6-14.

Knight, C. G., Willenbrock, F., & Murphy, G. (1992). A novel coumarin-labelled peptide for sensitive continuous assays of the matrix metalloproteinases. *FEBS Letters*, 296(3), 263–266.

Knisely, J. M., Li, Y., Griffith, J. M., Geuze, H. J., Schwartz, A. L., & Bu, G. (2007). Slow endocytosis of the LDL receptor-related protein 1B: implications for a novel cytoplasmic tail conformation. *Experimental Cell Research*, 313(15), 3298-3307.

Kobat, S. G., & Turgut, B. (2020). Importance of Müller cells. *Beyoglu Eye J*, 5(2), 59-63.

Konaniah, E. S., Kuhel, D. G., Basford, J. E., Weintraub, N. L., & Hui, D. Y. (2017). Deficiency of LRP1 in mature adipocytes promotes diet-induced inflammation and atherosclerosis-brief report. *Arteriosclerosis, Thrombosis, and Vascular Biology*, 37(6), 1046–1049.

Kristensen, T., Moestrup, S. K., Gliemann, J., Bendtsen, L., Sand, O., & Sottrup-Jensen, L. (1990). Evidence that the newly cloned low-density-lipoprotein receptor related protein (LRP) is the alpha 2-macroglobulin receptor. *FEBS Letters*, 276(1–2), 151–155.

Kumar, S., Rao, N., & Ge, R. (2012). Emerging roles of ADAMTSs in angiogenesis and cancer. *Cancers*, 4(4), 1252-1299.

Kwon, W., & Freeman, S. A. (2020). Phagocytosis by the retinal pigment epithelium: recognition, resolution, recycling. *Frontiers in immunology*, 11, 604205.

Lamb, T. D. (2015). Why rods and cones? *Eye* 30(2), 179–185.

Langlois, B., Perrot, G., Schneider, C., Henriet, P., Emonard, H., Martiny, L., & Dedieu, S. (2010). LRP-1 promotes cancer cell invasion by supporting ERK and inhibiting JNK signaling pathways. *PLoS One*, 5(7), e11584.

Langton, K. P., Barker, M. D., & McKie, N. (1998). Localization of the functional domains of human tissue inhibitor of metalloproteinases-3 and the effects of a Sorsby's fundus dystrophy mutation. *Journal of Biological Chemistry*, 273(27), 16778-16781.

Langton, K. P., McKie, N., Curtis, A., Goodship, J. A., Bond, P. M., Barker, M. D., & Clarke, M. (2000). A novel tissue inhibitor of metalloproteinases-3 mutation reveals a common molecular phenotype in Sorsby's Fundus Dystrophy. *Journal of Biological Chemistry*, 275(35), 27027–27031.

Langton, K. P., McKie, N., Smith, B. M., Brown, N. J., & Barker, M. D. (2005). Sorsby's fundus dystrophy mutations impair turnover of TIMP-3 by retinal pigment epithelial cells. *Human Molecular Genetics*, 14(23), 3579–3586.

Laudati, E., Gilder, A. S., Lam, M. S., Misasi, R., Sorice, M., Gonias, S. L., & Mantuano, E. (2016). The activities of LDL Receptor-related Protein-1 (LRP1) compartmentalize into distinct plasma membrane microdomains. *Molecular and Cellular Neuroscience*, 76, 42-51.

Leco, K. J., Khokha, R., Pavloff, N., Hawkes, S. P., & Edwards, D. R. (1994). Tissue inhibitor of metalloproteinases-3 (TIMP-3) is an extracellular matrix-associated protein with a distinctive pattern of expression in mouse cells and tissues. *Journal of Biological Chemistry*, 269(12), 9352–9360.

Leco, K. J., Waterhouse, P., Sanchez, O. H., Gowing, K. L., Poole, A. R., Wakeham, A., ... & Khokha, R. (2001). Spontaneous air space enlargement in the lungs of mice lacking tissue inhibitor of metalloproteinases-3 (TIMP-3). *The Journal of Clinical Investigation*, 108(6), 817-829.

Lee, D., Walsh, J. D., Migliorini, M., Yu, P., Cai, T., Schwieters, C. D., ... & Wang, Y. X. (2007). The structure of receptor-associated protein (RAP). *Protein Science*, 16(8), 1628-1640.

Lee, M. H., Atkinson, S., & Murphy, G. (2007). Identification of the Extracellular Matrix (ECM) Binding Motifs of Tissue Inhibitor of Metalloproteinases (TIMP)-3 and Effective Transfer to TIMP-1 \*. *Journal of Biological Chemistry*, 282(9), 6887–6898.

Lehmann, G. L., Benedicto, I., Philp, N. J., & Rodriguez-Boulan, E. (2014). Plasma membrane protein polarity and trafficking in RPE cells: past, present and future. *Experimental Eye Research*, 126, 5-15.

Lengyel, I., Tufail, A., Al Hosaini, H., Luthert, P., Bird, A. C., & Jeffery, G. (2004). Association of drusen deposition with choroidal intercapillary pillars in the aging human eye. *Investigative Ophthalmology & Visual Science*, 45(9), 2886–2892.

Li, R., Maminishkis, A., Zahn, G., Vossmeyer, D., & Miller, S. S. (2009). Integrin  $\alpha 5\beta 1$  mediates attachment, migration, and proliferation in human retinal pigment epithelium: relevance for proliferative retinal disease. *Investigative Ophthalmology & Visual Science*, 50(12), 5988–5996.

Li, R., McCourt, P., Liu, X., Smedsrød, B., & Sørensen, K. (2007). Endocytosis of advanced glycation end products in bovine retinal pigment epithelial cells. *Investigative Ophthalmology & Visual Science*, 48(13), 2206–2206.

Li, W. Q., Dehnade, F., & Zafarullah, M. (2001). Oncostatin M-induced matrix metalloproteinase and tissue inhibitor of metalloproteinase-3 genes expression in chondrocytes requires janus kinase/stat signaling pathway. *The Journal of Immunology*, 166(5), 3491–3498.

Li, Y., Marzolo, M. P., Van Kerkhof, P., Strous, G. J., & Bu, G. (2000). The YXXL motif, but not the two NPXY motifs, serves as the dominant endocytosis signal for low density lipoprotein receptor-related protein. *Journal of Biological Chemistry*, 275(22), 17187–17194.

Li, Z., Clarke, M. P., Barker, M. D., & McKie, N. (2005). TIMP3 mutation in Sorsby's fundus dystrophy: molecular insights. *Expert Reviews in Molecular Medicine*, 7(24), 1–15.

Lillis, A. P., Mikhailenko, I., & Strickland, D. K. (2005). Beyond endocytosis: LRP function in cell migration, proliferation and vascular permeability. *Journal of Thrombosis and Haemostasis*, 3(8), 1884–1893.

Lillis, A. P., Van Duyn, L. B., Murphy-Ullrich, J. E., & Strickland, D. K. (2008). LDL receptor-related protein 1: Unique tissue-specific functions revealed by selective gene knockout studies. *Physiological Reviews*, 88(3), 887–918.

Lin, R. J., Blumenkranz, M. S., Binkley, J., Wu, K., & Vollrath, D. (2006). A novel His158Arg mutation in TIMP3 causes a late-onset form of Sorsby fundus dystrophy. *American Journal of Ophthalmology*, 142(5), 839-848.

Liu, C. X., Li, Y., Obermoeller-McCormick, L. M., Schwartz, A. L., & Bu, G. (2001). The putative tumor suppressor Lrp1b, a novel member of the low density lipoprotein (ldl) receptor family, exhibits both overlapping and distinct properties with the ldl receptor-related protein. *Journal of Biological Chemistry*, 276(31), 28889–28896.

Liu, Q., Trotter, J., Zhang, J., Peters, M. M., Cheng, H., Bao, J., ... & Bu, G. (2010). Neuronal LRP1 knockout in adult mice leads to impaired brain lipid metabolism and progressive, age-dependent synapse loss and neurodegeneration. *Journal of Neuroscience*, 30(50), 17068-17078.

Liu, Q., Zhang, J., Tran, H., Verbeek, M. M., Reiss, K., Estus, S., & Bu, G. (2009). LRP1 shedding in human brain: Roles of ADAM10 and ADAM17. *Molecular Neurodegeneration*, 4(1), 1–7.

Liu, X., Yang, W., Guan, Z., Yu, W., Fan, B., Xu, N., & Liao, D. J. (2018). There are only four basic modes of cell death, although there are many ad-hoc variants adapted to different situations. *Cell and Bioscience*, 8(1), 1–12.

Loeven, M. A., van Gemst, J. J., Schophuizen, C. M., Tilakaratna, V., van Den Heuvel, L. P., Day, A. J., ... & van Der Vlag, J. (2018). A novel choroidal endothelial cell line has a decreased affinity for the age-related macular degeneration-associated complement factor h variant 402h. *Investigative Ophthalmology & Visual Science*, 59(2), 722-730.

Löffek, S., Schilling, O., & Franzke, C. W. (2011). Biological role of matrix metalloproteinases: a critical balance. *European Respiratory Journal*, 38(1), 191–208.

Lu, D., Li, J., Liu, H., Foxa, G. E., Weaver, K., Li, J., ... & Yang, T. (2018). LRP1 suppresses bone resorption in mice by inhibiting the RANKL-stimulated NF- $\kappa$ B and p38 pathways during osteoclastogenesis. *Journal of Bone and Mineral Research*, 33(10), 1773-1784.

Lynn, S. A., Keeling, E., Dewing, J. M., Johnston, D. A., Page, A., Cree, A. J., ... & Ratnayaka, J. A. (2018). A convenient protocol for establishing a human cell culture model of the outer retina. *F1000 Research*, 7.

Lynn, S. A., Ward, G., Keeling, E., Scott, J. A., Cree, A. J., Johnston, D. A., ... & Ratnayaka, J. A. (2017). Ex-vivo models of the Retinal Pigment Epithelium (RPE) in long-term culture faithfully recapitulate key structural and physiological features of native RPE. *Tissue and Cell*, 49(4), 447-460.

MacLaren, R. E., Groppe, M., Barnard, A. R., Cottrall, C. L., Tolmachova, T., Seymour, L., ... & Seabra, M. C. (2014). Retinal gene therapy in patients with choroideremia: initial findings from a phase 1/2 clinical trial. *The Lancet*, 383(9923), 1129-1137.

Mahabadi, N., & Khalili, Y. Al. (2023). Neuroanatomy, Retina. StatPearls.

Mahley, R. W., & Huang, Y. (2007). Atherogenic remnant lipoproteins: role for proteoglycans in trapping, transferring, and internalizing. *The Journal of Clinical Investigation*, 117(1), 94-98.

Mahmoodi, M., Sahebjam, S., Smookler, D., Khokha, R., & Mort, J. S. (2005). Lack of tissue inhibitor of metalloproteinases-3 results in an enhanced inflammatory response in antigen-induced arthritis. *The American Journal of Pathology*, 166(6), 1733–1740.

Majid, M. A., Smith, V. A., Easty, D. L., Baker, A. H., & Newby, A. C. (2002). Sorsby's fundus dystrophy mutant tissue inhibitors of metalloproteinase-3 induce apoptosis of retinal pigment epithelial and MCF-7 cells. *FEBS Letters*, 529(2–3), 281–285.

Majid, M. A., Smith, V. A., Newby, A. C., & Dick, A. D. (2007). Matrix bound SFD mutant TIMP-3 is more stable than wild type TIMP-3. *British Journal of Ophthalmology*, 91(8), 1073-1076.

Malfait, A. M., Liu, R. Q., Ijiri, K., Komiya, S., & Tortorella, M. D. (2002). Inhibition of ADAM-TS4 and ADAM-TS5 prevents aggrecan degradation in osteoarthritic cartilage. *Journal of Biological Chemistry*, 277(25), 22201-22208.

Mamipour, M., Yousefi, M., & Hasanzadeh, M. (2017). An overview on molecular chaperones enhancing solubility of expressed recombinant proteins with correct folding. *International Journal of Biological Macromolecules*, 102, 367-375.

Mao, H., Lockyer, P., Li, L., Ballantyne, C. M., Patterson, C., Xie, L., & Pi, X. (2017). Endothelial LRP1 regulates metabolic responses by acting as a co-activator of PPAR $\gamma$ . *Nature Communications*, 8(1), 1–11.

Margarucci, L., Monti, M. C., Fontanella, B., Riccio, R., & Casapullo, A. (2011). Chemical proteomics reveals bolinaquinone as a clathrin-mediated endocytosis inhibitor. *Molecular BioSystems*, 7(2), 480–485.

Marmorstein, L. Y., Munier, F. L., Arsenijevic, Y., Schorderet, D. F., McLaughlin, P. J., Chung, D., ... & Marmorstein, A. D. (2002). Aberrant accumulation of EFEMP1 underlies drusen formation in Malattia Leventinese and age-related macular degeneration. *Proceedings of the National Academy of Sciences*, 99(20), 13067–13072.

Martin, E. L., McCaig, L. A., Moyer, B. Z., Pape, M. C., Leco, K. J., Lewis, J. F., & Veldhuizen, R. A. (2005). Differential response of TIMP-3 null mice to the lung insults of sepsis, mechanical ventilation, and hyperoxia. *American Journal of Physiology-Lung Cellular and Molecular Physiology*, 289(2), L244-L251.

Maskos, K., Lang, R., Tschesche, H., & Bode, W. (2007). Flexibility and variability of TIMP binding: X-ray structure of the complex between collagenase-3/MMP-13 and TIMP-2. *Journal of Molecular Biology*, 366(4), 1222–1231.

Maurya, M., Bora, K., Blomfield, A. K., Pavlovich, M. C., Huang, S., Liu, C. H., & Chen, J. (2023). Oxidative stress in retinal pigment epithelium degeneration: From pathogenesis to therapeutic targets in dry age-related macular degeneration. *Neural regeneration research*, 18(10), 2173-2181.

Maxson, M. E., & Grinstein, S. (2014). The vacuolar-type H<sup>+</sup>-ATPase at a glance - more than a proton pump. *Journal of Cell Science*, 127(Pt 23), 4987–4993.

May, P., Woldt, E., Matz, R. L., & Boucher, P. (2007). The LDL receptor-related protein (LRP) family: An old family of proteins with new physiological functions. *Annals of Medicine*, 39(3), 219–228.

Mazzoni, F., Safa, H., & Finnemann, S. C. (2014). Understanding photoreceptor outer segment phagocytosis: use and utility of RPE cells in culture. *Experimental Eye Research*, 126, 51-60.

Meunier, I., Bocquet, B., Labesse, G., Zeitz, C., Defoort-Dhellembes, S., Lacroux, A., ... & Hamel, C. P. (2016). A new autosomal dominant eye and lung syndrome linked to mutations in TIMP3 gene. *Scientific Reports*, 6(1), 32544.

Mogensen, E. H., Poulsen, E. T., Thøgersen, I. B., Yamamoto, K., Brüel, A., & Enghild, J. J. (2022). The low-density lipoprotein receptor-related protein 1 (LRP1) interactome in the human cornea. *Experimental Eye Research*, 219, 109081.

Mohammed, F. F., Smookler, D. S., Taylor, S. E., Fingleton, B., Kassiri, Z., Sanchez, O. H., ... & Khokha, R. (2004). Abnormal TNF activity in Timp3<sup>-/-</sup> mice leads to chronic hepatic inflammation and failure of liver regeneration. *Nature Genetics*, 36(9), 969-977.

Morgunova, E., Tuuttila, A., Bergmann, U., & Tryggvason, K. (2002). Structural insight into the complex formation of latent matrix metalloproteinase 2 with tissue inhibitor of metalloproteinase 2. *Proceedings of the National Academy of Sciences of the United States of America*, 99(11), 7414-7419.

Morris, K. J., Cs-Szabo, G., & Cole, A. A. (2010). Characterization of TIMP-3 in human articular talar cartilage. *Connective Tissue Research*, 51(6), 478-490.

Mullooly, M., McGowan, P. M., Crown, J., & Duffy, M. J. (2016). The ADAMs family of proteases as targets for the treatment of cancer. *Cancer Biology & Therapy*, 17(8), 870-880.

Muratoglu, S. C., Mikhailenko, I., Newton, C., Migliorini, M., & Strickland, D. K. (2010). Low density lipoprotein receptor-related protein 1 (LRP1) forms a signaling complex with platelet-derived growth factor receptor-beta in endosomes and regulates activation of the MAPK pathway. *Journal of Biological Chemistry*, 285(19), 14308-14317.

Murphy, G. (2011). Tissue inhibitors of metalloproteinases. *Genome biology*, 12, 1-7.

Sitte, N., Huber, M., Grune, T., Ladhoff, A., Doecke, W. D., Zglinicki, T. V., & Davies, K. J. (2000). Proteasome inhibition by lipofuscin/ceroid during postmitotic aging of fibroblasts. *The FASEB Journal*, 14(11), 1490-1498.

Naessens, S., De Zaeytijd, J., Syx, D., Vandenbroucke, R. E., Smeets, F., Van Cauwenbergh, C., ... & Coppieters, F. (2019). The N-terminal p.(Ser38Cys) TIMP3 mutation underlying Sorsby fundus dystrophy is a founder mutation disrupting an intramolecular disulfide bond. *Human Mutation*, 40(5), 539-551.

Nagase, H., Suzuki, K., Morodomi, T., Enghild, J. J., & Salvesen, G. (1992). Activation mechanisms of the precursors of matrix metalloproteinases 1, 2 and 3. *Matrix (Stuttgart, Germany)*. Supplement, 1, 237-244.

Nagase, H., Visse, R., & Murphy, G. (2006). Structure and function of matrix metalloproteinases and TIMPs. *Cardiovascular Research*, 69(3), 562-573.

Nandhu, M. S., Hu, B., Cole, S. E., Erdreich-Epstein, A., Rodriguez-Gil, D. J., & Viapiano, M. S. (2014). Novel paracrine modulation of Notch-DLL4 signaling by Fibulin-3

promotes angiogenesis in high-grade gliomas. *Cancer Research*, 74(19), 5435–5448.

Nykjaer, A., Dragun, D., Walther, D., Vorum, H., Jacobsen, C., Herz, J., ... & Willnow, T. E. (1999). An endocytic pathway essential for renal uptake and activation of the steroid 25-(OH) vitamin D3. *Cell*, 96(4), 507-515.

Or, C., Wang, J., Kojic, L., Jia, W., Cynader, M. S., Cui, J. Z., & Matsubara, J. A. (2014). Expression of ADAMs (A Disintegrin and Metalloproteinase) 10 and 17 in Human Eyes and in Experimental Models of Age Related Macular Degeneration (AMD). *Investigative Ophthalmology & Visual Science*, 55(13), 3460–3460.

Ori, A., Wilkinson, M. C., & Fernig, D. G. (2011). A systems biology approach for the investigation of the heparin/heparan sulfate interactome. *Journal of Biological Chemistry*, 286(22), 19892–19904.

Panezai, J., Bergdahl, E., & Sundqvist, K. G. (2017). T-cell regulation through a basic suppressive mechanism targeting low-density lipoprotein receptor-related protein 1. *Immunology*, 152(2), 308–327.

Pauleikhoff, D., Harper, C. A., Marshall, J., & Bird, A. C. (1990). Aging Changes in Bruch's Membrane: A Histochemical and Morphologic Study. *Ophthalmology*, 97(2), 171–178.

Pedrero-Prieto, C. M., Flores-Cuadrado, A., Saiz-Sánchez, D., Úbeda-Bañón, I., Frontiñán-Rubio, J., Alcaín, F. J., ... & Peinado, J. R. (2019). Human amyloid- $\beta$  enriched extracts: evaluation of in vitro and in vivo internalization and molecular characterization. *Alzheimer's Research & Therapy*, 11, 1-16.

Peiretti, E., Klancnik, J. M., Spaide, R. F., & Yannuzzi, L. (2005). Choroidal neovascularization in sorsby fundus dystrophy treated with photodynamic therapy and intravitreal triamcinolone acetonide. *Retina*, 25(3), 377–379.

Penfold, P. L., Killingsworth, M. C., & Sarks, S. H. (1985). Senile macular degeneration: The involvement of immunocompetent cells. *Graefe's Archive for Clinical and Experimental Ophthalmology*, 223(2), 69–76.

Perera, R. M., & Zoncu, R. (2016). The Lysosome as a Regulatory Hub. *Annual Review of Cell and Developmental Biology*, 32, 223–253.

Petrushkin, K., Koisti, M. J., Bakall, B., Li, W., Xie, G., Marknell, T., ... & Wadelius, C. (1998). Identification of the gene responsible for Best macular dystrophy. *Nature Genetics*, 19(3), 241-247.

Polavarapu, R., Gongora, M. C., Yi, H., Ranganthan, S., Lawrence, D. A., Strickland, D., & Yepes, M. (2007). Tissue-type plasminogen activator-mediated shedding of

astrocytic low-density lipoprotein receptor-related protein increases the permeability of the neurovascular unit. *Blood*, 109(8), 3270-3278.

Porter, S., Clark, I. M., Kevorkian, L., & Edwards, D. R. (2005). The ADAMTS metalloproteinases. *Biochem. J*, 386, 15–27.

Prendergast, R. A., Iliff, C. E., Coskuncan, N. M., Caspi, R. R., Sartani, G., Tarrant, T. K., ... & McLeod, D. S. (1998). T cell traffic and the inflammatory response in experimental autoimmune uveoretinitis. *Investigative Ophthalmology & Visual Science*, 39(5), 754-762.

Qi, J. H., & Anand-Apte, B. (2022). Deglycosylation Increases the aggregation and angiogenic properties of mutant tissue inhibitor of metalloproteinase 3 protein: implications for Sorsby Fundus Dystrophy. *International Journal of Molecular Sciences*, 23(22), 14231.

Qi, J. H., Bell, B., Singh, R., Batoki, J., Wolk, A., Cutler, A., ... & Anand-Apte, B. (2019). Sorsby fundus dystrophy mutation in tissue inhibitor of metalloproteinase 3 (TIMP3) promotes choroidal neovascularization via a fibroblast growth factor-dependent mechanism. *Scientific Reports*, 9(1), 17429.

Qi, J. H., Dai, G., Luthert, P., Chaurasia, S., Hollyfield, J., Weber, B. H., ... & Anand-Apte, B. (2009). S156C mutation in tissue inhibitor of metalloproteinases-3 induces increased angiogenesis. *Journal of Biological Chemistry*, 284(30), 19927-19936.

Qi, J. H., Ebrahem, Q., Moore, N., Murphy, G., Claesson-Welsh, L., Bond, M., ... & Anand-Apte, B. (2003). A novel function for tissue inhibitor of metalloproteinases-3 (TIMP3): inhibition of angiogenesis by blockage of VEGF binding to VEGF receptor-2. *Nature Medicine*, 9(4), 407-415.

Qi, J. H., Ebrahem, Q., Yeow, K., Edwards, D. R., Fox, P. L., & Anand-Apte, B. (2002). Expression of Sorsby's fundus dystrophy mutations in human retinal pigment epithelial cells reduces matrix metalloproteinase inhibition and may promote angiogenesis. *Journal of Biological Chemistry*, 277(16), 13394-13400.

Qi, J., Liu, J., Yi, C., Deng, W., Cui, X., & Xu, H. (2023). The LRP2 is involved in the inflammatory and autophagy pathways in photoreceptors. *Investigative Ophthalmology & Visual Science*, 64(8), 4429–4429.

Qureshi, H. Y., Ahmad, R., Sylvester, J., & Zafarullah, M. (2007). Requirement of phosphatidylinositol 3-kinase/Akt signaling pathway for regulation of tissue inhibitor of metalloproteinases-3 gene expression by TGF- $\beta$  in human chondrocytes. *Cellular Signalling*, 19(8), 1643–1651.

Qureshi, H. Y., Sylvester, J., El Mabrouk, M., & Zafarullah, M. (2005). TGF-beta-induced expression of tissue inhibitor of metalloproteinases-3 gene in chondrocytes is

mediated by extracellular signal-regulated kinase pathway and Sp1 transcription factor. *Journal of Cellular Physiology*, 203(2), 345–352.

R Sparrow, J., Hicks, D., & P Hamel, C. (2010). The retinal pigment epithelium in health and disease. *Current Molecular Medicine*, 10(9), 802-823.

Ranganathan, S., Noyes, N. C., Migliorini, M., Winkles, J. A., Battey, F. D., Hyman, B. T., ... & Strickland, D. K. (2011). LRAD3, a novel low-density lipoprotein receptor family member that modulates amyloid precursor protein trafficking. *Journal of Neuroscience*, 31(30), 10836-10846.

Rapti, M., Atkinson, S. J., Lee, M. H., Trim, A., Moss, M., & Murphy, G. (2008). The isolated N-terminal domains of TIMP-1 and TIMP-3 are insufficient for ADAM10 inhibition. *The Biochemical Journal*, 411(2), 433–439.

Ravikiran, B., & Mahalakshmi, R. (2014). Unusual post-translational protein modifications: the benefits of sophistication. *RSC Advances*, 4(64), 33958–33974.

Reiss, K., & Saftig, P. (2009). The “a disintegrin and metalloprotease” (ADAM) family of sheddases: physiological and cellular functions. *Seminars in Cell & Developmental Biology*, 20(2), 126–137.

Ren, Q., Chen, J., & Liu, Y. (2021). LRP5 and LRP6 in Wnt signaling: similarity and divergence. *Frontiers in Cell and Developmental Biology*, 9, 670960.

Roebroek, A. J. M., Reekmans, S., Lauwers, A., Feyaerts, N., Smeijers, L., & Hartmann, D. (2006). Mutant Lrp1 knock-in mice generated by recombinase-mediated cassette exchange reveal differential importance of the NPXY motifs in the intracellular domain of LRP1 for normal fetal development. *Molecular and Cellular Biology*, 26(2), 605–616.

Rousselle, P., & Beck, K. (2013). Laminin 332 processing impacts cellular behavior. *Cell Adhesion & Migration*, 7(1), 122-134.

Rudolf, M., Clark, M. E., Chimento, M. F., Li, C. M., Medeiros, N. E., & Curcio, C. A. (2008). Prevalence and morphology of druse types in the macula and periphery of eyes with age-related maculopathy. *Investigative Ophthalmology & Visual Science*, 49(3), 1200–1209.

Rutar, M., Natoli, R., Valter, K., & Provis, J. M. (2011). Early focal expression of the chemokine Ccl2 by Müller cells during exposure to damage-inducing bright continuous light. *Investigative Ophthalmology & Visual Science*, 52(5), 2379–2388.

Safaiyan, F., Kolset, S. O., Prydz, K., Gottfridsson, E., Lindahl, U., & Salmivirta, M. (1999). Selective effects of sodium chlorate treatment on the sulfation of heparan sulfate. *Journal of Biological Chemistry*, 274(51), 36267–36273.

Saftig, P., & Reiss, K. (2011). The “A Disintegrin And Metalloproteases” ADAM10 and ADAM17: Novel drug targets with therapeutic potential? *European Journal of Cell Biology*, 90(6–7), 527–535.

Sahebjam, S., Khokha, R., & Mort, J. S. (2007). Increased collagen and aggrecan degradation with age in the joints of Timp3–/– mice. *Arthritis & Rheumatism*, 56(3), 905–909.

Saihan, Z., Li, Z., Rice, J., Rana, N. A., Ramsden, S., Schlottmann, P. G., Jenkins, S. A., Blyth, C., Black, G. C., McKie, N., & Webster, A. R. (2009). Clinical and biochemical effects of the E139K missense mutation in the TIMP3 gene, associated with Sorsby fundus dystrophy. *Molecular Vision*, 15, 1218–1230.

Sánchez, M. C., Barcelona, P. F., Luna, J. D., Ortiz, S. G., Juarez, P. C., Riera, C. M., & Chiabrando, G. A. (2006). Low-density lipoprotein receptor-related protein-1 (LRP-1) expression in a rat model of oxygen-induced retinal neovascularization. *Experimental Eye Research*, 83(6), 1378–1385.

Sarafanov, A. G., Ananyeva, N. M., Shima, M., & Saenko, E. L. (2001). Cell surface heparan sulfate proteoglycans participate in factor VIII catabolism mediated by low density lipoprotein receptor-related protein. *Journal of Biological Chemistry*, 276(15), 11970–11979.

Sarrazin, S., Lamanna, W. C., & Esko, J. D. (2011). Heparan Sulfate Proteoglycans. *Cold Spring Harbor Perspectives in Biology*, 3(7), 1–33.

Schoenberger, S. D., & Agarwal, A. (2013). A novel mutation at the N-terminal domain of the TIMP3 gene in sorsby fundus dystrophy. *Retina*, 33(2), 429–435.

Schubert, K., Collins, L. E., Green, P., Nagase, H., & Troeberg, L. (2019). LRP1 controls tnf release via the timp-3/adam17 axis in endotoxin-activated macrophages. *The Journal of Immunology*, 202(5), 1501–1509.

Schuksz, M., Fuster, M. M., Brown, J. R., Crawford, B. E., Ditto, D. P., Lawrence, R., ... & Esko, J. D. (2008). Surfen, a small molecule antagonist of heparan sulfate. *Proceedings of the National Academy of Sciences*, 105(35), 13075–13080.

Scilabra, S. D., Pigni, M., Pravatá, V., Schätzl, T., Müller, S. A., Troeberg, L., & Lichtenthaler, S. F. (2018). Increased TIMP-3 expression alters the cellular secretome through dual inhibition of the metalloprotease ADAM10 and ligand-binding of the LRP-1 receptor. *Scientific Reports*, 8(1), 14697.

Scilabra, S. D., Troeberg, L., Yamamoto, K., Emonard, H., Thøgersen, I., Enghild, J. J., ... & Nagase, H. (2013). Differential regulation of extracellular tissue inhibitor of metalloproteinases-3 levels by cell membrane-bound and shed low density

lipoprotein receptor-related protein 1. *Journal of Biological Chemistry*, 288(1), 332-342.

Scilabra, S. D., Yamamoto, K., Pigoni, M., Sakamoto, K., Müller, S. A., Papadopoulou, A., ... & Kadomatsu, K. (2017). Dissecting the interaction between tissue inhibitor of metalloproteinases-3 (TIMP-3) and low density lipoprotein receptor-related protein-1 (LRP-1): Development of a “TRAP” to increase levels of TIMP-3 in the tissue. *Matrix Biology*, 59, 69-79.

Shaw, E., & Lipinski, D. M. (2021). Optimizing transfection and transduction-based gene delivery in primary and immortalized RPE cells. *Investigative Ophthalmology & Visual Science*, 62(8), 2696–2696.

Singh, M., & Tyagi, S. C. (2017). Metalloproteinases as mediators of inflammation and the eyes: molecular genetic underpinnings governing ocular pathophysiology. *International Journal of Ophthalmology*, 10(8), 1308.

Sivaprasad, S., Webster, A. R., Egan, C. A., Bird, A. C., & Tufail, A. (2008). Clinical Course and Treatment Outcomes of Sorsby Fundus Dystrophy. *American Journal of Ophthalmology*, 146(2), 228-234.e2.

Smith, M. R., Kung, H. F., Durum, S. K., Colburn, N. H., & Sun, Y. (1997). TIMP-3 induces cell death by stabilizing TNF- $\alpha$  receptors on the surface of human colon carcinoma cells. *Cytokine*, 9(10), 770–780.

Smith, S. M., Baker, M., Halebian, M., & Smith, C. J. (2017). Weak molecular interactions in clathrin-mediated endocytosis. *Frontiers in Molecular Biosciences*, 4, 72.

Soboleva, G., Geis, B., Schrewe, H., & Weber, B. H. F. (2003). Sorsby fundus dystrophy mutation Timp3S156C affects the morphological and biochemical phenotype but not metalloproteinase homeostasis. *Journal of Cellular Physiology*, 197(1), 149–156.

Söderberg, L., Johannesson, M., Nygren, P., Laudon, H., Eriksson, F., Osswald, G., ... & Lannfelt, L. (2023). Lecanemab, aducanumab, and gantenerumab—binding profiles to different forms of amyloid-beta might explain efficacy and side effects in clinical trials for Alzheimer's disease. *Neurotherapeutics*, 20(1), 195-206.

Song, B., Wang, C., Liu, J., Wang, X., Lv, L., Wei, L., ... & Song, X. (2010). MicroRNA-21 regulates breast cancer invasion partly by targeting tissue inhibitor of metalloproteinase 3 expression. *Journal of Experimental & Clinical Cancer Research*, 29, 1-8.

Sorsby, A., & Mason, M. E. J. (1949). A fundus dystrophy With unusual features (Late onset and dominant inheritance of a central retinal lesion showing oedema, haemorrhage and exudates developing into generalised choroidal atrophy with massive pigment proliferation). *The British Journal of Ophthalmology*, 33(2), 67.

Spaide, R. F. (2021). Treatment of Sorsby fundus dystrophy with anti-tumor necrosis factor-alpha medication. *Eye*, 36(9), 1810–1812.

Spanò, D. P., & Scilabria, S. D. (2022). Tissue inhibitor of metalloproteases 3 (TIMP-3): in vivo analysis underpins its role as a master regulator of ectodomain shedding. *Membranes*, 12(2), 211.

Sparrow, J. R., & Boulton, M. (2005). RPE lipofuscin and its role in retinal pathobiology. *Experimental Eye Research*, 80(5), 595–606.

Sreekumar, P. G., Su, F., Spee, C., Araujo, E., Nusinowitz, S., Reddy, S. T., & Kannan, R. (2022). Oxidative stress and lipid accumulation augments cell death in LDLR-deficient RPE cells and Ldlr<sup>-/-</sup> mice. *Cells*, 12(1), 43.

Stern, J., & Temple, S. (2015). Retinal pigment epithelial cell proliferation. *Experimental Biology and Medicine*, 240(8), 1079-1086.

Stöhr, R., Cavalera, M., Menini, S., Mavilio, M., Casagrande, V., Rossi, C., ... & Federici, M. (2014). Loss of TIMP3 exacerbates atherosclerosis in ApoE null mice. *Atherosclerosis*, 235(2), 438-443.

Storm, T., Burgoyne, T., Dunaief, J. L., Christensen, E. I., Futter, C., & Nielsen, R. (2019). Selective ablation of megalin in the retinal pigment epithelium results in megaophthalmos, macromelanosome formation and severe retina degeneration. *Investigative Ophthalmology & Visual Science*, 60(1), 322-330.

Storm, T., Burgoyne, T., & Futter, C. E. (2020). Membrane trafficking in the retinal pigment epithelium at a glance. *Journal of Cell Science*, 133(16), jcs238279.

Storm, T., Heegaard, S., Christensen, E. I., & Nielsen, R. (2014). Megalin-deficiency causes high myopia, retinal pigment epithelium-macromelanosomes and abnormal development of the ciliary body in mice. *Cell and Tissue Research*, 358(1), 99–107.

Su, C. W., Lin, C. W., Yang, W. E., & Yang, S. F. (2019). TIMP-3 as a therapeutic target for cancer. *Therapeutic Advances in Medical Oncology*, 11.

Summerford, C., & Samulski, R. J. (1998). Membrane-associated heparan sulfate proteoglycan is a receptor for adeno-associated virus type 2 virions. *Journal of Virology*, 72(2), 1438–1445.

Sundelin, S., Wihlmark, Dr. U., Nilsson, S. E. G., & Brunk, U. T. (1998). Lipofuscin accumulation in cultured retinal pigment epithelial cells reduces their phagocytic capacity. *Current Eye Research*, 17(8), 851–857.

Szewczyk-Roszczenko, O. K., Roszczenko, P., Shmakova, A., Finiuk, N., Holota, S., Lesyk, R., ... & Bielawski, K. (2023). The chemical inhibitors of endocytosis: from mechanisms to potential clinical applications. *Cells*, 12(18), 2312.

Tabata, Y., Isashiki, Y., Kamimura, K., Nakao, K., & Ohba, N. (1998). A novel splice site mutation in the tissue inhibitor of the metalloproteinases-3 gene in Sorsby's fundus dystrophy with unusual clinical features. *Human Genetics*, 103, 179-182.

Takahashi, S., Kawarabayasi, Y., Nakai, T., Sakai, J., & Yamamoto, T. (1992). Rabbit very low density lipoprotein receptor: a low density lipoprotein receptor-like protein with distinct ligand specificity. *Proceedings of the National Academy of Sciences*, 89(19), 9252-9256.

Tanna, P., Strauss, R. W., Fujinami, K., & Michaelides, M. (2017). Stargardt disease: clinical features, molecular genetics, animal models and therapeutic options. *British Journal of Ophthalmology*, 101(1), 25-30.

Thevenard, J., Verzeaux, L., Devy, J., Etique, N., Jeanne, A., Schneider, C., ... & Emonard, H. (2014). Low-density lipoprotein receptor-related protein-1 mediates endocytic clearance of tissue inhibitor of metalloproteinases-1 and promotes its cytokine-like activities. *PLoS One*, 9(7), e103839.

Thottacherry, J. J., Sathe, M., Prabhakara, C., & Mayor, S. (2019). Spoiled for choice: diverse endocytic pathways function at the cell surface. *Annual Review of Cell and Developmental Biology*, 35, 55-84.

Thyboll, J., Kortesmaa, J., Cao, R., Soininen, R., Wang, L., Iivanainen, A., ... & Tryggvason, K. (2002). Deletion of the laminin  $\alpha 4$  chain leads to impaired microvessel maturation. *Molecular and Cellular Biology*, 22(4), 1194-1202.

Tian, X., Cui, Z., Liu, S., Zhou, J., & Cui, R. (2021). Melanosome transport and regulation in development and disease. *Pharmacology & Therapeutics*, 219, 107707.

Trinkle-Mulcahy, L. (2019). Recent advances in proximity-based labeling methods for interactome mapping. *F1000Research*, 8.

Troeberg, L., Fushimi, K., Khokha, R., Emonard, H., Ghosh, P., & Nagase, H. (2008). Calcium pentosan polysulfate is a multifaceted exosite inhibitor of aggrecanases. *The FASEB Journal*, 22(10), 3515.

Troeberg, L., Fushimi, K., Scilabria, S. D., Nakamura, H., Dive, V., Thøgersen, I. B., ... & Nagase, H. (2009). The C-terminal domains of ADAMTS-4 and ADAMTS-5 promote association with N-TIMP-3. *Matrix Biology*, 28(8), 463-469.

Troeberg, L., Lazenbatt, C., Anower-E-Khuda, M. F., Freeman, C., Federov, O., Habuchi, H., ... & Nagase, H. (2014). Sulfated glycosaminoglycans control the extracellular trafficking and the activity of the metalloprotease inhibitor TIMP-3. *Chemistry & Biology*, 21(10), 1300-1309.

Tsokolas, G., Almuhtaseb, H., & Lotery, A. (2018). Evaluation of pro-re-nata (prn) and treat and extend bevacizumab treatment protocols in Sorsby Fundus Dystrophy. *European Journal of Ophthalmology*, 30(1), 26–33.

Tuuttila, A., Morgunova, E., Bergmann, U., Lindqvist, Y., Maskos, K., Fernandez-Catalan, C., ... & Schneider, G. (1998). Three-dimensional structure of human tissue inhibitor of metalloproteinases-2 at 2.1 Å resolution. *Journal of Molecular Biology*, 284(4), 1133-1140.

Vallet, S. D., Berthollier, C., & Ricard-Blum, S. (2022). The glycosaminoglycan interactome 2.0. *American Journal of Physiology-Cell Physiology*, 322(6), C1271-C1278.

Van Den Biggelaar, M., Sellink, E., Klein Gebbinck, J. W. T. M., Mertens, K., & Meijer, A. B. (2011). A single lysine of the two-lysine recognition motif of the D3 domain of receptor-associated protein is sufficient to mediate endocytosis by low-density lipoprotein receptor-related protein. *The International Journal of Biochemistry & Cell Biology*, 43(3), 431–440.

van Soest, S. S., De Wit, G. M., Essing, A. H., ten Brink, J. B., Kamphuis, W., De Jong, P. T., & Bergen, A. A. (2007). Comparison of human retinal pigment epithelium gene expression in macula and periphery highlights potential topographic differences in Bruch's membrane. *Molecular Vision*, 13, 1608-1617.

Venkatesh, Y. P., & Levine, R. P. (1988). The esterase-like activity of covalently bound human third complement protein. *Molecular Immunology*, 25(9), 821–828.

Vergaro, A., Pankiewic, M., Jedlickova, J., Dudakova, L., Vajter, M., Michaelides, M., ... & Liskova, P. (2024). Disease-causing timp3 variants and deep phenotyping of two czech families with Sorsby Fundus Dystrophy associated with novel p.(Tyr152Cys) mutation. *International Journal of Molecular Sciences*, 25(7), 3744.

Vranka, J. A., Johnson, E., Zhu, X., Shepardson, A., Alexander, J. P., Bradley, J. M., ... & Acott, T. S. (1997). Discrete expression and distribution pattern of TIMP-3 in the human retina and choroid. *Current Eye Research*, 16(2), 102-110.

Wang, B., Hsu, S. H., Majumder, S., Kutay, H., Huang, W., Jacob, S. T., & Ghoshal, K. (2010). TGFbeta-mediated upregulation of hepatic miR-181b promotes hepatocarcinogenesis by targeting TIMP3. *Oncogene*, 29(12), 1787–1797.

Wang, F., Flanagan, J., Su, N., Wang, L. C., Bui, S., Nielson, A., ... & Luo, Y. (2012). RNAscope: a novel *in situ* RNA analysis platform for formalin-fixed, paraffin-embedded tissues. *The Journal of Molecular Diagnostics*, 14(1), 22-29.

Wang, J., Ohno-Matsui, K., Yoshida, T., Kojima, A., Shimada, N., Nakahama, K. I., ... & Morita, I. (2008). Altered function of factor I caused by amyloid β: implication for

pathogenesis of age-related macular degeneration from drusen. *The Journal of Immunology*, 181(1), 712-720.

Wang, L., Clark, M. E., Crossman, D. K., Kojima, K., Messinger, J. D., Mobley, J. A., & Curcio, C. A. (2010). Abundant lipid and protein components of drusen. *PLoS One*, 5(4), e10329.

Warwick, A., Gibson, J., Sood, R., & Lotery, A. (2016). A rare penetrant TIMP3 mutation confers relatively late onset choroidal neovascularisation which can mimic age-related macular degeneration. *Eye (London, England)*, 30(3), 488–491.

Weaver, A. M., McCabe, M., Kim, I., Allietta, M. M., & Gonias, S. L. (1996). Epidermal growth factor and platelet-derived growth factor-BB induce a stable increase in the activity of low density lipoprotein receptor-related protein in vascular smooth muscle cells by altering receptor distribution and recycling. *Journal of Biological Chemistry*, 271(40), 24894–24900.

Weber, B. H., Lin, B., White, K., Kohler, K., Soboleva, G., Herterich, S., ... & Schrewe, H. (2002). A mouse model for Sorsby fundus dystrophy. *Investigative Ophthalmology & Visual Science*, 43(8), 2732-2740.

Weber, B. H. F., Vogt, G., Pruitt, R. C., Stöhr, H., & Felbor, U. (1994a). Mutations in the tissue inhibitor of metalloproteinases-3 (TIMP3) in patients with Sorsby's fundus dystrophy. *Nature Genetics*, 8(4), 352–356.

Weber, B. H. F., Vogt, G., Wolz, W., Ives, E. J., & Ewing, C. C. (1994b). Sorsby's fundus dystrophy is genetically linked to chromosome 22q13-qter. *Nature Genetics*, 7(2), 158–161.

Weinlich, R., Brunner, T., & Amarante-Mendes, G. P. (2010). Control of death receptor ligand activity by posttranslational modifications. *Cellular and Molecular Life Sciences*, 67(10), 1631–1642.

Wetzel, M., Li, L., Harms, K. M., Roitbak, T., Ventura, P. B., Rosenberg, G. A., ... & Cunningham, L. A. (2008). Tissue inhibitor of metalloproteinases-3 facilitates Fas-mediated neuronal cell death following mild ischemia. *Cell Death & Differentiation*, 15(1), 143-151.

Whitmore, S. S., Sohn, E. H., Chirco, K. R., Drack, A. V., Stone, E. M., Tucker, B. A., & Mullins, R. F. (2015). Complement activation and choriocapillaris loss in early AMD: implications for pathophysiology and therapy. *Progress in Retinal and Eye Research*, 45, 1-29.

Wijesuriya, S. D., Evans, K., Jay, M. R., Davison, C., Weber, B. H., Bird, A. C., ... & Gregory, C. Y. (1996). Sorsby's fundus dystrophy in the British Isles: demonstration

of a striking founder effect by microsatellite-generated haplotypes. *Genome Research*, 6(2), 92-101.

Wilde, C. G., Hawkins, P. R., Coleman, R. T., Levine, W. B., Delegeane, A. M., Okamoto, P. M., ... & Seilhamer, J. J. (1994). Cloning and characterization of human tissue inhibitor of metalloproteinases-3. *DNA and Cell Biology*, 13(7), 711-718.

Williamson, R. A., Freedman, R. B., Martorell, G., Carr, M. D., Feeney, J., Murphy, G., & Docherty, A. J. P. (1994). Solution structure of the active domain of tissue inhibitor of metalloproteinases-2. A new member of the OB fold protein family. *Biochemistry*, 33(39), 11745–11759.

Willnow, T. E. (1999). The low-density lipoprotein receptor gene family: Multiple roles in lipid metabolism. *Journal of Molecular Medicine*, 77(3), 306–315.

Willnow, T. E., & Herz, J. (1994). Genetic deficiency in low density lipoprotein receptor-related protein confers cellular resistance to *Pseudomonas* exotoxin A evidence that this protein is required for uptake and degradation of multiple ligands. *Journal of Cell Science*, 107(3), 719–726.

Wisniewska, M., Goettig, P., Maskos, K., Belouski, E., Winters, D., Hecht, R., ... & Bode, W. (2008). Structural determinants of the ADAM inhibition by TIMP-3: crystal structure of the TACE-N-TIMP-3 complex. *Journal of Molecular Biology*, 381(5), 1307-1319.

Wolk, A., Upadhyay, M., Ali, M., Suh, J., Stoehr, H., Bonilha, V. L., & Anand-Apte, B. (2020). The retinal pigment epithelium in Sorsby Fundus Dystrophy shows increased sensitivity to oxidative stress-induced degeneration. *Redox Biology*, 37, 101681.

Wong, S. C., Fong, K. C. S., Lee, N., Gregory-Evans, K., & Gregory-Evans, C. Y. (2003). Successful photodynamic therapy for subretinal neovascularisation due to Sorsby's fundus dystrophy: 1 year follow up. *British Journal of Ophthalmology*, 87(6), 796–797.

Wong, W. L., Su, X., Li, X., Cheung, C. M. G., Klein, R., Cheng, C. Y., & Wong, T. Y. (2014). Global prevalence of age-related macular degeneration and disease burden projection for 2020 and 2040: a systematic review and meta-analysis. *The Lancet Global Health*, 2(2), e106–e116.

Xia, Z. M., Song, M. Y., Chen, Y. L., Cui, G., & Fan, D. (2023). TIMP3 induces gene expression partly through PI3K and their association with vascularization and heart rate. *Frontiers in Cardiovascular Medicine*, 10, 1130388.

Xu, H., Zhang, L., & Freitas, M. A. (2008). Identification and characterization of disulfide bonds in proteins and peptides from tandem MS data by use of the MassMatrix MS/MS search engine. *Journal of Proteome Research*, 7(01), 138-144.

Yamamoto, K., Okano, H., Miyagawa, W., Visse, R., Shitomi, Y., Santamaria, S., ... & Nagase, H. (2016). MMP-13 is constitutively produced in human chondrocytes and co-endocytosed with ADAMTS-5 and TIMP-3 by the endocytic receptor LRP1. *Matrix Biology*, 56, 57-73.

Yamamoto, K., Santamaria, S., Botkjaer, K. A., Duhdia, J., Troeberg, L., Itoh, Y., ... & Nagase, H. (2017). Inhibition of shedding of low-density lipoprotein receptor-related protein 1 reverses cartilage matrix degradation in osteoarthritis. *Arthritis & Rheumatology*, 69(6), 1246-1256.

Yamamoto, K., Scavenius, C., Meschis, M. M., Gremida, A. M., Mogensen, E. H., Thøgersen, I. B., ... & Nagase, H. (2022). A top-down approach to uncover the hidden ligandome of low-density lipoprotein receptor-related protein 1 in cartilage. *Matrix Biology*, 112, 190-218.

Yamamoto, K., Scavenius, C., Santamaria, S., Botkjaer, K. A., Duhdia, J., Troeberg, L., ... & Nagase, H. (2018). Inhibition of LRP1 shedding reverses cartilage degradation in osteoarthritis. *Osteoarthritis and Cartilage*, 26, S22.

Yamamoto, K., Troeberg, L., Scilabria, S. D., Pelosi, M., Murphy, C. L., Strickland, D. K., & Nagase, H. (2013). LRP-1-mediated endocytosis regulates extracellular activity of ADAMTS-5 in articular cartilage. *The FASEB Journal*, 27(2), 511.

Yan, W., Zheng, L., Xu, X., Hao, Z., Zhang, Y., Lu, J., ... & Jiang, Q. (2022). Heterozygous LRP1 deficiency causes developmental dysplasia of the hip by impairing triradiate chondrocytes differentiation due to inhibition of autophagy. *Proceedings of the National Academy of Sciences*, 119(37), e2203557119.

Yan, X., Lin, J., Rolfs, A., & Luo, J. (2011). Differential expression of the ADAMs in developing chicken retina. *Development, Growth & Differentiation*, 53(5), 726-739.

Yang, S., Zhou, J., & Li, D. (2021). Functions and diseases of the retinal pigment epithelium. *Frontiers in Pharmacology*, 12, 727870.

Yang, X., Wang, J., Guo, S. L., Fan, K. J., Li, J., Wang, Y. L., ... & Yang, X. (2011). miR-21 promotes keratinocyte migration and re-epithelialization during wound healing. *International Journal of Biological Sciences*, 7(5), 685-690.

Yeow, K. M., Kishnani, N. S., Hutton, M., Hawkes, S. P., Murphy, G., & Edwards, D. R. (2002). Sorsby's fundus dystrophy tissue inhibitor of metalloproteinases-3 (TIMP-3) mutants have unimpaired matrix metalloproteinase inhibitory activities, but affect cell adhesion to the extracellular matrix. *Matrix Biology*, 21(1), 75-88.

Yu, C., Muñoz, L. E., Mallavarapu, M., Herrmann, M., & Finnemann, S. C. (2019). Annexin A5 regulates surface  $\alpha\beta 5$  integrin for retinal clearance phagocytosis. *Journal of Cell Science*, 132(20), jcs232439.

Yu, W. H., Yu, S. S. C., Meng, Q., Brew, K., & Woessner, J. F. (2000). TIMP-3 binds to sulfated glycosaminoglycans of the extracellular matrix \*. *Journal of Biological Chemistry*, 275(40), 31226–31232.

Zarbin, M. A. (2003). Analysis of retinal pigment epithelium integrin expression and adhesion to aged submacular human Bruch's membrane. *Transactions of the American Ophthalmological Society*, 101, 499.

Zhong, Z., Baker, J. J., Zylstra-Diegel, C. R., & Williams, B. O. (2012). Lrp5 and Lrp6 play compensatory roles in mouse intestinal development. *Journal of Cellular Biochemistry*, 113(1), 31-38.

Zhou, Y. D., Yoshida, S., Peng, Y. Q., Kobayashi, Y., Zhang, L. S., & Tang, L. S. (2017). Diverse roles of macrophages in intraocular neovascular diseases: a review. *International Journal of Ophthalmology*, 10(12), 1902.

Zurhove, K., Nakajima, C., Herz, J., Bock, H. H., & May, P. (2008).  $\gamma$ -Secretase limits the inflammatory response through the processing of LRP1. *Science Signaling*, 1(47), ra15-ra15.